Proteins at Crossroads:

Regulating Dual Targeting of Tail-Anchored Proteins between Mitochondria and Peroxisomes

Dissertation

der Mathematisch-Naturwissenschaftlichen Fakultät

der Eberhard Karls Universität Tübingen

zur Erlangung des Grades eines

Doktors der Naturwissenschaften

(Dr. rer. nat.)

vorgelegt von

Nitya Aravindan

Aus Vashi-Maharashtra, Indien

Tübingen

2024

Gedruckt mit Genehmigung der Mathematisch-Naturwissenschaftlichen Fakultät der Eberhard Karls Universität Tübingen.

Tag der mündlichen Qualifikation:	16.08.2024
Dekan:	Prof. Dr. Thilo Stehle
1. Berichterstatter:	Prof. Dr. Doron Rapaport
2. Berichterstatter:	Prof. Dr. Ralf-Peter Jansen

Erklärung / Declaration: Ich erkläre, dass ich die zur Promotion eingereichte Arbeit mit dem Titel:

“Proteins at Crossroads: Regulating Dual Targeting of Tail-Anchored Proteins between Mitochondria and Peroxisomes”

Selbständig verfasst, nur die angegebenen Quellen und Hilfsmittel benutzt und wörtlich oder inhaltlich übernommene Stellen als solche gekennzeichnet habe. Ich versichere an Eides statt, dass diese Angaben wahr sind und dass ich nichts verschwiegen habe. Mir ist bekannt, dass die falsche Abgabe einer Versicherung an Eides statt mit Freiheitsstrafe bis zu drei Jahren oder mit Geldstrafe bestraft wird.

I hereby declare that I have produced the work entitled:

“Proteins at Crossroads: Regulating Dual Targeting of Tail-Anchored Proteins between Mitochondria and Peroxisomes”

submitted for the award of a doctorate, on my own (without external help), have used only the sources and aids indicated and have marked passages included from other works, whether verbatim or in content, as such. I swear upon oath that these statements are true and that I have not concealed anything. I am aware that making a false declaration under oath is punishable by a term of imprisonment of up to three years or by a fine.

Tübingen, den

Contents

List of abbreviations

ATP	Adenosine Triphosphate
BN-PAGE	Blue Native Polyacrylamide Gel Electrophoresis
ER	Endoplasmic Reticulum
Fis1	Fission 1
Gem1	GTPase EF-hand protein of Mitochondria 1
GFP	Green Fluorescent Protein
HA	Hemagglutinin
IF	Immunofluorescence
IMS	Intermembrane Space
IMPs	Integral Membrane Proteins
IMM	Inner Membrane of Mitochondria
MIM	Mitochondrial Import Machinery
MIA	Mitochondrial IMS Assembly
MOM	Mitochondrial Outer Membrane
Mpf1	Mitochondria and Peroxisomes Factor 1
MPP	Mitochondrial Processing Peptidases
mPTS	Membrane Peroxisomal Targeting Signal
PAM	Presequence translocase-Associated Motor
Pex3	Peroxisomal Biogenesis Factor 3
Pex19	Peroxisomal Biogenesis Factor 19
PH	Pleckstrin Homology
SGA	Synthetic Genetic Array
SS	Steady-State
TA	Tail-Anchored
TMD	Transmembrane Domain
Tom70	Translocase of Outer Mitochondrial Membrane 70
Tom71	Translocase of Outer Mitochondrial Membrane 71
TPR	Tetratricopeptide Repeat
WT	Wild Type
Yet1	Yeast Endoplasmic reticulum Transmembrane protein 1
Yet3	Yeast Endoplasmic reticulum Transmembrane protein 3

Summary

This summary provides an overview of the key findings and methodologies discussed in each chapter of this thesis, reflecting the research conducted on protein distribution, sterol biosynthesis, and organelle separation.

Chapter 2: Mpf1 is a novel factor that affects the dual distribution of tail-anchored proteins between mitochondria and peroxisomes

This study identifies factors influencing the dual targeting of tail-anchored proteins between mitochondria and peroxisomes. Using high-throughput microscopy and subcellular fractionation, we identified Ynl144c (renamed Mpf1), Tom70, and Tom71, as factors whose absence led to increased Fis1 and Gem1 population in peroxisomes. Overexpressing Tom71, unlike Tom70, resulted in more Fis1 in mitochondria, indicating a unique role for Tom71. Furthermore, characterizing Mpf1 revealed it as an unstable protein associated with the mitochondrial outer membrane and *MPF1* transcript levels were reduced upon the deletion of *TOM70/71*. We also discovered that mutating three conserved residues in the PH domain of Mpf1 increases its stability without affecting localization. Overall, these findings reveal unique roles of Mpf1, Tom70, and Tom71 in the dual targeting of proteins between mitochondria and peroxisomes

Chapter 3: On-Demand Sterol Biosynthesis at Organelle Contact Sites

This study explores the formation of membrane subdomains enriched in sterols at ER contact sites, shedding light on the function of Yet3 in regulating sterol biosynthesis and cellular homeostasis. This chapter mainly discusses my contribution to this study, focusing on identifying high molecular weight complexes involving Yet3 and the ergosterol biosynthesis enzymes, suggesting their assembly into large complexes at the ER contact sites. The study also emphasizes Yet1's importance in maintaining Yet3's proper localization and function. Notably, the BN-PAGE analysis revealed a Yet1-independent role of Yet3 in forming the high molecular weight complexes involved in sterol biosynthesis. Together, these findings reveal Yet3's role as a regulator of sterol biosynthesis and ER membrane subdomain formation.

Chapter 4: Separating Yeast Peroxisomes from Mitochondria

This chapter describes an optimized method for separating yeast peroxisomes from mitochondria, involving modified growth conditions, preparation of yeast spheroplasts, isolation of crude organelles, and a discontinuous gradient centrifugation. This technique improves purity of the organelles, enabling the study of proteins dually targeted to mitochondria and peroxisomes.

Zussammenfassung

Die vorliegenden Zusammenfassungen geben einen Überblick über die wichtigsten Ergebnisse und Methoden, die in den einzelnen Kapiteln dieser Arbeit erörtert werden. Sie spiegeln die Forschungsarbeiten zur Proteinverteilung, Sterolbiosynthese und Organellentrennung wider.

Kapitel 1: Mpf1 ist ein neuer Faktor, der die duale Verteilung von schwanzverankerten Proteinen zwischen Mitochondrien und Peroxisomen beeinflusst

In dieser Studie werden Faktoren identifiziert, die die duale Verteilung von schwanzverankerten Proteinen zwischen Mitochondrien und Peroxisomen beeinflussen. Mittels Hochdurchsatzmikroskopie und subzellulärer Fraktionierung konnten wir Ynl144c (umbenannt in Mpf1), Tom70 und Tom71 identifizieren, als Proteine deren Fehlen zu einer erhöhten Fis1- und Gem1-Population in Peroxisomen führte. Die Überexpression von Tom71 resultierte im Gegensatz zu Tom70 in einer erhöhten Fis1-Konzentration in Mitochondrien, was auf eine spezifische Funktion von Tom71 hindeutet. Des Weiteren konnte festgestellt werden, dass eine Mutante des Proteins Mpf1, die eine veränderte PH-Domäne aufweist, eine erhöhte Stabilität zeigt, ohne dass dies zu einer Beeinträchtigung der Lokalisierung führt. Die Ergebnisse legen nahe, dass Mpf1, Tom70 und Tom71 eine einzigartig Rolle bei der dualen Adressierung von Proteinen zwischen Mitochondrien und Peroxisomen spielen.

Kapitel 2: Sterol-Biosynthese auf Abruf an Organellen-Kontaktstellen

Die vorliegende Studie untersucht die Bildung von mit Sterolen angereicherten Membransubdomänen an ER-Kontaktstellen und wirft ein Licht auf die Funktion von Yet3 bei der Regulierung der Sterolbiosynthese und der zellulären Homöostase. In diesem Kapitel wird hauptsächlich mein Beitrag zu der vorliegenden Studie erörtert, wobei der Schwerpunkt auf der Identifizierung von Komplexen mit hohem Molekulargewicht liegt, an denen Yet3 und die Enzyme der Ergosterol-Biosynthese beteiligt sind. Dies deutet auf deren Zusammenschluss zu großen Komplexen an den ER-Kontaktstellen hin. Die Studie unterstreicht zudem die Bedeutung von Yet1 für die Aufrechterhaltung der richtigen Lokalisierung und Funktion von Yet3. Die BN-PAGE-Analyse ergab jedoch, dass Yet3 eine Yet1-unabhängige Rolle bei der Bildung von Komplexen mit hohem Molekulargewicht spielt, die an der Sterinbiosynthese beteiligt sind. Zusammenfassend zeigen diese Ergebnisse, dass Yet3 als Regulator der Sterol-Biosynthese und der Bildung von ER-Membransubdomänen fungiert.

Kapitel 3: Abtrennung von Hefe-Peroxisomen von Mitochondrien

In diesem Kapitel wird eine optimierte Methode zur Abtrennung von Hefe-Peroxisomen von Mitochondrien erörtert. Diese umfasst die modifizierte Wachstumsbedingungen, die Herstellung von Hefe-Sphäroplasten, die Isolierung von rohen Organellen sowie eine diskontinuierliche Gradientenzentrifugation. Die hier beschriebene Technik verbessert die Reinheit der Organellen und erlaubt die Untersuchung von Proteinen, die sowohl in Mitochondrien als auch in Peroxisomen vorkommen.

List of submitted publications contained in this thesis

a) Submitted original manuscripts

1. **Aravindan, N.**, Vitali, D. G., Oberst, J., Zalckvar, E., Schuldiner, M., & Rapaport, D. (2024). Mpf1 is a novel factor that affects the dual distribution of tail-anchored proteins between mitochondria and peroxisomes. bioRxiv. https://doi.org/10.1101/2024.04.30.591829

2. Zung, N., **Aravindan, N.**, Boshnakovska, A., Valenti, R., Preminger, N., Jonas, F., Yaakov, G., Willoughby, M. M., Homberg, B., Keller, J., Kupervaser, M., Dezorella, N., Dadosh, T., Wolf, S. G., Itkin, M., Malitsky, S., Brandis, A., Barkai, N., Fernández-Busnadiego, R., Reddi, A., Rehling, P., Rapaport, D., Schuldiner, M. (2024). The molecular mechanism of on-demand sterol biosynthesis at organelle contact sites bioRxiv. https://doi.org/10.1101/2024.05.09.593285

b) Submitted book chapter

3. **Aravindan, N.** and Rapaport, D. (2024). A modified procedure for separating yeast peroxisomes from mitochondria. In Methods in Enzymology book on "MITOCHONDRIAL TRANSLOCASES" (Editor: Nils Wiedemann).

Personal contribution to the submitted publications contained in this thesis.

a) Submitted original manuscripts

1. **Aravindan, N**., Vitali, D. G., Oberst, J., Zalckvar, E., Schuldiner, M., & Rapaport, D. (2024). Mpf1 is a novel factor that affects the dual distribution of tail-anchored proteins between mitochondria and peroxisomes. bioRxiv. https://doi.org/10.1101/2024.04.30.591829

   I designed and performed most experiments, analyzed data, prepared all the figures and co-wrote the manuscript with DR.

2. Zung, N., **Aravindan, N**., Boshnakovska, A., Valenti, R., Preminger, N., Jonas, F., Yaakov, G., Willoughby, M. M., Homberg, B., Keller, J., Kupervaser, M., Dezorella, N., Dadosh, T., Wolf, S. G., Itkin, M., Malitsky, S., Brandis, A., Barkai, N., Fernández-Busnadiego, R., Reddi, A., Rehling, P., Rapaport, D., Schuldiner, M. (2024). The molecular mechanism of on-demand sterol biosynthesis at organelle contact sites. bioRxiv. https://doi.org/10.1101/2024.05.09.593285

   I performed the BN-PAGE analysis shown in Figure S4 B in the pre-print.

b) Submitted book chapter

Aravindan and Rapaport (2024). A modified procedure for separating yeast peroxisomes from mitochondria. In Methods in Enzymology book on "MITOCHONDRIAL TRANSLOCASES" (Editor: Nils Wiedemann).

I optimized the protocol, prepared figures and co-wrote the book chapter with DR.

Chapter 1

Introduction

Chapter 1 introduces the intracellular sorting of membrane proteins, discusses the origin, function and biogenesis of mitochondria. It provides details into the processes involved in the import of proteins into mitochondria, particularly focusing on tail-anchored (TA) proteins. The chapter further focuses on the pathways for importing dually localized TA proteins like Fis1 and Gem1 into mitochondria and peroxisomes.

Intracellular sorting of membrane proteins

Saccharomyces cerevisiae, also known as baker's yeast, is one of the most studied eukaryotic model organisms. Studies in yeast have allowed the identification of many protein complexes, as well as trafficking and metabolic pathways, most of them also being conserved in higher eukaryotes. One of the unique properties of eukaryotic cells is their compartmentalization, leading complex metabolic processes to be organized within distinct cellular organelles. Each organelle provides an ideal condition to execute specific biochemical reactions as they host a distinct physical environment and a diverse mix of metabolites, enzymes, and cofactors (Cao et al., 2020; Moon et al., 2023). Since most proteins are synthesized in the cytosol, the presence of different organelles in the cell calls for a mechanism to correctly sort the proteins to their designated intracellular location. To achieve this, the proteins that are destined to reach a specific organelle bear a targeting signal sequence that with help of several cytosolic factors and chaperones is recognized by the membrane receptor of that organelle (Schlacht et al., 2014). This complex protein trafficking system is prone to mistargeting proteins to unintended organelles. To counteract this, cells have developed numerous quality control mechanisms to correct folding of proteins within their designated organelles and to clear out mistargeted protein from the wrong organelles (Johansson et al., 2023).

Such targeting mechanism is crucial for integral membrane proteins (IMPs), which constitute ~30 % of the proteome (Krogh et al., 2001). IMPs contain one or more transmembrane domains (TMDs) which consists of hydrophobic amino acids and are prone to aggregation in the site of their synthesis – the cytosol. Hence, for a membrane protein to be stably targeted into a specific lipid bilayer, it needs to be recognized by cytosolic factors that would protect the TMDs until it reaches the destined organelle (Guna & Hegde, 2018; Hann & Walter, 1991). IMPs can be imported across membranes either during their synthesis (co-translational) or after completing the synthesis (post-translational). (Pool, 2005; Shao & Hegde, 2011). These processes are important for delivering proteins to three main organelles: peroxisomes, mitochondria, and the endoplasmic reticulum (ER).

Mitochondria – Origin, structure, and function

Of these organelles, mitochondria are essential, ubiquitous, semi-autonomous and multifunctional. According to the endosymbiotic hypothesis, mitochondria were free living organisms (α-proteobacteria) that were engulfed by an archaeal cell in a single event over 1.5 billion years ago (Andersson et al., 2003; Cavalier-Smith, 2006; John & Whatley, 1975). Over time, the α-proteobacteria was fully incorporated into the host cell and became a permanent organelle that is now responsible for various cellular functions. This transition from an endosymbiotic organism to a permanent organelle led to many changes in the host cell. Among others, many genes from the endosymbiont got either lost or transferred to be encoded by the host nuclear genome. This required the evolution of protein import systems, that allowed the organelle the usage of proteins encoded by genes that had been previously transferred to the host genome (Dolezal et al., 2006; Schneider, 2020). As of now, 99% of mitochondrial proteins are nuclear encoded. In *S. cerevisiae* the proteins that are still encoded by the mitochondrial genome (mt DNA) includes seven respiratory chain subunits and one ribosomal subunit (Foury et al., 1998; Pfanner et al., 2019; Stenger et al., 2020).

Another unique feature of mitochondria is their enclosure by two membranes, which in-turn divides the organelle into four sub-compartments: the mitochondrial outer membrane (MOM), intermembrane space (IMS), inner mitochondrial membrane (IMM) and the matrix. The ability of the MOM to allow transport of metabolites is attributed to integral membrane proteins known as porins, that facilitate free movement of ions and small molecules. Consequently, the MOM does not establish a membrane potential (Kühlbrandt, 2015). The IMM forms a selective diffusion barrier for ions and small molecules, whose movement is facilitated by specific membrane transport proteins. The IMM harbors major components of the respiratory chain complex, essential for ATP production. The transport of protons by the respiratory complexes creates a membrane potential across the IMM (Kühlbrandt, 2015; Schneider, 2020; Zorova et al., 2018).

Apart from cellular energy production, mitochondria have other important functions. They are involved in synthesizing phospholipids, producing iron-sulfur clusters and heme, maintaining calcium balance, and triggering apoptosis and cell death (Osellame et al., 2012). Many dysfunctions in mitochondria have been associated with diseases and specially with several neurodegenerative disorders like Alzheimer's and Parkinson's disease (Nicolson, 2014)

Protein import into mitochondria

Overview of Import machineries

To effectively carry out their functions, mitochondria possess different sets of specialized enzymes and proteins. Most of these proteins are encoded in the nuclear genome and require translation by cytosolic ribosomes before being imported into mitochondria. The outer and inner mitochondrial membranes contain various protein complexes that facilitate the import and sorting of proteins synthesized in the cytosol.

The import pathways can be broadly grouped into five major categories, depending on the type of targeting signal and sub-mitochondrial localization. These are: 1) Presequence pathway; 2) Carrier pathway; 3) β-barrel pathway; 4) Mitochondria import

and assembly (MIA) pathway for Cysteine rich IMS proteins and 5) Import of α-helical outer-membrane proteins via MIM complex (Waizenegger et al., 2005; Wiedemann & Pfanner, 2017). A more detailed schematic overview is shown in Figure 1.1 (taken from Wiedemann & Pfanner, 2017).

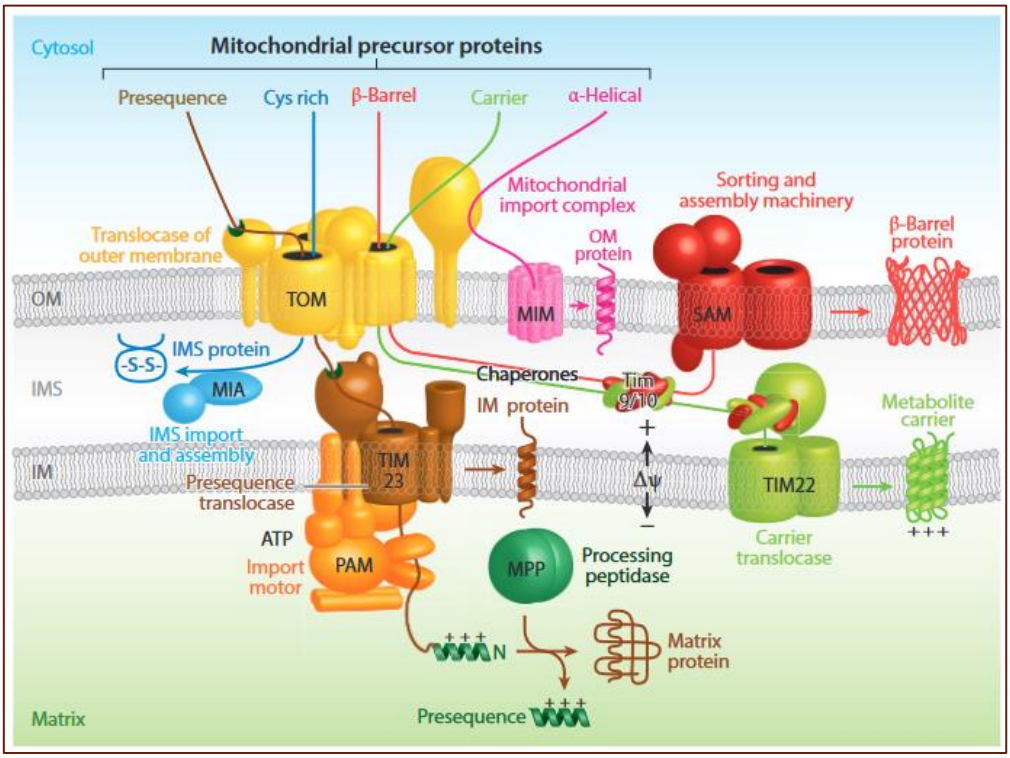

Figure 1.1: Protein import pathways of mitochondria. Precursor proteins carrying N-terminal presequences are recognized and imported via the translocase of the outer mitochondrial membrane (TOM) complex and further imported into the matrix by the translocase of the inner mitochondrial membrane (TIM23) complex. Inner membrane (IM) proteins with a hydrophobic transmembrane domain are released laterally into the IM, while hydrophilic matrix proteins are imported with the help of the presequence translocase-associated motor (PAM). The presequence of matrix proteins is removed by the mitochondrial processing peptidase (MPP). Cysteine-rich proteins in the intermembrane space (IMS) are imported by TOM and the import and assembly (MIA) system, which introduces disulfide bonds in the imported protein. β-barrel protein precursors move through TOM into the IMS where they interact with small TIM chaperones and are then inserted into the outer membrane (OM) by sorting and assembly machinery (SAM). IM metabolite carrier precursors are imported via TOM, small TIM chaperones, and TIM22 complex. Some α-helical OM proteins are integrated into the OM by the mitochondrial import (MIM) complex. The membrane potential across the IM drives translocation by TIM23 and TIM22. This figure taken from (Wiedemann & Pfanner, 2017)

Overall, the mitochondrial protein import pathways consist of eight important multiprotein machineries (Figure 1.1): 1) The translocase of outer membrane (TOM) machinery; 2) The sorting and assemble machinery (SAM); 3) Mitochondrial IMS import and assembly (MIA); 4) The mitochondrial import machinery; 5) Presequence translocase of inner membrane 23 (TIM23); 6) The Presequence- associated motor (PAM); 7) Carrier translocase of inner membrane 22 (TIM22) and 8) The Oxa1 complex. (Chacinska et al., 2009; Haastrup et al., 2023; Wiedemann & Pfanner, 2017)

The TOM complex is considered as the crucial and most important machinery since it serves as the initial point of recognition for the majority of nuclear-encoded mitochondrial proteins, facilitating their entry into the intermembrane space (Rapaport, 2005; Rapaport et al., 1997). Following this step, these proteins utilize various other pathways, dependent on their targeting signal, to reach their ultimate destinations (Chacinska et al., 2009; Haastrup et al., 2023).

The TOM complex consists of seven subunits. The main receptor proteins Tom20 and Tom70 (and its paralogue, Tom71 to a lesser extent) first recognize the approaching newly synthesized proteins (Chacinska et al., 2009). Tom70 functions as a major receptor for precursor proteins that are accompanied by cytosolic chaperones and containing internal targeting signals (Backes et al., 2021; Fan & Young, 2011). Proteins carrying an N-terminal presequence are mainly recognized by Tom20 (Chacinska et al., 2009; Sayyed & Mahalakshmi, 2022). However, all the three receptors have partially overlapping functions. After initial recognition by Tom20 and/or Tom70/71, precursor proteins are relayed to the central receptor Tom22. Then, with the help of Tom5 the precursor proteins are transferred to Tom40 (Neupert, 2015; Rapaport, 2005; Wiedemann & Pfanner, 2017). Tom22 is also very important for the integrity of the TOM complex, two Tom22 subunits holds together the Tom40 dimer and the small Toms that are associated with it (Nussberger et al., 2024). The β -barrel protein Tom40 is composed of 19 antiparallel β-strands that together form channel which contains hydrophobic and hydrophilic regions that transport different classes of precursor proteins (Gupta & Becker, 2021; Zeth, 2010).

The components of the TOM complex, Tom40, Tom7, and the IMS domain of Tom22 facilitate the transfer of presequence containing proteins to the TIM23 complex. For transporting precursors of carrier, IMS and β-barrel proteins, once these proteins exit the TOM channel, specific chaperones direct these precursor proteins to their respective sub-mitochondrial destinations (Genge & Mokranjac, 2022; Gupta & Becker, 2021; Neupert, 2015; Rapaport, 2003, 2005; Wiedemann & Pfanner, 2017)

Proteins harboring cleavable matrix-targeting presequence are translocated across the inner membrane to the matrix by the TIM23 complex. The TIM23 complex also transiently couples with the respiratory chain complexes and exhibits a membrane potential driven import step (Demishtein-Zohary & Azem, 2017; Genge & Mokranjac, 2022). This translocation also requires the function of the presequence translocase-associated motor (PAM) (Herrmann & Bykov, 2023; Li et al., 2004). Once the cleavable presequence reaches the matrix, the mitochondrial processing peptidase (MPP) cleaves the presequence (Gakh et al., 2002). Many precursor proteins contain also a hydrophobic α-helix located directly after the matrix-targeting sequence. Such precursor proteins follow the so-called "stop-transfer" route, in which after the presequence cleavage by MPP, they are laterally released into the lipid phase of the inner mitochondrial membrane (Chacinska et al., 2009). For some IMS proteins, this hydrophobic sorting signal is cleaved off by inner mitochondrial peptidase (IMP) (Herrmann & Bykov, 2023; Kunová et al., 2022; Pfanner et al., 2019). Carrier proteins of the inner membrane interact upon their exit from the TOM complex with the small Tim9/10 chaperones in the IMS which are then guiding them to the TIM22 complex (Sirrenberg et al., 1998).

Proteins destined to the IMS that are cysteine rich are imported into the IMS via the TOM complex and their correct folding in the IMS is ensured by the mitochondrial intermembrane space import and assembly (MIA) (Stojanovski et al., 2008).

For the sorting of outer membrane proteins, the TOM and SAM complexes are responsible to incorporate β-barrel proteins into the outer membrane (Herrmann &

Bykov, 2023; Jores et al., 2018). The integration of α-helical proteins is mostly dependent on the MIM machinery (Doan et al., 2020; Vitali et al., 2020). Two biogenesis pathways that do not involve the TOM complex are: the insertion of mitochondrially encoded proteins (components of the respiratory chain) by the OXA1 complex into the inner membrane (Stuart, 2002), and the spontaneous integration of certain tail-anchored proteins like Fis1 into the outer membrane (Kemper et al., 2008; Krumpe et al., 2012; Vitali et al., 2020).

Sorting of single-span α-helical mitochondrial outer membrane proteins

Mitochondrial outer membrane single-span proteins traverse the membrane once using a single hydrophobic α-helix structure and can be categorized into three subclasses based on their topology. These subclasses are: 1) Signal-anchored proteins that are anchored into the outer membrane through an N-terminal transmembrane segment (TMS), while a large soluble domain is exposed to either the cytosol or the intermembrane space; 2) Tail-anchored (TA) proteins, which are embed into the outer membrane with their transmembrane domain at the very C-terminus exposing a large soluble domain to the cytosol.; and 3) Proteins with large soluble domains exposed to both the cytosol and the IMS, and a transmembrane domain in the middle of the protein (Becker et al., 2012; Drwesh & Rapaport, 2020; Dukanovic & Rapaport, 2011).

Unlike proteins targeted to the matrix, which have a typical N-terminal cleavable presequence, the targeting signals for mitochondrial outer membrane proteins are located at their termini or within their internal structure (Rapaport, 2003). The import of signal anchored α-helical proteins does not follow a single import pathway but rather depends on a multitude of factors (Chacinska et al., 2009; Drwesh & Rapaport, 2020; Rapaport, 2003). While many signals anchored proteins like Tom20 and Tom70 rely on the MIM complex (an insertase on the outer membrane which comprises of Mim1 and Mim2) for their import (Ahting et al., 2005; Mnaimneh et al., 2004; Vitali et al., 2020), some proteins like Om45 requires the initial recognition by the receptors of the TOM complex, involvement of the TIM23 complex and final insertion by the MIM complex (Drwesh & Rapaport, 2020; Song et al., 2014). Other proteins like Mcr1 and

Fis1 can integrate to the outer membrane without the assistance of any import complexes (Dukanovic & Rapaport, 2011; Gupta & Becker, 2021).

Tail-anchored (TA) proteins

Tail-anchored (TA) proteins are type II-orientated membrane proteins and constitute ~3–5% of all cellular membrane proteins. They perform a range of essential functions ranging from apoptosis, membrane fission, and membrane biogenesis to protein translocation and enzyme catalysis, and are present on the membranes of various organelles like- ER, mitochondria, peroxisomes and Golgi (Borgese & Fasana, 2011; Hegde & Keenan, 2011). Of note, the TMD of TA proteins emerges out of the ribosome only after the termination of translation. Hence all TA proteins are targeted by post-translational pathways where dedicated targeting factors and/or chaperones recognize the hydrophobic TMD and shield it from the aqueous cytosol. These factors are also involved to a various extent in delivering the TA proteins to their destined organelle (Borgese et al., 2003; Mehlhorn et al., 2021)

Biogenesis of tail-anchored proteins

TA protein import into ER

Those IMPs targeted that are to the ER membrane and bear an N-terminal hydrophobic signal peptide are initially recognized by the by the signal recognition pathway (SRP) at the ribosome exit tunnel, while the nascent chain is still associated with the ribosome. The SRP then delivers the ribosome-bound chain to the Sec61 translocon and the integration into the endoplasmic reticulum membrane occurs co-translationally (Hann & Walter, 1991; Pool, 2005; Shao & Hegde, 2011). Tail-anchored (TA) proteins pose an exception to the SRP mediated targeting since the TMD cannot be recognized by the SRP (Rabu et al., 2009)

The GET pathway

A classic mechanism involved in post-translational insertion of TA proteins to the ER membrane is by the Guided Entry of Tail-anchored (GET) pathway which was originally described in yeast. This pathway is sometimes called in mammalian cells as

transmembrane domain recognition complex (TRC) pathway (Borgese et al., 2019; Farkas & Bohnsack, 2021; Schuldiner et al., 2008; Stefanovic & Hegde, 2007). As part of the GET pathway, the pre-targeting complex responsible for substrate recognition comprises of Sgt2, Get4, and Get5. Get5 was first recognized in a high-throughput screen for ribosome-associated proteins. Furthermore, high affinity interaction between Get4/Get5 and ribosomes, supported the fact that the pre-targeting complex is positioned on the ribosomes to safeguard emerging TA proteins (Chartron et al., 2012; Schuldiner et al., 2008). The co-chaperone Sgt2 binds to the transmembrane of the ER destined TA protein with its C-terminus, while the N-terminus binds to the ubiquitin-like domain of Get5 (Chartron et al., 2011). Get3 is then recruited by Get4 and by engaging with the ATP-bound Get3, Get4 maintains the chaperone in an open configuration, ready to receive the TA protein (Denic et al., 2013). Overall, the pre-targeting complex increases the concentration of Get3 near the TA proteins and also makes it more receptive (Denic et al., 2013).

The transfer of the TA protein from Sgt2 to Get3 occurs directly, not involving a soluble phase (Borgese et al., 2019; Wang et al., 2010). Once Get3 interacts with its substrate (TA protein), it causes a conformational change that induces its ATPase activity which results in the disassociation of Get3 from the Get4/Get5 complex (Rome et al., 2013; Schuldiner et al., 2008). Then, the Get3-TA protein complex interacts with Get1/Get2 on the ER membrane. The ADP-Get3-TA protein first interacts with the cytosolic domain of Get2 and its subsequent interaction with Get1 releases the ADP, further changing the conformation of Get3 and allows the release of the substrate to the lipid bilayer (Mariappan et al., 2011). Get3 is then recycled back to the cytosol where it binds another ATP molecule and interacts with the Get4/Get5 complex for another round of targeting TA proteins to the ER membrane (Mariappan et al., 2011; Wang et al., 2011).

Involvement of Hsp70

The process of how the newly synthesized TA protein is captured by Sgt2 has remained a puzzle until it was discovered that the tetratricopeptide repeat (TPR) domain of Sgt2 binds several chaperones including Hsp70 (Lin et al., 2021). Furthermore, it was found

that the chaperone Hsp70 (Ssa1 in yeast) is much more efficient in chaperoning the TA proteins and protecting them from aggregation than Sgt2 alone (Cho et al., 2021; Cho & Shan, 2018). Fluorescence and site-specific crosslinking assays observed interaction of Hsp70 with the Sgt2 TPR domain, which was essential for efficient transfer of TA substrates from Ssa1 to Sgt2 (Cho et al., 2021).

Import of TA protein (Fis1 and Gem1) into mitochondria and peroxisomes

The mitochondrial outer membrane harbours several tail anchored proteins. Among those are synaptojanin-binding protein Omp25 (Nemoto & De Camilli, 1999), small TOMs (Tom5, Tom6, Tom7) (Setoguchi et al., 2006), mitochondrial fission protein – Fis1 (Shaw & Nunnari, 2002), the apoptosis regulatory proteins such as Bak, Bcl-XL and Mcl-1 (Cory & Adams, 2002). However, the mechanisms of their selective targeting to the MOM is widely unknown (Chio et al., 2017).

The targeting of TA proteins to mitochondria is still ambiguous since they do not share any sequence conservation in the tail region (Kemper et al., 2008). A combination of physiochemical properties in the tail region, such as hydrophobicity and net charge is a driving force that determines the correct segregation of these proteins to its destined organelle (Chio et al., 2017; Rapaport, 2003). Accordingly, it was shown that the transmembrane segment (TMS) of Fis1 was sufficient for targeting the protein to mitochondria (Kemper et al., 2008). However, the mechanism involved in the correct targeting of TA proteins, especially for Fis1 and Gem1 that are dually targeted to mitochondria and peroxisomes is still widely unknown.

Surprisingly, removal or mutation of MOM import components did not have a drastic effect of TA protein import (Kemper et al., 2008). In line with these findings, Setoguchi and co-workers show that TA proteins can insert into the mammalian MOM in a TOM independent manner (Setoguchi et al., 2006).

In vitro import experiments show a partial and variable defect in the import of TA proteins Fis1 and Gem1 into the MOM of *mim1*Δ cells (Doan et al., 2020; Vitali et al., 2020). The biogenesis Gem1 is also compromised by the absence of Tom20, which

suggests that it is recognized by Tom20 on the surface of mitochondria and inserted into the outer membrane by the MIM complex (Vitali et al., 2020). Moreover, other reports suggested that the lipid composition of the MOM is a crucial factor for the specific insertion of Fis1, as it is also able to integrate in an unassisted manner into lipid vesicles with very low ergosterol content (Krumpe et al., 2012).

Surprisingly, the cytosolic chaperone Pex19 shows an involvement in targeting dually localized TA proteins like Fis1 and Gem1 to both mitochondria and peroxisomes (Cichocki et al., 2018). Initially, Pex19 was known for its role in stabilizing newly synthesized peroxisomal membrane proteins in the cytosol and facilitating their integration into the peroxisomal membrane by interacting with the membrane receptor Pex3 (Chen et al., 2014; Fujiki et al., 2006). Further studies suggested that along with Pex19, the cytosolic chaperones Hsp70 (Ssa1) and its co-chaperone Sti1 also facilitates the mitochondrial import of the tail-anchored proteins Fis1 and Gem1 (Cichocki et al., 2018; Jansen & van der Klei, 2019). The dual targeting of Fis1 and Gem1 to the outer membrane of mitochondria and peroxisomes explains their reliance on the common cytosolic chaperone Pex19. While Pex3 was identified as the receptor of Pex19 on the peroxisomal surface (Fang et al., 2004), it is still unknown whether Pex19 is recognized by a dedicated receptor on the mitochondrial surface.

Although studies suggest that differences in membrane composition between organelles are sufficient to determine correct localization, and despite the known role of Pex19 in the biogenesis of Fis1 and Gem1 to both mitochondria and peroxisomes, the regulation of this dual distribution remains puzzling. It is still unclear what factors dictate and regulate the targeting of these tail-anchored proteins to both mitochondria and peroxisomes.

Overview of Chapters in the thesis

This thesis comprises several chapters, each focusing on different aspects of the research conducted on protein distribution, sterol biosynthesis, and organelle separation. The results described in chapters 2-4 are included in three individual manuscripts.

Chapter 1 presents a brief overview on the biogenesis of mitochondrial proteins.

Chapter 2 provides detailed information on the main research conducted as part of the thesis. The research focuses on identification of Mpf1 as a novel factor influencing the dual distribution of tail-anchored (TA) proteins between mitochondria and peroxisomes. This chapter describes the research objectives, methodologies, and key findings on how the absence of Mpf1 and Tom71 affects the localization of the TA proteins Fis1 and Gem1 to mitochondria and peroxisomes. The research also indicates the unique role of Tom71, and further characterizes Mpf1 in terms of its stability and association with the mitochondrial outer membrane.

Chapter 3 provides a short overview of my role in a project conducted in collaboration with the lab of Prof. Maya Schuldiner. This chapter describes molecular mechanism of on-demand sterol biosynthesis at ER contact sites and discusses my contribution to this study. It provides background information on sterol biosynthesis, the experimental techniques used, and the findings on Yet3's role in forming high molecular weight complexes at such contact sites.

Chapter 4 introduces a modified technique for separating yeast peroxisomes from mitochondria, that was developed as a part of this thesis. This chapter outlines the importance for the new procedure, detailed methodology including the growth conditions, preparation of yeast spheroplasts, and the use of a discontinuous gradient for organelle separation. It also discusses the improved purity of organelles achieved with this technique and its application for studying dually targeted proteins.

Chapter 2

This chapter consists of sections adapted from the following manuscript submitted to *Review Commons*:

Mpf1 is a novel factor that affects the dual distribution of tail-anchored proteins between mitochondria and peroxisomes

Nitya Aravindan[1], Daniela G. Vitali[1], Jessica Oberst[1], Einat Zalckvar[2,3], Maya Schuldiner[2], Doron Rapaport[1, *]

1. Interfaculty Institute of Biochemistry, University of Tübingen, Tübingen, Germany

2. Department of Molecular Genetics, Weizmann Institute of Science, Rehovot, Israel

3. Current address: Bar-Ilan University, Ramat-Gan, Israel

bioRxiv. https://doi.org/10.1101/2024.04.30.591829

Author contributions

N.A., D.G.V., designed and conducted experiments, J.O. performed experiments; E.Z., M.S., and D.R. designed experiments and analyzed data, N.A. and D. R. wrote the initial version of the manuscript. All authors read and contributed to the final manuscript.

Research Objectives

Most cellular proteins are synthesized in the cytosol and must be targeted to their specific cellular compartments to function. Extensive research led to major progress in understanding protein targeting to individual organelles, however, little is known about how proteins are distributed to two or more organelles.

In this study, our broad aim is to gain a better understanding of how tail-anchored (TA) proteins – Fis1 and Gem1 are dually targeted in yeast cells to both mitochondria and peroxisomes.

Previous studies have shown the involvement of proteins like Pex19 and the MIM complex in targeting Fis1 and Gem1. In addition, the hydrophobicity of the transmembrane domain and the presence of charged residues in its flanking regions as well as the composition of target membranes were suggested to influence this process. However, the regulation of the distribution of these dually localized proteins remains unclear.

To understand the dual targeting process, these specific open questions are addressed in this study:

1) What factors influence the dual distribution of TA proteins Fis1 and Gem1 between mitochondria and peroxisomes?
2) How does the absence/overexpression of the identified factors (Tom70, Tom71 and Mpf1) affect the dual distribution of Fis1?
3) Does Tom71, the barely expressed paralog of Tom70 play a unique role in regulating Fis1 distribution?
4) What is the role of the uncharacterized gene *YNL144C* (renamed Mpf1) in the dual targeting process? What is the subcellular localization of Mpf1, and which factors are essential for its biogenesis?

Introduction

Eukaryotic cells have evolved complex machineries that direct cytosolically synthesized proteins to their specific intracellular location. Most proteins are directed to a specific organelle using targeting signals. However, some proteins are destined to two (or even more) cellular destinations through a process called dual/multiple targeting. For instance, metabolic enzymes like fumarase and aconitase are found not only in mitochondria but also in the cytosol or nucleus. Additionally, different forms of Mcr1 are localized to distinct compartments within the same organelle (Haucke et al., 1997; Regev-Rudzki & Pines, 2007; Stein et al., 1994; Yogev et al., 2011).

Mitochondria and peroxisomes share several proteins that are dually targeted to their membranes. These organelles engage in extensive crosstalk and form multiple transient contact sites. In high-throughput screening studies showed peroxisomes were associated in close proximity to mitochondria at sites enriched in pyruvate dehydrogenase (PDH) complex responsible for acetyl-CoA synthesis in the mitochondrial matrix. This indicated that the spatial positioning of these organelles are strategic to support the necessary metabolic processes (Cohen & Schuldiner, 2011; Mattiazzi Ušaj et al., 2015; Shai et al., 2016).

One of the proteins involved in mediating these contact sites is Pex11, a key protein involved in initiating peroxisome division, which interacts with Mdm34, a constituent of the ER-mitochondria encounter structure (ERMES) (Mattiazzi Ušaj et al., 2015; Shai et al., 2016). Furthermore, a high-content microscopy identified two peroxisome-mitochondria (PerMit) tethers which involve the MOM mitofusin protein– Fzo1 or the peroxisomal membrane protein Pex34 (Shai et al., 2018). It was observed that PerMit contacts, were enhanced when Fzo1 was overexpressed (Alsayyah et al., 2024). Additionally, Pex34 was not found to be uniformly distributed on the peroxisomal surface, but rather in distinct niches that colocalized with the PerMit signal (Shai et al., 2018). However, the mitochondrial binding partner of Pex34 and the peroxisomal binding partner of Fzo1 remains to be found (Figure 2.1).

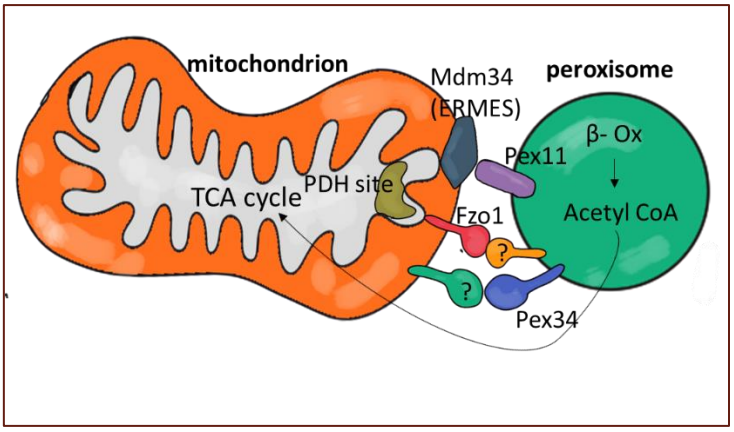

Figure 2.1: Contact sites between mitochondrial and peroxisomal membranes. Beta-oxidation of fatty acids in yeast occurs solely in peroxisomes. The by-product of beta-oxidation, Acetyl CoA is transferred to the mitochondria for the TCA cycle. Peroxisomes were found to concentrate in proximity to mitochondrial sites rich in pyruvate dehydrogenase (PDH). The organelles are co-dependent for their metabolic processes and share multiple contact sites. Pex11 on the peroxisomal membrane tethers with Mdm34 on the mitochondrial outer membrane (MOM). Pex34 interacts with an unknown receptor on the MOM, while Fzo1 interacts with an unidentified receptor on the peroxisomal membrane.

Besides their close physical and metabolic connections, mitochondria and peroxisomes also share several outer membrane proteins and the fission machinery used for their division (Figure 2.2).

A key element of this fission machinery is Fis1, a TA protein that can be targeted to both mitochondrial and peroxisomal membranes in yeast, plants, and mammalian cells (Koch et al., 2005; Kuravi et al., 2006; M. Schrader et al., 2016). Fis1 recruits the adapter protein Mdv1 to the site of fission, in both mitochondria and peroxisomes. Fis1-Mdv1 complex then recruits dimers of the dynamin-like protein Dnm1 to the site to complete the final fission step (Bleazard et al., 1999; Mozdy et al., 2000; Shaw & Nunnari, 2002; Yoon et al., 2003) (Figure 2.2).

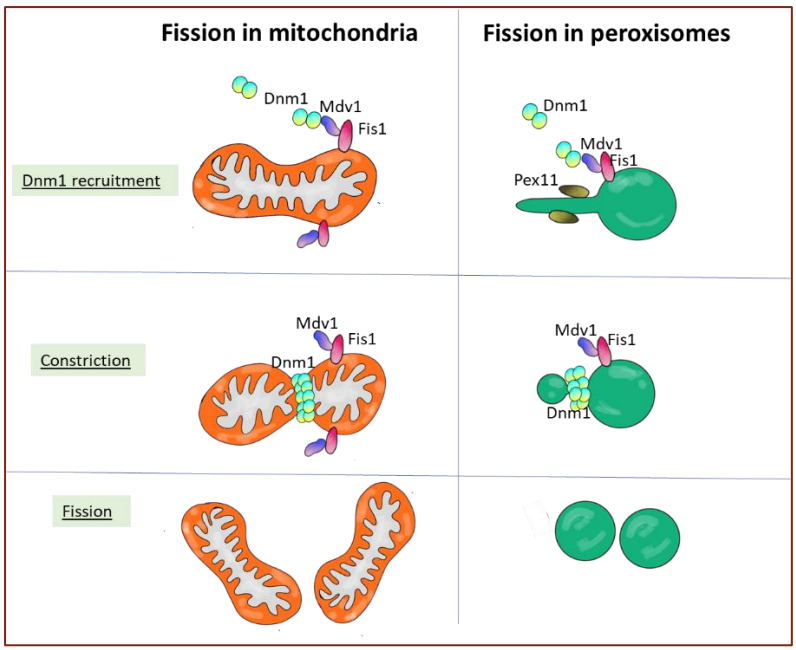

Figure 2.2: Fission in mitochondria and peroxisomes. Fission in yeast mitochondria is facilitated by the OM protein Fis1, which via the adaptor protein Mdv1 recruits the GTPase Dnm1 to the site of fission. In peroxisomes, the process starts with elongation of peroxisomes by Pex11 and recruitment of Dnm1 to the site of fission via Fis1 and Mdv1. Dnm1 constricts the organelles and facilitates the fission.

Interestingly, mammalian homologues of these fission components are also found in both mitochondria and peroxisomes. Defects in the fission of these organelles have been linked to several pathophysiological conditions, making it crucial to understand the biogenesis of the proteins involved in these processes (Ong et al., 2013; Schrader et al., 2022). Apart from Fis1, other examples for proteins dually localized to both mitochondria and peroxisomes are the tail-anchored protein Gem1 (MIRO1 in mammals) and the quality control protein AAA-ATPase Msp1 (ATAD1 in mammals)(Costello et al., 2017; Okreglak & Walter, 2014).

Over the years, a clear understanding of the targeting of TA proteins to the secretory pathway has been established (Schuldiner et al., 2008; Stefanovic & Hegde, 2007), however, the precise mechanism for the accurate targeting of TA proteins to mitochondria remains widely unknown. Previous studies have shown that the targeting information is encoded in part by the physio-chemical properties of the tail region (Rao et al., 2016). A combination of transmembrane domain (TMD) hydrophobicity along with the number of charged residues in the C-terminal segment, is crucial for the accurate targeting of TA proteins (Bittner et al., 2022a; Borgese et al., 2007; Chio et al., 2017; Costello et al., 2017). On average, TMDs of ER TA proteins have higher hydrophobicity compared to mitochondrial and/or peroxisomal ones (Rao et al., 2016).

When Fis1 TMD residues were replaced by more hydrophobic residues, the protein was mistargeted to the ER (Beilharz et al., 2003). Additionally, the TA region of Fis1 is characterized by an enrichment of basic residues immediately following the TMD at the C-terminal end and mutating these residues abolished mitochondrial targeting of Fis1. Furthermore, moderately hydrophobic TMDs combined with the presence of basic residues direct TA proteins also to the peroxisome and how shared mitochondrial and peroxisomal TA proteins (Fis1 and Gem1) are distinguished is still unclear (Chen et al., 2014; Chio et al., 2017).

Some studies have shown that the biogenesis of the TA proteins Fis1 and Gem1 is facilitated by the mitochondrial import (MIM) (Doan et al., 2020), while other studies have also reported that the insertion of Fis1 depends on the lipid composition of the MOM and that Fis1 can insert into lipid vesicles in an unassisted manner (Kemper et al., 2008; Krumpe et al., 2012; Vitali et al., 2020).

In contrast, membrane targeting of for peroxisomal TA proteins is mediated by Pex19 and Pex3 (Fujiki et al., 2006). Pex19 is important for the biogenesis of peroxisomal proteins with a peroxisomal membrane targeting signal (mPTS). Such proteins are identified by Pex19 in the cytoplasm and delivered to the peroxisomal membrane through an interaction with the membrane receptor Pex3 (Chen et al., 2014; Götte et al., 1998). Surprisingly, depletion of *PEX19* led to a reduction in the steady state levels of Fis1 and Gem1 in mitochondrial fractions, pointing out an unexpected role of Pex19 in the biogenesis of mitochondrial TA proteins (Cichocki et al., 2018). Hence, despite some understanding of the biogenesis of Fis1 and Gem1 on the mitochondrial or peroxisomal membranes, the regulation of the distribution of these dually localized proteins remains quite puzzling.

To obtain new insights on the factors governing dual targeting of proteins to both mitochondria and peroxisomes, we employed a high-throughput microscopy screen with fluorescently labeled TA proteins. The identified hits were subsequently validated through subcellular fractionation assays to assess their impact on Fis1 distribution. We

found that the deletion of the uncharacterized gene *YNL144C* (re-named in this study as Mitochondrial and Peroxisomal Factor 1 (Mpf1)), as well as each of the paralogous proteins, *TOM70* and *TOM71* led to an enhanced localization of Fis1 to peroxisomes. Accordingly, overexpressing Tom71 caused Fis1 to localize more to mitochondria, suggesting a unique role for Tom71. We further characterized Mpf1 and identified it as an unstable protein, loosely associated with the mitochondrial outer membrane. We also observed that the biogenesis of Mpf1 is controlled by the presence of Tom70 and Tom71. Furthermore, mutations in the Pleckstrin homology (PH) domain of Mpf1 did not affect its localization to the MOM and displayed elevated steady state levels as well as a partial enhancement in its stability compared to its native counterpart. Altogether, our results suggest that Mpf1, Tom70, and Tom71 play a role in regulating the dual localization of Fis1 and Gem1 to both mitochondria and peroxisomes.

Materials and methods

The details of Materials and Methods related to Chapter 2 (including tables describing strains, primers, plasmids, and antibodies used in this study) can be found in the Appendix containing the pre-print:

"Mpf1 is a novel factor that affects the dual distribution of tail-anchored proteins between mitochondria and peroxisomes."

Results and discussion

This section contains an adapted and brief version of results and discussion from the pre-print:

"**Mpf1 is a novel factor that affects the dual distribution of tail-anchored proteins between mitochondria and peroxisomes."**

Nitya Aravindan, Daniela G. Vitali, Jessica Oberst, Einat Zalckvar, Maya Schuldiner and Doron Rapaport

The full version of results and discussion for Chapter 2 can be found in Appendix.

Author contributions

I (Nitya Aravindan) designed and conducted most experiments and contributed to most of the results in this manuscript. Daniela G. Vitali (D.G.V) designed and conducted the high-throughput microscopy screen in the lab of Maya Schuldiner and Einat Zalckvar (M.S and E.Z), and the images were analyzed and quantified by me. Jessica Oberst (J.O) performed some experiments to understand the role of Tom71 in the dual distribution of Fis1 and contributed to Figure 2.7 D, E and F.

Einat Zalckvar (E.Z.), Maya Schuldiner (M.S.), and Doron Rapaport (D.R.) designed experiments and analyzed data.

N.A. and D. R. wrote the initial version of the manuscript. All authors read and contributed to the final manuscript.

High-throughput screen reveals factors that influence the dual distribution of TA proteins

Some yeast TA proteins, such as Fis1 and Gem1, are found on both mitochondria and peroxisomes. To identify factors influencing their dual distribution, we employed a high-throughput microscopy screen. We generated strains expressing mCherry-tagged Fis1 or Gem1 alongside the peroxisomal marker Pex3-GFP or mitochondrial marker Om45-GFP. Then, using an automated procedure and synthetic genetic assay (SGA) (Cohen & Schuldiner, 2011), we integrated these two tagged proteins into a collection that included deletion strains for all non-essential yeast genes and depletion strains for all essential genes (Figure 2.3A). The new collection of yeast deletion/depletion strains expressing the mCherry tagged TA proteins Fis1/Gem1 along with Pex3-GFP/Om45-GFP were subjected to a high-throughput microscopy screen to identify those strains where the distribution of the TA proteins Fis1 and Gem1 between mitochondria and peroxisomes is altered (Figure 2.3A).

While many proteins altered the distribution of Fis1 between the two organelles, some changes seemed to be secondary effects due to defects in the biogenesis or morphology of the respective organelles. Hence, for a strain to be a real hit, it had to fulfil two phenotypes: (i) have normal biogenesis of peroxisomes (as reflected by the number of GFP puncta structures), and (ii) display normal mitochondrial morphology, as observed with the mCherry-Fis1/Om45-GFP. Considering these factors, we could identify many proteins that altered Fis1/Gem1 distribution (see Table S1 in the pre-print for the full list). Further manual examination highlighted the uncharacterized protein Ynl144c (renamed Mpf1) and the paralogous proteins Tom70 and Tom71. The absence of any of these three proteins increased mCherry-Fis1 co-localization with Pex3-GFP-stained peroxisomes compared to control cells (Figure 2.3B and C). When this phenotype was quantified, the co-localization of mCherry-Fis1 was with 20% of peroxisomes in the wild type (WT/control) cells and this number was considerably increased in cells lacking Mpf1 (31%), Tom70 (40%), or Tom71 (43%) (Figure 2.3C).

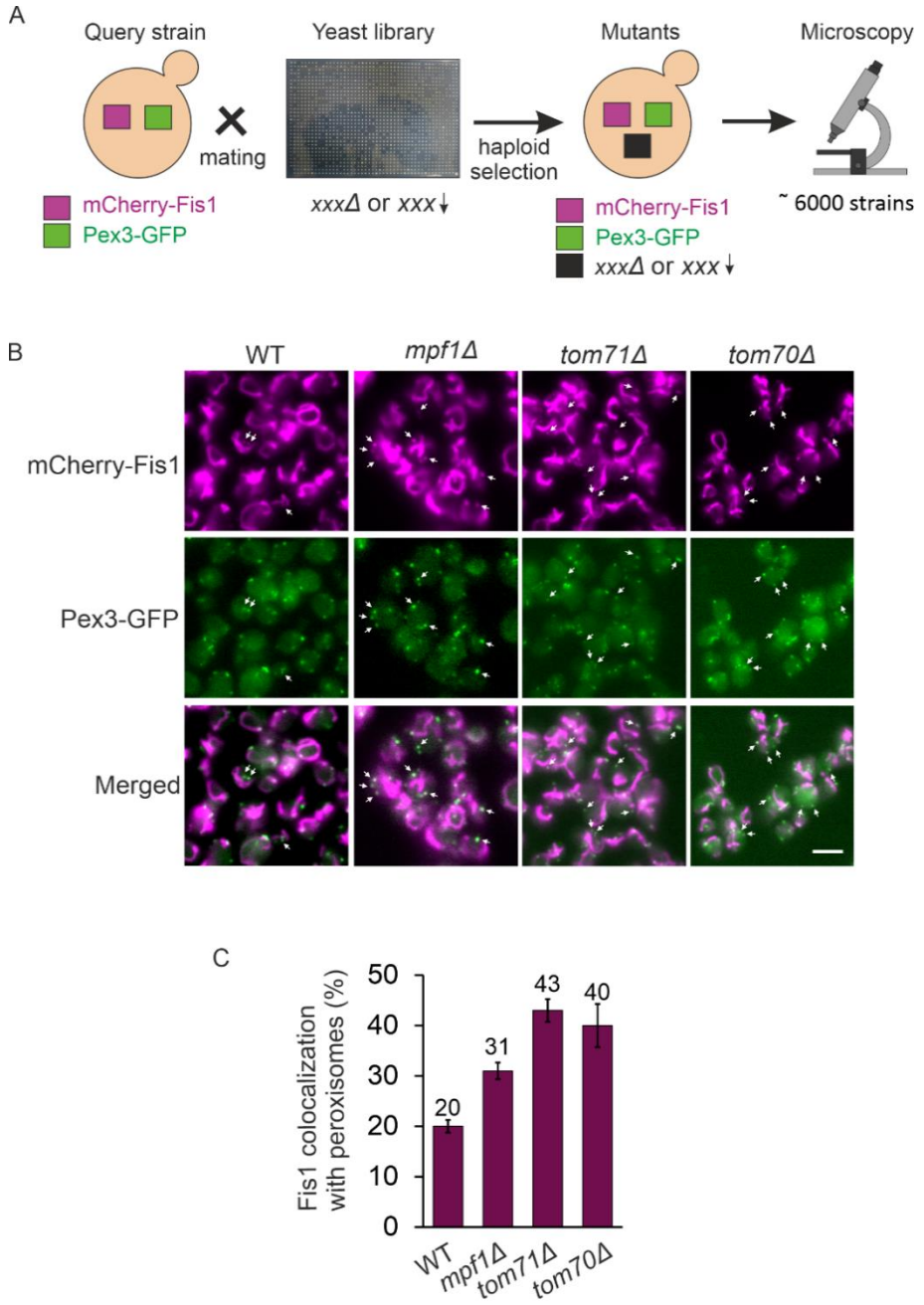

Figure 2.3: A high-throughput microscopy screen reveals proteins that affect dual distribution of Fis1. **(A)** Illustration of the screen aiming to find factors that affect dual targeting of Fis1. mCherry-Fis1 and Pex3-GFP were integrated into a yeast deletion and depletion libraries. The resultant strains, each containing a unique gene deletion/depletion and carrying the fluorescently labelled target proteins were visualized using automated microscopy. **(B)** Representative images of WT and three deletions strains with altered distribution of Fis1. The phenotype was observed by detecting co-localization of mCherry-Fis1 with Pex3-GFP (shown with white arrows). Scale bar, 5 µm. **(C)** Quantification of the co-localization of mCherry-Fis1 with peroxisomes. Total number of peroxisomes (visualized by Pex3-GFP) were counted in 100 cells in each of three independent experiments. Subsequently, the percentage of mCherry-Fis1 puncta co-localized with peroxisomes was determined. The graph represents the average of three independent experiments, error bars represent standard error.

We observed a similar phenotype with mCherry-Gem1, another dually localized TA protein. In the control strain *tim13*Δ, co-localization was 22% with Pex3-GFP and this was increased to 25% in *mpf1*Δ*,* 30% *in tom70*Δ and 34% in *tom71*Δ, indicating that the identified proteins have a general effect on dually distributed TA proteins (Figure 2.4A and B).

Furthermore, we observed that none of the identified proteins have a strong influence on the distribution of Fis1/Gem1, but rather a partial effect. Surprisingly, among the three hits, Tom71 (a lesser expressed paralog of Tom70) has a more dominant effect in altering the TA proteins' distribution, attributing a unique role that has not been identified previously.

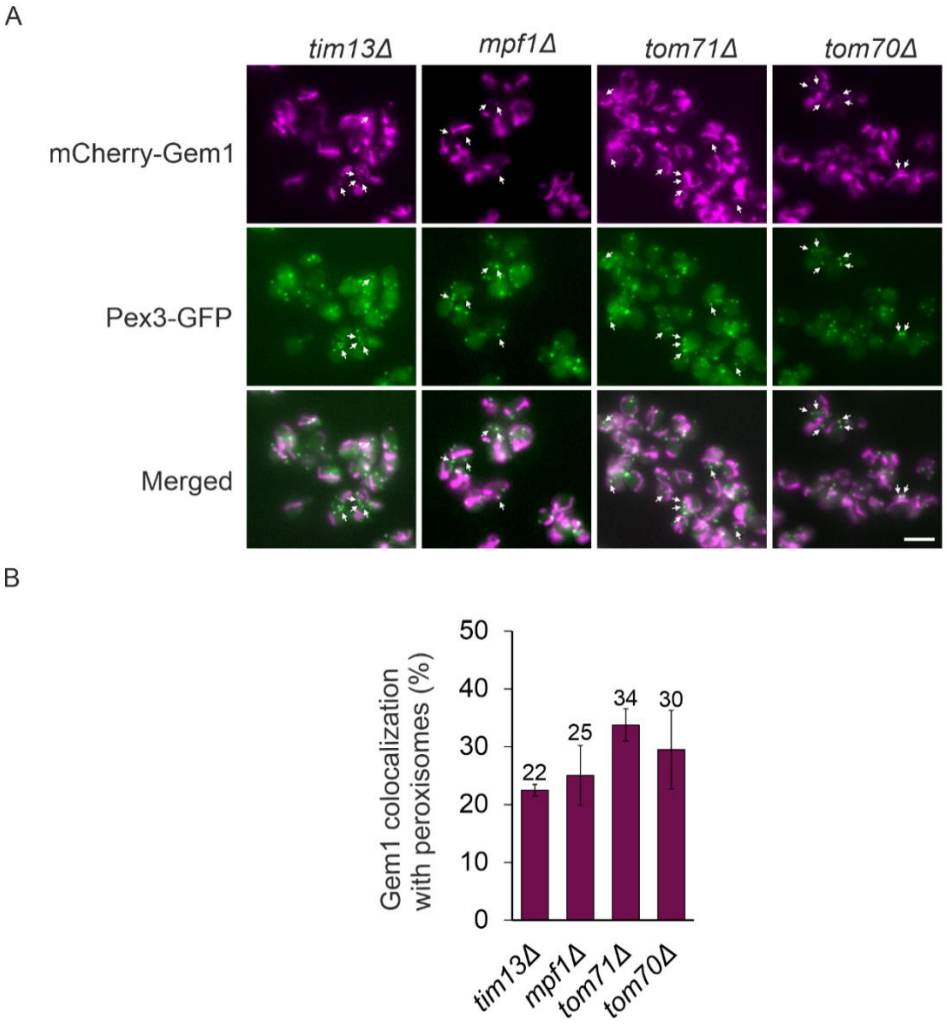

Figure 2.4: The hits influencing Fis1's distribution to mitochondria and peroxisomes also impact the dual distribution of another TA protein, Gem1. (A) Representative images of three strains (*mpf1Δ*, *tom71Δ*, and *tom70Δ*) with altered distribution of Gem1 between mitochondria and peroxisomes. The strains co-express mCherry-Gem1 and GFP-Pex3 (as peroxisomal marker). Note that these strains maintain normal mitochondrial morphology and peroxisome number. *tim13*Δ cells were used as control. Co-localization of mCherry-Gem1 (as magenta puncta, shown with white arrows) with Pex3-GFP (as green puncta, shown with white arrows) is indicated. Scale bar, 5 µm. **(B)** Quantification of the co-localization of Gem1 with peroxisomes. The percentage of co-localization of mCherry-Gem1 puncta with the peroxisomes was determined in 100 cells in three independent experiments. Error bars represent standard error. Subsequently, the percentage of co-localization of mCherry-Gem1 puncta with the peroxisomes was determined.

We further confirmed that these observations were not the result of fragmented mitochondria that were misinterpreted as peroxisomal puncta. We visualized mitochondrial morphology using Om45-GFP and found no alteration in mitochondrial morphology in *mpf1*Δ and *tom71*Δ cells compared to control cells (*tim13*Δ) (Figure 2.5). We noticed a slightly altered mitochondrial morphology in *tom70*Δ cells (Figure

2.5), which is not surprising since Tom70 plays a crucial role in the biogenesis of many outer membrane proteins (Backes et al., 2021; Kreimendahl & Rassow, 2020; Yamamoto et al., 2009; Young et al., 2003).

Altogether, the visual screen identified three potential novel factors: Mpf1, Tom70, and Tom71 that affect the dual distribution of TA proteins.

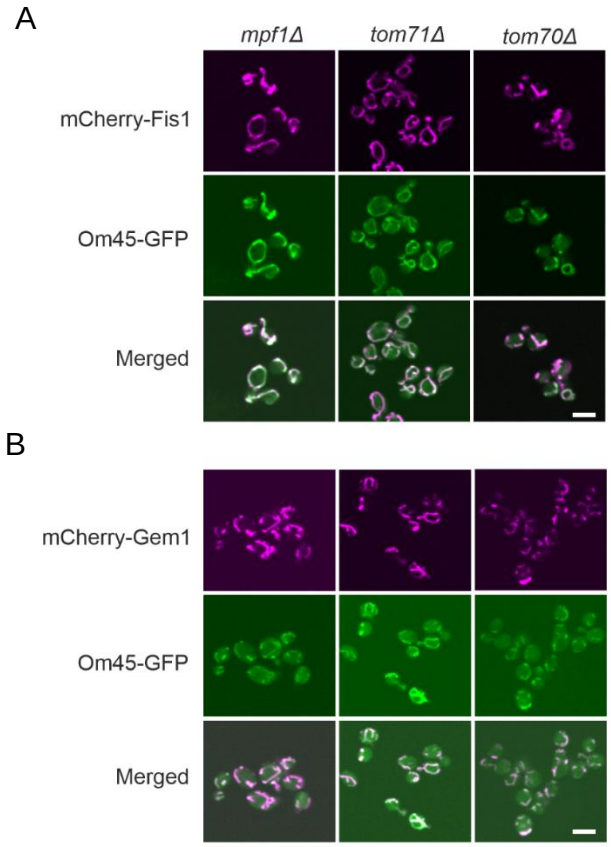

Figure 2.5: Regular mitochondrial morphology in *mpf1Δ*, *tom71Δ*, and *tom70Δ* cells. Mitochondrial morphology was visualized by imaging mCherry-Fis1 (top panel) and mCherry-Gem1 (bottom panel) in the indicated strains. Om45-GFP served as a marker for mitochondrial structures. Scale bar, 5 µm.

Fis1 and Gem1 distribute more towards peroxisomes in cells lacking Mpf1 and Tom71

To validate the aforementioned findings, we utilized subcellular fractionation assays to physically separate mitochondria from peroxisomes. Subsequently, we quantified the levels of both mitochondrial and peroxisomal Fis1 in cells lacking the identified factors. To obtain optimal separation, cells were grown on oleate to induce proliferation of peroxisomes. Using a Histodenz gradient and ultracentrifugation, a total of 12 fractions were collected from the gradient. Tom20, a mitochondrial marker, was enriched in the first four fractions (lanes 1-4), while the peroxisomal marker Pex14 was present in the last four (lanes 9-12). Thus, fractions that were enriched in either pure mitochondria or peroxisomes could be obtained and Fis1, being dually targeted, was found in both sets (Figure 2.6A).

To compare the distribution of Fis1 among the various strains, Fis1 levels in fractions 1-12 were quantified. The amount of Fis1 in fractions 1-4 were considered as mitochondrial Fis1 whereas the Fis1 population in fractions 9-12 was counted as peroxisomal. Using this approach, we found that in WT cells, 70% of Fis1 was present in the mitochondrial fraction and this portion decreased to 57% and 52% in *mpf1*Δ and *tom71*Δ cells, respectively (Figure 2.6). In these strains, alongside the decrease in mitochondrial Fis1, we observed an increase in its peroxisomal portion. While we found 23% of Fis1 in peroxisomes in WT cells, this fraction increased to 34% in *mpf1*Δ and 37% in *tom71*Δ (Figure 2.6). Surprisingly, in the double deletion *tom71*Δ*/mpf1*Δ cells, the distribution of Fis1 was comparable to WT cells (Figure 2.6). Since mitochondrial fission is crucial for maintaining healthy cells and the depletion of Fis1 leads to hyperfused mitochondria (Das & Chakrabarti, 2020; Hoppins et al., 2007), we speculate that *tom71*Δ*/mpf1*Δ leads to activation/upregulation of other factors to maintain correct distribution of Fis1 molecules.

Unfortunately, due to technical reasons, I could not obtain a separation of mitochondria and peroxisomes in an adequate quality in *tom70*Δ and *tom70*Δ*/tom71*Δ

cells. Hence, using this method we could not validate Tom70 as a factor that regulates the distribution of TA proteins.

Altogether, by physically separating mitochondria from peroxisomes, we could confirm the involvement (direct or indirect) of Mpf1 and Tom71 in regulating Fis1 dual distribution between mitochondria and peroxisomes.

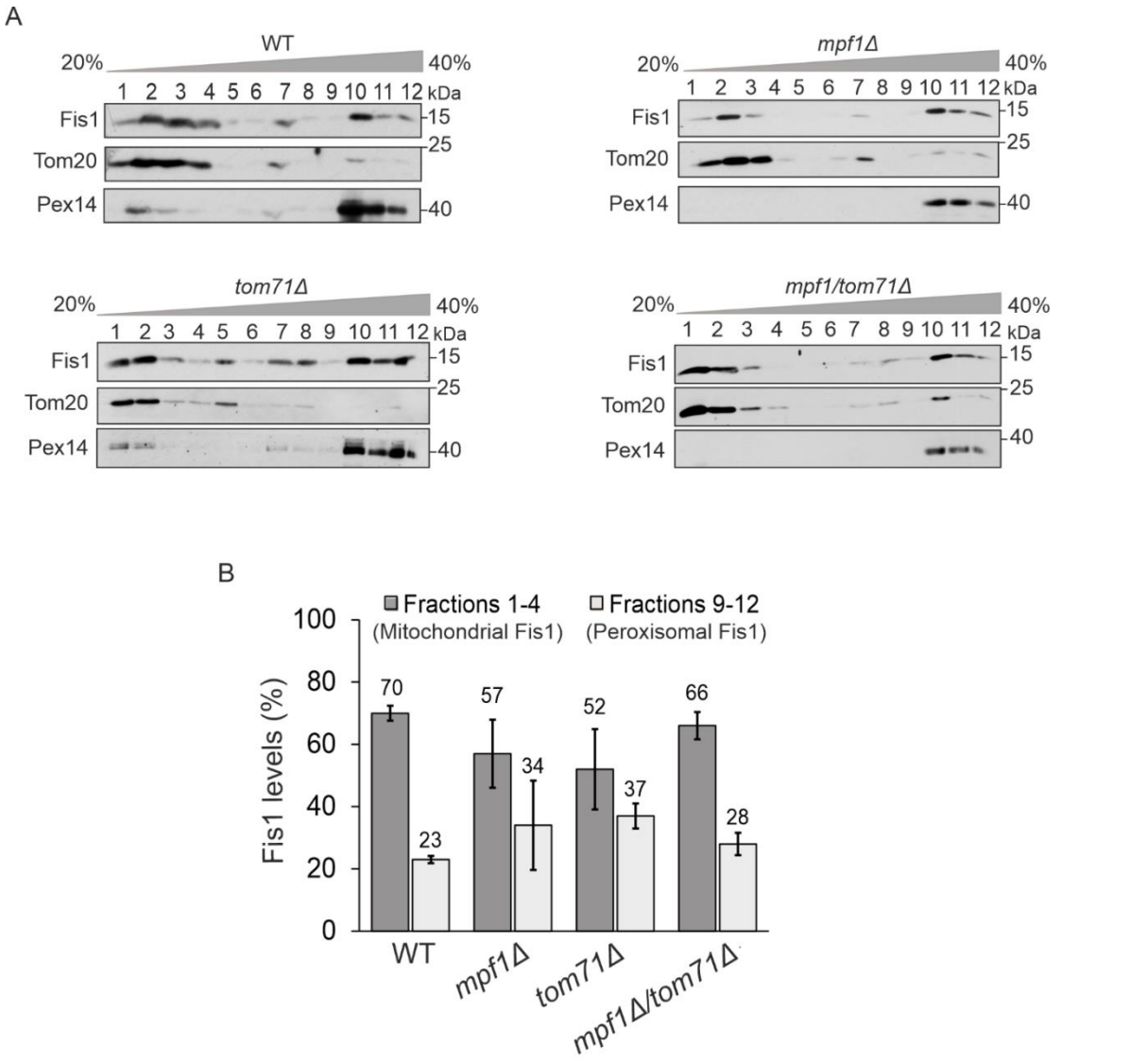

Figure 2.6: Physical separation of mitochondria and peroxisomes validates the hits. **(A)** Gradient centrifugation procedure was employed to separate mitochondria and peroxisomes from the indicated strains and 12 fractions from the top of the gradient were collected. The fractions were analyzed by SDS-PAGE and immunodecorated with antibodies against Fis1 (dually localized to mitochondria and peroxisomes), Tom20 (mitochondrial marker), and Pex14 (peroxisome marker). **(B)** The intensities of Fis1 obtained in each fraction was quantified and the sum of all the 12 intensities was set to 100%. Fis1 signal in fractions 1-4 was considered mitochondrial, while that within fractions 9-12 was designated as peroxisomal. The graph represents the average of three independent experiments, error bars representing standard error.

Tom71 has a unique role in Fis1 distribution, setting it apart from Tom70

Tom71 is a paralogue of Tom70, sharing with the latter 53% sequence identity and constituting only around 10% of Tom70 levels (Morgenstern et al., 2021; Schlossmann et al., 1996). Tom70 plays a crucial role as an import receptor and docking site for chaperones carrying newly synthesized mitochondrial proteins, and hence is required for the biogenesis of many mitochondrial proteins (Backes et al., 2021; Kreimendahl & Rassow, 2020; Yamamoto et al., 2009; Young et al., 2003). Tom71 was shown to compensate for the absence of Tom70 to some degree and Tom70 and Tom71 might have overlapping functions (Morgenstern et al., 2021; Schlossmann et al., 1996). However, a specialized role unique to Tom71 has not been found yet.

Our work might hint towards a unique role for Tom71, since its deletion caused change in the distribution of Fis1, even in the presence of Tom70 (Figure2.6 B).

To understand the involvement Tom70 and Tom71 in the dual distribution of Fis1, we created strains where each of the proteins was overexpressed. This was done by replacing the endogenous promoter with a strong *GPD* promoter in WT, *mpf1*Δ and *tom71*Δ cells (Figure 2.7A and D). We then quantified the mitochondrial and peroxisomal Fis1 in each of these strains (Figure 2.7B and C). We observed that increased levels of Tom70 led to normalization of Fis1 distribution in *mpf1*Δ cells, suggesting that the function of Mpf1 in regulating Fis1 distribution is dispensable in the presence of higher amounts of Tom70 (Figure 2.7B and C). Interestingly, elevated levels of Tom70 in *tom71*Δ cells led to only a partial correction of Fis1 distribution, indicating a unique and dominant role of Tom71 that cannot be replaced by elevated levels of Tom70 (Figure 2.7B and C).

Surprisingly, although we expected the overexpression of Tom70 in WT cells to drive Fis1 distribution more towards mitochondria, we observed a minor reduction in mitochondrial Fis1 (62%) and a slight increase in peroxisomal Fis1 (33%) (Figure 2.7B and C). This observation was unexpected since previous studies show that overexpression of Tom70 enhances the biogenesis of many mitochondrial proteins (Liu

et al., 2022). I propose that the targeting of Fis1 towards mitochondria might prefer Tom71 over Tom70 and over-crowding the mitochondrial surface with Tom70 and/or possibly engaging Tom71 in Tom71/Tom70 heterodimers creates a competing effect, thereby reducing Fis1 levels in mitochondria.

To further test if Tom71 had a unique role, we analyzed mitochondrial and peroxisomal Fis1 levels in the strains overexpressing Tom71 (Figure 2.7E and F). Interestingly, we observed that Tom71 overexpression in both WT and *mpf1*Δ cells led to an increased distribution of Fis1 towards mitochondria (Figure 2.7E and F). These findings substantiate the independent and unique contribution of Tom71 to the targeting of Fis1 to mitochondria, whose absence cannot be compensated by Tom70. Notably, the role of Mpf1 in regulating Fis1 distribution is dispensable upon overexpression of either Tom70 or Tom71. This observation suggests that Mpf1, Tom70, and Tom71 might share the same pathway regulating the distribution of Fis1 and further experiments could reveal if Mpf1 directly interacts with Tom70 and/or Tom71.

Previous studies have shown that the cytosolic chaperone/receptor Pex19 is important for the biogenesis of mitochondrial Fis1 (Cichocki et al., 2018). Since overexpression of Tom71 brought 81% of Fis1 towards mitochondria, we wondered whether Tom71 could function as a receptor for Pex19. To test this, we created a strain co-expressing Tom71-HA and Flag-Pex19 in *tom70*Δ cells. We used *tom70*Δ cells to prevent potential competition of Tom70 in binding to Pex19. However, using affinity purification method, we could not co-elute Flag-Pex19 with Tom71-HA (Figure 2.7G). Although we were unable to detect an interaction between Tom71 and Pex19, it is possible that these proteins interact only transiently, making it difficult to capture this association using the applied conditions.

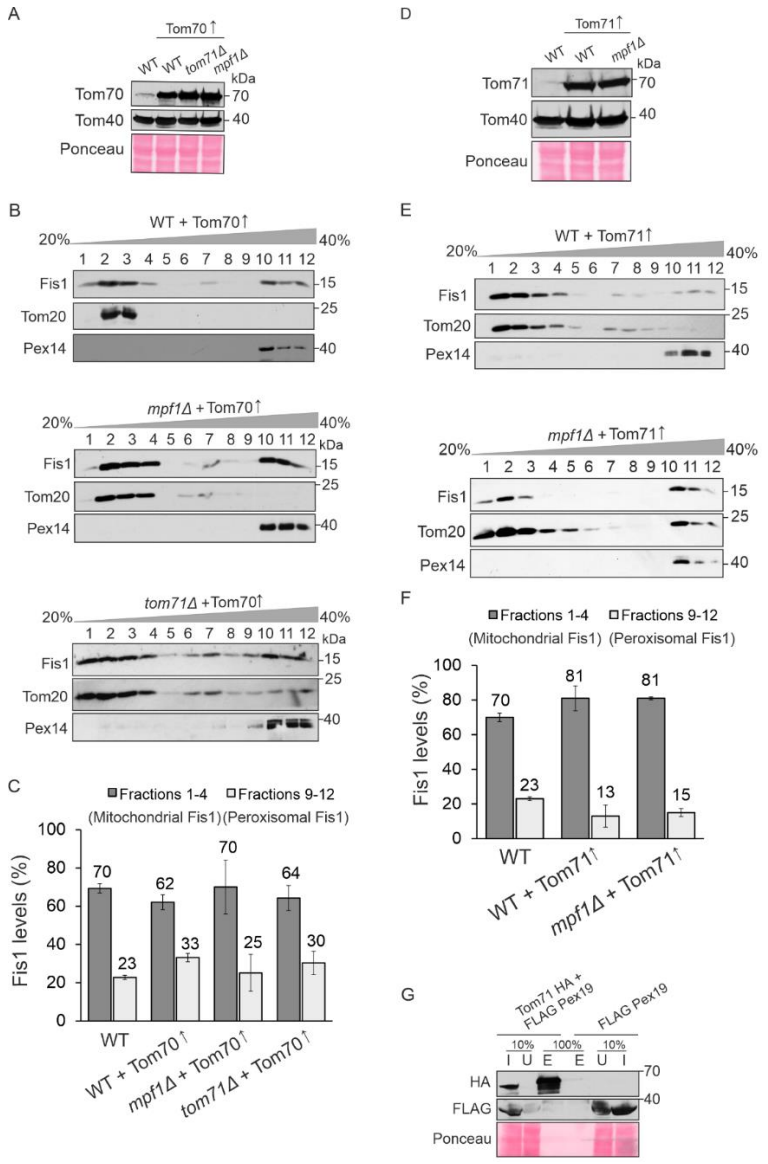

Figure 2.7: Tom71 has a unique effect on the distribution of Fis1. **(A)** Tom70 was overexpressed in the indicated strains by replacing the endogenous promoter with the *GPD* promoter. Cells of the resulting strains were grown on galactose and whole cell lysate was obtained by alkaline lysis. Extracted proteins were analyzed by SDS-PAGE and immunodecorated with the indicated antibodies. Ponceau staining was employed to verify equal loading in all lanes. **(B, C)** Gradient separation of mitochondria and peroxisomes from the indicated strains were performed as described in the legend to Fig. 2.6A and B. **(D)** Tom71 was overexpressed in the indicated strains by replacing the endogenous promoter with the *GPD* promoter. Proteins from the obtained strains were analyzed as described in part (A). **(E-F)** Gradient separation of mitochondria and peroxisomes from the indicated strains were performed as described in the legend to Fig. 2.6A and B. Note: to allow easier comparison, the Fis1 levels in WT cells in panels C and F were taken from Figure 2.6B. The graph represents the average of three independent experiments, error bars representing standard error. **(G)** Cells expressing either Flag-Pex19 alone or co-expressing Flag-Pex19 and Tom71-HA were lysed with Triton X-100 and the suspension was incubated with anti-HA beads. Fractions representing the input (I), unbound material (U), and the eluate (E) were analyzed by SDS-PAGE and immunodecorated with the indicated antibodies.

Characterizing Mpf1 – protein stability and effect on cell growth

Since Mpf1 is an uncharacterized protein with an unknown function, we investigated whether its loss would impact the growth of yeast cells. We noticed that *mpf1*Δ cells grew like WT cells in rich medium, in all the three carbon sources – glucose, glycerol and oleate (YPD, YPG and YPO respectively) (Figure2.8 A). However, on a synthetic medium, when oleic acid was used as the sole carbon source, absence of Mpf1 improved the cell growth (Figure 2.8 A).

β-oxidation of fatty acids like oleate takes place exclusively in peroxisomes in yeast (Hiltunen et al., 2003), and fully functional peroxisomes is crucial for optimal growth on oleate. Furthermore, previous studies have shown that upon absence of Fis1, the number of peroxisomes on oleate are reduced (Kuravi et al., 2006), and specifically re-directing Fis1 only to peroxisomes by expressing Fis1-Pex15, a fusion protein, increased the number of peroxisomes per cell (Motley et al., 2008). Therefore, consistent with our previous observations, the improved growth of *mpf1*Δ cells on oleate can be explained by the increased presence of Fis1 in peroxisomes. This, in turn, enhances the number of peroxisomes which might improve oleate utilization. This observation hints towards a physiological role of Mpf1.

A previous high-throughput study suggested that Mpf1 and its uncharacterized paralog Yhr131c might be substrates of Grr1, a subunit of the SCF ubiquitin ligase complex. In that study, both Mpf1 and Yhr131c were shown to be partially stabilized in *grr1*Δ cells (Mark et al., 2014).

To verify this previous observation, we overexpressed Mpf1-3HA in WT and *grr1*Δ cells and monitored the life span of Mpf1 in these cells by cycloheximide (CHX) chase assay. In line with the previous findings, we observed that Mpf1 is a highly unstable protein which is almost completely degraded within 45 minutes in WT cells (Figure 2.8B and C). We also observed that the absence of Grr1 resulted in only a minor effect on the stability of Mpf1 (Figure 2.8 A and B), suggesting that there might be other factors that affect the stability of this protein. Mpf1's short lifespan raises the question of why cells

produce proteins that are degraded so quickly. It might be that Mpf1 is needed immediately under some conditions and further investigations to find out circumstances that enhance Mpf1 could provide valuable insights into its function.

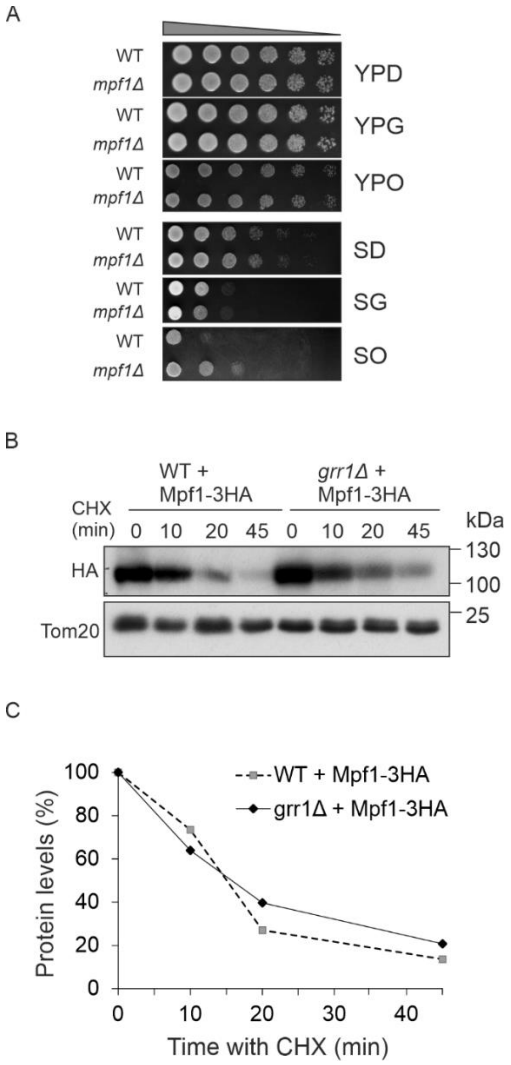

Figure 2.8: Absence of Mpf1 is beneficial for growth on oleate; Mpf1 is an unstable protein. (A) Growth of wild-type (WT) and *mpf1Δ* cells at 30°C was analyzed by drop-dilution assay. The cells were grown on either rich media (YP) or synthetic media (S) containing glucose (YPD or SD), glycerol (YPG or SG), or oleate (YPO or SOleate). **(B)** WT and *grr1Δ* cells were transformed with a vector encoding Mpf1-3HA. The cells were grown on SD-Ura and then on time = 0 the translation inhibitor cycloheximide (CHX) was added (Time=0). Proteins were extracted at each time point by alkaline lysis and analyzed by SDS-PAGE and immunodecorated with antibodies against HA or Tom20 (as loading control). **(C)** The bands representing either Mpf1-3HA or Tom20 were quantified and for each lane, the intensity of the band corresponding to Mpf1-3HA was normalized to the loading control (Tom20). The signal at time point = 0 was set to 100%. One representative experiment out of three independent ones is shown.

Mpf1 loosely associates with the MOM

To characterize Mpf1 further, we aimed to determine its subcellular location by fractionating WT cells expressing Mpf1-3HA into whole cell lysate (WCL), ER, cytosol and mitochondria. These fractions were analyzed by Western blotting and immunodecorated with antibodies recognizing marker proteins for the mitochondria (Tom40), ER (Erv2), cytosol (Hexokinase), and peroxisomes (Pex14).

We primarily detected Mpf1-3HA in the mitochondrial fraction, with a portion also in the ER fraction. However, these latter fractions also contained the peroxisomal marker Pex14. Hence, at this stage, we could only conclude that Mpf1-3HA might localize to mitochondria, peroxisomes, and/or the ER (Figure 2.9A).

To pinpoint the localization of Mpf1-3HA, we turned to fluorescence microscopy. Tagging Mpf1 with GFP resulted in cytosolic staining, contrary to fractionation results. This observation could be due to cleavage of the GFP tag from Mpf1 or mis-targeting because of the size of GFP. We then conducted immunofluorescence (IF) assays using anti-HA antibodies conjugated to a fluorophore to detect Mpf1-3HA. As an IF technique control, we visualized Tom22-HA, a bona-fide MOM protein. We found Mpf1-3HA stained tubular structures that co-localize with RFP-MTS (mitochondrial targeting signal) but not with RFP-PTS1 (Peroxisomal targeting signal 1) (Figure 2.9B). These findings confirm that Mpf1-3HA localizes mainly to the mitochondria.

Next, we investigated the sub-mitochondrial localization of Mpf1-3HA by treating isolated mitochondria from cells expressing Mpf1-3HA with proteinase K (PK). We observed Mpf1-3HA to be susceptible to PK digestion, similar to surface proteins like Tom70 and an Mcr1 isoform on the outer membrane ($Mcr1_{OM}$) (Figure 2.9C). In contrast as expected for mitochondrial internal proteins, the Mcr1 isoform in the intramembrane space ($Mcr1_{IMS}$) and the matrix protein Hep1 remained protected from PK by the outer membrane and both outer and inner membranes, respectively (Figure 2.9C). Hence, we concluded that Mpf1 is situated on the MOM, exposed to the cytosol.

We next determined whether Mpf1-3HA is an integral or peripheral membrane protein by conducting alkaline extraction of mitochondrial proteins. Using this assay, one could separate soluble and peripheral membrane proteins in the supernatant and integral membrane proteins in the pellet. We performed this assay under varying pH conditions since alkaline pH decreases non-covalent protein-protein interactions and releases peripheral membrane proteins to the supernatant (Kim et al., 2015).

The control *bona fide* integral membrane protein, $Mcr1_{OM}$ isoform remained in the pellet fractions across all pH conditions, and as expected, the soluble IMS isoform of Mcr1 remained in the supernatant (Figure 2.9D). Mpf1-3HA was present in the membrane fraction (P) only under milder extraction condition (pH 10.5). However, as the pH was raised to 11, 11.5, and 12, larger quantities of Mpf1 were detected in the supernatant fraction. This behavior was similar to the partially extractable MOM protein, Om14 (Burri et al., 2006; Zhou et al., 2022) (Figure 2.9D). In summary, these results suggest that Mpf1-3HA is bound peripherally to the cytosolic side of the mitochondrial OM.

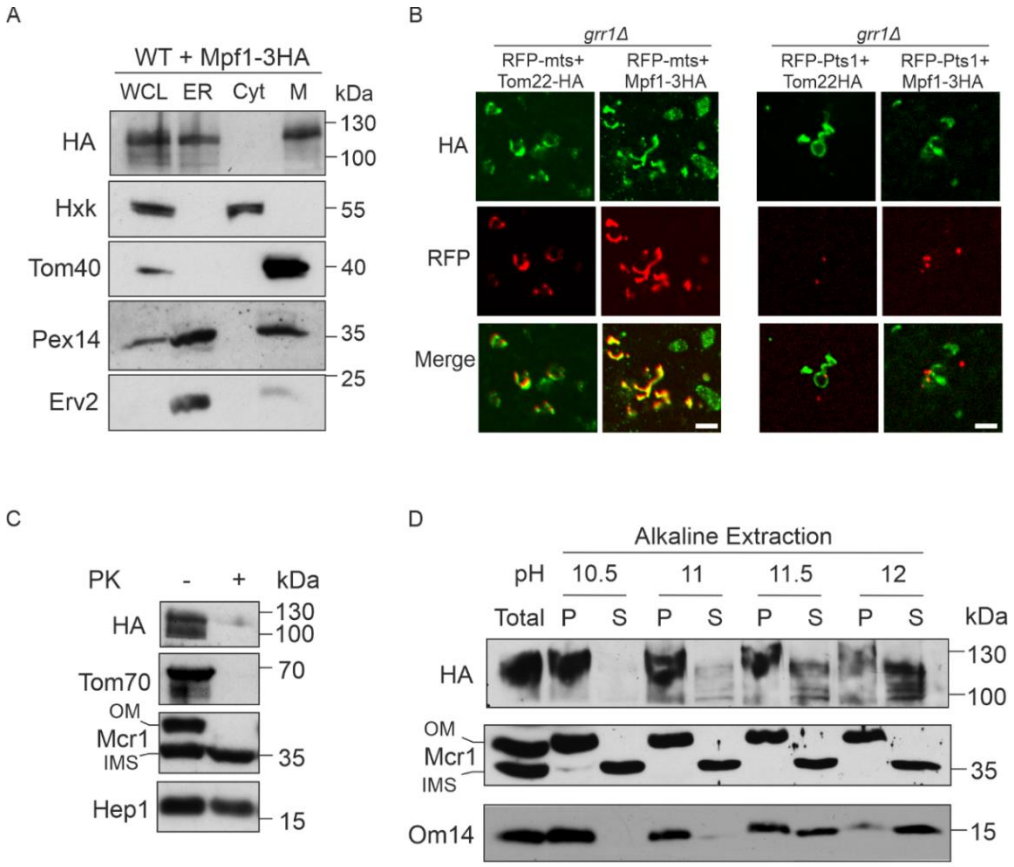

Figure 2.9: Mpf1 shows a loose association with the mitochondrial outer membrane. (A) Cells overexpressing Mpf1-3HA were subjected to sub-cellular fractionation. The isolated fractions of whole cell lysate (WCL), microsomes (ER), cytosol (Cyt), and mitochondria (M) were analyzed by SDS-PAGE and immunodecorated with the indicated antibodies. Tom40 (mitochondria), Hexokinase (cytosol), Pex14 (peroxisomes), and Erv2 (ER) were used as marker proteins. **(B)** Cells expressing Mpf1-3HA were analyzed by immunofluorescence microscopy. *grr1*Δ cells were used to increase the half-life of the protein. The HA tagged proteins were visualized with anti-HA antibody conjugated with Alexa Fluor™ 488. Tom22-HA, a bona-fide mitochondrial protein was used as a control for the antibody. To visualize mitochondria and peroxisomes, the cells expressing the HA-tagged proteins were co-transformed with mitochondrial targeting signal fused to RFP (MTS-RFP) or RFP-PTS1 (peroxisomal targeting signal 1). Scale bar, 5 µm. **(C)** Isolated mitochondria from cells expressing Mpf-3HA were either left intact (-PK) or treated with proteinase K (+PK). Then, the samples were analyzed by SDS-PAGE and immunodecorated with the indicated antibodies. Tom70 and $Mcr1_{OM}$ are exposed on the mitochondrial surface whereas $Mcr1_{IMS}$ and Hep1 (matrix) are protected by mitochondrial membranes. **(D)** Isolated mitochondria from cells expressing Mpf1-3HA were subjected to alkaline extraction using solution at the indicated pH values. "Total" represents untreated mitochondria. Membrane proteins were isolated in the pellet (P) fraction and soluble and membrane-peripheral proteins in the supernatant (S) fraction. The samples were analyzed by SDS-PAGE and immune-decoration against the specified antibodies. $Mcr1_{OM}$ and $Mcr1_{IMS}$ served as controls for integral membrane protein and soluble protein, respectively. Om14 acted as a control for MOM-associated protein extractable under extreme alkaline conditions.

Tom70 and Tom71 play a role in the biogenesis of Mpf1

Considering the location of Mpf1 on the surface of mitochondria, we explored whether Tom70, Tom71, or both facilitated its biogenesis. Previous research on Tom70 and to a lesser extent its paralog Tom71, highlighted a tetratricopeptide (TPR) structure, capable of binding cytosolic chaperones like Hsp70 and Hsp90 while recruiting several nascent proteins to the mitochondria (Backes et al., 2018; Jores et al., 2018; Young et al., 2003; Zanphorlin et al., 2016). Microscopy analysis of many GFP tagged proteins showed their reduced levels in *tom70Δ/71Δ* cells (Backes et al., 2021).

To examine the potential role of Tom70/71 in the biogenesis of Mpf1, we observed the steady state levels of Mpf1-3HA in *tom70Δ*, *tom71Δ,* and *tom70Δ/71Δ* cells. Remarkably, the absence of either Tom70 or Tom71, did not significantly alter Mpf1-3HA levels compared to WT cells. However, the double deletion of both Tom70 and Tom71 led to a tenfold decrease in Mpf1-3HA levels compared to WT cells (Figure 2.10A and B).

We wondered if this dramatic reduction of Mpf1-3HA in *tom70Δ/71Δ* cells was due to an effect on its stability or subcellular localization.

Though initial levels of Mpf1-3HA were tenfold lower in the double deletion cells at the time-point 0, the protein's lifespan was similar to that in WT cells (Figure 2.10C and D). Furthermore, both subcellular fractionation and immunofluorescence microscopy assays demonstrated that Mpf1-3HA remained predominantly localized to the mitochondria in *tom70Δ/71Δ* cells (Figure 2.10E and F).

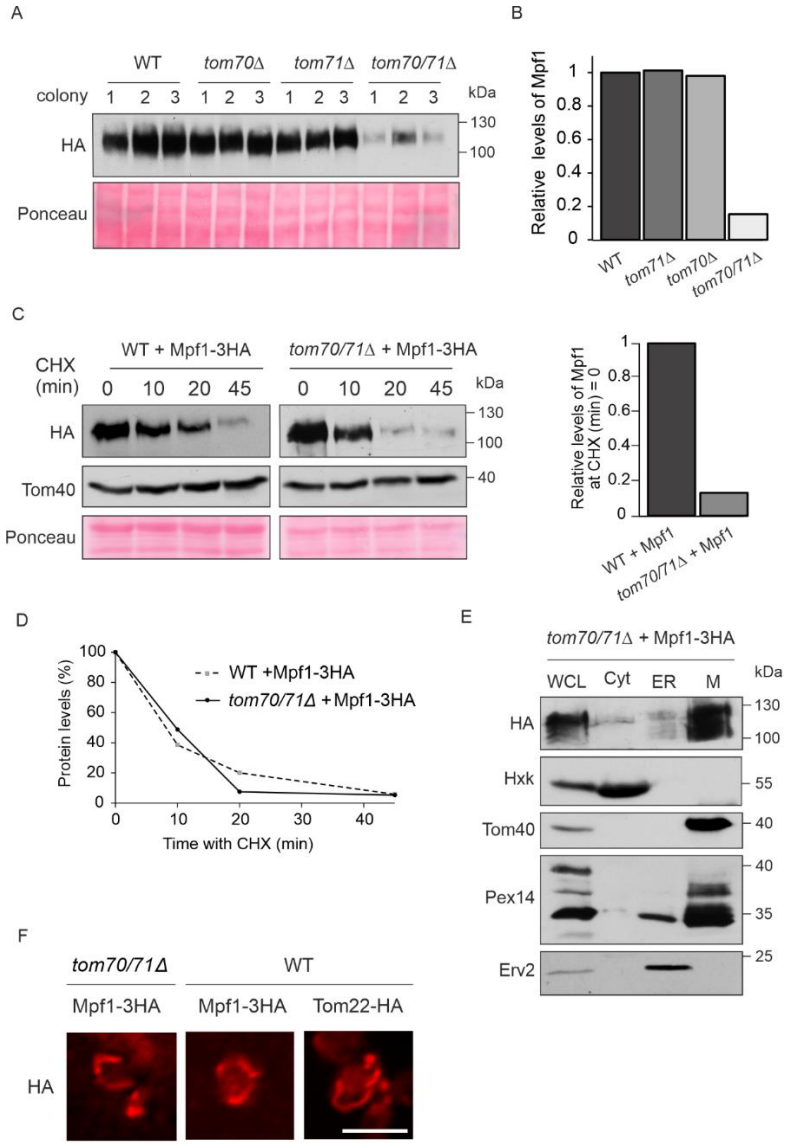

Figure 2.10: The absence of Tom70 and Tom71 reduces the expression of Mpf1. **(A)** Proteins were extracted using alkaline lysis from the indicated cells (three independent colonies) expressing Mpf1-3HA. Samples were analyzed by immunodecorated with HA antibody. Ponceau staining was used as the loading control. **(B)** The bands representing Mpf1-3HA were quantified and for each lane normalized to the intensity of the Ponceau staining. The average of the three colonies for each strain was calculated and the value for WT cells was set as 1. **(C)** Left panel: WT and *tom70/71Δ* cells expressing Mpf1-3HA were subjected to cycloheximide (CHX) assay as described in the legend to Fig. 2.8A. Right panel: Quantification of Mpf1-HA levels relative to Ponceau at time point = 0. **(D)** The bands corresponding to Mpf1-3HA in the experiment presented in panel (C) were quantified as described in the legend to Fig. 2.8B. One representative experiment out of three independent ones is presented. **(E)** Sub-cellular fractionation of *tom70/71Δ* strain expressing Mpf1-3HA. The isolated fractions of whole cell lysate (WCL), microsomes (ER), cytosol (Cyt), and mitochondria (M) were analyzed by SDS-PAGE and immuno-decoration against the indicated antibodies. Tom40 (mitochondria), Hexokinase (cytosol), Pex14 (peroxisomes), and Erv2 (ER) were used as marker proteins. **(F)** Immunofluorescence microscopy to visualize Mpf1-3HA in *tom70/71Δ* and WT cells. Tom22-HA was used as a control for the IF technique. The HA-tagged proteins were visualized using an anti-HA antibody conjugated with Alexa Fluor™ 594. Scale bar, 5 μm

Previous study suggested that Tom70 might be involved in signaling pathways through multiple transcription factors to regulate the transcription of genes encoding mitochondrial proteins. Accordingly, deletion of Tom70 resulted in reduced levels of mRNAs encoding mitochondrial proteins (Liu et al., 2022).

Hence, we then asked if the low protein levels of Mpf1-3HA in *tom70Δ/71Δ* cells were due to low transcript levels of *MPF1*.

Our RT-qPCR analysis found that deleting both *TOM70* and *TOM71* resulted in approximately a 50% reduction in transcript levels of both endogenous *MPF1* and overexpressed *MPF1-3HA* compared to WT cells (Figure 2.11). The mRNA reduction may be due to decreased transcription, increased degradation, or mRNA sequestration to P-bodies. Our findings suggest Tom70 and Tom71 play a role in Mpf1-3HA transcriptional control. Despite reduced mRNA and protein levels in the absence of Tom70/71, Mpf1-3HA still localizes to mitochondria, hinting at the involvement of other factors in its proper targeting.

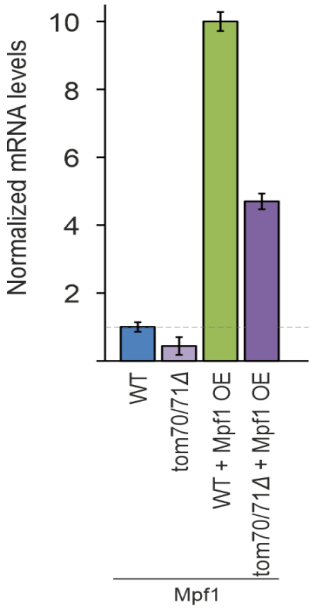

Figure 2.11: The transcript levels of Mpf1 are reduced in *tom70/71Δ* cells. RT-qPCR analysis was performed to detect transcript levels of *MPF1* in either WT or *tom70/71Δ* cells. The transcript levels of endogenous *MPF1* or upon transformation of cells with overexpression plasmid encoding *MPF1-3HA* were determined. The transcript levels of *ACT1* (encoding the abundant protein Actin) served as a reference.

Mutating the PH domain of Mpf1 increases protein stability

Pleckstrin homology (PH) domains interact with phosphoinositide (PI) species as well as other lipids on biological membranes. Large scale studies and structural analysis predicted the presence of a PH domain in Mpf1 (Gallego et al., 2010; Isakoff et al., 1998; Lemmon, 2004), and previous attempts to investigate PI binding of a recombinant PH domain from Mpf1 was unsuccessful due to inadequate expression levels.

Previous studies have shown that mutating the basic residues in the β1/β2 loop can abolish membrane targeting of PH domains that strongly bind to PIs (Yu et al., 2004). The PH domains of Mpf1 consists of two anti-parallel β-sheets followed by a C-terminal α-helix, and we found three basic residues potentially in the β1/β2 loop. Thus, I decided to mutate the lysine and arginine residues by replacing them with alanine (K144A, K147A, and R157A) (Figure 2.12A). Next, I investigated the stability and/or subcellular localization of the PH domain mutant Mpf1(PH*)-3HA.

Compared to native Mpf1-3HA, Mpf1(PH*)-3HA exhibited elevated stability, with steady-state levels ~60% higher than that of the native protein (Figure 2.12B and C). PH domain is known to facilitate protein-protein interactions (Lemmon, 2004; Scheffzek & Welti, 2012), and mutating the basic residues in the PH domain of Mpf1 might have disrupted its interactions with Ubiquitin/proteasome degradation pathway factors, thereby increasing its stability. Alternatively, the mutations might stabilize Mpf1's interaction with a protein or lipid on the MOM and the increased stability could be associated through these interactions.

Of note, cells overexpressing Mpf1(PH*)-3HA grew slightly better than WT cells on oleate-containing medium, (Figure 2.12D). We speculate that this variant might have a dominant negative effect on recruiting Fis1 to mitochondria, and thereby increases the number of peroxisomes on oleate, promoting cell survival.

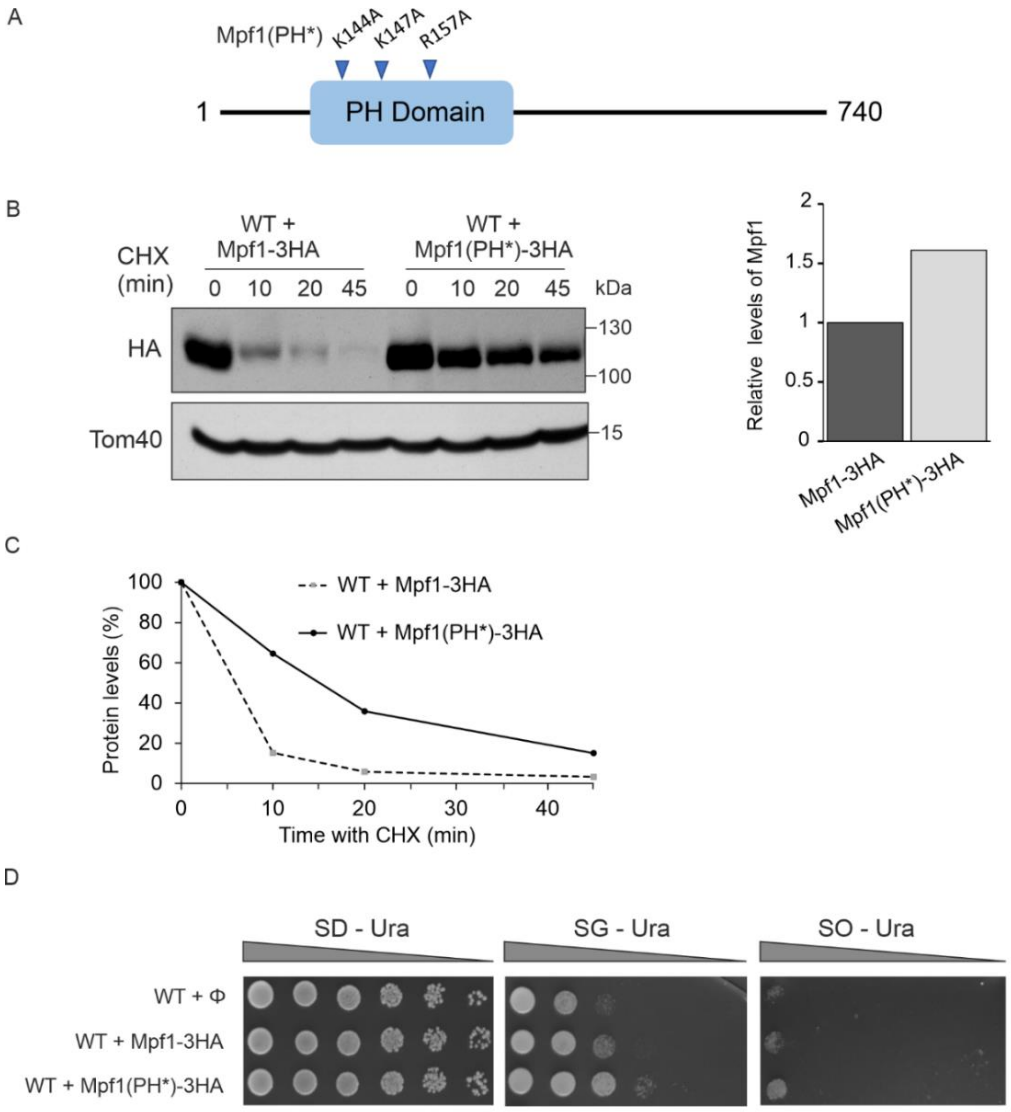

Figure 2.12: Mutating the Pleckstrin homology (PH) domain of Mpf1 stabilizes the protein. **(A)** Schematic diagram of the mutations in the PH domain of Mpf1 with K144, K147, and R157 replaced by alanine (A) residues (the mutant is indicated as Mpf1(PH*). The mutated basic residues in the in the β1/β2 loop of the PH domain are indicated with blue arrowheads. **(B)** Left panel: WT cells overexpressing either Mpf1-3HA or Mpf1(PH)*-3HA were subjected to cycloheximide (CHX) assay for the indicated time periods. Proteins were then extracted by alkaline lysis and analyzed by SDS-PAGE and immunodecorated with antibodies against either HA or Tom40 (as loading control). Right panel: Quantification of Mpf1-HA and Mpf1(PH)*-3HA levels relative to Tom40 at time point = 0. **(C)** Quantification of Mpf1-3HA and Mpf1(PH)*-3HA was performed as described in the legend to Fig. 2.5B. One representative experiment out of three independent ones is presented. **(D)** Growth analysis by drop dilution assay of WT cells harboring either an empty vector (Φ), a plasmid encoding Mpf1-3HA, or a plasmid encoding Mpf1(PH*)-3HA. Cells were grown at 30°C on synthetic media containing glucose (SD-Ura), glycerol (SG-Ura), or oleic acid (SO-Ura).

Next, I investigated whether the basic residues in the PH domain of Mpf1 are essential for mitochondrial targeting and OM association. Using IF and subcellular fractionation, we found that Mpf1(PH*)-3HA still localizes to the mitochondria (Figure 2.13A and B).

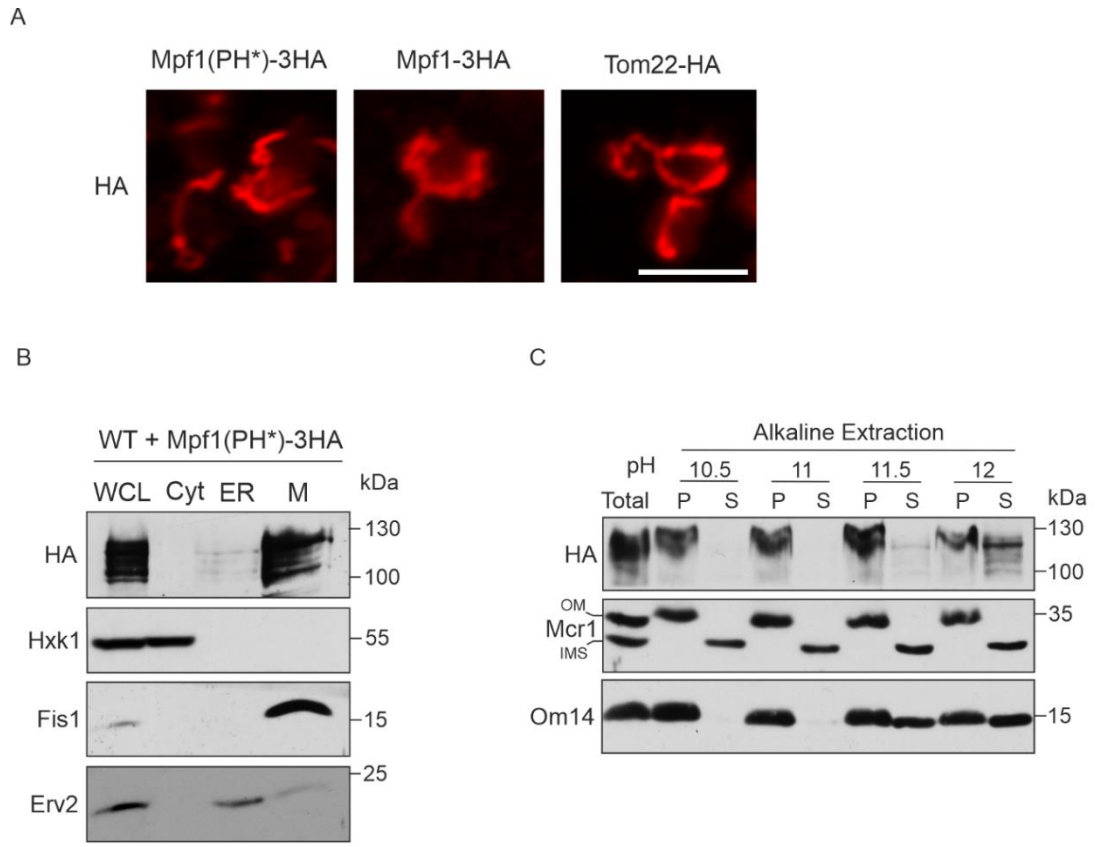

Figure 2.13: The mutations in the PH domain do not affect the location of Mpf1. (A) Immunofluorescence microscopy localization of Mpf1(PH*)-3HA in WT cells. Tom22-HA was used as a control for the technique. The HA-tagged proteins were visualized using an anti-HA antibody conjugated with Alexa Fluor™ 594. Scale bar, 5 µm. **(B)** Sub-cellular fractionation of WT cells expressing Mpf1(PH*)-3HA. Cells were analyzed as described in the legend to Fig. 2.9A. **(C)** Isolated mitochondria from cells expressing Mpf1(PH*)-3HA were subjected to alkaline extraction as described in the legend to Fig. 2.9D.

Not all PH domains show strong and specific interactions with PIs and binds to membranes with low affinity and specificity. Effective binding of such "weak" PH domains to biological membranes may be enhanced by interactions with other membrane-bound proteins (Maffucci & Falasca, 2001). Furthermore, molecular modelling of the PH domain of Mpf1 revealed that it indeed has a weak or no positive

charge, while effective membrane targeting or binding to PIs might require stronger positive charges (Yu et al., 2004).

To investigate whether the association of Mpf1(PH*)-3HA with MOM is affected, we then performed an alkaline extraction. We detected Mpf1(PH*)-3HA predominantly in the pellet fraction in pH 10.5, with an increase in the supernatant only at pH 12. This indicates that Mpf1(PH*)-3HA exhibits a similar, or even somewhat stronger association to the MOM than its native counterpart (Figure 2.13C). Collectively, these findings indicate that mutating key residues in the PH domain of Mpf1 increased its stability and did not alter its association with mitochondria.

Altogether, our findings contribute to novel insights on factors responsible for regulating the dual distribution of Fis1 to mitochondria and peroxisomes. We identified for the first time three proteins Tom70, its paralogue Tom71, and Mpf1 as involved in this process. In addition to recognizing a unique function of Tom71, we could provide a function for a so far uncharacterized protein – Mpf1. We identify the latter as an unstable protein at the surface of mitochondria. Collectively, the current study provides the first glimpse into the process of dual distribution of TA proteins between mitochondria and peroxisomes.

Chapter 3

This chapter consists of sections adapted from the following pre-print submitted to Cell. The methods and results presented in this chapter are exclusively derived from the experiments I conducted as part of my doctoral thesis.

The molecular mechanism of on-demand sterol biosynthesis at organelle contact sites.

Naama Zung[1], Nitya Aravindan[2], Angela Boshnakovska[3,3a,3b,3c], Rosario Valenti[1], Noga Preminger[1], Felix Jonas[1], Gilad Yaakov[1], Mathilda M. Willoughby[4,4a], Bettina Homberg[3,3a,3b,3c], Jenny Keller[5,5a], Meital Kupervaser[6], Nili Dezorella[7], Tali Dadosh[7], Sharon G. Wolf [7], Maxim Itkin[8], Sergey Malitsky[8], Alexander Brandis[7], Naama Barkai[1], Rubén Fernández-Busnadiego[5,5a,9,9a], Amit R. Reddi[4], Peter Rehling[3,3a,3b,3c], Doron Rapaport[2], Maya Schuldiner[1]

[1]Department of Molecular Genetics, Weizmann Institute of Science, Israel
[2]Interfaculty Institute of Biochemistry, University of Tuebingen, Germany
[3]Department of Cellular Biochemistry, University Medical Center Göttingen, Germany
[3a]Cluster of Excellence "Multiscale Bioimaging: from Molecular Machines to Networks of Excitable Cells" (MBExC), University of Göttingen, Germany
[3b]Fraunhofer Institute for Translational Medicine and Pharmacology ITMP, Translational Neuroinflammation and Automated Microscopy, Germany.
[3c]Max Planck Institute for Multidisciplinary Sciences, D-37077, Germany
[4]School of Chemistry and Biochemistry, Georgia Institute of Technology, USA
[4a]Biochemistry and Molecular Biology Department, University of Nebraska Medical Center, USA
[5]University Medical Center Göttingen, Institute for Neuropathology, 37077, Germany
[5a]Collaborative Research Center 1190 "Compartmental Gates and Contact Sites in Cells", University of Göttingen, Germany
[6]The De Botton Protein Profiling institute of the Nancy and Stephen Grand Israel National Center for Personalized Medicine, Weizmann Institute of Science, Israel
[7]Electron Microscopy Unit, Chemical Research Support, Weizmann Institute of Science, Israel
[8]Life Sciences Core Facilities, Weizmann Institute of Science, Israel
[9]Cluster of Excellence "Multiscale Bioimaging: from Molecular Machines to Networks of Excitable Cells" (MBExC), University of Göttingen, 37077, Germany
[9a]Faculty of Physics, University of Göttingen, 37077, Germany

bioRxiv DOI: 10.1101/2024.05.09.593285

Author contributions

I performed Blue Native PAGE experiments to identify potential complexes of the ERGosome with Yet3, which can be found in Figure S4 B in the pre-print.

Introduction

In cells, organellar communication is crucial to ensure transfer of metabolites and efficient cellular homeostasis. This communication is enabled by the presence of contact sites, which are areas where the organelles are in close proximity, held together by tethering proteins (Scorrano et al., 2019; Zung et al., 2024). All organelles create contact sites or "contacts" and the most well studied ones are those of the endoplasmic reticulum (ER). Although, extensive efforts have been made to identify the proteins at these contact sites, there is still limited knowledge about the lipid composition within these regions.

Previous studies have shown that ER contacts form specific micro-environment that are rich in sterols and sphingolipids (ARDAIL et al., 2003). Specifically, ER-mitochondria contact sites have been shown to possess sterol concentrations that are seven times greater than those of the adjacent bulk ER membrane (Fujimoto et al., 2012). The major sterols in yeast and mammals is ergosterol and cholesterol respectively. These sterols are essential to maintain membrane fluidity and ensure optimum activity of membrane proteins. The precursor Farnesyl-PP, once processed to squalene is converted to either ergosterol or cholesterol by post-squalene enzymes. Sterol production primarily occurs in the ER and to a lesser extent in lipid droplets (LD). From these sites, sterols are transported to other organelles and specially to the plasma membrane (PM). The plasma membrane contains the highest concentration of cholesterol, comprising 30-50% of its total lipids (Lange, 1991; Ridsdale et al., 2006). In contrast, the ER membrane has the very low cholesterol content, with only 3-6% of its total lipids, despite being the site of sterol synthesis (Ridsdale et al., 2006), which raises the question of how sterol-rich subdomains are formed and maintained in the contact sites amidst the sterol-deficient environment of the ER (Zung et al., 2024).

This study aimed to identify the protein(s) within the contact sites responsible for maintaining these sterol-rich subdomains. Our work identified Yet3 as a contact site protein located on the ER membrane, interacting with an assembly of post-squalene ergosterol biosynthesis enzymes that were named ERGosome. The findings of the

project suggest that Yet3 is responsible for recruiting this ERGosome to the ER contact sites, thereby creating sterol-rich environments (Mo & Bard, 2005; Zung et al., 2024). Furthermore, the study emphasizes the function of Yet3 as a crucial regulator of sterol biosynthesis and distribution. It suggests that Yet3 maintains the balance of sterols between the PM and the ER. Overexpression of Yet3 leads to increase in sterol concentration on ER and depletion of sterols from the PM, significantly effecting the biogenesis of other organelles (Zung et al., 2024).

My contribution to this study revealed potential high molecular weight complexes involving Yet3 and sterol biosynthesis enzymes, indicating that these enzymes and Yet3 might assemble into large complexes at the ER contact sites. While the results in this study also indicate the importance of Yet1 (paralog of Yet3) in maintaining the proper localization of function of Yet3, the BN-PAGE analysis reveal a Yet1-independent role of Yet3 in the formation of high molecular weight complexes involved in sterol biosynthesis.

Methods

Isolation of crude organelles

Yeast cells (200 ml) overexpressing the indicated GFP tagged proteins were cultured in rich media (YP) supplemented with 2% glucose till logarithmic phase. The cells were harvested (3000 x g, 5 min, RT), resuspended in DTT buffer (100 mM Tris, 10 mM DTT) and incubated at 30 °C for 15 min. The cells were then washed once with spheroplasting buffer (1.2 M Sorbitol, 20 mM KPI, pH 7.2) and then, to digest the cell wall, the cells were incubated with spheroplasting buffer supplemented with zymolyase (6mg/g of cells) for 1 hour at 30 °C. Further steps were carried out on ice. The spheroplasts were resuspended in homogenization buffer (0.6 M Sorbitol, 10 mm Tris, pH 7.4, 1 mM EDTA, 0.2% fatty acid-free BSA with 2 mM PMSF). To obtain cell lysate, the spheroplasts were dounce homogenized. The cell debris and nuclei were removed by centrifugation (2000 x g, 10 min, 4 °C). The supernatant containing the crude organelles were isolated by centrifugation (18,000 x g, 15 min, 4 °C). The pellets were resuspended in SEM buffer (250 mM Sucrose, 1 mM EDTA, 10 mM MOPS) containing 2 mM PMSF and stored at -80 °C.

Blue Native PAGE

Isolated organelles (150 µg) were solubilized in 100 µL SEM buffer supplemented with Triton X-100 at a protein to detergent ratio of 1:2. The sample was incubated for 30 min on ice. The supernatant containing the solubilized fraction was isolated by centrifugation (30,000 x g, 30 min, 4 °C), and was mixed with the 10X loading dye (5% (w/v) Coomassie blue G, 500 mM 6-amino-N-caproic acid, 100 mM Bis-Tris, pH 7.0). The sample was loaded on a gel containing 6-16% acrylamide gradient. The gels were run (150 V, 15 mA, 2 hours, 4 °C) with Cathode buffer A (500 mM Tricine, 150 mM Bis-Tris, 0.2 % Coomassie blue G, pH 7.0). The buffer was replaced with Cathode buffer B (500 mM Tricine, 150 mM Bis-Tris, pH 7.0) after the 3/4th of the gel is stained and the gels run was continued (50 V, 15 mA, 16 hours, 4 °C). The proteins were blotted onto a polyvinylidene fluoride (PVDF) membrane and immunodecorated with an antibody against GFP.

Results and discussion

Yet3 potentially forms high molecular weight complexes

To study the potential formation of complexes containing Yet3 and/or enzymes involved in ergosterol biosynthesis, the relevant proteins were overexpressed as GFP fusion proteins. BN-PAGE followed by immunodecoration with an antibody against GFP provides insights into the formation of two potential high molecular weight complexes at approximately 480 and 720 kDa (Figure 3.1). Of note, these complexes are specific as they are not detected when a GFP fusion protein is not expressed (Figure 3.1). These observations might suggest an assembly of Yet3 and the ergosterol biosynthesis enzymes (Hmg1, Erg9, Erg11 and Erg24) into large complexes at the ER contact sites.

Furthermore, Yet1 (a paralog of Yet3) has been shown to play a significant role in modulating the distribution of Yet3, which in turn affects the localization of sterol biosynthesis enzymes and the overall sterol distribution within the cell (Zung et al.,2024). The BN-PAGE analysis shows that the absence of Yet1 did not affect the migration of both high molecular weight complexes, suggesting that the formation of these complexes can occur independently of Yet1 (Figure 3.1).

However, GFP-Yet3 forms also some lower molecular weight complexes. These complexes either disappear completely or diminish when Yet1 is absent (Figure 3.1). Previous research demonstrated that Yet3 and its paralog Yet1 form a heterodimeric complex that regulates the inositol biosynthesis pathway (Wilson et al., 2011). Therefore, the disappearance of these lower molecular weight complexes can be attributed to the absence of the heterodimeric complex due to the lack of Yet1. Some lower molecular weight complexes are partially diminished, suggesting that Yet1 may play a role in forming other complexes that are moderately destabilized in *yet1Δ* cells.

Altogether, these findings suggest that Yet1's regulatory role is more relevant to the localization and distribution of Yet3 than its complex formation with the ergosterol biosynthesis enzymes.

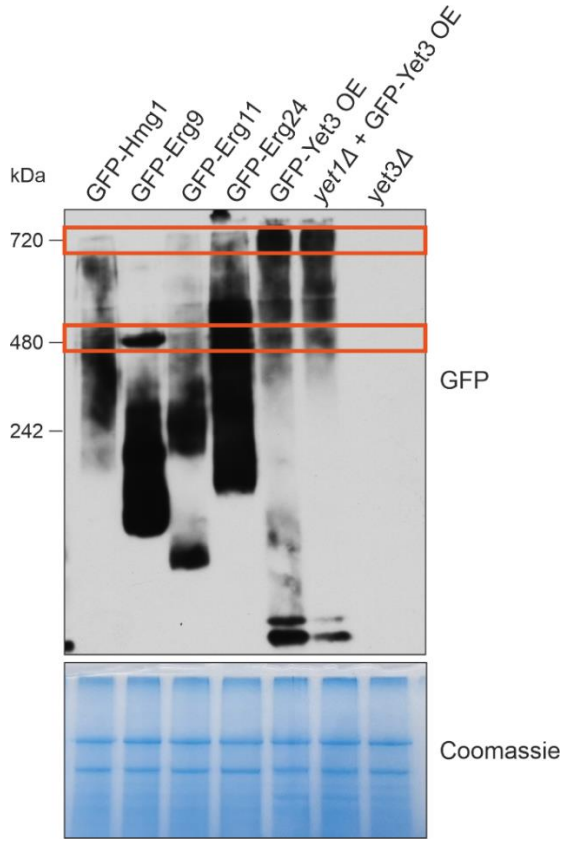

Figure 3.1: Yet3 potentially forms high molecular weight complexes with ergosterol biosynthesis enzymes. Isolated organelles from strains overexpressing the indicated proteins were subjected to BN-PAGE analysis. The membrane was immunodecorated with antibodies against GFP. The Coomassie staining of the membrane serves as a loading control.

The absence of Yet1 reduced levels of Yet3 and other ER proteins in isolated microsomes

To further investigate whether the absence of Yet1 affects the steady-state levels of ER proteins, I isolated whole cell lysates (WCL) and ER (microsomes) from WT and *yet1Δ* cells. The fractions were analyzed by SDS-PAGE followed by immunodecoration with

antibodies against Yet3, and other *bona fide* ER proteins like Sec61 and Erv2. The results indicated that upon the deletion of Yet1, the protein levels of the tested ER proteins were reduced and not enriched in the isolated microsomes compared to WT samples (Figure 3.2A).

A previous study demonstrated the interdependence of Yet1 and Yet3 for normal stability and localization, suggesting their co-assembly into a functional heterodimeric complex (Wilson & Barlowe, 2010). It was also shown that Yet proteins interact and form a complex with the core component of the ER Sec translocon, Sec61, and other proteins of the Sec complex such as Sec63 (Wilson & Barlowe, 2010). The Sec complex is crucial for facilitating the transport of secretory pathway proteins into the endoplasmic reticulum and for integrating membrane proteins into the ER membrane (Bhadra et al., 2021).

Furthermore, the study discovered that the quantity of Sec61 co-immunoprecipitated with Yet3-HA was significantly diminished in *yet1Δ* cells, suggesting that the interaction of Yet3 with Yet1 is crucial for effective association with the Sec complex (Wilson & Barlowe, 2010). Although the study speculated that Yet-Sec complex interaction might not be crucial for translocation in general, I observed decreased levels of Yet3, Sec61 and Erv2 in the microsomes of *yet1Δ* cells, potentially due to the absence of the Yet-Sec complex (Figure 3.2A). However, the protein levels of Yet3, Sec61, and Erv2 in the whole cell lysate (WCL) of *yet1Δ* cells remained unchanged (Figure 3.2A). This suggests that Yet1 does not affect the steady-state levels of these proteins in the WCL, but rather influences their localization to the isolated microsomes.

Next, I wondered whether elevated levels of Yet3 can compensate for the absence of Yet1. Thus, I monitored the levels of the ER proteins in *yet1Δ* cells overexpressing GFP tagged Yet3. Interestingly, I observed that this overexpression restored protein levels in the microsomes to levels comparable to those in wild-type cells (Figure 3.2B). This suggests that overexpressing Yet3 might compensate for the loss of Yet1 in forming the Yet-Sec complex. Notably, I observed that GFP-Yet3 levels were lower in the

microsomes compared to the whole cell lysates in both WT and *yet1Δ* cells overexpressing GFP-Yet3, indicating that GFP-Yet3 was not enriched (Figure 3.2B). This could potentially be due to the bulky GFP tag affecting the correct localization of Yet3.

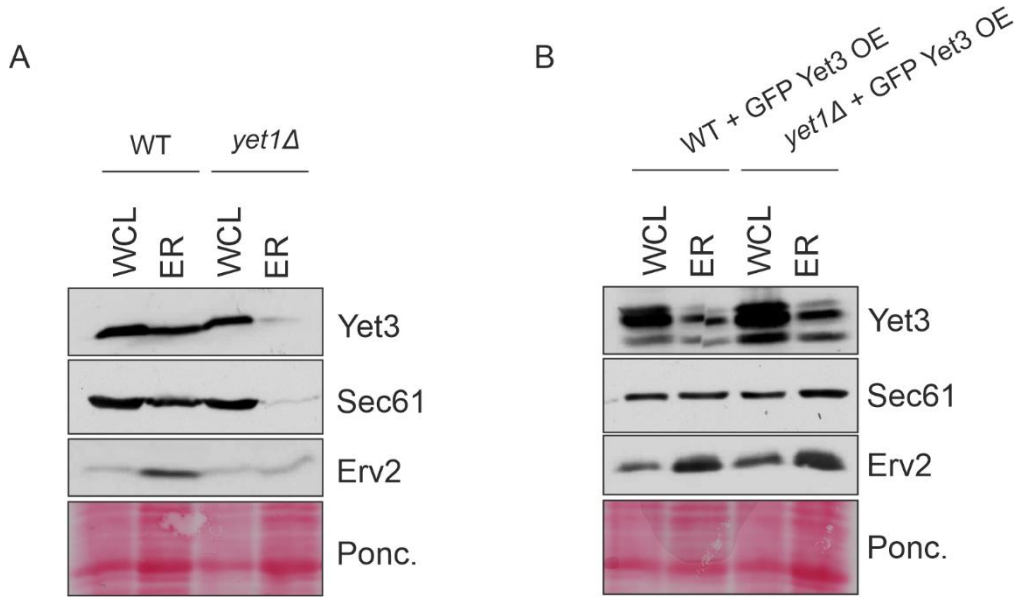

Figure 3.2: The absence of Yet1 effects protein levels of Yet3, Sec61 and Erv2 in isolated microsomes. A and B) Whole cell lysates (WCL) and ER (microsomes) were isolated from the specified strains and subjected to SDS-PAGE analysis followed by immunodecoration with the indicated antibodies. The Ponceau staining serves as a loading control.

Altogether, the key takeaway is that Yet3 forms high molecular weight complexes potentially with ergosterol biosynthesis enzymes. Yet1 influences the localization and distribution of Yet3, but the formation of these complexes can occur independently of Yet1. In Yet1's absence, some lower molecular weight complexes disappear or diminish, likely due to the absence of Yet1-Yet3 heterodimers, or other complexes involving Yet1 that are not yet identified. Furthermore, the absence of Yet1 reduces the levels of Yet3 and other ER proteins in isolated microsomes but not in whole cell lysates, indicating its potential role in ensuring proper protein localization. Overexpression of Yet3 in *yet1Δ* cells restores protein levels in microsomes, suggesting that elevated Yet3 can compensate for the loss of Yet1, although the bulky GFP tag might affect Yet3's proper localization.

Chapter 4

This chapter consists of brief sections adapted from the book chapter submitted to Methods in Enzymology as a part of my doctoral thesis.

A modified procedure for separating yeast peroxisomes from mitochondria.

Nitya Aravindan and Doron Rapaport*

Interfaculty Institute of Biochemistry, University of Tuebingen, Tuebingen, Germany

Corresponding author e-mail address: doron.rapaport@uni-tuebingen.de

Author Contributions

I optimized a method for the effective separation of mitochondria and peroxisomes in yeast cells. This method has been submitted as a book chapter, co-authored by me and Doron Rapaport.

Introduction

Subcellular compartmentalization in eukaryotic cells aids in providing optimal conditions to execute specific biochemical reactions as each compartment provides a unique physical environment and houses different combinations of metabolites, enzymes, and cofactors (Cao et al., 2020; Moon et al., 2023). Early studies suggested that these micro-environments are independent of each other, but recent discoveries demonstrate extensive crosstalk, which is partially mediated by contact sites, between the different organelles.

Mitochondria and peroxisomes communicate extensively, which is mediated by several contact sites. Furthermore, these organelles are mutually dependent and share several membrane proteins that carry out the same function in both organelles (Bittner et al., 2022b). A well-studied example is about the components of the organellar fission machinery. The dually localized fission protein Fis1 recruits the adapter protein Mdv1 and the GTPase Dnm1 to the site of division (Ihenacho et al., 2021; Mozdy et al., 2000). A similar dual distribution of fission components is observed also in mammalian cells (Koch et al., 2004, 2005; Yoon et al., 2003).

To better understand the mechanism of such dual-localization and the overall biogenesis of mitochondria and peroxisomes, it is important to develop techniques to separate these two organelles from each other and to obtain each one of them in a high purity. Subcellular fractionation techniques based on distinct density of the different organelles and various differential centrifugation steps are often used for such purposes. However, when yeast cells are grown under normal conditions, certain organelles like mitochondria and peroxisomes share strikingly similar densities. This similarity challenges the separation of these organelles from one another.

To obtain optimal yield and quality of organelles, the cultivation conditions of yeast cells, like the growth temperature and composition of growth media, are adjusted to suit the isolation requirements of the specific organelle of interest. Caution is required while disrupting the cell wall and the plasma membrane, in order to obtain a cell lysate with minimal harm to the integrity of the organelles (Rieder & Emr, 2000)

In this chapter, we describe an optimized method designed to effectively separate mitochondria and peroxisomes from each other, which is based on previous procedures (Cramer et al., 2015; Distel et al., 1996; Leighton et al., 1968; Stehlik et al., 2020). Obtaining pure fractions exclusive to each organelle has been challenging due to their remarkably similar densities, as well as the fragility and low amounts of peroxisomes under normal growth conditions. We discuss growth conditions that would favor induction of peroxisomes to increase their number and density, and portray organellar isolation followed by gradient centrifugation, enabling an improved separation from mitochondria. Additionally, we illustrate the advantage of the procedure to study the dual localization of the membrane protein Fis1.

This chapter presents a modified tool that enables the exploration of proteins' subcellular localization and facilitates the determination of whether they localize to mitochondria, peroxisomes, or both (See Figure 4.1 for a general scheme).

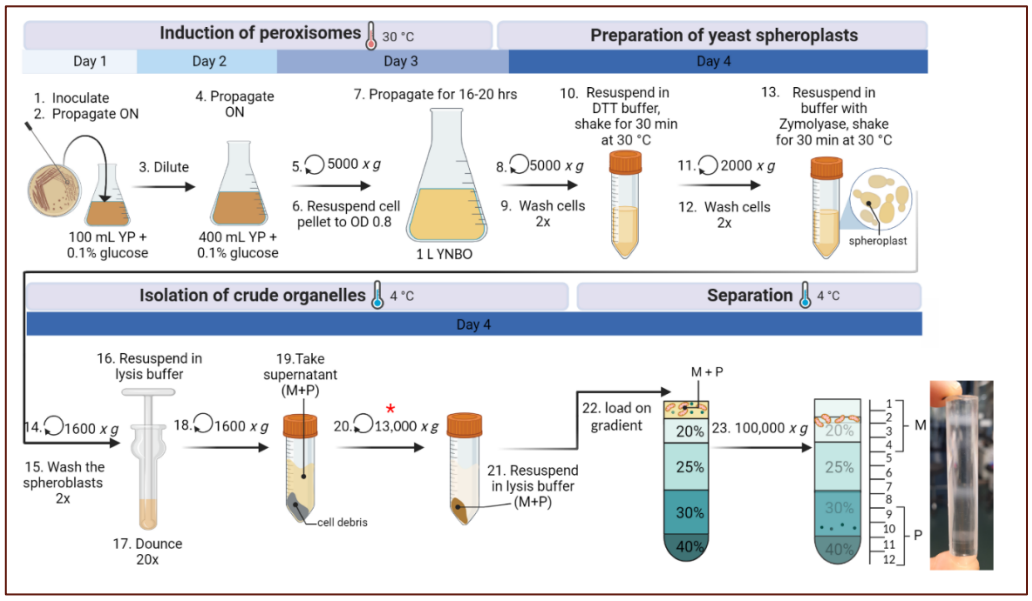

Figure 4.1: Schematic overview of the optimized procedure for separating yeast mitochondria from peroxisomes

Method

Growth conditions to induce peroxisomes

A final culture volume of 1 L is required to have enough starting material for the subcellular fractionation assay. It is important to induce peroxisomes to obtain an optimal separation of mitochondria and peroxisomes.

- For peroxisome induction, transfer generous amounts of cells from a plate into a 300 mL Erlenmeyer flask containing 100 mL of YP (2% (w/v) bacto peptone, 1% (w/v) yeast extract) + 0.1% glucose medium. Incubate the culture at 30 °C overnight in an incubator shaker.
- Next morning, increase the volume of the culture to 400 mL in a 1 L Erlenmeyer flask by adding 300 mL YP + 0.1% glucose medium to the existing 100 mL preculture. This new culture should be cultivated for 16-20 hours.
- The final step to induce peroxisomes includes transitioning the preculture grown in YP + 0.1% glucose to YNBO medium (0.1% (w/v) yeast extract, 0.17% (w/v) yeast nitrogen base, 0.5% (w/v) (NH4)2SO4, 0.0002 % (w/v) uracil, 0.0002% (w/v) adenine sulfate, a 10x mixture of 1.2% oleic acid and 2% Tween40 was sterile filtered and was added to 1x concentration together with 1% AA shortly before use). For this purpose, transfer the cell culture to a centrifuge bottle (for example, Thermo Scientific™ 1000 mL Fiberlite Bottles) and harvest the cells by centrifugation (5000 *x* g, 6 min, RT). Wash the resulting cell pellet with 50 mL sterile water once and pellet the cells again (5000 *x* g, 6 min, RT). Next, resuspend the cells in 25 mL sterile water and measure the $OD_{600\ nm}$.

Yeast cells grow very slowly when oleate is the sole carbon source. Therefore, dilute the cells to a relatively high $OD_{600\ nm}$ of 0.8 in a final 1 L culture in YNBO medium. Incubate the culture at 30 °C overnight for approximately 16 hours in an incubator shaker. To obtain optimal results, ensure that the $OD_{600\ nm}$ does not exceed 2.0 before proceeding to the next steps.

Preparation of yeast spheroplasts

Yeast cells contain a rigid polysaccharide wall that has to be removed in order to extract cell contents using osmotic stress. Prior to digesting this cell wall to obtain spheroplasts, yeast cells are treated with an EDTA-based buffer, priming the cell wall for better digestion by subsequent lytic enzymes. This breakdown is efficiently achieved by the lytic activity of Zymolyase, which hydrolyzes glucose polymers linked by β-1,3-bonds (Kitamura et al., 1971; Suzuki & Iwahashi, 2013). To prevent osmotic lysis during this process, an osmotic stabilizer like sorbitol is included in the buffer. Optimal digestion of yeast cell wall is achieved upon incubation with the enzyme at 30 °C for 45-60 min. It is possible to check whether spheroplasts have efficiently been produced by resuspending the cell suspension in either water or sorbitol buffer. Spheroplasts, in contrast to intact cells, are ruptured in water due to osmotic stress, whereas both forms are stable in sorbitol-containing solution. A five-fold decrease in the $OD_{600\,nm}$ of cells in water as compared to the absorption in sorbitol buffer is a good indication for an efficient production of spheroplasts.

- Transfer the culture from the 1 L Erlenmeyer flask to 1 L centrifuge bottles. Harvest the cells by centrifugation (5000 × g, 6 min, RT) and discard the supernatant.
- Wash the cells twice by resuspending the pellet in 30 mL of pure water, transfer them to a 50 mL tube and centrifuge (5000 × g, 6 min, RT). Weigh the cell pellet following the second wash step.
- Resuspend the pellet in 10 mL Resuspension buffer (100 mM Tris, 10 mM DTT, pH 7.4) per gram of cell weight. Incubate the cell suspension at 30 °C for 30 min with gentle agitation in a shaker incubator.
- Centrifuge the cell suspension (2000 × g, 5 min, RT) to harvest the cell pellet. Wash the cells by resuspending the pellet in 10 mL of Sorbitol buffer (20 mM HEPES, 1.2 M sorbitol, pH 7.2) per gram of cell weight and then centrifuge again as above. Repeat the washing step one more time.
- Centrifuge the cell suspension (2000 × g, 5 min, RT) to harvest the cell pellet. As a final step to digest the yeast cell wall efficiently, resuspend the cell pellet in 10 mL

Spheroplasting buffer (Sorbitol buffer + 8.58mg Zymolyase/g of cells) per gram of cell weight. Incubate this cell suspension at 30 °C for one hour with gentle agitation in a shaker incubator.

- To check if yeast spheroplasts were produced efficiently, resuspend 100 µL of the cell suspension in 900 µL of either water or Sorbitol buffer. Wait for 2 min and measure the OD_{600}. An ideal indicator for the optimal production of spheroplasts would be if the absorbance of the cell suspension in water is 5-fold lower than that in the Sorbitol buffer. If such a decrease is not observed, it is recommended to extend the incubation with zymolyase by an additional 15 min.

Preparation of yeast cell lysates and isolation of crude organelles

The basic method to obtain cell lysate relies on a controlled osmotic shock combined with mechanical homogenization (Daum et al., 1982). Dounce homogenization forces the cell suspension to pass through a very narrow space and thereby shears the cell membranes (Dey et al., 1997). This lysing process is facilitated by employing a hypotonic solution, causing cell swelling and rapid bursting under shearing forces. To isolate crude organelles from the whole cell lysates, differential centrifugation is commonly used. This technique relies on the different densities and size of the individual organelles that allow them to have variable sedimentation rates. This allows for pelleting larger organelles like the nuclei along with cell debris and unbroken cells upon low-speed centrifugation at around 2000 *x* g (Bourne, 1970). At higher centrifugation speeds of 13,000 -18,000 *x* g, mitochondria, peroxisomes, and parts of the ER sediment. To obtain purer fractions of these organelles, density gradient centrifugations must be employed. Here, we focus only on obtaining pure mitochondria and peroxisomal fractions.

Preparation of yeast cell lysate

- Centrifuge the spheroplasts (1600 *x* g, 10 min, 4 °C) to harvest them. To remove zymolyase from the spheroplast suspension, wash them by gently resuspending them in 10 mL of cold Sorbitol buffer per gram of cell weight and repeat the

centrifugation as above. Altogether, wash the spheroplasts three times to ensure the removal of zymolyase.

- Resuspend the pelleted spheroplasts gently by using a cut pipette tip. Use 15 mL Lysis buffer (5mM MES, 0.5 mM EDTA, 1mM KCL. Add 0.6 M Sorbitol, 1x Proteinase Inhibitor and 2 mM PMSF before use, pH 5.5) per gram of cell weight.
- In an ice bath, transfer the suspension to a Dounce homogenizer and dounce it 20 times (counting up and down strokes as one). This mechanical action, combined with the hypotonic buffer, ruptures the yeast spheroplasts, releasing their cellular contents into the buffer.

Isolating crude organelles from yeast cell lysate

- Clarify the cell lysate by centrifuging it (1600 *x* g, 10 min, 4 °C). The resulting pellet contains nuclei and cell debris, while the post nuclear supernatant (PNS) contains cytosol and organelles. Carefully transfer the supernatant to another 50 mL falcon tube, ensuring that cell debris are not included. Repeat this clarifying spin twice to remove most of the impurities in the cell lysate and keep the supernatant after each step.
- To isolate crude organelle fraction, which contains mitochondria and peroxisomes, the cell lysate is centrifuged (13,000 *x* g, 10 min, 4 °C). The pellet contains the crude organelles while the supernatant represents the cytosol. Resuspend the pelleted organelles in approximately 1 mL of Lysis buffer and dilute the suspension to an $OD_{600\ nm}$ of 4.

Discontinuous gradient to separate mitochondria and peroxisomes

To further separate mitochondria and peroxisomes from each other, we employ density gradient centrifugation. We layer the sample that comprises of a mixture of both organelles on top of a step gradient of different percentages of Histodenz, where the highest percentage is present in the bottom of the tube (Figure 4.1). Upon centrifugation, the organelles sediment to a position on the gradient that is in equilibrium to the density of the organelle itself. Mitochondria were found to be

concentrated at the top third of the gradient whereas peroxisomes were found at the bottom third of the gradient.

- For one gradient, prepare aliquots of 415 µL 40%, 830 µL 30%, 830 µL 25%, and 415 µL 20% Histodenz solution. Carefully layer these volumes starting from the highest to lowest density in a polycarbonate centrifuge tube using a Pasteur pipette. Once the gradient is layered, distinct lines at the interfaces between the different solutions should be visible.
- Add the crude organelles mixture that was isolated on top of the gradient, using a cut pipette tip. The samples in the tubes opposite of each other must be carefully balanced against one another.
- Place the tubes in an appropriate swing-out bucket rotor (we have had good experience with SW60Ti) and make sure to include all the buckets of the rotor (including the empty ones) before starting the spin.
- Centrifuge the gradients in an ultracentrifuge (100,000 x g, 90 min, 4 °C) with acceleration at 7 and brakes/deceleration at 0 to prevent disturbing the gradient by sudden braking.
- Meanwhile, if the samples are intended to be used directly for SDS-PAGE and Western blot, prepare 12 tubes, each with 30 µL of 8X Laemmli solution including 5% β-mercaptoethanol.
- Once the centrifuge has stopped completely, carefully remove the gradient tubes out of the rotor buckets using forceps and place them on ice. The gradient can be divided into 12 equal fractions of 234 µL. Take 12 such fractions out cautiously from the top of the gradient using an extended pipette tip and transfer them into the tubes containing the sample solution.
- Heat the samples in the loading dye at 95 °C for 5 minutes. These samples can be directly analyzed by SDS-PAGE or stored at -20 °C.

To check the effectiveness of organelle separation, we analyze the fractions by loading 100 µL of each fraction on a 12.5% SDS-PAGE, followed by blotting onto a nitrocellulose membrane. We immunodecorated the membranes with antibodies

against mitochondrial and peroxisomal marker membrane proteins. We observe that the first four fractions (fractions 1-4) are enriched in the mitochondrial marker protein Tom20, whereas the last four fractions (fractions 9-12) are enriched in the peroxisomal marker protein Pex14. Fis1, which is a dually localized protein that is present at the membranes of both organelles, is indeed detectable in fractions 1-4 and fractions 9-12 (Figure 4.2)

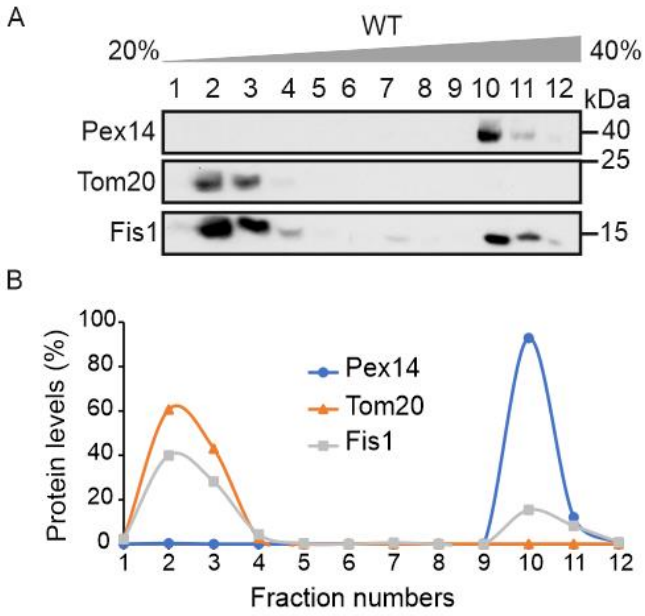

Figure 4.2: The gradient centrifugation provides a reliable method to separate mitochondria from peroxisomes. (A) A mixture of both organelles, mitochondria and peroxisome from WT yeast cells grown on rich oleate-containing medium was loaded on top a step gradient and 12 fractions were collected from the gradient and analyzed by SDS-PAGE and immunodecoration antibodies against Pex14 (peroxisomal membrane), Tom20 (mitochondrial outer membrane), and Fis1 (dually localized to mitochondria and peroxisomes). **(B)** The intensities of the different bands in the gels shown in (A) were quantified and the relative portion in each fraction is shown. The sum of each protein in all the fractions was set to 100%.

Acknowledgements

I would like to express my sincere gratitude to my supervisor, Prof. Dr. Doron Rapaport, for giving me the opportunity to work on this project and for guiding me through every obstacle in this scientific journey. I am also immensely thankful to my collaborators, Prof. Dr. Maya Schuldiner and Dr. Einat Zalckvar, for their invaluable scientific input, encouragement, and support. Special thanks to Dr. Daniela Vitali for initiating this project, and to Jessica Oberst, whose bachelor thesis generated valuable results for this work. I also had the incredible opportunity to work on a second project, and I am grateful to Maya, Doron, and Naama for providing this chance.

I would like to extend my heartfelt thanks to Prof. Dr. Ralf-Peter Jansen for being my second supervisor and for reviewing this thesis despite the tight timeline. I am grateful to my Ph.D. defense examiners, Prof. Gabriele Dodt and Prof. Michael Filarsky, for making the time to be part of the committee. My sincere thanks go to Dr. Kai Dimmer for his valuable scientific inputs.

To Vitasta, Roza, Zak, John, Alex, Julia, Elena, and the entire lab team, I am very grateful for your support and cheerfulness during the challenging times in the lab and for the fun moments outside of it. I am especially thankful to Julia for her current help with the project revisions.

Lastly, I would like to give special thanks to my family—Amma, Appa, Anna and Manni—who have been a great pillar of strength throughout this process. To Nikas, for assisting me with all the German translations and for all the support. To Srishti, Rupsa, and Avani, for being amazing friends.

References

Ahting, U., Waizenegger, T., Neupert, W., & Rapaport, D. (2005). Signal-anchored Proteins Follow a Unique Insertion Pathway into the Outer Membrane of Mitochondria *. *Journal of Biological Chemistry*, *280*(1), 48–53. https://doi.org/10.1074/jbc.M410905200

Alsayyah, C., Singh, M. K., Morcillo-Parra, M. A., Cavellini, L., Shai, N., Schmitt, C., Schuldiner, M., Zalckvar, E., Mallet, A., Belgareh-Touzé, N., Zimmer, C., & Cohen, M. M. (2024). Mitofusin-mediated contacts between mitochondria and peroxisomes regulate mitochondrial fusion. *PLOS Biology*, *22*(4), e3002602. https://doi.org/10.1371/journal.pbio.3002602

Andersson, S. G. E., Karlberg, O., Canbäck, B., & Kurland, C. G. (2003). On the origin of mitochondria: A genomics perspective. *Philosophical Transactions of the Royal Society of London. Series B, Biological Sciences*, *358*(1429), 165–177; discussion 177-179. https://doi.org/10.1098/rstb.2002.1193

ARDAIL, D., POPA, I., BODENNEC, J., LOUISOT, P., SCHMITT, D., & PORTOUKALIAN, J. (2003). The mitochondria-associated endoplasmic-reticulum subcompartment (MAM fraction) of rat liver contains highly active sphingolipid-specific glycosyltransferases. *Biochemical Journal*, *371*(3), 1013–1019. https://doi.org/10.1042/bj20021834

Backes, S., Bykov, Y. S., Flohr, T., Räschle, M., Zhou, J., Lenhard, S., Krämer, L., Mühlhaus, T., Bibi, C., Jann, C., Smith, J. D., Steinmetz, L. M., Rapaport, D., Storchová, Z., Schuldiner, M., Boos, F., & Herrmann, J. M. (2021). The chaperone-binding activity of the mitochondrial surface receptor Tom70

protects the cytosol against mitoprotein-induced stress. *Cell Reports*, *35*(1), 108936. https://doi.org/10.1016/j.celrep.2021.108936

Backes, S., Hess, S., Boos, F., Woellhaf, M. W., Gödel, S., Jung, M., Mühlhaus, T., & Herrmann, J. M. (2018). Tom70 enhances mitochondrial preprotein import efficiency by binding to internal targeting sequences. *Journal of Cell Biology*, *217*(4), 1369–1382. https://doi.org/10.1083/jcb.201708044

Becker, T., Wenz, L. S., & Pfanner, N. (2012). Biogenesis of alpha-helical outer membrane proteins. *Biochimica et Biophysica Acta (BBA) - Bioenergetics*, *1817*, S67–S68. https://doi.org/10.1016/j.bbabio.2012.06.191

Beilharz, T., Egan, B., Silver, P. A., Hofmann, K., & Lithgow, T. (2003). Bipartite Signals Mediate Subcellular Targeting of Tail-anchored Membrane Proteins in Saccharomyces cerevisiae *. *Journal of Biological Chemistry*, *278*(10), 8219–8223. https://doi.org/10.1074/jbc.M212725200

Bhadra, P., Yadhanapudi, L., Römisch, K., & Helms, V. (2021). How does Sec63 affect the conformation of Sec61 in yeast? *PLOS Computational Biology*, *17*(3), e1008855. https://doi.org/10.1371/journal.pcbi.1008855

Bittner, E., Stehlik, T., & Freitag, J. (2022a). Sharing the wealth: The versatility of proteins targeted to peroxisomes and other organelles. *Frontiers in Cell and Developmental Biology*, *10*. https://doi.org/10.3389/fcell.2022.934331

Bittner, E., Stehlik, T., & Freitag, J. (2022b). Sharing the wealth: The versatility of proteins targeted to peroxisomes and other organelles. *Frontiers in Cell and Developmental Biology*, *10*. https://doi.org/10.3389/fcell.2022.934331

Bleazard, W., McCaffery, J. M., King, E. J., Bale, S., Mozdy, A., Tieu, Q., Nunnari, J., & Shaw, J. M. (1999). The dynamin-related GTPase Dnm1 regulates

mitochondrial fission in yeast. *Nature Cell Biology*, *1*(5), 298–304. https://doi.org/10.1038/13014

Borgese, N., Brambillasca, S., & Colombo, S. (2007). How tails guide tail-anchored proteins to their destinations. *Current Opinion in Cell Biology*, *19*(4), 368–375. https://doi.org/10.1016/j.ceb.2007.04.019

Borgese, N., Colombo, S., & Pedrazzini, E. (2003). The tale of tail-anchored proteins. *The Journal of Cell Biology*, *161*(6), 1013–1019. https://doi.org/10.1083/jcb.200303069

Borgese, N., Coy-Vergara, J., Colombo, S. F., & Schwappach, B. (2019). The Ways of Tails: The GET Pathway and more. *The Protein Journal*, *38*(3), 289–305. https://doi.org/10.1007/s10930-019-09845-4

Borgese, N., & Fasana, E. (2011). Targeting pathways of C-tail-anchored proteins. *Biochimica et Biophysica Acta (BBA) - Biomembranes*, *1808*(3), 937–946. https://doi.org/10.1016/j.bbamem.2010.07.010

Bourne, G. H. (Ed.). (1970). TWO - The structure of the cell membrane. In *Division of Labor in Cells (Second Edition)* (pp. 12–35). Academic Press. https://doi.org/10.1016/B978-0-12-119259-4.50006-6

Burri, L., Vascotto, K., Gentle, I. E., Chan, N. C., Beilharz, T., Stapleton, D. I., Ramage, L., & Lithgow, T. (2006). Integral membrane proteins in the mitochondrial outer membrane of Saccharomyces cerevisiae. *The FEBS Journal*, *273*(7), 1507–1515. https://doi.org/10.1111/j.1742-4658.2006.05171.x

Cao, X., Yang, S., Cao, C., & Zhou, Y. J. (2020). Harnessing sub-organelle metabolism for biosynthesis of isoprenoids in yeast. *Synthetic and Systems Biotechnology*, *5*(3), 179–186. https://doi.org/10.1016/j.synbio.2020.06.005

Cavalier-Smith, T. (2006). Origin of mitochondria by intracellular enslavement of a photosynthetic purple bacterium. *Proceedings of the Royal Society B: Biological Sciences*, *273*(1596), 1943–1952. https://doi.org/10.1098/rspb.2006.3531

Chacinska, A., Koehler, C. M., Milenkovic, D., Lithgow, T., & Pfanner, N. (2009). Importing Mitochondrial Proteins: Machineries and Mechanisms. *Cell*, *138*(4), 628–644. https://doi.org/10.1016/j.cell.2009.08.005

Chartron, J. W., Clemons, W. M., & Suloway, C. J. (2012). The complex process of GETting tail-anchored membrane proteins to the ER. *Current Opinion in Structural Biology*, *22*(2), 217–224. https://doi.org/10.1016/j.sbi.2012.03.001

Chartron, J. W., Gonzalez, G. M., & Clemons, W. M. (2011). A Structural Model of the Sgt2 Protein and Its Interactions with Chaperones and the Get4/Get5 Complex *. *Journal of Biological Chemistry*, *286*(39), 34325–34334. https://doi.org/10.1074/jbc.M111.277798

Chen, Y., Pieuchot, L., Loh, R. A., Yang, J., Kari, T. M. A., Wong, J. Y., & Jedd, G. (2014). Hydrophobic handoff for direct delivery of peroxisome tail-anchored proteins. *Nature Communications*, *5*(1), 5790. https://doi.org/10.1038/ncomms6790

Chio, U. S., Cho, H., & Shan, S.-O. (2017). Mechanisms of Tail-Anchored Membrane Protein Targeting and Insertion. *Annual Review of Cell and Developmental Biology*, *33*, 417–438. https://doi.org/10.1146/annurev-cellbio-100616-060839

Cho, H., & Shan, S. (2018). Substrate relay in an Hsp70-cochaperone cascade safeguards tail-anchored membrane protein targeting. *The EMBO Journal*, *37*(16), e99264. https://doi.org/10.15252/embj.201899264

Cho, H., Shim, W. J., Liu, Y., & Shan, S. (2021). J-domain proteins promote client relay from Hsp70 during tail-anchored membrane protein targeting. *Journal of Biological Chemistry*, *296*, 100546. https://doi.org/10.1016/j.jbc.2021.100546

Cichocki, B. A., Krumpe, K., Vitali, D. G., & Rapaport, D. (2018). Pex19 is involved in importing dually targeted tail-anchored proteins to both mitochondria and peroxisomes. *Traffic*, *19*(10), 770–785. https://doi.org/10.1111/tra.12604

Cohen, Y., & Schuldiner, M. (2011). Advanced Methods for High-Throughput Microscopy Screening of Genetically Modified Yeast Libraries. In G. Cagney & A. Emili (Eds.), *Network Biology* (Vol. 781, pp. 127–159). Humana Press. https://doi.org/10.1007/978-1-61779-276-2_8

Cory, S., & Adams, J. M. (2002). The Bcl2 family: Regulators of the cellular life-or-death switch. *Nature Reviews Cancer*, *2*(9), Article 9. https://doi.org/10.1038/nrc883

Costello, J. L., Castro, I. G., Camões, F., Schrader, T. A., McNeall, D., Yang, J., Giannopoulou, E.-A., Gomes, S., Pogenberg, V., Bonekamp, N. A., Ribeiro, D., Wilmanns, M., Jedd, G., Islinger, M., & Schrader, M. (2017). Predicting the targeting of tail-anchored proteins to subcellular compartments in mammalian cells. *Journal of Cell Science*, *130*(9), 1675–1687. https://doi.org/10.1242/jcs.200204

Cramer, J., Effelsberg, D., Girzalsky, W., & Erdmann, R. (2015). Large-Scale Purification of Peroxisomes for Preparative Applications. *Cold Spring Harbor Protocols*, *2015*(9), pdb.prot083725. https://doi.org/10.1101/pdb.prot083725

Das, R., & Chakrabarti, O. (2020). Mitochondrial hyperfusion: A friend or a foe. *Biochemical Society Transactions*, *48*(2), 631–644. https://doi.org/10.1042/BST20190987

Daum, G., Böhni, P. C., & Schatz, G. (1982). Import of proteins into mitochondria. Cytochrome b2 and cytochrome c peroxidase are located in the intermembrane space of yeast mitochondria. *Journal of Biological Chemistry*, *257*(21), 13028–13033. https://doi.org/10.1016/S0021-9258(18)33617-2

Demishtein-Zohary, K., & Azem, A. (2017). The TIM23 mitochondrial protein import complex: Function and dysfunction. *Cell and Tissue Research*, *367*(1), 33–41. https://doi.org/10.1007/s00441-016-2486-7

Denic, V., Dötsch, V., & Sinning, I. (2013). Endoplasmic Reticulum Targeting and Insertion of Tail-Anchored Membrane Proteins by the GET Pathway. *Cold Spring Harbor Perspectives in Biology*, *5*(8), a013334. https://doi.org/10.1101/cshperspect.a013334

Dey, P. M., Brownleader, M. D., & Harborne, J. B. (1997). 1—The Plant, the Cell and its Molecular Components. In P. M. Dey & J. B. Harborne (Eds.), *Plant Biochemistry* (pp. 1–47). Academic Press. https://doi.org/10.1016/B978-012214674-9/50002-3

Distel, B., van der Leij, I., & Kos, W. (1996). Peroxisome Isolation. In I. H. Evans (Ed.), *Yeast Protocols: Methods in Cell and Molecular Biology* (pp. 133–138). Humana Press. https://doi.org/10.1385/0-89603-319-8:133

Doan, K. N., Grevel, A., Mårtensson, C. U., Ellenrieder, L., Thornton, N., Wenz, L.-S., Opaliński, Ł., Guiard, B., Pfanner, N., & Becker, T. (2020). The Mitochondrial Import Complex MIM Functions as Main Translocase for α-Helical Outer Membrane Proteins. *Cell Reports*, *31*(4), 107567. https://doi.org/10.1016/j.celrep.2020.107567

Dolezal, P., Likic, V., Tachezy, J., & Lithgow, T. (2006). Evolution of the molecular machines for protein import into mitochondria. *Science (New York, N.Y.)*, *313*(5785), 314–318. https://doi.org/10.1126/science.1127895

Drwesh, L., Heim, B., Graf, M., Kehr, L., Hansen-Palmus, L., Franz-Wachtel, M., Macek, B., Kalbacher, H., Buchner, J., & Rapaport, D. (2022). A network of cytosolic (co)chaperones promotes the biogenesis of mitochondrial signal-anchored outer membrane proteins. *eLife*, *11*, e77706. https://doi.org/10.7554/eLife.77706

Drwesh, L., & Rapaport, D. (2020). Biogenesis pathways of α-helical mitochondrial outer membrane proteins. *Biological Chemistry*, *401*(6–7), 677–686. https://doi.org/10.1515/hsz-2019-0440

Dukanovic, J., & Rapaport, D. (2011). Multiple pathways in the integration of proteins into the mitochondrial outer membrane. *Biochimica et Biophysica Acta (BBA) - Biomembranes*, *1808*(3), 971–980. https://doi.org/10.1016/j.bbamem.2010.06.021

Fan, A. C. Y., & Young, J. C. (2011). Function of Cytosolic Chaperones in Tom70-Mediated Mitochondrial Import. *Protein and Peptide Letters*, *18*(2), 122–131.

Fang, Y., Morrell, J. C., Jones, J. M., & Gould, S. J. (2004). PEX3 functions as a PEX19 docking factor in the import of class I peroxisomal membrane proteins. *Journal of Cell Biology*, *164*(6), 863–875. https://doi.org/10.1083/jcb.200311131

Farkas, Á., & Bohnsack, K. E. (2021). Capture and delivery of tail-anchored proteins to the endoplasmic reticulum. *Journal of Cell Biology*, *220*(8), e202105004. https://doi.org/10.1083/jcb.202105004

Foury, F., Roganti, T., Lecrenier, N., & Purnelle, B. (1998). The complete sequence of the mitochondrial genome of Saccharomyces cerevisiae. *FEBS Letters*, *440*(3), 325–331. https://doi.org/10.1016/s0014-5793(98)01467-7

Fujiki, Y., Matsuzono, Y., Matsuzaki, T., & Fransen, M. (2006). Import of peroxisomal membrane proteins: The interplay of Pex3p- and Pex19p-mediated interactions. *Biochimica Et Biophysica Acta*, *1763*(12), 1639–1646. https://doi.org/10.1016/j.bbamcr.2006.09.030

Fujimoto, M., Hayashi, T., & Su, T.-P. (2012). The role of cholesterol in the association of endoplasmic reticulum membranes with mitochondria. *Biochemical and Biophysical Research Communications*, *417*(1), 635–639. https://doi.org/10.1016/j.bbrc.2011.12.022

Gakh, O., Cavadini, P., & Isaya, G. (2002). Mitochondrial processing peptidases. *Biochimica et Biophysica Acta (BBA) - Molecular Cell Research*, *1592*(1), 63–77. https://doi.org/10.1016/S0167-4889(02)00265-3

Gallego, O., Betts, M. J., Gvozdenovic-Jeremic, J., Maeda, K., Matetzki, C., Aguilar-Gurrieri, C., Beltran-Alvarez, P., Bonn, S., Fernández-Tornero, C., Jensen, L. J., Kuhn, M., Trott, J., Rybin, V., Müller, C. W., Bork, P., Kaksonen, M., Russell, R. B., & Gavin, A. (2010). A systematic screen for protein–lipid interactions in Saccharomyces cerevisiae. *Molecular Systems Biology*, *6*(1), 430. https://doi.org/10.1038/msb.2010.87

Genge, M. G., & Mokranjac, D. (2022). Coordinated Translocation of Presequence-Containing Precursor Proteins Across Two Mitochondrial Membranes: Knowns and Unknowns of How TOM and TIM23 Complexes Cooperate With Each Other. *Frontiers in Physiology*, *12*, 806426. https://doi.org/10.3389/fphys.2021.806426

Götte, K., Girzalsky, W., Linkert, M., Baumgart, E., Kammerer, S., Kunau, W.-H., & Erdmann, R. (1998). Pex19p, a Farnesylated Protein Essential for Peroxisome Biogenesis. *Molecular and Cellular Biology*, *18*(1), 616–628. https://doi.org/10.1128/MCB.18.1.616

Guna, A., & Hegde, R. S. (2018). Transmembrane Domain Recognition during Membrane Protein Biogenesis and Quality Control. *Current Biology: CB*, *28*(8), R498–R511. https://doi.org/10.1016/j.cub.2018.02.004

Gupta, A., & Becker, T. (2021). Mechanisms and pathways of mitochondrial outer membrane protein biogenesis. *Biochimica et Biophysica Acta (BBA) - Bioenergetics*, *1862*(1), 148323. https://doi.org/10.1016/j.bbabio.2020.148323

Haastrup, M. O., Vikramdeo, K. S., Singh, S., Singh, A. P., & Dasgupta, S. (2023). The Journey of Mitochondrial Protein Import and the Roadmap to Follow. *International Journal of Molecular Sciences*, *24*(3), 2479. https://doi.org/10.3390/ijms24032479

Hann, B. C., & Walter, P. (1991). The signal recognition particle in S. cerevisiae. *Cell*, *67*(1), 131–144. https://doi.org/10.1016/0092-8674(91)90577-L

Haucke, V., Ocana, C. S., Hönlinger, A., Tokatlidis, K., Pfanner, N., & Schatz, G. (1997). Analysis of the Sorting Signals Directing NADH-Cytochrome b5 Reductase to Two Locations within Yeast Mitochondria. *Molecular and Cellular Biology*, *17*(7), 4024–4032. https://doi.org/10.1128/MCB.17.7.4024

Hegde, R. S., & Keenan, R. J. (2011). Tail-anchored membrane protein insertion into the endoplasmic reticulum. *Nature Reviews. Molecular Cell Biology*, *12*(12), 787–798. https://doi.org/10.1038/nrm3226

Herrmann, J. M., & Bykov, Y. (2023). Protein translocation in mitochondria: Sorting out the Toms, Tims, Pams, Sams and Mia. *FEBS Letters*, *597*(12), 1553–1554. https://doi.org/10.1002/1873-3468.14614

Hiltunen, J. K., Mursula, A. M., Rottensteiner, H., Wierenga, R. K., Kastaniotis, A. J., & Gurvitz, A. (2003). The biochemistry of peroxisomal β-oxidation in the yeast Saccharomyces cerevisiae. *FEMS Microbiology Reviews*, *27*(1), 35–64. https://doi.org/10.1016/S0168-6445(03)00017-2

Hoppins, S., Lackner, L., & Nunnari, J. (2007). The Machines that Divide and Fuse Mitochondria. *Annual Review of Biochemistry*, *76*(Volume 76, 2007), 751–780. https://doi.org/10.1146/annurev.biochem.76.071905.090048

Ihenacho, U. K., Meacham, K. A., Harwig, M. C., Widlansky, M. E., & Hill, R. B. (2021). Mitochondrial Fission Protein 1: Emerging Roles in Organellar Form and Function in Health and Disease. *Frontiers in Endocrinology*, *12*. https://doi.org/10.3389/fendo.2021.660095

Isakoff, S. J., Cardozo, T., Andreev, J., Li, Z., Ferguson, K. M., Abagyan, R., Lemmon, M. A., Aronheim, A., & Skolnik, E. Y. (1998). Identification and analysis of PH domain-containing targets of phosphatidylinositol 3-kinase using a novel in vivo assay in yeast. *The EMBO Journal*, *17*(18), 5374–5387. https://doi.org/10.1093/emboj/17.18.5374

Janke, C., Magiera, M. M., Rathfelder, N., Taxis, C., Reber, S., Maekawa, H., Moreno-Borchart, A., Doenges, G., Schwob, E., Schiebel, E., & Knop, M. (2004). A versatile toolbox for PCR-based tagging of yeast genes: New fluorescent proteins, more markers and promoter substitution cassettes. *Yeast (Chichester, England)*, *21*(11), 947–962. https://doi.org/10.1002/yea.1142

Jansen, R. L. M., & van der Klei, I. J. (2019). The peroxisome biogenesis factors Pex3 and Pex19: Multitasking proteins with disputed functions. *FEBS Letters*, *593*(5), 457–474. https://doi.org/10.1002/1873-3468.13340

Johansson, K. E., Mashahreh, B., Hartmann-Petersen, R., Ravid, T., & Lindorff-Larsen, K. (2023). Prediction of Quality-control Degradation Signals in Yeast Proteins. *Journal of Molecular Biology*, *435*(2), 167915. https://doi.org/10.1016/j.jmb.2022.167915

John, P., & Whatley, F. R. (1975). Paracoccus denitrificans and the evolutionary origin of the mitochondrion. *Nature*, *254*(5500), 495–498. https://doi.org/10.1038/254495a0

Jores, T., Lawatscheck, J., Beke, V., Franz-Wachtel, M., Yunoki, K., Fitzgerald, J. C., Macek, B., Endo, T., Kalbacher, H., Buchner, J., & Rapaport, D. (2018). Cytosolic Hsp70 and Hsp40 chaperones enable the biogenesis of mitochondrial β-barrel proteins. *Journal of Cell Biology*, *217*(9), 3091–3108. https://doi.org/10.1083/jcb.201712029

Kemper, C., Habib, S. J., Engl, G., Heckmeyer, P., Dimmer, K. S., & Rapaport, D. (2008). Integration of tail-anchored proteins into the mitochondrial outer membrane does not require any known import components. *Journal of Cell Science*, *121*(12), 1990–1998. https://doi.org/10.1242/jcs.024034

Kim, H., Botelho, S. C., Park, K., & Kim, H. (2015). Use of carbonate extraction in analyzing moderately hydrophobic transmembrane proteins in the mitochondrial inner membrane. *Protein Science : A Publication of the Protein Society*, *24*(12), 2063–2069. https://doi.org/10.1002/pro.2817

Kitamura, K., Kaneko, T., & Yamamoto, Y. (1971). Lysis of viable yeast cells by enzymes of Arthrobacter luteus. *Archives of Biochemistry and Biophysics*, *145*(1), 402–404. https://doi.org/10.1016/0003-9861(71)90053-1

Koch, A., Schneider, G., Lüers, G. H., & Schrader, M. (2004). Peroxisome elongation and constriction but not fission can occur independently of dynamin-like protein 1. *Journal of Cell Science*, *117*(17), 3995–4006. https://doi.org/10.1242/jcs.01268

Koch, A., Yoon, Y., Bonekamp, N. A., McNiven, M. A., & Schrader, M. (2005). A Role for Fis1 in Both Mitochondrial and Peroxisomal Fission in Mammalian Cells. *Molecular Biology of the Cell*, *16*(11), 5077–5086. https://doi.org/10.1091/mbc.E05-02-0159

Kreimendahl, S., & Rassow, J. (2020). *The mitochondrial outer membrane protein Tom70-mediator in protein traffic, membrane contact cites and innate immunity*. https://hss-opus.ub.ruhr-uni-bochum.de/opus4/frontdoor/index/index/year/2021/docId/7875

Krogh, A., Larsson, B., von Heijne, G., & Sonnhammer, E. L. L. (2001). Predicting transmembrane protein topology with a hidden markov model: Application to complete genomes11Edited by F. Cohen. *Journal of Molecular Biology*, *305*(3), 567–580. https://doi.org/10.1006/jmbi.2000.4315

Krumpe, K., Frumkin, I., Herzig, Y., Rimon, N., Özbalci, C., Brügger, B., Rapaport, D., & Schuldiner, M. (2012). Ergosterol content specifies targeting of tail-anchored proteins to mitochondrial outer membranes. *Molecular Biology of the Cell*, *23*(20), 3927–3935. https://doi.org/10.1091/mbc.E11-12-0994

Kühlbrandt, W. (2015). Structure and function of mitochondrial membrane protein complexes. *BMC Biology*, *13*(1), 89. https://doi.org/10.1186/s12915-015-0201-x

Kunová, N., Havalová, H., Ondrovičová, G., Stojkovičová, B., Bauer, J. A., Bauerová-Hlinková, V., Pevala, V., & Kutejová, E. (2022). Mitochondrial Processing Peptidases—Structure, Function and the Role in Human Diseases. *International Journal of Molecular Sciences*, *23*(3), 1297. https://doi.org/10.3390/ijms23031297

Kuravi, K., Nagotu, S., Krikken, A. M., Sjollema, K., Deckers, M., Erdmann, R., Veenhuis, M., & van der Klei, I. J. (2006). Dynamin-related proteins Vps1p and Dnm1p control peroxisome abundance in Saccharomyces cerevisiae. *Journal of Cell Science*, *119*(19), 3994–4001. https://doi.org/10.1242/jcs.03166

Lange, Y. (1991). Disposition of intracellular cholesterol in human fibroblasts. *Journal of Lipid Research*, *32*(2), 329–339. https://doi.org/10.1016/S0022-2275(20)42093-0

Leighton, F., Poole, B., Beaufay, H., Baudhuin, P., Coffey, J. W., Fowler, S., & De Duve, C. (1968). THE LARGE-SCALE SEPARATION OF PEROXISOMES, MITOCHONDRIA, AND LYSOSOMES FROM THE LIVERS OF RATS INJECTED WITH TRITON WR-1339. *The Journal of Cell Biology*, *37*(2), 482–513. https://doi.org/10.1083/jcb.37.2.482

Lemmon, M. A. (2004). Pleckstrin homology domains: Not just for phosphoinositides. *Biochemical Society Transactions*, *32*(5), 707–711. https://doi.org/10.1042/BST0320707

Li, Y., Dudek, J., Guiard, B., Pfanner, N., Rehling, P., & Voos, W. (2004). The presequence translocase-associated protein import motor of mitochondria.

Pam16 functions in an antagonistic manner to Pam18. *The Journal of Biological Chemistry*, *279*(36), 38047–38054. https://doi.org/10.1074/jbc.M404319200

Lin, K.-F., Fry, M. Y., Saladi, S. M., & Clemons, W. M. (2021). Molecular basis of tail-anchored integral membrane protein recognition by the cochaperone Sgt2. *The Journal of Biological Chemistry*, *296*, 100441. https://doi.org/10.1016/j.jbc.2021.100441

Liu, Q., Chang, C. E., Wooldredge, A. C., Fong, B., Kennedy, B. K., & Zhou, C. (2022). Tom70-based transcriptional regulation of mitochondrial biogenesis and aging. *eLife*, *11*, e75658. https://doi.org/10.7554/eLife.75658

Maffucci, T., & Falasca, M. (2001). Specificity in pleckstrin homology (PH) domain membrane targeting: A role for a phosphoinositide–protein co-operative mechanism. *FEBS Letters*, *506*(3), 173–179. https://doi.org/10.1016/S0014-5793(01)02909-X

Mariappan, M., Mateja, A., Dobosz, M., Bove, E., Hegde, R. S., & Keenan, R. J. (2011). The mechanism of membrane-associated steps in tail-anchored protein insertion. *Nature*, *477*(7362), 61–66. https://doi.org/10.1038/nature10362

Mark, K. G., Simonetta, M., Maiolica, A., Seller, C. A., & Toczyski, D. P. (2014). Ubiquitin Ligase Trapping Identifies an SCFSaf1 Pathway Targeting Unprocessed Vacuolar/Lysosomal Proteins. *Molecular Cell*, *53*(1), 148–161. https://doi.org/10.1016/j.molcel.2013.12.003

Mattiazzi Ušaj, M., Brložnik, M., Kaferle, P., Žitnik, M., Wolinski, H., Leitner, F., Kohlwein, S. D., Zupan, B., & Petrovič, U. (2015). Genome-Wide Localization Study of Yeast Pex11 Identifies Peroxisome–Mitochondria Interactions through the ERMES Complex. *Journal of Molecular Biology*, *427*(11), 2072–2087. https://doi.org/10.1016/j.jmb.2015.03.004

Mehlhorn, D. G., Asseck, L. Y., & Grefen, C. (2021). Looking for a safe haven: Tail-anchored proteins and their membrane insertion pathways. *Plant Physiology*, *187*(4), 1916–1928. https://doi.org/10.1093/plphys/kiab298

Mnaimneh, S., Davierwala, A. P., Haynes, J., Moffat, J., Peng, W.-T., Zhang, W., Yang, X., Pootoolal, J., Chua, G., Lopez, A., Trochesset, M., Morse, D., Krogan, N. J., Hiley, S. L., Li, Z., Morris, Q., Grigull, J., Mitsakakis, N., Roberts, C. J., … Hughes, T. R. (2004). Exploration of Essential Gene Functions via Titratable Promoter Alleles. *Cell*, *118*(1), 31–44. https://doi.org/10.1016/j.cell.2004.06.013

Mo, C., & Bard, M. (2005). A systematic study of yeast sterol biosynthetic protein–protein interactions using the split-ubiquitin system. *Biochimica et Biophysica Acta (BBA) - Molecular and Cell Biology of Lipids*, *1737*(2), 152–160. https://doi.org/10.1016/j.bbalip.2005.11.002

Moon, S. Y., Son, S.-H., Oh, S. S., & Lee, J. Y. (2023). Harnessing Cellular Organelles to Bring New Functionalities into Yeast. *Biotechnology and Bioprocess Engineering*. https://doi.org/10.1007/s12257-022-0195-5

Morgenstern, M., Peikert, C. D., Lübbert, P., Suppanz, I., Klemm, C., Alka, O., Steiert, C., Naumenko, N., Schendzielorz, A., Melchionda, L., Mühlhäuser, W. W. D., Knapp, B., Busch, J. D., Stiller, S. B., Dannenmaier, S., Lindau, C., Licheva, M., Eickhorst, C., Galbusera, R., … Warscheid, B. (2021). Quantitative high-confidence human mitochondrial proteome and its dynamics in cellular context. *Cell Metabolism*, *33*(12), 2464-2483.e18. https://doi.org/10.1016/j.cmet.2021.11.001

Motley, A. M., Ward, G. P., & Hettema, E. H. (2008). Dnm1p-dependent peroxisome fission requires Caf4p, Mdv1p and Fis1p. *Journal of Cell Science*, *121*(10), 1633–1640. https://doi.org/10.1242/jcs.026344

Mozdy, A. D., McCaffery, J. M., & Shaw, J. M. (2000). Dnm1p GTPase-mediated mitochondrial fission is a multi-step process requiring the novel integral membrane component Fis1p. *The Journal of Cell Biology*, *151*(2), 367–380. https://doi.org/10.1083/jcb.151.2.367

Nemoto, Y., & De Camilli, P. (1999). Recruitment of an alternatively spliced form of synaptojanin 2 to mitochondria by the interaction with the PDZ domain of a mitochondrial outer membrane protein. *The EMBO Journal*, *18*(11), 2991–3006. https://doi.org/10.1093/emboj/18.11.2991

Neupert, W. (2015). A Perspective on Transport of Proteins into Mitochondria: A Myriad of Open Questions. *Journal of Molecular Biology*, *427*(6, Part A), 1135–1158. https://doi.org/10.1016/j.jmb.2015.02.001

Nicolson, G. L. (2014). Mitochondrial Dysfunction and Chronic Disease: Treatment With Natural Supplements. *Integrative Medicine: A Clinician's Journal*, *13*(4), 35–43.

Nussberger, S., Ghosh, R., & Wang, S. (2024). New insights into the structure and dynamics of the TOM complex in mitochondria. *Biochemical Society Transactions*, *52*(2), 911–922. https://doi.org/10.1042/BST20231236

Okreglak, V., & Walter, P. (2014). The conserved AAA-ATPase Msp1 confers organelle specificity to tail-anchored proteins. *Proceedings of the National Academy of Sciences*, *111*(22), 8019–8024. https://doi.org/10.1073/pnas.1405755111

Ong, S.-B., Hall, A. R., & Hausenloy, D. J. (2013). Mitochondrial Dynamics in Cardiovascular Health and Disease. *Antioxidants & Redox Signaling*, *19*(4), 400–414. https://doi.org/10.1089/ars.2012.4777

Osellame, L. D., Blacker, T. S., & Duchen, M. R. (2012). Cellular and molecular mechanisms of mitochondrial function. *Best Practice & Research. Clinical Endocrinology & Metabolism*, *26*(6), 711–723. https://doi.org/10.1016/j.beem.2012.05.003

Pfanner, N., Warscheid, B., & Wiedemann, N. (2019). Mitochondrial proteins: From biogenesis to functional networks. *Nature Reviews Molecular Cell Biology*, *20*(5), Article 5. https://doi.org/10.1038/s41580-018-0092-0

Pool, M. R. (2005). Signal recognition particles in chloroplasts, bacteria, yeast and mammals (Review). *Molecular Membrane Biology*, *22*(1–2), 3–15. https://doi.org/10.1080/09687860400026348

Rabu, C., Schmid, V., Schwappach, B., & High, S. (2009). Biogenesis of tail-anchored proteins: The beginning for the end? *Journal of Cell Science*, *122*(20), 3605–3612. https://doi.org/10.1242/jcs.041210

Rao, M., Okreglak, V., Chio, U. S., Cho, H., Walter, P., & Shan, S. (2016). Multiple selection filters ensure accurate tail-anchored membrane protein targeting. *eLife*, *5*, e21301. https://doi.org/10.7554/eLife.21301

Rapaport, D. (2003). Finding the right organelle. *EMBO Reports*, *4*(10), 948–952. https://doi.org/10.1038/sj.embor.embor937

Rapaport, D. (2005). How does the TOM complex mediate insertion of precursor proteins into the mitochondrial outer membrane? *Journal of Cell Biology*, *171*(3), 419–423. https://doi.org/10.1083/jcb.200507147

Rapaport, D., Neupert, W., & Lill, R. (1997). Mitochondrial Protein Import: Tom40 PLAYS A MAJOR ROLE IN TARGETING AND TRANSLOCATION OF PREPROTEINS BY FORMING A SPECIFIC BINDING SITE FOR THE PRESEQUENCE*. *Journal of Biological Chemistry*, *272*(30), 18725–18731. https://doi.org/10.1074/jbc.272.30.18725

Regev-Rudzki, N., & Pines, O. (2007). Eclipsed distribution: A phenomenon of dual targeting of protein and its significance. *BioEssays*, *29*(8), 772–782. https://doi.org/10.1002/bies.20609

Ridsdale, A., Denis, M., Gougeon, P.-Y., Ngsee, J. K., Presley, J. F., & Zha, X. (2006). Cholesterol Is Required for Efficient Endoplasmic Reticulum-to-Golgi Transport of Secretory Membrane Proteins. *Molecular Biology of the Cell*, *17*(4), 1593–1605. https://doi.org/10.1091/mbc.e05-02-0100

Rieder, S. E., & Emr, S. D. (2000). Overview of Subcellular Fractionation Procedures for the Yeast Saccharomyces cerevisiae. *Current Protocols in Cell Biology*, *7*(1), 3.7.1-3.7.25. https://doi.org/10.1002/0471143030.cb0307s07

Rome, M. E., Rao, M., Clemons, W. M., & Shan, S. (2013). Precise timing of ATPase activation drives targeting of tail-anchored proteins. *Proceedings of the National Academy of Sciences of the United States of America*, *110*(19), 7666–7671. https://doi.org/10.1073/pnas.1222054110

Sayyed, U. Mohd. H., & Mahalakshmi, R. (2022). Mitochondrial protein translocation machinery: From TOM structural biogenesis to functional regulation. *The Journal of Biological Chemistry*, *298*(5), 101870. https://doi.org/10.1016/j.jbc.2022.101870

Scheffzek, K., & Welti, S. (2012). Pleckstrin homology (PH) like domains – versatile modules in protein–protein interaction platforms. *FEBS Letters*, *586*(17), 2662–2673. https://doi.org/10.1016/j.febslet.2012.06.006

Schlacht, A., Herman, E. K., Klute, M. J., Field, M. C., & Dacks, J. B. (2014). Missing pieces of an ancient puzzle: Evolution of the eukaryotic membrane-trafficking system. *Cold Spring Harbor Perspectives in Biology*, *6*(10), a016048. https://doi.org/10.1101/cshperspect.a016048

Schlossmann, J., Lill, R., Neupert, W., & Court, D. A. (1996). Tom71, a Novel Homologue of the Mitochondrial Preprotein Receptor Tom70*. *Journal of Biological Chemistry*, *271*(30), 17890–17895. https://doi.org/10.1074/jbc.271.30.17890

Schneider, A. (2020). Evolution of mitochondrial protein import – lessons from trypanosomes. *Biological Chemistry*, *401*(6–7), 663–676. https://doi.org/10.1515/hsz-2019-0444

Schrader, M., Costello, J. L., Godinho, L. F., Azadi, A. S., & Islinger, M. (2016). Proliferation and fission of peroxisomes—An update. *Biochimica et Biophysica Acta (BBA) - Molecular Cell Research*, *1863*(5), 971–983. https://doi.org/10.1016/j.bbamcr.2015.09.024

Schrader, T. A., Carmichael, R. E., Islinger, M., Costello, J. L., Hacker, C., Bonekamp, N. A., Weishaupt, J. H., Andersen, P. M., & Schrader, M. (2022). PEX11β and FIS1 cooperate in peroxisome division independently of mitochondrial fission factor. *Journal of Cell Science*, *135*(13), jcs259924. https://doi.org/10.1242/jcs.259924

Schuldiner, M., Metz, J., Schmid, V., Denic, V., Rakwalska, M., Schmitt, H. D., Schwappach, B., & Weissman, J. S. (2008). The GET Complex Mediates

Insertion of Tail-Anchored Proteins into the ER Membrane. *Cell*, *134*(4), 634–645. https://doi.org/10.1016/j.cell.2008.06.025

Scorrano, L., De Matteis, M. A., Emr, S., Giordano, F., Hajnóczky, G., Kornmann, B., Lackner, L. L., Levine, T. P., Pellegrini, L., Reinisch, K., Rizzuto, R., Simmen, T., Stenmark, H., Ungermann, C., & Schuldiner, M. (2019). Coming together to define membrane contact sites. *Nature Communications*, *10*(1), 1287. https://doi.org/10.1038/s41467-019-09253-3

Setoguchi, K., Otera, H., & Mihara, K. (2006). Cytosolic factor- and TOM-independent import of C-tail-anchored mitochondrial outer membrane proteins. *The EMBO Journal*, *25*(24), 5635–5647. https://doi.org/10.1038/sj.emboj.7601438

Shai, N., Schuldiner, M., & Zalckvar, E. (2016). No peroxisome is an island—Peroxisome contact sites. *Biochimica et Biophysica Acta (BBA) - Molecular Cell Research*, *1863*(5), 1061–1069. https://doi.org/10.1016/j.bbamcr.2015.09.016

Shai, N., Yifrach, E., van Roermund, C. W. T., Cohen, N., Bibi, C., IJlst, L., Cavellini, L., Meurisse, J., Schuster, R., Zada, L., Mari, M. C., Reggiori, F. M., Hughes, A. L., Escobar-Henriques, M., Cohen, M. M., Waterham, H. R., Wanders, R. J. A., Schuldiner, M., & Zalckvar, E. (2018). Systematic mapping of contact sites reveals tethers and a function for the peroxisome-mitochondria contact. *Nature Communications*, *9*(1), 1761. https://doi.org/10.1038/s41467-018-03957-8

Shao, S., & Hegde, R. S. (2011). Membrane Protein Insertion at the Endoplasmic Reticulum. *Annual Review of Cell and Developmental Biology*, *27*(1), 25–56. https://doi.org/10.1146/annurev-cellbio-092910-154125

Shaw, J. M., & Nunnari, J. (2002). Mitochondrial dynamics and division in budding yeast. *Trends in Cell Biology*, *12*(4), 178–184.

Sirrenberg, C., Endres, M., Fölsch, H., Stuart, R. A., Neupert, W., & Brunner, M. (1998). Carrier protein import into mitochondria mediated by the intermembrane proteins Tim10/Mrs11 and Tim12/Mrs5. *Nature*, *391*(6670), 912–915. https://doi.org/10.1038/36136

Song, J., Tamura, Y., Yoshihisa, T., & Endo, T. (2014). A novel import route for an N-anchor mitochondrial outer membrane protein aided by the TIM23 complex. *EMBO Reports*, *15*. https://doi.org/10.1002/embr.201338142

Stefanovic, S., & Hegde, R. S. (2007). Identification of a Targeting Factor for Posttranslational Membrane Protein Insertion into the ER. *Cell*, *128*(6), 1147–1159. https://doi.org/10.1016/j.cell.2007.01.036

Stehlik, T., Kremp, M., Kahnt, J., Bölker, M., & Freitag, J. (2020). Peroxisomal targeting of a protein phosphatase type 2C via mitochondrial transit. *Nature Communications*, *11*(1), Article 1. https://doi.org/10.1038/s41467-020-16146-3

Stein, I., Peleg, Y., Even-Ram, S., & Pines, O. (1994). The Single Translation Product of the FUM1 Gene (Fumarase) Is Processed in Mitochondria before Being Distributed between the Cytosol and Mitochondria in Saccharomyces cerevisiae. *Molecular and Cellular Biology*, *14*(7), 4770–4778. https://doi.org/10.1128/mcb.14.7.4770-4778.1994

Stenger, M., Le, D. T., Klecker, T., & Westermann, B. (2020). Systematic analysis of nuclear gene function in respiratory growth and expression of the mitochondrial genome in S. cerevisiae. *Microbial Cell*, *7*(9), 234–249. https://doi.org/10.15698/mic2020.09.729

Stojanovski, D., Müller, J. M., Milenkovic, D., Guiard, B., Pfanner, N., & Chacinska, A. (2008). The MIA system for protein import into the mitochondrial intermembrane

space. *Biochimica et Biophysica Acta (BBA) - Molecular Cell Research*, *1783*(4), 610–617. https://doi.org/10.1016/j.bbamcr.2007.10.004

Stuart, R. (2002). Insertion of proteins into the inner membrane of mitochondria: The role of the Oxa1 complex. *Biochimica Et Biophysica Acta*, *1592*(1), 79–87. https://doi.org/10.1016/s0167-4889(02)00266-5

Suzuki, T., & Iwahashi, Y. (2013). RNA Preparation of Saccharomyces cerevisiae Using the Digestion Method may Give Misleading Results. *Applied Biochemistry and Biotechnology*, *169*(5), 1620–1632. https://doi.org/10.1007/s12010-012-0051-8

Vitali, D. G., Drwesh, L., Cichocki, B. A., Kolb, A., & Rapaport, D. (2020). The Biogenesis of Mitochondrial Outer Membrane Proteins Show Variable Dependence on Import Factors. *iScience*, *23*(1), 100779. https://doi.org/10.1016/j.isci.2019.100779

Waizenegger, T., Schmitt, S., Zivkovic, J., Neupert, W., & Rapaport, D. (2005). Mim1, a protein required for the assembly of the TOM complex of mitochondria. *EMBO Reports*, *6*(1), 57–62. https://doi.org/10.1038/sj.embor.7400318

Wang, F., Brown, E. C., Mak, G., Zhuang, J., & Denic, V. (2010). A Chaperone Cascade Sorts Proteins for Posttranslational Membrane Insertion into the Endoplasmic Reticulum. *Molecular Cell*, *40*(1), 159–171. https://doi.org/10.1016/j.molcel.2010.08.038

Wang, F., Whynot, A., Tung, M., & Denic, V. (2011). The mechanism of tail-anchored protein insertion into the ER membrane. *Molecular Cell*, *43*(5), 738–750. https://doi.org/10.1016/j.molcel.2011.07.020

Wiedemann, N., & Pfanner, N. (2017). Mitochondrial Machineries for Protein Import and Assembly. *Annual Review of Biochemistry*, *86*(Volume 86, 2017), 685–714. https://doi.org/10.1146/annurev-biochem-060815-014352

Wilson, J. D., & Barlowe, C. (2010). Yet1p and Yet3p, the Yeast Homologs of BAP29 and BAP31, Interact with the Endoplasmic Reticulum Translocation Apparatus and Are Required for Inositol Prototrophy. *Journal of Biological Chemistry*, *285*(24), 18252–18261. https://doi.org/10.1074/jbc.M109.080382

Wilson, J. D., Thompson, S. L., & Barlowe, C. (2011). Yet1p-Yet3p interacts with Scs2p-Opi1p to regulate ER localization of the Opi1p repressor. *Molecular Biology of the Cell*, *22*(9), 1430–1439. https://doi.org/10.1091/mbc.E10-07-0559

Yamamoto, H., Fukui, K., Takahashi, H., Kitamura, S., Shiota, T., Terao, K., Uchida, M., Esaki, M., Nishikawa, S., Yoshihisa, T., Yamano, K., & Endo, T. (2009). Roles of Tom70 in Import of Presequence-containing Mitochondrial Proteins*. *Journal of Biological Chemistry*, *284*(46), 31635–31646. https://doi.org/10.1074/jbc.M109.041756

Yogev, O., Naamati, A., & Pines, O. (2011). Fumarase: A paradigm of dual targeting and dual localized functions. *The FEBS Journal*, *278*(22), 4230–4242. https://doi.org/10.1111/j.1742-4658.2011.08359.x

Yoon, Y., Krueger, E. W., Oswald, B. J., & McNiven, M. A. (2003). The Mitochondrial Protein hFis1 Regulates Mitochondrial Fission in Mammalian Cells through an Interaction with the Dynamin-Like Protein DLP1. *Molecular and Cellular Biology*, *23*(15), 5409–5420. https://doi.org/10.1128/MCB.23.15.5409-5420.2003

Young, J. C., Hoogenraad, N. J., & Hartl, F. U. (2003). Molecular Chaperones Hsp90 and Hsp70 Deliver Preproteins to the Mitochondrial Import Receptor Tom70. *Cell*, *112*(1), 41–50. https://doi.org/10.1016/S0092-8674(02)01250-3

Yu, J. W., Mendrola, J. M., Audhya, A., Singh, S., Keleti, D., DeWald, D. B., Murray, D., Emr, S. D., & Lemmon, M. A. (2004). Genome-Wide Analysis of Membrane Targeting by *S. cerevisiae* Pleckstrin Homology Domains. *Molecular Cell*, *13*(5), 677–688. https://doi.org/10.1016/S1097-2765(04)00083-8

Zanphorlin, L. M., Lima, T. B., Wong, M. J., Balbuena, T. S., Minetti, C. A. S. A., Remeta, D. P., Young, J. C., Barbosa, L. R. S., Gozzo, F. C., & Ramos, C. H. I. (2016). Heat Shock Protein 90 kDa (Hsp90) Has a Second Functional Interaction Site with the Mitochondrial Import Receptor Tom70*. *Journal of Biological Chemistry*, *291*(36), 18620–18631. https://doi.org/10.1074/jbc.M115.710137

Zeth, K. (2010). Structure and evolution of mitochondrial outer membrane proteins of beta-barrel topology. *Biochimica Et Biophysica Acta*, *1797*(6–7), 1292–1299. https://doi.org/10.1016/j.bbabio.2010.04.019

Zhou, J., Jung, M., Dimmer, K. S., & Rapaport, D. (2022). The multi-factor modulated biogenesis of the mitochondrial multi-span protein Om14. *Journal of Cell Biology*, *221*(4), e202112030. https://doi.org/10.1083/jcb.202112030

Zorova, L. D., Popkov, V. A., Plotnikov, E. Y., Silachev, D. N., Pevzner, I. B., Jankauskas, S. S., Babenko, V. A., Zorov, S. D., Balakireva, A. V., Juhaszova, M., Sollott, S. J., & Zorov, D. B. (2018). Mitochondrial membrane potential. *Analytical Biochemistry*, *552*, 50–59. https://doi.org/10.1016/j.ab.2017.07.009

Zung, N., Aravindan, N., Boshnakovska, A., Valenti, R., Preminger, N., Jonas, F., Yaakov, G., Willoughby, M. M., Homberg, B., Keller, J., Kupervaser, M.,

Dezorella, N., Dadosh, T., Wolf, S. G., Itkin, M., Malitsky, S., Brandis, A., Barkai, N., Fernández-Busnadiego, R., … Schuldiner, M. (2024). *The molecular mechanism of on-demand sterol biosynthesis at organelle contact sites* (p. 2024.05.09.593285). bioRxiv. https://doi.org/10.1101/2024.05.09.593285

Appendix

A.1: List of Strains, Primers, Plasmids and Antibodies used in this study

Table S1: Strains used in this study.

Name	Genotype	Source
WT (BY4741)	MATa his3Δ1 leu2Δ0 met15Δ0 ura3Δ0	Lab stock
TEF2 mCherry *FIS1* (BY4741)	MATa his3Δ1 leu2Δ0 met15Δ0 ura3Δ0 lys+ can1Δ::GAL1pr-SceI::STE2pr-SpHIS5 lyp1Δ::STE3pr-LEU2 NAT::TEF2pr-mCherry-Fis1	Maya Schuldiner
TEF2-mCherry *GEM1* (BY4741)	MATa his3Δ1 leu2Δ0 met15Δ0 ura3Δ0 lys+ can1Δ::GAL1pr-SceI::STE2pr-SpHIS5 lyp1Δ::STE3pr-LEU2 NAT::TEF2pr-mCherry-Gem1	Maya Schuldiner
TEF2 mCherry *FIS1*, *OM45* GFP (BY4741)	MATa his3Δ1 leu2Δ0 met15Δ0 ura3Δ0 lys+ can1Δ::GAL1pr-SceI::STE2pr-SpHIS5 lyp1Δ::STE3pr-LEU2 NAT::TEF2pr-mCherry-Fis1 OM45-GFP::hph	This study
TEF2 mCherry *FIS1*, *PEX3* GFP (BY4741)	MATa his3Δ1 leu2Δ0 met15Δ0 ura3Δ0 lys+ can1Δ::GAL1pr-SceI::STE2pr-SpHIS5 lyp1Δ::STE3pr-LEU2 NAT::TEF2pr-mCherry-Fis1 PEX3-GFP::hph	This study
TEF2-mCherry *GEM1*, *OM45* GFP (BY4741)	MATa his3Δ1 leu2Δ0 met15Δ0 ura3Δ0 lys+ can1Δ::GAL1pr-SceI::STE2pr-SpHIS5 lyp1Δ::STE3pr-LEU2 NAT::TEF2pr-mCherry-Gem1 OM45-GFP::hph	This study
TEF2-mCherry *GEM1, PEX3* GFP (BY4741)	MATa his3Δ1 leu2Δ0 met15Δ0 ura3Δ0 lys+ can1Δ::GAL1pr-SceI::STE2pr-SpHIS5, lyp1Δ::STE3pr-LEU2 NAT::TEF2pr-mCherry-Gem1 PEX3-GFP::hph	This study
mpf1Δ (BY4741)	MATa, his3Δ1, leu2Δ0, met15Δ0, ura3Δ0, YNL144C::KAN	Euroscarf
tom71Δ (BY4741)	MATa, his3Δ1, leu2Δ0, met15Δ0, ura3Δ0, YHR117W::KAN	Euroscarf
tom70Δ (BY4741)	MATa, his3Δ1, leu2Δ0, met15Δ0, ura3Δ0, YNL121C::KAN	This study
tom70/71Δ (BY4741)	MATa his3Δ1 leu2Δ0 met15Δ0 ura3Δ0 TOM70::KAN, TOM71::Nat2	This study
mpf1/tom71Δ (BY4741)	MATa his3Δ1 leu2Δ0 met15Δ0 ura3Δ0 YNL144C::KAN, YHR117W::NAT	This study
GPD Tom70 (BY4741)	MATa his3Δ1 leu2Δ0 met15Δ0 ura3Δ0 NAT::GPDpr TOM70	This study
tom71Δ, GPD *TOM70* (BY4741)	MATa his3Δ1 leu2Δ0 met15Δ0 ura3Δ0 NAT::GPDpr TOM70	This study
mpf1Δ, GPD *TOM70* (BY4741)	MATa his3Δ1 leu2Δ0 met15Δ0 ura3Δ0 NAT::GPDpr TOM70	This study
GPD *TOM71* (BY4741)	MATa his3Δ1 leu2Δ0 met15Δ0 ura3Δ0 NAT::GPDpr TOM71	This study
mpf1Δ, GPD *TOM71* (BY4741)	MATa his3Δ1 leu2Δ0 met15Δ0 ura3Δ0 NAT::GPDpr TOM71	This study
grr1Δ (BY4741)	MATa his3Δ1 leu2Δ0 met15Δ0 ura3Δ0 GRR1::kanMX4	Euroscarf

Table S2: Primers used in this study

Primer name	Sequence 5′ to 3′	Note
OM45 C' tag pYM F	TGATAAGGGTGATGGTAAATTCTGGAGCTCGA AAAAGGACcgtacgctgcaggtcgac	Genomically C-tagging Om45-GFP. Om45 flanking region + forward primer to amplify cassette from pYMS271
OM45 C' tag pYM R	TTATGCGGGAACCAACCCTTTACAATTAGCTA TCTAACTAatcgatgaattcgagctcg	Genomically C-tagging Om45-GFP. Om45 flanking region + reverse primer to amplify cassette from pYMS271
PEX3 C' tag pYM F	CAGCAACTTTGGCGTCTCCAGCTCGTTTTCCTT CAAGCCTcgtacgctgcaggtcgac	Genomically C-tagging Pex3-GFP. Pex3 flanking region + forward primer to amplify cassette from pYMS271
PEX3 C' tag pYM R	ATATATTCTGGTGTGAGTGTCAGTACTTATTCA GAGATTAatcgatgaattcgagctcg	Genomically C-tagging Pex3-GFP. Pex3 flanking region + reverse primer to amplify cassette from pYMS271
OM45 WT CHK F	ATCTTCAATTGGGGGTTTAG	Check primer for screening PCR
OM45 WT CHK R	TCTCTACCAAACTCCTGTGC	Check primer for screening PCR
PEX3 WT CHK F	TGAGCAAGCTTTCCTATCAC	Check primer for screening PCR
PEX3 WT CHK R	CTTTCGATACATTGGGTCAG	Check primer for screening PCR
DLT_Tom71_Nat_Fwd	GTATATATCTCTACATACTTGTATATACCGAAC ATAAGAAGCTCTTATG gcg cgc cag atc tgt tta g	Forward primer from *TOM71* deletion. *TOM71* flanking regions + forward primer to amplify cassette from pFA6ANATN2
DLT_Tom71_Rev	CCAGTATTAACTAAAAGTATATATTTGACCAAT ACCTGACATATCTTCTA gag ctc gat tac aac agg tg	Reverse primer from *TOM71* deletion. *TOM71* flanking regions + reverse primer to amplify cassette from pFA6ANATN2
CHK Tom71 del F	ATGGCCGAAAACTCCCTCCTGA	Check primer for screening PCR
CHK Tom71 del R	AAG CAT GCC TTT AGC CCT ATA ACG AGC TA	Check primer for screening PCR
GPD_Tom71_Nat F	TGTATATATCTCTACATACTTGTATATACCGAA CATAAGAAGCTCTTATGcgtacgctgcaggtcgac	Forward primer for overexpression of *TOM71*. *TOM71* flanking regions + forward primer that binds to pYMN15
GPD_Tom71_Nat R	AGGATGGCCACTTTGTTCTTGGTGATAAACCT CAGGAGGGAGTTTTCGGCcatcgatgaattctctgtc g	Reverse primer for overexpression of *TOM71*. *TOM71* flanking regions + reverse primer that binds to pYMN15
CHK GPD Tom71 F	GAC CCA CGC ATG TAT CTA TC	Check primer for screening PCR
CHK GPD Tom71 R	CAG GTC TGC AGC GAG GAG	Check primer for screening PCR
GPD_Tom70_Nat F	AGATTCGGAAGTGAAATTACAGCTCACATCTA GGTTCTCAATTGCCAATGcgtacgctgcaggtcgac	Forward primer from *TOM70* deletion. *TOM70* flanking regions + forward primer to amplify cassette from pFA6ANATN2
GPD_Tom70_Nat R	GCAGCAACGGTTGCCAAAATGGCTGTCTTGTT CCTTGTAATGAAGCTCTTcatcgatgaattctctgtcg	Reverse primer from *TOM70* deletion. *TOM70* flanking regions + reverse primer to amplify cassette from pFA6ANATN2
CHK GPD Tom70 F	GAA AGA AACACTGTGCAGGC	Check primer for screening PCR
CHK GPD Tom70 R	CAG GTC TGC AGC GAG GAG	Check primer for screening PCR
Mpf1- SACI F	GGGgagctcATG TCC TCC AGC ATC TTT GAA ATG AC	Forward primer to clone *MPF1* in pRS426-3HA. SAC1 restriction site.
Mpf1- XMAI R	GGGcccgggTCATAAATTCGTAAGGTCGTTAGT TC	Reverse primer to clone *MPF1* in pRS426-TPI-3HA. XMA1 restriction site.
Ynl PHD K144A_K147A F	GGTTTCTATGGCAATGGAAGCACTATCGCC	Forward primer for site-directed mutagenesis (K144A, K147A) in pRS426-3HA

Ynl PHD K144A_K147A R	GGCGATAGTGCTTCCATTGCCATAGAAACC	Reverse primer for site-directed mutagenesis (K144A, K147A) in pRS426-3HA
Ynl PHD K157A F	ATGCTTCTTCTGCATTATGGAACA	Forward primer for site-directed mutagenesis (K157A) in pRS426-3HA
Ynl PHD K157A R	TGTTCCATAATGCAGAAGAAGCAT	Forward primer for site-directed mutagenesis (K157A) in pRS426-3HA
Tom71 HA F AvrII	GGGcctaggATGGCCGAAAACTCCCTCCTGA	Forward primer to clone *TOM71* in pYX142.AVRII restriction site.
Tom71 HA R SALI	GGGgtcgacCTAAGCGTAATCTGGAACATCGTA TGGGTA AAGCATGCCTTTAGCCC	Reverse primer to clone *TOM71* in pYX142. SALI restriction site. HA tag
Flag Pex19 F EcoRI	GGGgaattc ATG GAC TAC AAA GAC GAT GAC GAC AAGAATGAAAACGAGTACGATAATT	Forward primer to clone *PEX19* in pRS426. ECORI restriction site. FLAG tag.
Flag Pex19 R BamHI	GGGggatccTTATTGTTGTTTGCAACCGTC	Reverse primer to clone *PEX19* in pRS426. BAMHI restriction site
Flag Mpf1 F XmaI	GGGcccgggATGTCCTCCAGCATCTTTGAAATG AC	Forward primer to clone *MPF1* in pRS426. XMAI restriction site.
Flag Mpf1 R SacI	GGGgagctcTCACTTGTCGTCATCGTCTTTGTAG TCTAAATTCGTAAGGTCGTTAGTTC	Reverse primer to clone *MPF1* in pRS426. SACI restriction site. FLAG tag.
Actin 1F qPCR	TGGTGATGAAGCTCAATCCAAG	qPCR Actin forward primer
Actin 1R qPCR	TGGATGGAAACGTAGAAGGC	qPCR Actin reverse primer
Ynl 1F qPCR	TCGCCCTTTGAAAATGCTTCT	qPCR Mpf1 forward primer
Ynl 1R qPCR	TCGTCTCGTGCTATTTCCCC	qPCR Mpf1 reverse primer
qPCRTgl2-1_For	GGGACTAGACTGCCGATATCTAA	qPCR Tgl2 forward primer
qPCRTgl2-1_Rev	GGCCATTTCTGACCCTCTATG	qPCR Tgl2 reverse primer

Table S3: Plasmids used in this study

Plasmid	Promoter	Markers	Source
pYMS271	TPI	Amp^R, Hph^R	Maya Schuldiner, This study
pFa6aNatN2		Amp^R, Nat^R	Lab stock
pFa6aKanMX6		Amp^R, Kan^R	Lab stock
pYM-N15	GPD	Amp^R, Nat^R	(Janke et al., 2004)
pRS426-3HA	TPI	Amp^R, URA3	Lab stock
pRS426-Mpf1-3HA	TPI	Amp^R, URA3	This study
pRs426-Tom22-HA	TPI	Amp^R, URA3	This study
pYX142-RFP-MTS	TPI	Amp^R, LEU2	This study
pRS426-Mpf1(PH*)-3HA	TPI	Amp^R, URA3	This study
pRS426-Flag-Pex19	TPI	Amp^R, URA3	This study
pYX142	TPI	Amp^R, LEU2	Lab stock
pYX142-Tom71-HA	TPI	Amp^R, LEU2	This study

Table S4: Antibodies used in this study

Antibody	Dilution	Source
Polyclonal rat anti-HA	1:1000	11867423001 (Roche)
Polyclonal rabbit anti-Erv2	1:1000	Roland Lill
Polyclonal rabbit anti-Hexokinase	1:1000	Bio-Trend (#100-4159)
Polyclonal rabbit anti-Tom20	1:1000	Lab stocks
Polyclonal rabbit anti-Tom40	1:2000	Lab stocks
Polyclonal rabbit anti-Tom70	1:2000	Lab stocks
Polyclonal rabbit anti-Mcr1	1:1000	Lab stocks
Polyclonal rabbit anti-Om14	1:1000	Lab stocks
Polyclonal rabbit anti-Fis1	1:1000	Lab stocks
Polyclonal rabbit anti-Pex14	1:2000	R. Erdmann & W. Girzalsky
Polyclonal rabbit anti-Hep1	1:1000	Lab stocks
Polyclonal rabbit anti-Tom71	1:1000	Lab stocks
Goat anti-rabbit IgG HRP conjugate	1:10000	#1721019, Bio-Rad
Goat anti-rat IgG HRP conjugate	1.2000	#ab6845, Abcam

Mpf1 is a novel factor that affects the dual distribution of tail-anchored proteins between mitochondria and peroxisomes

Nitya Aravindan[1], Daniela G. Vitali[1], Jessica Oberst[1], Einat Zalckvar[2], Maya Schuldiner[2], Doron Rapaport[1,*]

1. Interfaculty Institute of Biochemistry, University of Tübingen, Tübingen, Germany

2. Department of Molecular Genetics, Weizmann Institute of Science, Rehovot, Israel

* To whom correspondence should be addressed: doron.rapaport@uni-tuebingen.de;

Tel: +0049-7071-2974184; ORCID: 0000-0003-3136-1207

Keywords: dual targeting, Fis1, Gem1, mitochondria, peroxisomes, tail-anchored proteins,

Abstract

Over half of cellular proteins must target upon their translation to distinct cellular compartments to function. Whereas considerable progress has been made in our understanding of targeting to individual organelles, we know truly little about how proteins distribute their targeting between two, or more, destinations – a process called dual/multiple targeting. In this study, we shine mechanistic insight into the process of dual targeting of proteins between the yeast mitochondria and peroxisomes. We performed a high throughput systematic microscopy screen in which we visualized the location of the model tail-anchored (TA) proteins Fis1 and Gem1 on the background of mutants in all yeast genes. This screen identified three proteins, whose absence resulted in a higher portion of the TA proteins in peroxisomes: the two paralogues Tom70, Tom71, as well as the uncharacterized gene *YNL144C* that we renamed mitochondria peroxisomes factor 1 (Mpf1). We characterized Mpf1 to be an unstable protein that associated with the cytosolic face of the mitochondrial outer membrane. Furthermore, our study uncovers a unique contribution of Tom71 for the regulation of the dual targeting and reveals a link between *TOM70/71* and the quantity of transcripts of *MPF1*. Collectively, our study revealed, for the first-time, factors that influence the dual targeting of proteins between mitochondria and peroxisomes.

Introduction

Eukaryotic cells have evolved complex machineries that direct, with the help of targeting signals, cytosolically synthesized proteins to specific intracellular locations. While most proteins target to a single compartment, there are those that are targeted to two (or even more) cellular destinations. Some examples of such proteins include the metabolic enzymes fumarase and aconitase, where in addition to the mitochondrial population a certain portion of the protein is also found in the cytosol or even the nucleus (Regev-Rudzki & Pines, 2007; Stein et al., 1994; Yogev et al., 2011).

Several cases of such dually targeted membrane proteins are those that distribute between mitochondria and peroxisomes. These two organelles maintain extensive crosstalk and are transiently associated by multiple contact sites. Pex11, a key protein involved in initiating peroxisome division was found to interact with Mdm34, a constituent of the ER-mitochondria

encounter structure (ERMES) complex, thus mediating these mitochondria-peroxisome contact sites (Mattiazzi Ušaj et al., 2015). Furthermore, peroxisomes were found in close proximity to sites enriched in pyruvate dehydrogenase (PDH) complex responsible for acetyl-CoA synthesis in the mitochondrial matrix, further validating the organelles' co-dependency in their metabolic processes (Cohen & Schuldiner, 2011; Mattiazzi Ušaj et al., 2015; Shai et al., 2016). In a high throughput screen, Fzo1 and Pex34 were found to contribute to the formation of mitochondria-peroxisomes tethers (Shai et al., 2016). In addition to their close physical and metabolic relationships, mitochondria and peroxisomes also utilize many similar outer membrane proteins, such as the same fission machinery, for their division.

A central component of this fission machinery is Fis1, a tail anchored (TA) protein that can be targeted to both mitochondrial and peroxisomal membranes in yeast, plants, and mammalian cells (Koch et al., 2005; Kuravi et al., 2006; M. Schrader et al., 2016). The adapter protein Mdv1, which, is recruited by Fis1 to the site of fission, engages in turn the dynamin-like protein Dnm1 that mediates the final fission step (Bleazard et al., 1999; Mozdy et al., 2000; Shaw & Nunnari, 2002; Yoon et al., 2003). Notably, mammalian homologues of these fission components were also found to be dually localized to mitochondria and peroxisomes. Combined defects in the organellar fission have been linked to several pathophysiological conditions and therefore it is important to understand the biogenesis of proteins involved in these cellular machineries (Ong et al., 2013; Schrader et al., 2022). Additional examples for proteins dually localized to both mitochondria and peroxisomes are the TA protein Gem1 (MIRO1 in mammals) and the ATPase Msp1 (ATAD1 in mammals)(Costello et al., 2017; Okreglak & Walter, 2014).

While a clear mechanism for targeting TA proteins to the secretory pathway has been worked out (Schuldiner et al., 2008; Stefanovic & Hegde, 2007), the mechanism involved in the correct targeting of TA proteins to mitochondria is still widely unknown. It has been previously shown that optimal hydrophobicity of the transmembrane domain and the presence of charged residues is essential for the correct targeting of TA proteins to mitochondria and/or peroxisomes (Bittner et al., 2022a; Borgese et al., 2007; Costello et al., 2017). While the mitochondrial import (MIM) complex was suggested to promote the biogenesis of the TA proteins Fis1 and Gem1 (Doan et al., 2020), other studies have also reported insertion of Fis1 to the mitochondrial outer membrane (MOM) and to lipid vesicles in an unassisted manner (Krumpe et al., 2012, Vitali et al., 2020).

For peroxisomal TA proteins, a dedicated pathway for membrane targeting – mediated by Pex19 and Pex3 exists (Fujiki et al., 2006). Nascent TA proteins with a peroxisomal membrane targeting signal (mPTS) are recognized by Pex19 in the cytoplasm and delivered to the peroxisomal membrane by interacting with the membrane receptor Pex3 (Chen et al., 2014; Götte et al., 1998). Surprisingly, depletion of *PEX19* resulted in reduced steady state levels of Fis1 and Gem1 also in mitochondrial fractions, suggesting an unexpected contribution of Pex19 to the biogenesis of mitochondrial TA proteins (Cichocki et al., 2018). Hence, despite some understanding of how TA proteins arrive to either mitochondria or peroxisomes, how the distribution of such dually localized proteins is regulated is still quite puzzling.

To obtain new insights on the mechanisms that control dual targeting of proteins to both mitochondria and peroxisomes and to unravel novel factors involved in this process, we used a high-throughput visual screen with fluorescently labeled TA proteins in the bakers' yeast *Saccharomyces cerevisiae*. We found that the deletion of the uncharacterized gene *YNL144C* (in this study, re-named as Mitochondria and Peroxisomes Factor 1 (Mpf1)), as well as each of the paralogous proteins, *TOM70* and *TOM71* led to an enhanced localization of Fis1 to peroxisomes. Accordingly, overexpressing Tom71 caused Fis1 to localize more to mitochondria. We further characterized Mpf1 and identified it as an unstable protein on the surface of mitochondria controlled by the presence of Tom70 and Tom71. Collectively, our findings describe the involvement of Mpf1, Tom70, and Tom71 in regulating the dual distribution of Fis1 and Gem1 to mitochondria and peroxisomes.

Results

A high throughput visual screen reveals candidates that affect the dual distribution of TA proteins to mitochondria and peroxisomes

Some yeast TA proteins like Fis1 and Gem1 are found on both organelles - mitochondria and peroxisomes. To identify factors that influence the dual distribution of these proteins, we decided to employ a high throughput microscopy screen. To visualize the TA proteins of interest, we generated strains expressing mCherry tagged versions of either Fis1 or Gem1 on the background of a peroxisomal marker, Pex3-GFP. Then, using an automated procedure (Cohen & Schuldiner, 2011), we introduced these two tagged proteins into the background of a collection containing deletion strains of all the yeast non-essential genes and depletion strains

of all the essential ones (Figure 1A). Thus, a new collection of deletion/depletion strains expressing the mCherry tagged TA protein along with GFP tagged Pex3 was created. This new collection was subjected to a high-throughput microscopy screen to identify those strains where the distribution of the TA proteins Fis1 and Gem1 between mitochondria and peroxisomes is altered (Figure 1A).

While many proteins altered the distribution between the two organelles, it appeared that this was often secondary to biogenesis and/or morphology defects of the respective organelles. Hence, we decided to consider as a real hit only strains that fulfilled two criteria: (i) have normal biogenesis of peroxisomes (as reflected by the number of GFP puncta structures), and (ii) display normal mitochondrial morphology, as observed with the mCherry-Fis1. Considering these requirements, the screen allowed us to identify several proteins that might influence the distribution of Fis1 and Gem1 to peroxisomes (see Table S1 for the full list). Further manual examination of the complete list led us to focus on the uncharacterized protein Ynl144c (that we re-named as mitochondrial and peroxisomal factor 1, Mpf1), and the two paralogue proteins Tom70 and Tom71. The absence of each of these three proteins led to a greater co-localization of mCherry-Fis1 with Pex3-GFP stained peroxisomes compared to control cells (Figure 1B and C). When we quantified this phenotype, we could detect co-localization of mCherry-Fis1 with 20% of peroxisomes in the wild type (WT) cells and this number was considerably increased in cells lacking Mpf1, Tom70, or Tom71 (Figure 1C).

To investigate whether this observation was limited only to mCherry-Fis1, we quantified the co-localization of mCherry-Gem1 with Pex3-GFP and observed the same trend, indicating that the identified proteins have a general effect on dually distributed TA proteins (Figure S1). We further confirmed that these observations were not the result of fragmented mitochondria that were misinterpreted for peroxisomal puncta. To this aim, we visualized mitochondrial morphology by staining the organelle with Om45-GFP and observed that the mitochondrial morphology was not altered in *mpf1*Δ and *tom71*Δ cells as compared to control cells (*tim13*Δ) (Figure S2). We noticed a slightly altered mitochondrial morphology in *tom70*Δ cells (Figure S2), which is not surprising considering the functions of Tom70 as an important mitochondrial import receptor and a docking site for cytosolic chaperones (Backes et al., 2021; Kreimendahl & Rassow, 2020; Yamamoto et al., 2009; Young et al., 2003). Collectively, the visual screen identified Mpf1, Tom70, and Tom71 as potential factors affecting the dual distribution of TA proteins.

Physical separation of mitochondria and peroxisomes validates the involvement of the identified hits in the dual distribution of Fis1

To confirm by another unrelated approach, that the candidates that we picked by the visual screen truly affect the dual distribution of Fis1 to mitochondria and peroxisomes, we monitored the distribution of Fis1 by subcellular fractionation. To obtain optimal separation, the cells were grown on oleate as a carbon source, a condition known to induce proliferation of peroxisomes. After obtaining a crude mitochondrial fraction, we used centrifugation of a Histodenz gradient to separate mitochondria from peroxisomes and 12 fractions of the gradient were collected. Our protocol could nicely differentiate between the two organelles despite their strong physical associations: Tom20, a *bona-fide* mitochondrial marker protein was enriched in the first four fractions (lanes 1-4), whereas the peroxisomal marker protein Pex14 was found preferentially in the last four fractions (9-12). As expected for a dually targeted protein, Fis1 was present in both sets of fractions (lanes 1-4 and 9-12) (Figure 2A). Fis1 levels in the various fractions were quantified and the total amount in fractions 1-4 was considered as mitochondrial Fis1 whereas the material in fractions 9-12 was counted as peroxisomal population.

Using this approach, we compared the distribution of native Fis1 in wild type (WT) cells to that in the mutated strains. Whereas in WT cells, 70% of Fis1 were found to be mitochondrial, this portion decreased to 57% and 52% in *mpf1*Δ and *tom71*Δ cells, respectively (Figure 2A and B). In parallel to the decrease in mitochondrial Fis1, we observed an increase in the peroxisomal portion of the protein. We found 23% of Fis1 in peroxisomes in WT cells whereas this fraction had increased to 34% and 37% in *mpf1*Δ and *tom71*Δ cells, respectively (Figure 2A and B). Unfortunately, we could not analyze the distribution of Fis1 in *tom70Δ* cells because, for unknown reasons, the separation of mitochondria from peroxisomes did not work well with cells from this strain. Hence, this technique could not validate Tom70 as a factor regulating the distribution of TA proteins.

We were then interested to explore the distribution phenotype upon the parallel deletion of both *MPF1* and *TOM71*. Surprisingly, we observed that in *tom71*Δ*/mpf1*Δ double deletion cells, the alteration in the Fis1 distribution was less profound than in the corresponding single deletion strains (Figure 2A and B). It might be that loss of both Mpf1 and Tom71 leads to compensatory upregulation of alternative factors to restore mitochondrial Fis1 levels to those observed in control cells. Taken together, the physical separation of mitochondria from peroxisomes

confirmed the (direct or indirect) involvement of Mpf1 and Tom71 in regulating the dual distribution of Fis1 between mitochondria and peroxisomes.

Tom71 has a unique role in Fis1 distribution, setting it apart from Tom70

Tom71 is a paralogue of Tom70, sharing 53% sequence identity, whose abundance is rather low – only about 10% of the levels of Tom70 (Morgenstern et al., 2021; Schlossmann et al., 1996). Tom70 plays a pivotal role as a mitochondrial import receptor and chaperones' docking site and is required for the biogenesis of many mitochondrial proteins (Backes et al., 2021; Kreimendahl & Rassow, 2020; Yamamoto et al., 2009; Young et al., 2003). Tom70 and Tom71 are thought to have overlapping functions, and a specialized role unique to Tom71 has not been reported yet.

Our work suggested a unique role for Tom71 since its deletion led to a distribution phenotype even in the presence of Tom70. To better understand the involvement of both proteins in the dual distribution of Fis1, we created strains where each of the protein is over-expressed. To that aim, the endogenous promoter of *TOM70* in WT, *mpf1*Δ and *tom71*Δ cells was replaced by the strong *GPD* promoter, resulting in a dramatic overexpression (Figure 3A). We then separated mitochondria and peroxisomes and quantified mitochondrial and peroxisomal levels of Fis1 (Figure 3B and C). We observed that elevated levels of Tom70 led to a correction of Fis1 distribution in *mpf1*Δ cells with 70% mitochondrial and 25% peroxisomal Fis1, similar to the distribution observed in WT cells (Figure 3B and C). Thus, it seems that the role of Mpf1 in regulating Fis1 distribution is dispensable in the presence of higher amounts of Tom70. Interestingly, only a partial correction of Fis1 distribution was observed upon overexpression of Tom70 in *tom71*Δ cells with 64% in mitochondria and 30% in peroxisomes (Figure 3B and C), indicating that Tom71 has a unique role in Fis1 distribution that cannot be replaced by elevated levels of Tom70.

Remarkably, although we expected that overexpression of Tom70 in WT cells would drive Fis1 distribution more towards mitochondria, we observed a minor reduction in mitochondrial Fis1 (62%) and a slight increase in peroxisomal Fis1 (33%) (Figure 3B and C). This observation is specially intriguing considering the report that the biogenesis of many mitochondrial proteins is enhanced upon overexpression of Tom70 (Liu et al., 2022). We can speculate that targeting of Fis1 towards mitochondria might prefer Tom71 over Tom70 and over-crowding the mitochondrial surface with Tom70 and/or engaging Tom71 in

Tom71/Tom70 heterodimers creates a competing effect, thereby reducing Fis1 levels in mitochondria.

To further study the role of Tom71 in regulating the distribution of Fis1, we next constructed WT and *mpf1*Δ strains where Tom71 expression is under the control of the strong *GPD* promoter and could confirm the massive overexpression of Tom71 in these cells (Figure 3D). Then, we separated mitochondria and peroxisomes from these strains and quantified the levels of mitochondrial and peroxisomal Fis1 (Figure 3E and F). Interestingly, we observed that Tom71 over expression in both WT and *mpf1*Δ cells led to an increased distribution of Fis1 towards mitochondria (Figure 3E and F). These findings substantiate the independent and unique contribution of Tom71 to the targeting of Fis1 to mitochondria.

It has previously been shown that the cytosolic chaperone/receptor Pex19 assists the biogenesis of mitochondrial Fis1 (Cichocki et al., 2018). Since overexpression of Tom71 drove 81% of Fis1 towards mitochondria, we wondered whether Tom71 functions as a receptor for Pex19 on the surface of mitochondria. To test this possibility, we created a strain where Tom71-HA and Flag-Pex19 are co-overexpressed in *tom70*Δ cells. We deleted Tom70 from these cells to prevent potential competition of Tom70 in binding to Pex19. Next, pull down analysis to detect potential interaction was performed. However, we could not co-elute Flag-Pex19 with Tom71-HA (Figure 3G). This outcome proposes that the proteins might not interact, or that the interaction is very transient. Taken together, these results demonstrate a unique role of Tom71, whose absence cannot be compensated by Tom70, while the contribution of Mpf1 to regulating Fis1 distribution is dispensable upon overexpression of either Tom70 or Tom71.

Deletion of *MPF1* is beneficial to cells grown on oleic acid

Since Mpf1 is an uncharacterized protein with an unknown function, we wanted to investigate whether loss of Mpf1 would have an effect on growth of yeast cells. We noticed that *mpf1*Δ cells grew similar to WT cells when glucose (YPD), glycerol (YPG), or oleate (YPO) were used as carbon sources in a rich medium. However, when oleic acid was used as the sole carbon source on a synthetic medium, cells lacking Mpf1 grew better than WT cells (Figure 4).

In yeast, β-oxidation of fatty acids such as oleate takes place solely in peroxisomes (Hiltunen et al., 2003). Thus, yeast cells require fully functional peroxisomes for optimal growth on oleate as the exclusive carbon source. Previous studies have shown that absence of Fis1 reduces the

number of peroxisomes in cells grown on oleate (Kuravi et al., 2006). Moreover, re-directing Fis1 only to peroxisomes by expressing Fis1-Pex15 fusion protein increased Dnm1-dependent peroxisome fission, and thereby increased the number of peroxisomes per cell (Motley et al., 2008). Hence, the better growth of *mpf1*Δ cells on oleate can be explained by the increased portion of Fis1 in peroxisomes in these cells which in turn, enhances the number of peroxisomes and thus improves the utilization of oleate.

Mpf1 is a highly unstable protein

A previous high throughput study proposed that Mpf1 might be a substrate of Grr1, an SCF ubiquitin ligase complex subunit. Both Mpf1 and its uncharacterized paralog, Yhr131c were suggested to interact with Grr1 and were reported to be partially stabilized in *grr1*Δ cells (Mark et al., 2014). To verify this previous report, we transformed a plasmid encoding Mpf1-3HA into WT and *grr1*Δ cells and monitored the life span of Mpf1 in these cells. In line with the previous findings, we observed that Mpf1 is indeed a highly unstable protein in WT cells and is almost completely degraded within 45 minutes after inhibition of translation by addition of cycloheximide (CHX) (Figure 5A and B). However, in our hands, the deletion of *GRR1* had only a minor effect on the stability of Mpf1 (Figure 5 A and B), suggesting that there are other factors that affect the lifespan of this protein.

Mpf1 loosely associates with the mitochondrial outer membrane

To further characterize Mpf1, we aimed to determine its subcellular location. WT cells expressing Mpf1-3HA were fractionated into whole cell lysate (WCL), ER, cytosol and mitochondria and these fractions were analyzed by Western blotting. Antibodies recognizing marker proteins for the mitochondria (Tom40), ER (Erv2), cytosol (Hexokinase) and peroxisomes (Pex14) were used to verify the fractionation. We detected Mpf1-3HA mainly in the mitochondrial fraction with some portion also in the ER fraction. Given the presence of the peroxisomal marker Pex14 in both fractions, we could only conclude that Mpf1-3HA might localize to mitochondria, peroxisomes, and/or the ER (Figure 6A).

To obtain a more precise localization of Mpf1, we then chose to employ fluorescence microscopy techniques. Tagging Mpf1 with GFP led to a cytosolic staining, which was not in line with the subcellular fractionation assays. This observation can be explained by either

cleaving of the GFP tag and/or mis-targeting due to the bulky GFP moiety. Hence, we opted for immunofluorescence (IF) assays. Anti-HA antibodies conjugated to a fluorophore were used to detect Mpf1-3HA. As a control for the IF technique, we also visualized Tom22-HA, a *bona-fide* mitochondrial outer membrane protein. We observed that Mpf1-3HA stained tubular structures that co-localize with RFP fused to mitochondrial targeting signal (RFP-MTS) but not with RFP-PTS1 (Peroxisomal targeting signal 1) (Figure 6B). These findings support the notion that Mpf1-3HA localizes to mitochondria.

Since mitochondria have four different sub-compartments, we investigated the sub-mitochondrial localization of Mpf1-3HA by treating mitochondria isolated from cells expressing Mpf1-3HA with proteinase K (PK). We found Mpf1-3HA to be susceptible to PK digestion comparable to that of the surface proteins Tom70 and an Mcr1 isoform on the outer membrane ($Mcr1_{OM}$) (Figure 6C). As expected for mitochondrial internal proteins, the Mcr1 isoform in the intramembrane space ($Mcr1_{IMS}$) and the matrix protein Hep1 were protected from PK by the outer membrane and both outer and inner membranes, respectively (Figure 6C). Hence, we concluded that Mpf1 is exposed to the cytosol on the surface of mitochondria.

We next determined whether Mpf1-3HA is an integral or peripheral membrane protein by performing alkaline extraction of mitochondrial proteins followed by centrifugation to separate membrane embedded proteins in the pellet from soluble and peripheral membrane proteins in the supernatant. To obtain a better resolution of the assay, we performed it under varying pH conditions. The alkaline pH decreases non-covalent protein-protein interactions and releases peripheral membrane proteins to the supernatant (Kim et al., 2015). As expected, $Mcr1_{OM}$ isoform remained in the pellet fractions under all pH conditions, confirming its behavior as a *bona fide* integral membrane protein. In contrast and as anticipated, the soluble IMS isoform of Mcr1 was in the supernatant fraction under all the employed conditions (Figure 6D). We found that Mpf1-3HA was in the membrane fraction only in milder extraction condition (pH 10.5). As the pH was raised to 11, 11.5, and 12, increasing amounts of Mpf1 were found in the supernatant fraction. This behavior is similar to that of the outer membrane proteins Om14, which is known to be partially extractable under alkaline conditions (Burri et al., 2006; Zhou et al., 2022) (Figure 6D). Altogether, these results indicate that Mpf1-3HA is peripherally associated with the cytosolic face of the mitochondrial OM.

The combined loss of Tom70 and Tom71 affects the steady state levels of Mpf1

Considering the location of Mpf1 on the mitochondrial surface, we wondered whether Tom70, Tom71, or both are involved in targeting of Mpf1 to the organelle. Several studies on Tom70 and its paralog Tom71 (to a lesser extent) have identified a tetratricopeptide (TPR) structure that can bind to the cytosolic chaperones Hsp70 and Hsp90 and enable the recruitment of several precursor proteins together with chaperones to the mitochondrial surface (Backes et al., 2018; Jores et al., 2018; Young et al., 2003; Zanphorlin et al., 2016). Moreover, microscopy analysis of many GFP tagged proteins showed their reduced levels upon the absence of Tom70/71 (Backes et al., 2021). To investigate potential involvement of Tom70/71 in the biogenesis of Mpf1, we monitored the steady state levels of Mpf1-3HA in *tom70*Δ, *tom71*Δ, and double deletion *tom70*Δ*/71*Δ cells. Of note, in the absence of either Tom70 or Tom71 alone, Mpf1-3HA levels were comparable to those in WT cells. However, double deletion of both proteins resulted in tenfold decrease compared to WT cells (Figure 7A and B).

To understand the reason for such a dramatic reduction in the steady-state levels, we investigated whether the stability of Mpf1-3HA was affected in *tom70*Δ*/71*Δ cells. Though the relative levels of Mpf1-3HA was tenfold lower in the double deletion cells at the beginning of the assay (time-point 0), the life span of the protein in the mutated cells was comparable to that in WT cells (Figure 7C and D). Furthermore, both subcellular fractionation and immunofluorescence microscopy revealed that Mpf1-3HA still localized predominantly to the mitochondria in *tom70*Δ*/71*Δ cells (Figure 7E and F).

Recent studies suggested that Tom70 can be involved in signaling through multiple transcription factors to control the transcription levels of genes encoding for many mitochondrial proteins. Accordingly, upon the selective removal of Tom70 from the mitochondrial surface, the levels of mRNAs encoding mitochondrial proteins were reduced (Liu et al., 2022). Along the same line, our RT-qPCR analysis revealed that the transcript levels of endogenous *MPF1* as well as overexpressed *MPF1-3HA* were reduced by around 50% as compared to WT cells upon the deletion of both *TOM70/71* (Figure S3). These lower mRNA levels can explain (at least partially) the dramatically reduced levels of Mpf1 protein in the double deletion strain. It should be mentioned that such reduction in the detection of mRNA can result from less transcription of *MPF1,* increased degradation of the mRNA, and/or sequestering of the mRNA to P-bodies. Collectively, our findings suggest an involvement of both Tom70 and Tom71 in the transcriptional control of Mpf1-3HA. Although the mRNA and

the protein steady-state levels of Mpf1-3HA are dramatically reduced in the absence of Tom70/71, Mpf1-3HA still localizes to mitochondria, suggesting the involvement of other factor(s) in its biogenesis.

The PH domain of Mpf1 is involved in the stability of the protein but not in its localization

Large scale studies and structural analysis predicted the presence of a Pleckstrin homology (PH) domain in Mpf1 (Gallego et al., 2010; Isakoff et al., 1998; Lemmon, 2004)**.** This domain can interact with phosphoinositide (PI) species as well as other lipids on biological membranes. Previous attempts to investigate binding of a recombinant PH domain from Mpf1 to PI were unsuccessful due to inadequate quantities (Yu et al., 2004). PH domains occur in a wide range of proteins with varying functions, and are stretches of ~120 amino acid residues with two anti-parallel β-sheets followed by a C-terminal α-helix (Riddihough, 1994). Membrane targeting of PH domains that strongly bind to PIs could be abolished by mutating the basic residues in the β1/β2 loop (Yu et al., 2004). To investigate if the PH domain of Mpf1 is essential for the stability and/or subcellular localization of the protein, we created a mutant of Mpf1 with lysine and arginine residues in the PH domain replaced by alanine (K144A, K147A, and R157A) (Figure 8A, Mpf1(PH*)-3HA). Compared to regular Mpf1-3HA, Mpf1(PH*)-3HA exhibited elevated stability, with steady-state levels ~60% higher than that of the native protein (Figure 8B and C). The PH domain is known to serve as a platform for protein-protein interactions (Lemmon, 2004; Scheffzek & Welti, 2012), and mutating the basic residues in the PH domain of Mpf1 might have disrupted its interactions with some factors of the proteasome degradation pathway and thereby increasing its stability. Of note, cells overexpressing Mpf1(PH*)-3HA grew slightly better than WT cells on oleate-containing medium (Figure 8D). It can be speculated that this variant might have a dominant negative effect on the recruitment of Fis1 to mitochondria and thus enhances the number of peroxisomes under these conditions.

We next asked whether the basic residues in the PH domain of Mpf1 are required for its targeting to mitochondria and its association with the OM. Employing immunofluorescence microscopy and subcellular fractionation, we found that Mpf1(PH*)-3HA still localizes to the mitochondria (Figure 9A and B). Molecular modelling revealed that the PH domain of Mpf1 has an overall weak or no positive charge, and membrane targeting or binding to PIs may depend on strong positive charges (Yu et al., 2004). Furthermore, not all PH domains exhibit

strong and specific interactions with PIs and many of them bind to PIs with low affinity and specificity. Effective binding of such "weak" PH domains to biological membranes might be strengthened by interactions with other membrane-bound proteins (Maffucci & Falasca, 2001). To explore this option, we then performed an alkaline extraction to see if the association of Mpf1(PH*)-3HA with the MOM is affected. Mpf1(PH*)-3HA predominantly remained in the pellet fraction in pH 10.5 and there was an increase of the protein portion in the supernatant only at pH 12, indicating that Mpf1(PH*)-3HA exhibits a similar, or even somewhat stronger association to the MOM than its native counterpart (Figure 9C). Collectively, these results suggest that mutating key residues in the PH domain of Mpf1 did not change its association with mitochondria.

Discussion

Considering the number of shared proteins between mitochondria and peroxisomes and the *de novo* formation of peroxisomes via mitochondria-derived vesicles (at least in mammalian cells), several studies speculate that peroxisomes evolved to facilitate the quality control of mitochondria under periods of stress and to relieve mitochondria from the burden of hosting oxidation enzymes of the β-oxidation pathway (Bittner et al., 2022b; Speijer, 2017). This symbiotic relationship between mitochondria and peroxisomes might have allowed peroxisomes to utilize several mitochondrial proteins for their own needs like those proteins involved in fission (Fis1) and quality control (Msp1). Moreover, mitochondria contribute indirectly to the targeting of the phosphatase Ptc5p to peroxisomes via a mitochondrial transit. These cross-talks are proposed to eventually lead to targeting of these proteins to both organelles when peroxisomes became autonomous over time (Bittner et al., 2022b; Stehlik et al., 2020). Distribution of the dually localized TA protein Fis1 to mitochondria and peroxisomes is aided by Pex19 (Cichocki et al., 2018). However, regulatory mechanisms to understand how the distribution of these cytosolically synthesized TA proteins is controlled have remained elusive.

In this study, we used comprehensive techniques to find factors that regulate the dual distribution of TA proteins Fis1 and Gem1 to the membranes of mitochondria and peroxisomes. Using high-throughput microscopy screens, we first identified the involvement of Tom70, Tom71, and an uncharacterized protein Ynl144c (re-named as Mpf1 in this study) in regulating the distribution of Fis1 and Gem1 to mitochondria and peroxisomes. Subsequently, we verified

the involvement of these candidates via subcellular fractionation assays and confirmed that in *tom71Δ* and *mpf1Δ* cells, Fis1 distributed more to peroxisomes. Surprisingly, the double deletion cells *tom71/mpf1Δ* showed Fis1 distribution comparable to WT cells. Since mitochondrial fission is crucial for the maintenance of healthy cells and the depletion of Fis1 leads to hyperfused mitochondria (Das & Chakrabarti, 2020; Hoppins et al., 2007), *tom71/mpf1Δ* potentially leads to activation of other factors to maintain proper distribution of Fis1 molecules. Further investigations on which factors could be upregulated in *tom71/mpf1Δ* cells would enhance our understanding of this regulatory mechanism. Unfortunately, due to technical difficulties, we were unable to optimally separate mitochondria and peroxisomes in *tom70Δ* and *tom70/71Δ* cells, and thereby the impact of the absence of Tom70 on the distribution of Fis1 could not be verified and remains unclear.

However, we were able to show that enhanced levels of Tom70 in *mpf1Δ* cells could fully correct the Fis1 distribution to WT levels but only partially reverse the distribution in *tom71Δ*. This observation suggests that Tom71 might have a more dominant role in affecting Fis1 distribution, that is not entirely rectified by higher levels of Tom70. Tom71 is a barely expressed paralog of Tom70 and until this study, a distinct function of Tom71 distinguishing it from Tom70 was not found. Our hypothesis that Tom71 plays a unique role in regulating Fis1 distribution is further validated by our finding that overexpression of Tom71 has a significant effect (compared to that of Tom70) in driving Fis1 distribution more towards mitochondria. A possible explanation for the effect of Tom71 is a putative role as a mitochondrial receptor for Pex19. However, so far, we could not detect a physical interaction between Tom71 and Pex19. It could be that the interaction is rather transient and might be dependent on the presence of substrate protein *in transit*.

The fact that the distribution of Fis1 in *mpf1Δ* cells could be completely corrected by higher levels of either Tom70 or Tom71 shows that the role of Mpf1 in regulating Fis1 is dispensable upon overexpression of one of these paralogues. This complementation can also suggest that Mpf1, Tom70, and Tom71 potentially share the same pathway in regulating the trafficking of Fis1 to mitochondria and peroxisomes. Further experiments to test whether Mpf1 directly interacts with Tom70 and/or Tom71 can shed light on the question if these proteins work together.

Although the precise molecular function of Mpf1 is not known yet, a hint for its physiological role is provided by our finding that yeast cells grown on fatty acid (oleate) benefit from the

deletion of *MPF1*. We assume that this phenotype is due to an increase in the number of Fis1 molecules targeted towards peroxisomes, which subsequently enhance the number of peroxisomes, which could be particularly beneficial when oleate is the sole carbon source. However, we did not observe this effect on oleate upon deleting *TOM71 or TOM70* (data not shown), suggesting that other functions of Tom70/71 are still important when oleate is the sole carbon source. An alternative explanation is that in the absence of Mpf1 other cellular mechanisms (beside increased peroxisomal Fis1 levels) cause beneficial effects for growth in oleate media.

Another interesting aspect about Mpf1 is its rather short life-span. This inherent instability raises the question why cells produce protein molecules that will be degraded within minutes. Currently, we can only speculate that under some special conditions the presence of Mpf1 could be required immidiately and obtaining new molecules via enhancing transcription and translation might be too time consuming. In the future, it will be of interest to identify conditions that support enhanced stability of Mpf1.

Characterizing the sub-cellular localization of Mpf1 indicated it to be a peripheral membrane protein, loosely associated to the mitochondrial OM. Interestingly, even in the absence of both Tom70 and Tom71, Mpf1 still makes its way to the mitochondrial surface, suggesting the involvement of other factors that can mediate its association to the organelle. Mutating the conserved basic residues in the β1/β2 loop and thereby potentially disrupting the PH domain of Mpf1 did not hamper its mitochondrial localization either. Thus, it seems that either the triple mutation did not interfere completely with the function of the PH domain or other regions of the protein facilitate the association with mitochondria. Our finding that Mpf1(PH*) exhibited enhanced stability might indicate that certain proteins in the Ubiquitin/proteasome degradation pathway usually recognize a degron element in the PH domain but are unable to do so with the mutated PH domain. Alternatively, it might be that the mutations stabilize the interaction of Mpf1 with a protein and/or a lipid in the mitochondria outer membrane and through these interactions Mpf1 is stabilized.

Altogether, our findings contribute to novel insights on factors responsible for regulating the dual distribution of Fis1 to mitochondria and peroxisomes. We identified for the first time three proteins Tom70, its paralogue Tom71, and Mpf1 as involved in this process. In addition to recognizing a unique function of Tom71, we could provide a function for a so far uncharacterized protein – Mpf1. We identify the latter as an unstable protein at the surface of

mitochondria. Collectvely, the current study provides the first glimpse into the process of dual distribution of TA proteins between mitochondria and peroxisomes.

Materials and Methods

Yeast strains and growth conditions

Saccharomyces cerevisiae strains used in this study are listed in Table S2. For induction of peroxisomes, yeast strains were grown at 30 °C on oleate-containing YNBO media (0.1% (w/v) yeast extract, 0.17% (w/v) yeast nitrogen base, 0.5% (w/v) ammonium sulphate, 0.0002% (w/v) uracil, 0.0002% (w/v) adenine sulphate, 0.12% oleic acid, 0.2% Tween40, supplied with amino acids). Generally, cells were grown at 30 °C on selective or rich media (YP) supplemented with 2% of either glucose or galactose. Yeast transformation was performed by the lithium acetate method (Gietz & Woods, 2006).

Yeast growth assay

Yeast strains were cultivated till mid-logarithmic phase and after harvesting them, cells were resuspended to 1 ml of $OD_{600} = 2$. The cell suspension was fivefold serially diluted and 5 µl of each dilution was spotted on the indicated solid media. The plates were incubated at 30° C in a humid box and the growth was monitored for 2-10 days.

High-throughput microscopy screening

The following query strains were made to cross with the yeast deletion library: (i) mCherry-Fis1, Pex3-GFP, (ii) mCherry-Fis1, Om45-GFP, (iii) mCherry-Gem1, Pex3-GFP, and (iv) mCherry-Gem1, Om45-GFP. To generate these query strains a DNA sequence encoding the mCherry tag was genomically inserted by homologous recombination at the 5' of the sequence encoding either Fis1 or Gem1, with the strong and constitutive *TEF2* promoter and the Nourseothricin N-acetyl transferase (NAT) selection cassette. Subsequently, in these strains the DNA sequence encoding GFP was integrated by homologous recombination into the 3' region of either Pex3 or Om45 also with the *TEF2* promoter and the hygromycin B phosphotransferase (HPH) selection cassette. Query strains were crossed by synthetic genetic array (SGA) with two libraries – the knock out (KO) library and the decreased abundance by mRNA perturbation (DAmP) library, as previously described (Cohen & Schuldiner, 2011; Tong & Boone, 2006). The high-throughput screen was performed by growing cells overnight

at 30 °C in rich media (YP) supplemented with galactose, diluting them 1:10 in the next morning and letting them divide at 30 °C for 4 hours before imaging with an automated system (Breker et al., 2013).

Recombinant DNA techniques

Full lists of primers and plasmids used in this study are found in Tables S3 and S4, respectively. The plasmid pGEM4-Mpf1-3HA was used as a template for site directed mutagenesis to create the PH domain mutant of Mpf1. The PCR product was digested with Dpn1 and transformed into *E. coli* cells. For gene deletion and manipulation, PCR product containing the selection cassette with flanking regions complementary to DNA sequences of the gene of interest were transformed into yeast cells by the Li-acetate method. Colonies were analysed by screening PCR. All constructs were verified by DNA sequencing.

Separation of mitochondria and peroxisomes by gradient centrifugation

Yeast cells were precultured overnight in 100 ml YP medium supplemented with 0.1% glucose. Next morning, the culture was upscaled to 400 ml and incubated overnight. For induction of peroxisomes, cells were harvested (5000 x g, 6 min, RT) and washed with 20 ml sterile water and centrifuged again (5000 x g, 6 min, RT). Cells were then resuspended in 1000 ml YNBO medium and incubated for 16 – 20 hours. Then, cells were harvested (5000 x g, 6 min, RT) and washed twice with 30 ml sterile water followed by centrifugation (5000 x g, 6 min, RT). The cells were then incubated in 20 ml Dithiothreitol (DTT) buffer (100 mM Tris, 10 mM DTT) for 30 min and were harvested (1500 × g, 6 min, RT) and washed twice with 20 ml sorbitol buffer (20 mM 4-(2-hydroxyethyl)-1-piperazineethanesulfonic acid (HEPES), 1.2 M sorbitol, pH 7.2). Next, cells were incubated for 1 hour in 20 ml sorbitol buffer containing Zymolyase. Digestion of yeast cell walls was monitored by measuring the OD_{600} of small sample of cells to detect their rupturing upon addition of water.

All further steps were carried out on ice. Spheroplasts were washed twice with 20 ml sorbitol buffer and centrifuged (1500 × g, 6 min, 4 °C). Then, cells were homogenized using a dounce homogenizer in a solution of 15 ml lysis buffer (5 mM 2-(N-Morpholino)-ethane sulphonic acid (MES), 0.5 mM EDTA, 1 mM KCl) containing 0.6 M Sorbitol, Proteases inhibitors cocktail (PIC), 2 mM phenylmethylsulfonyl fluoride (PMSF), pH 5.5). Cell debris were removed by two centrifugation runs (1600 × g, 10 min, 4 °C). The resulting supernatant (containing mitochondria and peroxisomes) was centrifuged (13,000 × g, 5 min, 4 °C) and the pellet was resuspended in lysis buffer to OD_{600}= 4. The organelles were loaded on top a density

gradient consisting of 415 µl of 20%, 830 µl of 25%, 415 µl of 30%, and 830 µl of 40% Histodenz in gradient buffer A (5 mM MES, 1 mM EDTA, 1 mM KCl, and 0.1% (v/v) ethanol, pH 5.5). Gradients were centrifuged in a Beckman ultracentrifuge optima XE with a swinging bucket rotor, SW 60 Ti (100,000 × g, 90 min, 4 °C, acceleration 7, brake off). A total of 12 fractions with 235 µl in each were collected from the top of the gradient and mixed with 8x sample buffer (0.5 M Tris pH 6.8, 16% SDS, 80% glycerol, 8 mg/mL bromophenol blue) to a final 2x concentration. Then 5% (v/v) β-mercaptoethanol was added and the samples were heated at 95 °C. Fractions were subjected to SDS-PAGE followed by Western blotting.

Isolation of Mitochondria

Yeast cells were grown in liquid media (volume of 2-6 L) to logarithmic phase. The cells were harvested (3000 x g, 5 min, RT), resuspended in DTT buffer and incubated at 30 °C for 15 min. Cells were harvested (2000 x g, 5 min, RT), washed once with spheroplasting buffer (1.2 M Sorbitol, 20 mM KPI, pH 7.2), harvested again and resuspended in spheroplasting buffer with Zymolyase (6 mg/g of cells) and incubated at 30 °C for 1 hour.

Further steps were carried out on ice. Spheroplasts were homogenized in homogenization buffer (0.6 M Sorbitol, 10 mm Tris, pH 7.4, 1 mM EDTA, 0.2% fatty acid-free BSA with 2 mM PMSF) using a dounce homogenizer to obtain a cell lysate. Cell debris and nuclei were removed by two clarifying spins (2000 x g, 10 min, 4 °C). The supernatant (cytosol + organelles) was centrifuged (18,000 x g, 15 min, 4 °C) to pellet crude mitochondria. The resulting post nuclear supernatant (PNS) consisted of ER/microsomal and cytosolic fractions. The crude mitochondria were washed twice with SEM buffer (250 mM Sucrose, 1 mM EDTA, 10 mM MOPS) containing 2 mM PMSF and were pelleted again (18,000 x g, 15 min, 4 °C).

Subcellular fractionation

All the steps were carried out at 4 °C. Whole cell lysate and crude mitochondria were obtained as described above. To further purify mitochondria from potential contaminants, the mitochondrial fraction was layered on a Percoll gradient (25% Percoll, 2 M sucrose, 100 mM MOPS/KOH pH 7.2, 100 mM EDTA, 200 mM PMSF) and centrifuged (80,000 x g, 45 min, 4 °C, slow acceleration, slow brake). Highly pure mitochondria were found as a brownish layer close to the bottom of the tube and was removed carefully with a Pasteur pipette. The mitochondria were washed several times with SEM buffer containing 2 mM PMSF and pelleted again (18, 000 x g, 15 min, 4 °C).

To isolate ER/microsomal and cytosolic fractions, 20 ml of PNS was clarified (18,000 x g, 15 min, 4 °C) and centrifuged (200,000 x g, 1 hour, 4 °C). The supernatant contained the cytosolic fraction, and the brownish sticky pellet (consisting of ER) was resuspended in 2 ml of SEM buffer containing 2 mM PMSF and homogenized with a dounce homogenizer. The sample was centrifuged (18,000 x g, 20 min, 4 °C) to obtain ER/microsomes in the supernatant.

The obtained fractions were precipitated with chloroform-methanol mixture and the pellet was resuspended in 2x sample buffer (125 mM Tris pH 6.8, 4% SDS, 20% glycerol, 10% β-ME, 2 mg/mL bromophenol blue) to obtain protein concentration of 2 mg/ml. Samples were heated at 95 °C for 10 min and further analysed by SDS-PAGE and immunoblotting. Table S5 indicates the antibodies used in the current study.

Proteinase K (PK) assay

Isolated mitochondria (100 µg) were incubated on ice for 15 minutes in 50 µL of either SEM buffer (untreated) or SEM buffer containing 10 µg/mL proteinase K (PK). Then, PK activity was inhibited by addition of 2 mM PMSF. The samples were centrifuged (18,000 x g, 15 min, 4 °C) and the pellets were resuspended in 2x sample buffer. Samples were heated at 95 °C for 10 min and further analysed by SDS-PAGE and immunoblotting.

Carbonate (Alkaline) Extraction

Isolated mitochondria (100 µg) were resuspended on ice in 100 µL solution containing 20 mM HEPES, 2 mM PMSF and 1x PIC, pH 7.5. This was followed by the addition of 100 µL of carbonate solution 200 mM Na_2CO_3, 5 mM PMSF, 1x PIC) at various pH values (10.5, 11, 11.5, or 12), and further incubation for 20 min at 4 °C. Next, pellet (membrane proteins) and supernatant fraction (soluble proteins) were separated by centrifugation (75,000 x g, 30 min, 4 °C). The supernatant was precipitated by trichloroacetic acid (TCA). The pellet and precipitated proteins from the supernatant were resuspended in 40 µL 2x sample buffer, heated at 95 °C for 10 min and further analysed by SDS-PAGE and immunoblotting.

Protein stability assay

Yeast strains were grown to mid-logarithmic phase. For each time point, cells corresponding to OD_{600} of 2 were collected and resuspended in 1 ml of media. Cycloheximide (CHX) at final conc. of 0.1 mg/ml was added at time=0 and the cells were incubated further at 30 °C for different time periods. Then, cells were harvested (3000 x g, 5 min, room temperature (RT)) and the proteins were extracted by alkaline lysis using 0.2 M NaOH, followed by heating with

2x sample buffer at 95 °C for 10 min. The samples were analysed by SDS-PAGE and immunoblotting.

(Immuno) Fluorescence microscopy

Yeast cells were grown on synthetic media containing 2% glucose till mid-logarithmic phase. The cells (1 ml) were centrifuged (3000 x g, 5 min, RT) and the cells pellet was resuspended in 50 µl water. A small portion (5 µl) of this solution was mixed with 1% (w/v) low melting point agarose and was spread on a glass slide. Confocal spinning disc microscope was used to capture images and they were analysed using ImageJ (more details are given in the next section).

For immunofluorescene microscopy, a published protocol was optimized (Pemberton, 2014). Yeast cells were grown till mid-logarithmic phase and to fix them, they were incubated at 30 °C for 10 min with 1% (v/v) of 37% formaldehyde. Cells were washed twice and centrifuged (3000 x g, 5 min, RT) with Phosphate buffer (100 mM KH_2PO_4, 37.4 mM KOH, pH 6.5). Then, cells were resuspended in DTT buffer (100 mM Tris-HCl and 100 mM DTT) and incubated for 10 min at 30 °C. Cells were then washed twice with SPC buffer (1.2 M Sorbitol, 127 mM KH_2PO_4, 36 mM Citric acid) and spheroplasts were produced by incubating the cells for 45 min at 30 °C in SPC buffer + Zymolyase (6 mg/gram of cells). Spheroplasts were washed with SPC buffer and centrifuged (2000 x g, 5 min, 4 °C) and the pellets were resuspended in 100 µl SPC buffer, snap frozen, and stored at -80 °C.

Glass slides with 15 wells were treated with 0.1% (w/v) Poly-L-Lysine for 15 min at RT to enhance cell attachment. The poly-l-lysine was washed off by gently passing a stream of distilled water and the slides were air-dried. Next, 5 µl of spheroplasts solution were added to each well and were allowed to attach for 15 min. Excess liquid was removed, the slides were immersed in ice-cold MeOH for 5 min and were moved up and down 2-3 times. To further permeabilize the cell membrane, the slides were then immersed in acetone for 30 sec. Following this, the slides were air-dried and placed in a humid box for further steps. The cells were blocked with blocking buffer (PBS, 2% (w/v) milk, 0.1% (v/v) Tween-20) for 10 min at RT. The blocking solution was discarded, and cells were incubated at dark with 5 µg/ml primary antibody in the blocking buffer for 2 h at RT. Excess liquid was aspirated, and the cells were washed 3 times with PBS before mounting with 80% (v/v) glycerol. Cells were imaged using spinning disk microscope Zeiss Axio Examiner Z1 with a CSU-X1 real-time confocal system (Visitron) and SPOT Flex charge-coupled device camera (Visitron). Samples were

observed using Zeiss Objective Plan-Apochromat 63×/1.4 Oil DIC M27. Images in Brightfield, GFP, and RFP channels were acquired through AxioVision software., Subsequent cropping and merging was done using Fiji software.

Rapid protein extraction

Cells grown to mid logarithmic phase were harvested and resuspended such that 1 ml consisted of 2.5 units of OD_{600}. The corresponding cell pellets were resuspended in 200 µl NaOH (100 mM) and incubated for 5 min at RT. The cells were centrifuged (3000 x g, 5 min, RT), resuspended in 2x sample buffer and heated for 5 min at 95 °C. The samples were centrifuged (3000 x g, 5 min, RT) and the supernatant was analysed using SDS-PAGE followed by immunoblotting.

Pull-down assays

Cell pellets from 500 ml cultures were resuspended in 5 ml DTT buffer and incubated for 15 min in a 30 °C shaker. Cells were harvested (2000 x g, 5 min, RT), washed once with spheroplasting buffer (1.2 M Sorbitol, 20 mM KPI, pH 7.2), resuspended in spheroplasting buffer with Zymolyase (6 mg/g of cells), and then incubated for 1 hour in a 30 °C shaker. Cell pellets were resuspended in 1 ml lysis buffer (Tris-buffered saline (TBS), 2 mM PMSF, 1x EDTA free protease inhibitor cocktail, 5 mM EDTA) and homogenized using a douncer. Whole cell lysate (WCL) corresponding to 3 mg proteins was solubilized with 1% Triton X-100 and incubated in overhead shaker for 30 min at 4 °C. The solubilized sample was centrifuged (30000 g, 30 min, 4 °C) to clear out cell debris and the supernatant was incubated with anti-HA magnetic beads for 2 hours at 4 °C. The beads were washed with wash buffer (TBS, 0.5% Triton X-100, 5 mM EDTA, 350 mM NaCl) and the bound proteins were eluted by incubating the beads for 10 min at 55 °C with 2x sample buffer supplemented with 0.05% H_2O_2. Eluted material was supplemented with 5% β-ME, incubated at 95 °C for 5 min and analysed by SDS-PAGE followed by immunoblotting.

Real-time quantitative PCR

RNA from 10 mL yeast culture was isolated using a mini kit for RNA isolation (Macherey-NAGEL, REF 740933.50). Next, 2.5 mg of RNA was used to prepare cDNA using the reagents and program mentioned in GoScript™ Reverse Transcription Mix, Oligo(dT) Protocol (Promega, A2791). RT-qPCR was set up in Thermo Fisher Scientific QuantStudio™ 5 Real-

Time PCR System and the results were analyzed using Design and Analysis software 2.6.0. Primers used for the qPCR are listed in Table S3 and Actin was used as a reference.

Acknowledgments

We thank E. Kracker for excellent technical assistance, H. Meyer and A. Fadel for help with the high-throughput screen, Marie Helmke and Luca Brenner for help with cloning, W. Girzalsky and R. Erdmann for anti-Pex14 antibody, and K.S. Dimmer for helpful discussions. This work was supported by the Deutsche Forschungsgemeinschaft (RA 1028/11-1 to D.R. and M.S.), the German-Israel Foundation (grant I-1458-412.13/2018 to M.S. and D.R.), and the Elisabeth and Franz Knoop-Foundation (fellowship to D.G.V.). All targeting work in the Schuldiner lab is also supported by an ERC CoG from the European Union (OnTarget, 864068). The robotic system of the Schuldiner lab was purchased through the kind support of the Blythe Brenden-Mann Foundation. MS is an Incumbent of the Dr. Gilbert Omenn and Martha Darling Professorial Chair in Molecular Genetics.

The authors declare no competing financial interests.

Author contributions

N.A., D.G.V., designed and conducted experiments, J.O. performed experiments; E.Z., M.S., and D.R. designed experiments and analyzed data, N.A. and D. R. wrote the initial version of the manuscript. All authors read and contributed to the final manuscript.

References

Backes, S., Bykov, Y. S., Flohr, T., Räschle, M., Zhou, J., Lenhard, S., Krämer, L., Mühlhaus, T., Bibi, C., Jann, C., Smith, J. D., Steinmetz, L. M., Rapaport, D., Storchová, Z., Schuldiner, M., Boos, F., & Herrmann, J. M. (2021). The chaperone-binding activity of the mitochondrial surface receptor Tom70 protects the cytosol against mitoprotein-induced stress. *Cell Reports*, *35*(1), 108936. https://doi.org/10.1016/j.celrep.2021.108936

Backes, S., Hess, S., Boos, F., Woellhaf, M. W., Gödel, S., Jung, M., Mühlhaus, T., & Herrmann, J. M. (2018). Tom70 enhances mitochondrial preprotein import efficiency by binding to internal targeting sequences. *Journal of Cell Biology*, *217*(4), 1369–1382. https://doi.org/10.1083/jcb.201708044

Bittner, E., Stehlik, T., & Freitag, J. (2022a). Sharing the wealth: The versatility of proteins targeted to peroxisomes and other organelles. *Frontiers in Cell and Developmental Biology*, *10*. https://doi.org/10.3389/fcell.2022.934331

Bittner, E., Stehlik, T., & Freitag, J. (2022b). Sharing the wealth: The versatility of proteins targeted to peroxisomes and other organelles. *Frontiers in Cell and Developmental Biology*, *10*. https://doi.org/10.3389/fcell.2022.934331

Bleazard, W., McCaffery, J. M., King, E. J., Bale, S., Mozdy, A., Tieu, Q., Nunnari, J., & Shaw, J. M. (1999). The dynamin-related GTPase Dnm1 regulates mitochondrial fission in yeast. *Nature Cell Biology*, *1*(5), 298–304. https://doi.org/10.1038/13014

Borgese, N., Brambillasca, S., & Colombo, S. (2007). How tails guide tail-anchored proteins to their destinations. *Current Opinion in Cell Biology*, *19*(4), 368–375. https://doi.org/10.1016/j.ceb.2007.04.019

Breker, M., Gymrek, M., & Schuldiner, M. (2013). A novel single-cell screening platform reveals proteome plasticity during yeast stress responses. *Journal of Cell Biology*, *200*(6), 839–850. https://doi.org/10.1083/jcb.201301120

Burri, L., Vascotto, K., Gentle, I. E., Chan, N. C., Beilharz, T., Stapleton, D. I., Ramage, L., & Lithgow, T. (2006). Integral membrane proteins in the mitochondrial outer membrane of Saccharomyces cerevisiae. *The FEBS Journal*, *273*(7), 1507–1515. https://doi.org/10.1111/j.1742-4658.2006.05171.x

Chen, Y., Pieuchot, L., Loh, R. A., Yang, J., Kari, T. M. A., Wong, J. Y., & Jedd, G. (2014). Hydrophobic handoff for direct delivery of peroxisome tail-anchored proteins. *Nature Communications*, *5*(1), 5790. https://doi.org/10.1038/ncomms6790

Cichocki, B. A., Krumpe, K., Vitali, D. G., & Rapaport, D. (2018). Pex19 is involved in importing dually targeted tail-anchored proteins to both mitochondria and peroxisomes. *Traffic*, *19*(10), 770–785. https://doi.org/10.1111/tra.12604

Cohen, Y., & Schuldiner, M. (2011). Advanced Methods for High-Throughput Microscopy Screening of Genetically Modified Yeast Libraries. In G. Cagney & A. Emili (Eds.), *Network Biology* (Vol. 781, pp. 127–159). Humana Press. https://doi.org/10.1007/978-1-61779-276-2_8

Costello, J. L., Castro, I. G., Camões, F., Schrader, T. A., McNeall, D., Yang, J., Giannopoulou, E.-A., Gomes, S., Pogenberg, V., Bonekamp, N. A., Ribeiro, D., Wilmanns, M., Jedd, G., Islinger, M., & Schrader, M. (2017). Predicting the targeting of tail-anchored proteins to subcellular compartments in mammalian cells. *Journal of Cell Science*, *130*(9), 1675–1687. https://doi.org/10.1242/jcs.200204

Das, R., & Chakrabarti, O. (2020). Mitochondrial hyperfusion: A friend or a foe. *Biochemical Society Transactions*, *48*(2), 631–644. https://doi.org/10.1042/BST20190987

Doan, K. N., Grevel, A., Mårtensson, C. U., Ellenrieder, L., Thornton, N., Wenz, L.-S., Opaliński, Ł., Guiard, B., Pfanner, N., & Becker, T. (2020). The Mitochondrial Import Complex MIM Functions as Main Translocase for α-Helical Outer Membrane Proteins. *Cell Reports*, *31*(4), 107567. https://doi.org/10.1016/j.celrep.2020.107567

Fujiki, Y., Matsuzono, Y., Matsuzaki, T., & Fransen, M. (2006). Import of peroxisomal membrane proteins: The interplay of Pex3p- and Pex19p-mediated interactions. *Biochimica Et Biophysica Acta*, *1763*(12), 1639–1646. https://doi.org/10.1016/j.bbamcr.2006.09.030

Gallego, O., Betts, M. J., Gvozdenovic-Jeremic, J., Maeda, K., Matetzki, C., Aguilar-Gurrieri, C., Beltran-Alvarez, P., Bonn, S., Fernández-Tornero, C., Jensen, L. J., Kuhn, M., Trott, J., Rybin, V., Müller, C. W., Bork, P., Kaksonen, M., Russell, R. B., & Gavin, A. (2010). A systematic screen for protein–lipid interactions in Saccharomyces cerevisiae. *Molecular Systems Biology*, *6*(1), 430. https://doi.org/10.1038/msb.2010.87

Gietz, R. D., & Woods, R. A. (2006). Yeast Transformation by the LiAc/SS Carrier DNA/PEG Method. In W. Xiao (Ed.), *Yeast Protocol* (pp. 107–120). Humana Press. https://doi.org/10.1385/1-59259-958-3:107

Götte, K., Girzalsky, W., Linkert, M., Baumgart, E., Kammerer, S., Kunau, W.-H., & Erdmann, R. (1998). Pex19p, a Farnesylated Protein Essential for Peroxisome Biogenesis. *Molecular and Cellular Biology*, *18*(1), 616–628. https://doi.org/10.1128/MCB.18.1.616

Hiltunen, J. K., Mursula, A. M., Rottensteiner, H., Wierenga, R. K., Kastaniotis, A. J., & Gurvitz, A. (2003). The biochemistry of peroxisomal β-oxidation in the yeast Saccharomyces cerevisiae. *FEMS Microbiology Reviews*, *27*(1), 35–64. https://doi.org/10.1016/S0168-6445(03)00017-2

Hoppins, S., Lackner, L., & Nunnari, J. (2007). The Machines that Divide and Fuse Mitochondria. *Annual Review of Biochemistry*, *76*(Volume 76, 2007), 751–780. https://doi.org/10.1146/annurev.biochem.76.071905.090048

Isakoff, S. J., Cardozo, T., Andreev, J., Li, Z., Ferguson, K. M., Abagyan, R., Lemmon, M. A., Aronheim, A., & Skolnik, E. Y. (1998). Identification and analysis of PH domain-containing targets of phosphatidylinositol 3-kinase using a novel in vivo assay in yeast. *The EMBO Journal*, *17*(18), 5374–5387. https://doi.org/10.1093/emboj/17.18.5374

Jores, T., Lawatscheck, J., Beke, V., Franz-Wachtel, M., Yunoki, K., Fitzgerald, J. C., Macek, B., Endo, T., Kalbacher, H., Buchner, J., & Rapaport, D. (2018). Cytosolic Hsp70 and

Hsp40 chaperones enable the biogenesis of mitochondrial β-barrel proteins. *Journal of Cell Biology*, *217*(9), 3091–3108. https://doi.org/10.1083/jcb.201712029

Kim, H., Botelho, S. C., Park, K., & Kim, H. (2015). Use of carbonate extraction in analyzing moderately hydrophobic transmembrane proteins in the mitochondrial inner membrane. *Protein Science : A Publication of the Protein Society*, *24*(12), 2063–2069. https://doi.org/10.1002/pro.2817

Koch, A., Yoon, Y., Bonekamp, N. A., McNiven, M. A., & Schrader, M. (2005). A Role for Fis1 in Both Mitochondrial and Peroxisomal Fission in Mammalian Cells. *Molecular Biology of the Cell*, *16*(11), 5077–5086. https://doi.org/10.1091/mbc.E05-02-0159

Kreimendahl, S., & Rassow, J. (2020). *The mitochondrial outer membrane protein Tom70-mediator in protein traffic, membrane contact cites and innate immunity*. https://hss-opus.ub.ruhr-uni-bochum.de/opus4/frontdoor/index/index/year/2021/docId/7875

Krumpe, K., Frumkin, I., Herzig, Y., Rimon, N., Özbalci, C., Brügger, B., Rapaport, D., & Schuldiner, M. (2012). Ergosterol content specifies targeting of tail-anchored proteins to mitochondrial outer membranes. *Molecular Biology of the Cell*, *23*(20), 3927–3935. https://doi.org/10.1091/mbc.E11-12-0994

Kuravi, K., Nagotu, S., Krikken, A. M., Sjollema, K., Deckers, M., Erdmann, R., Veenhuis, M., & van der Klei, I. J. (2006). Dynamin-related proteins Vps1p and Dnm1p control peroxisome abundance in Saccharomyces cerevisiae. *Journal of Cell Science*, *119*(19), 3994–4001. https://doi.org/10.1242/jcs.03166

Lemmon, M. A. (2004). Pleckstrin homology domains: Not just for phosphoinositides. *Biochemical Society Transactions*, *32*(5), 707–711. https://doi.org/10.1042/BST0320707

Liu, Q., Chang, C. E., Wooldredge, A. C., Fong, B., Kennedy, B. K., & Zhou, C. (2022). Tom70-based transcriptional regulation of mitochondrial biogenesis and aging. *eLife*, *11*, e75658. https://doi.org/10.7554/eLife.75658

Maffucci, T., & Falasca, M. (2001). Specificity in pleckstrin homology (PH) domain membrane targeting: A role for a phosphoinositide–protein co-operative mechanism. *FEBS Letters*, *506*(3), 173–179. https://doi.org/10.1016/S0014-5793(01)02909-X

Mark, K. G., Simonetta, M., Maiolica, A., Seller, C. A., & Toczyski, D. P. (2014). Ubiquitin Ligase Trapping Identifies an SCFSaf1 Pathway Targeting Unprocessed Vacuolar/Lysosomal Proteins. *Molecular Cell*, *53*(1), 148–161. https://doi.org/10.1016/j.molcel.2013.12.003

Mattiazzi Ušaj, M., Brložnik, M., Kaferle, P., Žitnik, M., Wolinski, H., Leitner, F., Kohlwein, S. D., Zupan, B., & Petrovič, U. (2015). Genome-Wide Localization Study of Yeast Pex11 Identifies Peroxisome–Mitochondria Interactions through the ERMES Complex. *Journal of Molecular Biology*, *427*(11), 2072–2087. https://doi.org/10.1016/j.jmb.2015.03.004

Morgenstern, M., Peikert, C. D., Lübbert, P., Suppanz, I., Klemm, C., Alka, O., Steiert, C., Naumenko, N., Schendzielorz, A., Melchionda, L., Mühlhäuser, W. W. D., Knapp, B., Busch, J. D., Stiller, S. B., Dannenmaier, S., Lindau, C., Licheva, M., Eickhorst, C.,

Galbusera, R., … Warscheid, B. (2021). Quantitative high-confidence human mitochondrial proteome and its dynamics in cellular context. *Cell Metabolism*, *33*(12), 2464-2483.e18. https://doi.org/10.1016/j.cmet.2021.11.001

Motley, A. M., Ward, G. P., & Hettema, E. H. (2008). Dnm1p-dependent peroxisome fission requires Caf4p, Mdv1p and Fis1p. *Journal of Cell Science*, *121*(10), 1633–1640. https://doi.org/10.1242/jcs.026344

Mozdy, A. D., McCaffery, J. M., & Shaw, J. M. (2000). Dnm1p GTPase-mediated mitochondrial fission is a multi-step process requiring the novel integral membrane component Fis1p. *The Journal of Cell Biology*, *151*(2), 367–380. https://doi.org/10.1083/jcb.151.2.367

Okreglak, V., & Walter, P. (2014). The conserved AAA-ATPase Msp1 confers organelle specificity to tail-anchored proteins. *Proceedings of the National Academy of Sciences*, *111*(22), 8019–8024. https://doi.org/10.1073/pnas.1405755111

Ong, S.-B., Hall, A. R., & Hausenloy, D. J. (2013). Mitochondrial Dynamics in Cardiovascular Health and Disease. *Antioxidants & Redox Signaling*, *19*(4), 400–414. https://doi.org/10.1089/ars.2012.4777

Pemberton, L. F. (2014). Preparation of Yeast Cells for Live-Cell Imaging and Indirect Immunofluorescence. In J. S. Smith & D. J. Burke (Eds.), *Yeast Genetics: Methods and Protocols* (pp. 79–90). Springer. https://doi.org/10.1007/978-1-4939-1363-3_6

Regev-Rudzki, N., & Pines, O. (2007). Eclipsed distribution: A phenomenon of dual targeting of protein and its significance. *BioEssays*, *29*(8), 772–782. https://doi.org/10.1002/bies.20609

Riddihough, G. (1994). More meanders and sandwiches. *Nature Structural Biology*, *1*(11), 755–757. https://doi.org/10.1038/nsb1194-755

Scheffzek, K., & Welti, S. (2012). Pleckstrin homology (PH) like domains – versatile modules in protein–protein interaction platforms. *FEBS Letters*, *586*(17), 2662–2673. https://doi.org/10.1016/j.febslet.2012.06.006

Schlossmann, J., Lill, R., Neupert, W., & Court, D. A. (1996). Tom71, a Novel Homologue of the Mitochondrial Preprotein Receptor Tom70*. *Journal of Biological Chemistry*, *271*(30), 17890–17895. https://doi.org/10.1074/jbc.271.30.17890

Schrader, M., Costello, J. L., Godinho, L. F., Azadi, A. S., & Islinger, M. (2016). Proliferation and fission of peroxisomes—An update. *Biochimica et Biophysica Acta (BBA) - Molecular Cell Research*, *1863*(5), 971–983. https://doi.org/10.1016/j.bbamcr.2015.09.024

Schrader, T. A., Carmichael, R. E., Islinger, M., Costello, J. L., Hacker, C., Bonekamp, N. A., Weishaupt, J. H., Andersen, P. M., & Schrader, M. (2022). PEX11β and FIS1 cooperate in peroxisome division independently of mitochondrial fission factor. *Journal of Cell Science*, *135*(13), jcs259924. https://doi.org/10.1242/jcs.259924

Schuldiner, M., Metz, J., Schmid, V., Denic, V., Rakwalska, M., Schmitt, H. D., Schwappach, B., & Weissman, J. S. (2008). The GET Complex Mediates Insertion of Tail-Anchored

Proteins into the ER Membrane. *Cell*, *134*(4), 634–645. https://doi.org/10.1016/j.cell.2008.06.025

Shai, N., Schuldiner, M., & Zalckvar, E. (2016). No peroxisome is an island—Peroxisome contact sites. *Biochimica et Biophysica Acta (BBA) - Molecular Cell Research*, *1863*(5), 1061–1069. https://doi.org/10.1016/j.bbamcr.2015.09.016

Shaw, J. M., & Nunnari, J. (2002). Mitochondrial dynamics and division in budding yeast. *Trends in Cell Biology*, *12*(4), 178–184.

Speijer, D. (2017). Evolution of peroxisomes illustrates symbiogenesis. *BioEssays*, *39*(9), 1700050. https://doi.org/10.1002/bies.201700050

Stefanovic, S., & Hegde, R. S. (2007). Identification of a Targeting Factor for Posttranslational Membrane Protein Insertion into the ER. *Cell*, *128*(6), 1147–1159. https://doi.org/10.1016/j.cell.2007.01.036

Stehlik, T., Kremp, M., Kahnt, J., Bölker, M., & Freitag, J. (2020). Peroxisomal targeting of a protein phosphatase type 2C via mitochondrial transit. *Nature Communications*, *11*(1), Article 1. https://doi.org/10.1038/s41467-020-16146-3

Stein, I., Peleg, Y., Even-Ram, S., & Pines, O. (1994). The Single Translation Product of the FUM1 Gene (Fumarase) Is Processed in Mitochondria before Being Distributed between the Cytosol and Mitochondria in Saccharomyces cerevisiae. *Molecular and Cellular Biology*, *14*(7), 4770–4778. https://doi.org/10.1128/mcb.14.7.4770-4778.1994

Tong, A. H. Y., & Boone, C. (2006). Synthetic genetic array analysis in Saccharomyces cerevisiae. *Methods in Molecular Biology (Clifton, N.J.)*, *313*, 171–192. https://doi.org/10.1385/1-59259-958-3:171

Vitali, D. G., Drwesh, L., Cichocki, B. A., Kolb, A., & Rapaport, D. (2020). The Biogenesis of Mitochondrial Outer Membrane Proteins Show Variable Dependence on Import Factors. *iScience*, *23*(1), 100779. https://doi.org/10.1016/j.isci.2019.100779

Yamamoto, H., Fukui, K., Takahashi, H., Kitamura, S., Shiota, T., Terao, K., Uchida, M., Esaki, M., Nishikawa, S., Yoshihisa, T., Yamano, K., & Endo, T. (2009). Roles of Tom70 in Import of Presequence-containing Mitochondrial Proteins*. *Journal of Biological Chemistry*, *284*(46), 31635–31646. https://doi.org/10.1074/jbc.M109.041756

Yogev, O., Naamati, A., & Pines, O. (2011). Fumarase: A paradigm of dual targeting and dual localized functions. *The FEBS Journal*, *278*(22), 4230–4242. https://doi.org/10.1111/j.1742-4658.2011.08359.x

Yoon, Y., Krueger, E. W., Oswald, B. J., & McNiven, M. A. (2003). The Mitochondrial Protein hFis1 Regulates Mitochondrial Fission in Mammalian Cells through an Interaction with the Dynamin-Like Protein DLP1. *Molecular and Cellular Biology*, *23*(15), 5409–5420. https://doi.org/10.1128/MCB.23.15.5409-5420.2003

Young, J. C., Hoogenraad, N. J., & Hartl, F. U. (2003). Molecular Chaperones Hsp90 and Hsp70 Deliver Preproteins to the Mitochondrial Import Receptor Tom70. *Cell*, *112*(1), 41–50. https://doi.org/10.1016/S0092-8674(02)01250-3

Yu, J. W., Mendrola, J. M., Audhya, A., Singh, S., Keleti, D., DeWald, D. B., Murray, D., Emr, S. D., & Lemmon, M. A. (2004). Genome-Wide Analysis of Membrane Targeting by *S. cerevisiae* Pleckstrin Homology Domains. *Molecular Cell*, *13*(5), 677–688. https://doi.org/10.1016/S1097-2765(04)00083-8

Zanphorlin, L. M., Lima, T. B., Wong, M. J., Balbuena, T. S., Minetti, C. A. S. A., Remeta, D. P., Young, J. C., Barbosa, L. R. S., Gozzo, F. C., & Ramos, C. H. I. (2016). Heat Shock Protein 90 kDa (Hsp90) Has a Second Functional Interaction Site with the Mitochondrial Import Receptor Tom70*. *Journal of Biological Chemistry*, *291*(36), 18620–18631. https://doi.org/10.1074/jbc.M115.710137

Zhou, J., Jung, M., Dimmer, K. S., & Rapaport, D. (2022). The multi-factor modulated biogenesis of the mitochondrial multi-span protein Om14. *Journal of Cell Biology*, *221*(4), e202112030. https://doi.org/10.1083/jcb.202112030

Figure legends

Figure 1: A high-throughput microscopy screen reveals proteins that affect dual distribution of Fis1. **(A)** Illustration of the screen aiming to find factors that affect dual targeting of Fis1. mCherry-Fis1 and Pex3-GFP were integrated into a yeast deletion and depletion libraries. The resultant strains, each containing a unique gene deletion/depletion and carrying the fluorescently labelled target proteins were visualized using automated microscopy. **(B)** Representative images of WT and three deletions strains with altered distribution of Fis1. The phenotype was observed by detecting co-localization of mCherry-Fis1 with Pex3-GFP (shown with white arrows). Scale bar, 5 µm. **(C)** Quantification of the co-localization of mCherry-Fis1 with peroxisomes. Total number of peroxisomes (visualized by Pex3-GFP) were counted in 100 cells in each of three independent experiments. Subsequently, the percentage of mCherry-Fis1 puncta co-localized with peroxisomes was determined. The graph represents the average of three independent experiments, error bars represent standard error.

Figure 2: Physical separation of mitochondria and peroxisomes validates the hits. **(A)** Gradient centrifugation procedure was employed to separate mitochondria and peroxisomes from the indicated strains and 12 fractions from the top of the gradient were collected. The fractions were analyzed by SDS-PAGE and immunodecoration with antibodies against Fis1 (dually localized to mitochondria and peroxisomes), Tom20 (mitochondrial marker), and Pex14 (peroxisome marker). **(B)** The intensities of Fis1 obtained in each fraction was quantified and the sum of all the 12 intensities was set to 100%. Fis1 signal in fractions 1-4 was considered mitochondrial, while that within fractions 9-12 was designated as peroxisomal. The graph represents the average of three independent experiments, error bars representing standard error.

Figure 3: Tom71 has a unique effect on the distribution of Fis1. **(A)** Tom70 was overexpressed in the indicated strains by replacing the endogenous promoter with the *GPD* promoter. Cells of the resulting strains were grown on galactose and whole cell lysate was obtained by alkaline lysis. Extracted proteins were analyzed by SDS-PAGE and immunodecoration with the indicated antibodies. Ponceau staining was employed to verify equal loading in all lanes. **(B, C)** Gradient separation of mitochondria and peroxisomes from

the indicated strains were performed as described in the legend to Fig. 2A and B. **(D)** Tom71 was overexpressed in the indicated strains by replacing the endogenous promoter with the *GPD* promoter. Proteins from the obtained strains were analyzed as described in part (A). **(E-F)** Gradient separation of mitochondria and peroxisomes from the indicated strains were performed as described in the legend to Fig. 2A and B. Note: to allow easier comparison, the Fis1 levels in WT cells in panels C and F were taken from Figure 2B. The graph represents the average of three independent experiments, error bars representing standard error. **(G)** Cells expressing either Flag-Pex19 alone or co-expressing Flag-Pex19 and Tom71-HA were lysed with Triton X-100 and the suspension was incubated with anti-HA beads. Fractions representing the input (I), unbound material (U), and the eluate (E) were analyzed by SDS-PAGE and immunodecoration with the indicated antibodies.

Figure 4: Loss of Mpf1 is beneficial for cells grown on oleic acid as a carbon source. Growth of wild-type (WT) and *mpf1Δ* cells at 30°C was analyzed by drop-dilution assay. The cells were grown on either rich media (YP) or synthetic media (S) containing glucose (YPD or SD), glycerol (YPG or SG), or oleate (YPO or SOleate).

Figure 5: Mpf1 is an unstable protein. **(A)** WT and *grr1Δ* cells were transformed with a vector encoding Mpf1-3HA. The cells were grown on SD-Ura and then at time = 0 the translation inhibitor cycloheximide (CHX) was added. Cells were further incubated and proteins were extracted at each time point by alkaline lysis and analyzed by SDS-PAGE and immunodecoration with antibodies against HA or Tom20 (as a loading control). **(B)** The bands representing either Mpf1-3HA or Tom20 were quantified and for each lane, the intensity of the band corresponding to Mpf1-3HA was normalized to the loading control (Tom20). The signal at time point = 0 was set to 100%. One representative experiment out of three independent ones is shown.

Figure 6: Mpf1 shows a loose association with the mitochondrial outer membrane. (A) Cells overexpressing Mpf1-3HA were subjected to subcellular fractionation. The isolated fractions of whole cell lysate (WCL), microsomes (ER), cytosol (Cyt), and mitochondria (M) were analyzed by SDS-PAGE and immunodecoration with the indicated antibodies. Tom40

(mitochondria), Hexokinase (cytosol), Pex14 (peroxisomes), and Erv2 (ER) were used as marker proteins. **(B)** Cells expressing Mpf1-3HA were analyzed by immunofluorescence microscopy. *grr1*Δ cells were used to increase the half-life of the protein. The HA tagged proteins were visualized with anti-HA antibody conjugated with Alexa Fluor™ 488. Tom22-HA, a *bona-fide* mitochondrial protein was used as a control for the procedure. To visualize mitochondria and peroxisomes, the cells expressing the HA-tagged proteins were co-transformed with MTS-RFP (mitochondrial targeting signal) or RFP-PTS1 (peroxisomal targeting signal 1). Scale bar, 5 µm. **(C)** Isolated mitochondria from cells expressing Mpf-3HA were either left intact (-PK) or treated with proteinase K (+PK). Then, the samples were analyzed by SDS-PAGE and immunodecoration with the indicated antibodies. Tom70 and $Mcr1_{OM}$ are exposed on the mitochondrial surface whereas $Mcr1_{IMS}$ and Hep1 (matrix) are protected by mitochondrial membranes. **(D)** Isolated mitochondria from cells expressing Mpf-3HA were subjected to alkaline extraction using solution at the indicated pH values. "Total" represents untreated mitochondria. Membrane proteins were isolated in the pellet (P) fraction and soluble and membrane-peripheral proteins in the supernatant (S) fraction. The samples were analyzed by SDS-PAGE and immune-decoration against the specified antibodies. $Mcr1_{OM}$ and $Mcr1_{IMS}$ served as controls for integral membrane protein and soluble protein, respectively. Om14 acted as a control for MOM-associated protein extractable under extreme alkaline conditions.

Figure 7: The absence of Tom70 and Tom71 reduces the expression of Mpf1. **(A)** Proteins were extracted from the indicated cells (three independent colonies) expressing Mpf1-3HA. Samples were analyzed by immunodecoration with HA antibody. Ponceau staining was used as the loading control. **(B)** The bands representing Mpf1-3HA were quantified and for each lane normalized to the intensity of the Ponceau staining. The average of the three colonies for each strain was calculated and the value for WT cells was set as 1. **(C)** Left panel: WT and *tom70/71Δ* cells expressing Mpf1-3HA were subjected to cycloheximide (CHX) assay as described in the legend to Fig. 5A. Right panel: Quantification of Mpf1-HA levels relative to Ponceau at time point = 0. **(D)** The bands corresponding to Mpf1-3HA in the experiment presented in panel (C) were quantified as described in the legend to Fig. 5B. One representative experiment out of three independent ones is presented. **(E)** Subcellular fractionation of *tom70/71Δ* cells expressing Mpf1-3HA. The isolated fractions of whole cell lysate (WCL), microsomes (ER), cytosol (Cyt), and mitochondria (M) were analyzed by SDS-PAGE and

immunodecoration with the indicated antibodies. Tom40 (mitochondria), Hexokinase (cytosol), Pex14 (peroxisomes), and Erv2 (ER) were used as marker proteins. **(F)** Immunofluorescence microscopy to visualize Mpf1-3HA in *tom70/71Δ* and WT cells. Tom22-HA was used as a control for the IF procedure. The HA-tagged proteins were visualized using an anti-HA antibody conjugated with Alexa Fluor™ 594. Scale bar, 5 µm.

Figure 8: Mutating the Pleckstrin homology (PH) domain of Mpf1 stabilizes the protein. **(A)** Schematic diagram of the mutations in the PH domain of Mpf1 with K144, K147, and R157 replaced by alanine (A) residues (the mutant is indicated as Mpf1(PH*). The mutated basic residues in the in the β1/β2 loop of the PH domain are indicated with blue arrowheads. **(B)** Left panel: WT cells overexpressing either Mpf1-3HA or Mpf1(PH)*-3HA were subjected to cycloheximide (CHX) assay for the indicated time periods. Proteins were then extracted and analyzed by SDS-PAGE and immunodecoration with antibodies against either HA or Tom40 (as loading control). Right panel: Quantification of Mpf1-HA and Mpf1(PH)*-3HA levels relative to Tom40 at time point = 0. **(C)** Quantification of Mpf1-3HA and Mpf1(PH)*-3HA was performed as described in the legend to Fig. 5B. One representative experiment out of three independent ones is presented. **(D)** Growth analysis by drop dilution assay of WT cells harboring either an empty vector (Φ), a plasmid encoding Mpf1-3HA, or a plasmid encoding Mpf1(PH*)-3HA. Cells were grown at 30°C on synthetic media containing glucose (SD-Ura), glycerol (SG-Ura), or oleic acid (SO-Ura).

Figure 9: The mutations in the PH domain do not affect the location of Mpf1. (A) Immunofluorescence microscopy localization of Mpf1(PH*)-3HA in WT cells. Native Mpf1-3HA and Tom22-HA were used as a control for the procedure. The HA-tagged proteins were visualized using an anti-HA antibody conjugated with Alexa Fluor™ 594. Scale bar, 5 µm. **(B)** Subcellular fractionation of WT cells expressing Mpf1(PH*)-3HA. Cells were analyzed as described in the legend to Fig. 6A. (C) Isolated mitochondria from cells expressing Mpf1(PH*)-3HA were subjected to alkaline extraction as described in the legend to Fig. 6D.

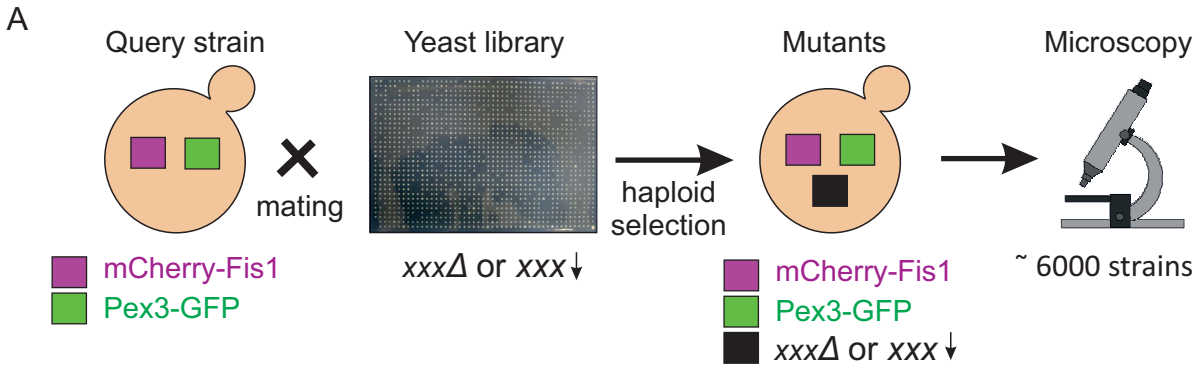

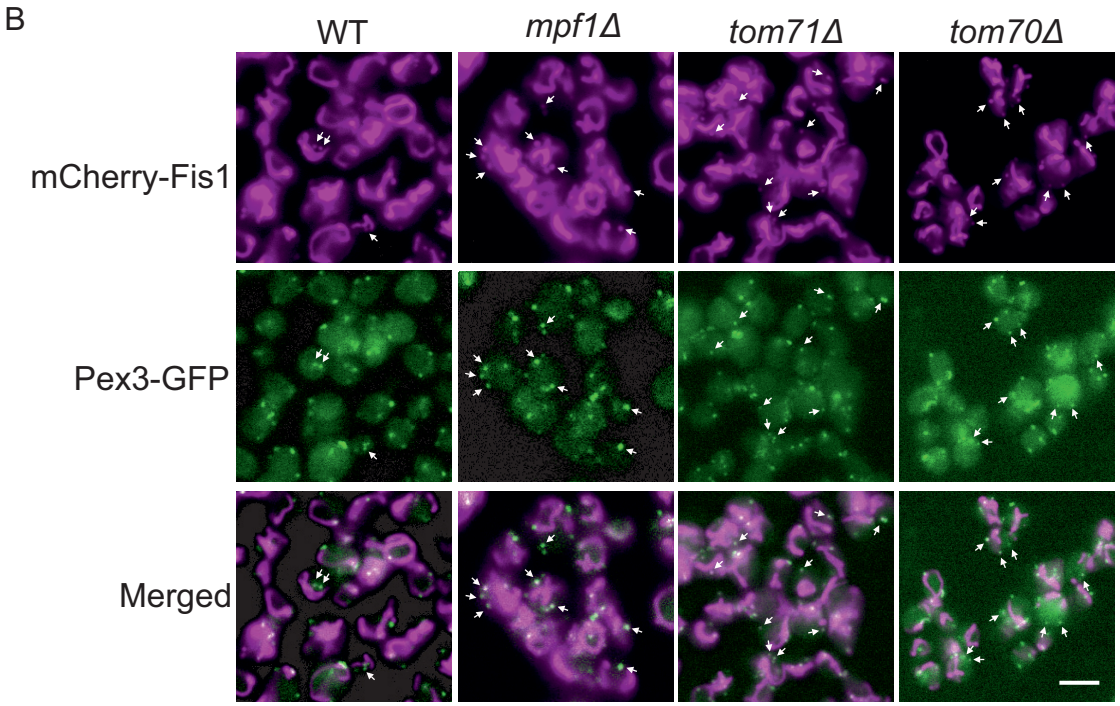

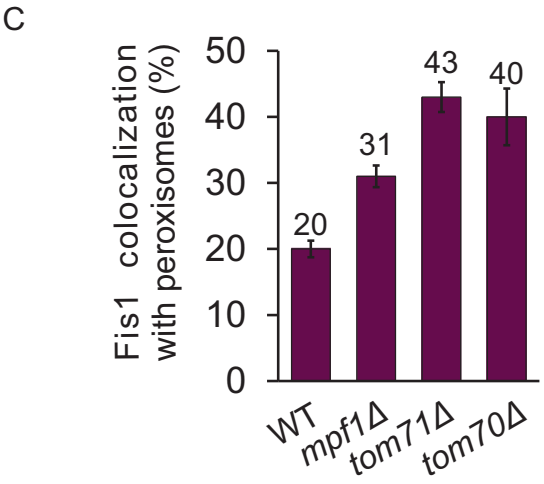

Fig.1, Aravindan et al.

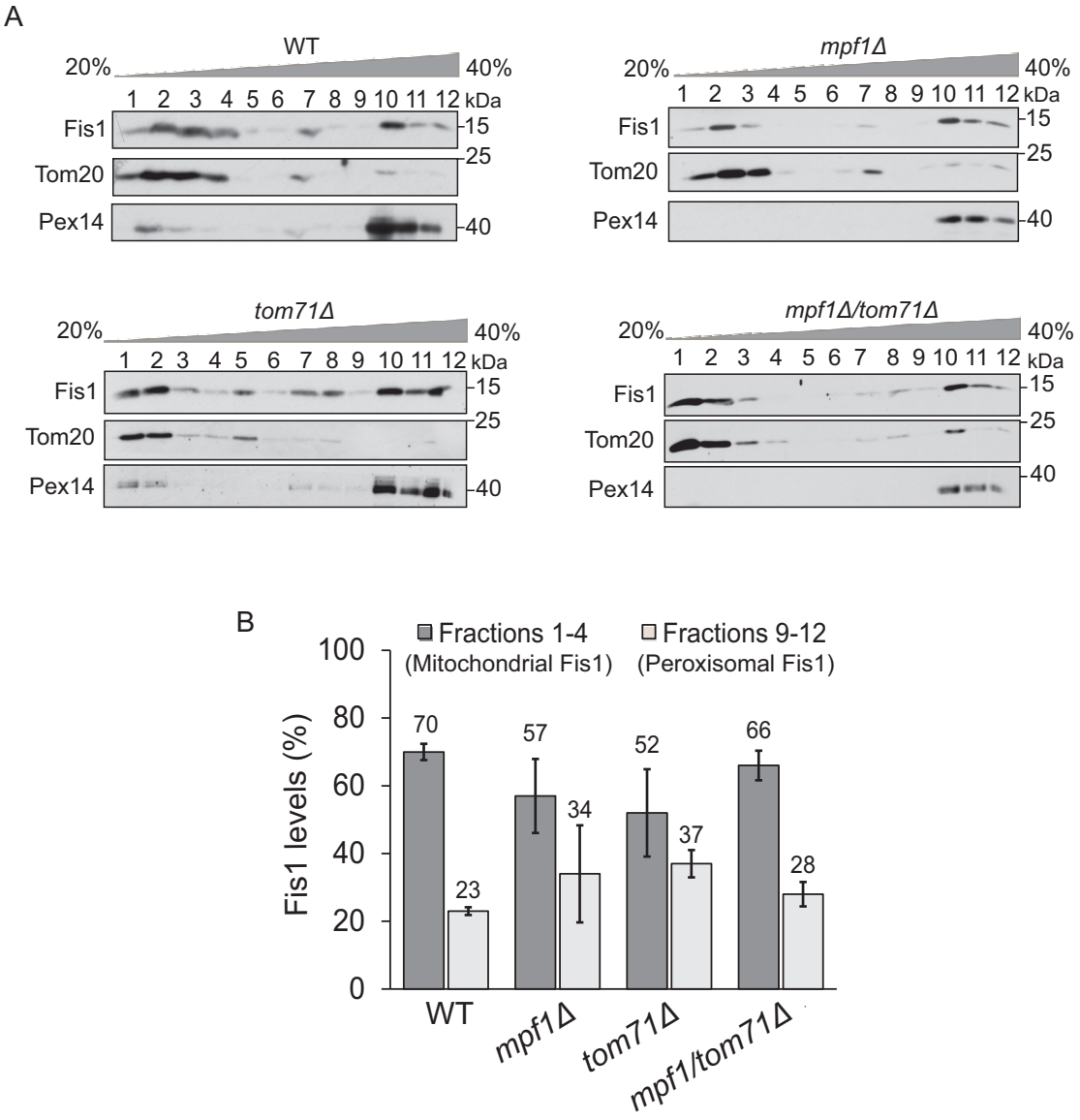

Fig. 2, Aravindan et al.

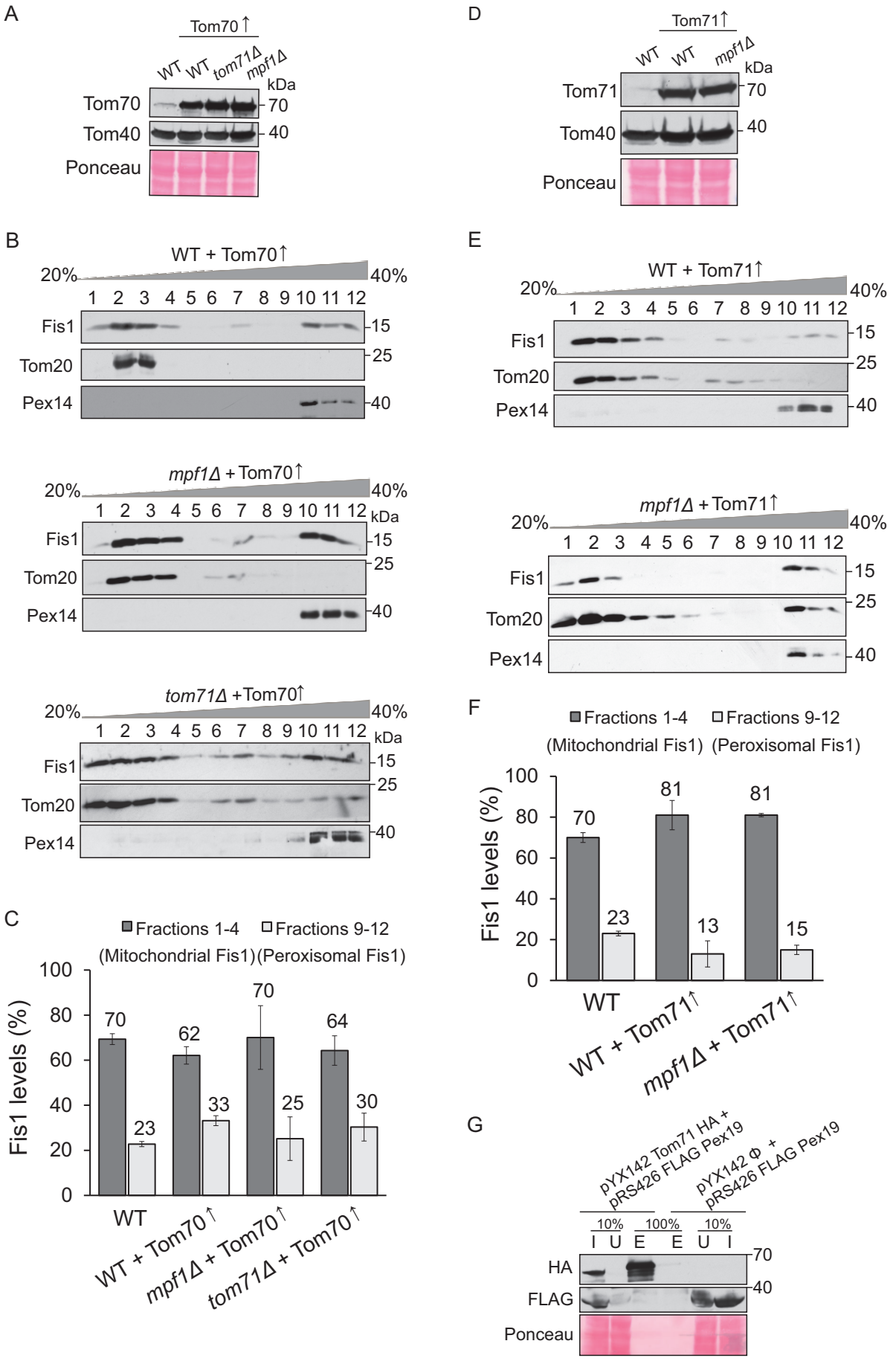

Fig. 3, Aravindan et al.

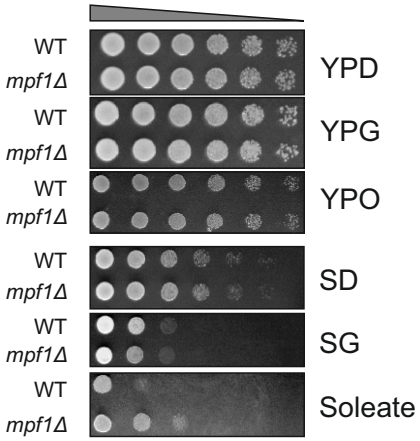

Fig. 4, Aravindan et al.

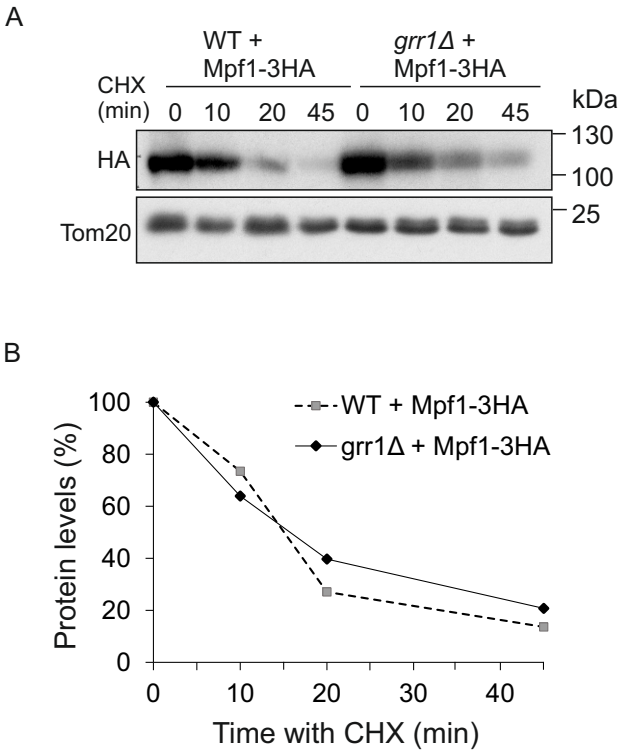

Fig. 5, Aravindan et al.

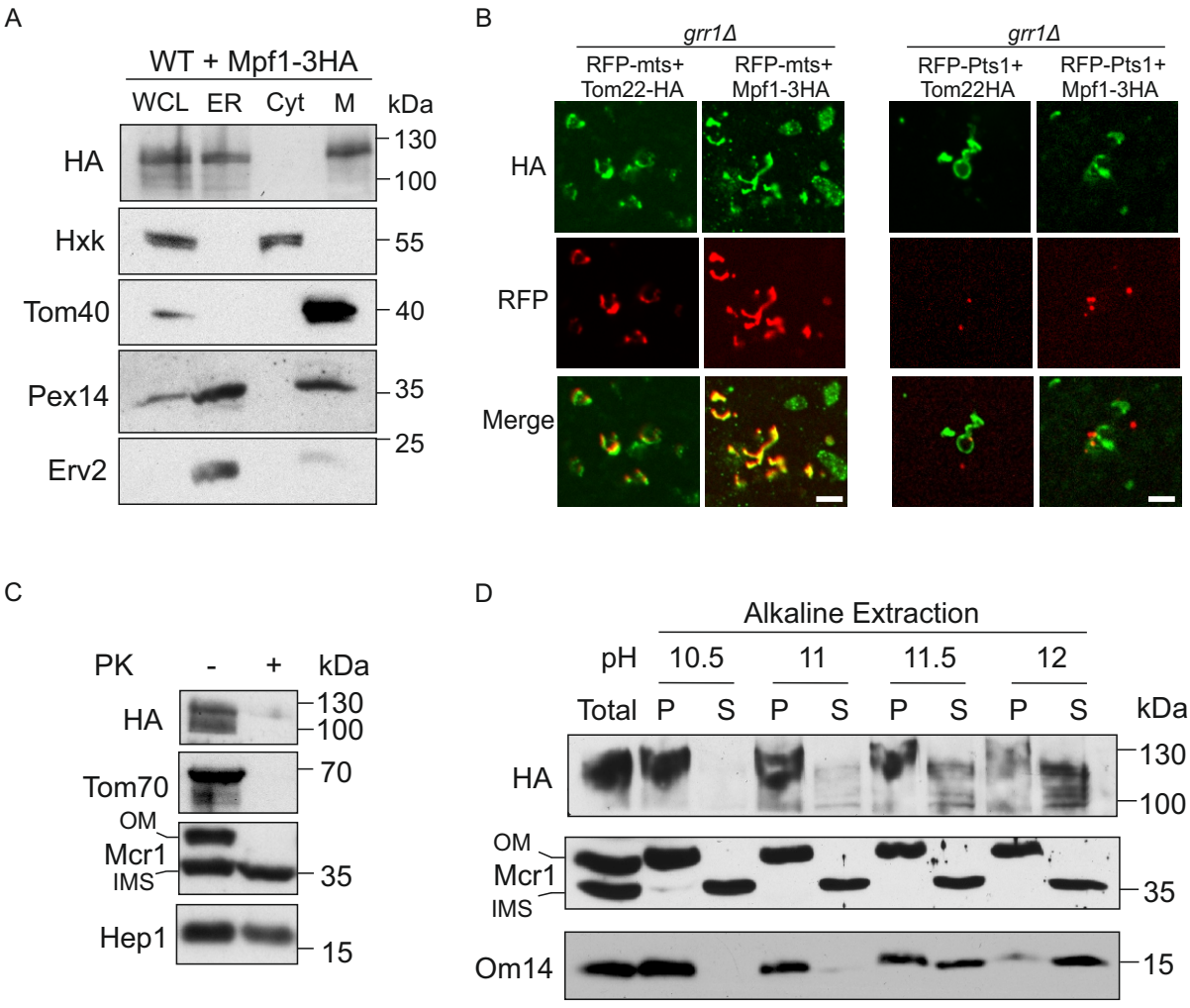

Fig. 6, Aravindan et al.

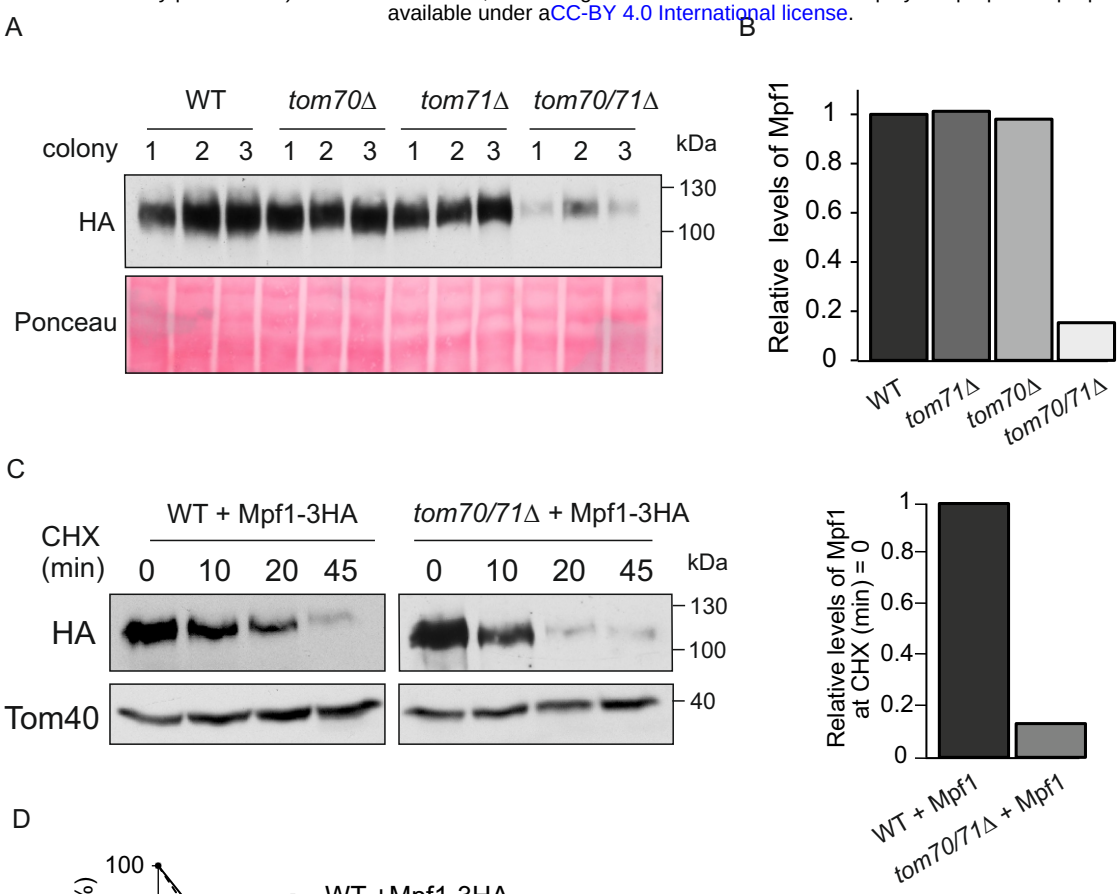

Fig. 7, Aravindan et al.

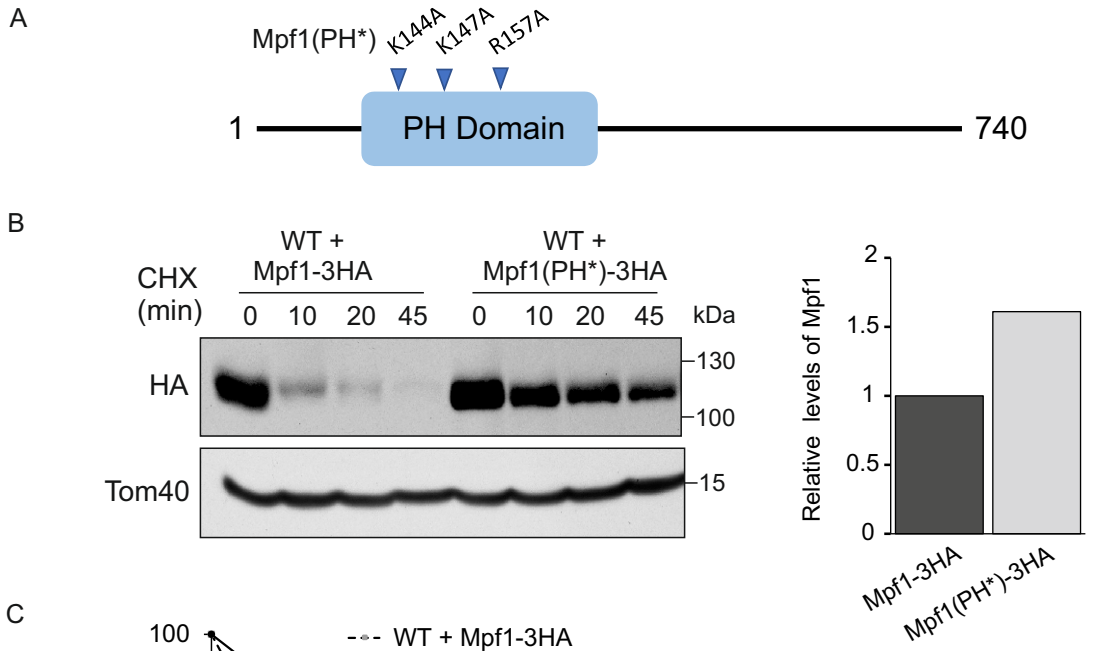

Fig. 8, Aravindan et al.

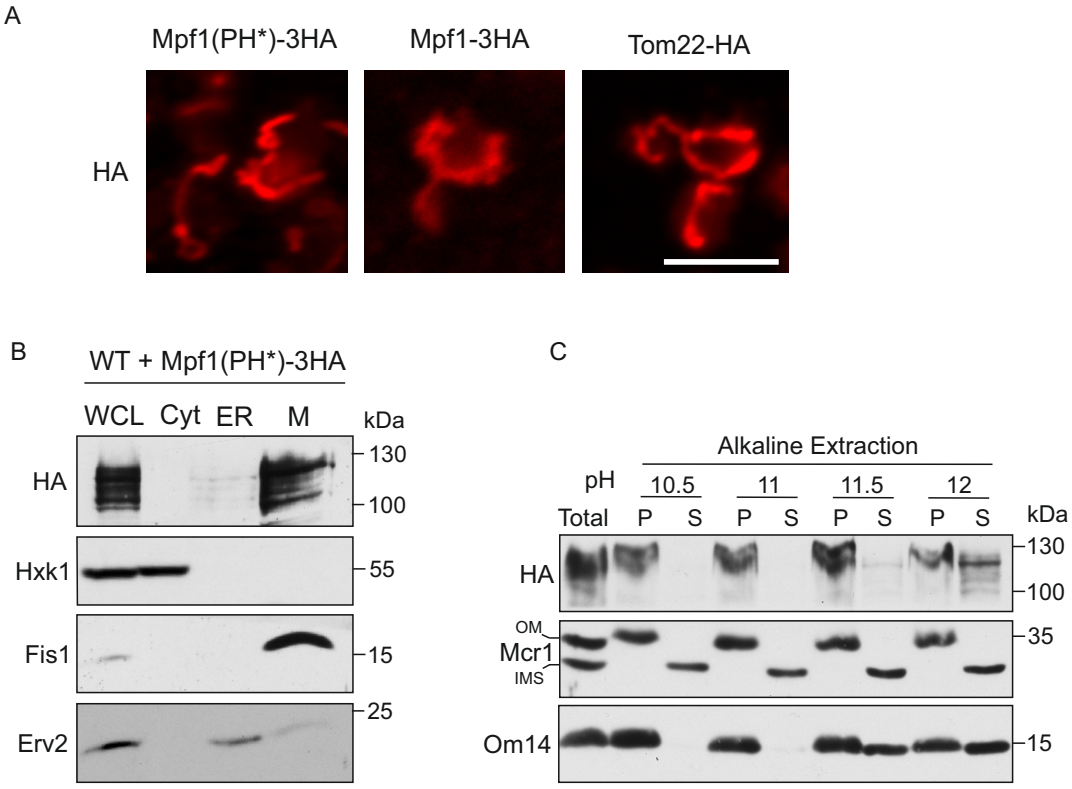

Fig. 9, Aravindan et al.

The molecular mechanism of on-demand sterol biosynthesis at organelle contact sites

Naama Zung[1], Nitya Aravindan[2], Angela Boshnakovska[3,3a,3b,3c], Rosario Valenti[1], Noga Preminger[1], Felix Jonas[1], Gilad Yaakov[1], Mathilda M. Willoughby[4,4a], Bettina Homberg[3,3a,3b,3c], Jenny Keller[5,5a], Meital Kupervaser[6], Nili Dezorella[7], Tali Dadosh[7], Sharon G. Wolf [7], Maxim Itkin[8], Sergey Malitsky[8], Alexander Brandis[8], Naama Barkai[1], Rubén Fernández-Busnadiego[5,5a,9,9a], Amit R. Reddi[4], Peter Rehling[3,3a,3b,3c], Doron Rapaport[2], Maya Schuldiner[1]

[1]Department of Molecular Genetics, Weizmann Institute of Science, Israel
[2]Interfaculty Institute of Biochemistry, University of Tuebingen, Germany
[3]Department of Cellular Biochemistry, University Medical Center Göttingen, Germany
[3a]Cluster of Excellence "Multiscale Bioimaging: from Molecular Machines to Networks of Excitable Cells" (MBExC), University of Göttingen, Germany
[3b]Fraunhofer Institute for Translational Medicine and Pharmacology ITMP, Translational Neuroinflammation and Automated Microscopy, Germany.
[3c]Max Planck Institute for Multidisciplinary Sciences, D-37077, Germany
[4]School of Chemistry and Biochemistry, Georgia Institute of Technology, USA
[4a]Biochemistry and Molecular Biology Department, University of Nebraska Medical Center, USA
[5]University Medical Center Göttingen, Institute for Neuropathology, 37077, Germany
[5a]Collaborative Research Center 1190 "Compartmental Gates and Contact Sites in Cells", University of Göttingen, Germany
[6]The De Botton Protein Profiling institute of the Nancy and Stephen Grand Israel National Center for Personalized Medicine, Weizmann Institute of Science, Israel
[7]Electron Microscopy Unit, Chemical Research Support, Weizmann Institute of Science, Israel
[8]Life Sciences Core Facilities, Weizmann Institute of Science, Israel
[9]Cluster of Excellence “Multiscale Bioimaging: from Molecular Machines to Networks of Excitable Cells” (MBExC), University of Göttingen, 37077, Germany
[9a]Faculty of Physics, University of Göttingen, 37077, Germany

Abstract

Contact-sites are specialized zones of proximity between two organelles, essential for organelle communication and coordination. The formation of contacts between the Endoplasmic Reticulum (ER), and other organelles, relies on a unique membrane environment enriched in sterols. However, how these sterol-rich domains are formed and maintained had not been understood. We found that the yeast membrane protein Yet3, the homolog of human BAP31, is localized to multiple ER contact sites. We show that Yet3 interacts with all the enzymes of the post-squalene ergosterol biosynthesis pathway and recruits them to create sterol-rich domains. Increasing sterol levels at ER contacts causes its depletion from the plasma membrane leading to a compensatory reaction and altered cell metabolism. Our data shows that Yet3 provides on-demand sterols at contacts thus shaping organellar structure and function. A molecular understanding of this protein's functions gives new insights into the role of BAP31 in development and pathology.

Introduction

The evolution of organelles was a key event in enabling efficient biophysical isolation of metabolic reactions in eukaryotic cells. However, this necessitated the concomitant formation of ways for organelles to communicate and transfer metabolites to ensure cellular homeostasis. One fundamental mode of communication between organelles is by the creation of areas of proximity between their membranes, termed contact sites[1,2]. Contact sites (in short, contacts) are specialized zones with a unique lipid and protein composition, held by tethering molecules[3]. While it is now clear that all organelles can create contacts[4], the first ones that were described[5] and the most well studied ones since, are those that are formed by the largest organelle in the cell, the Endoplasmic Reticulum (ER)[6].

The proteome of contact sites comprises many proteins that can function in tethering; transfer of lipids, ions, and other small molecules; as well as regulation of contact extent and/or function[7]. Extensive efforts have been undertaken to map the protein repertoire of various contacts[8–11], uncovering important information about their activity and regulation. In contrast, much less is understood about the unique lipid composition of contacts.

It has been clearly demonstrated that ER contacts are enriched with sterols and sphingolipids that create a specific membrane micro-environment within the continuous membrane of the ER. These subdomains have been dubbed "detergent resistant" or "raft-like"[12–15] and in ER-mitochondria contacts were shown to contain seven times higher sterols than the surrounding ER membrane[13]. These lipid subdomains are essential for ER compartmentalization and the initiation of cellular actions that are contact regulated, such as apoptosis and autophagy[16–18]. Hence, it is no surprise that these subdomains are important for optimal cellular and organismal function. For example, it was shown that their absence from the ER-mitochondria contact may promote tumor progression[19] and affect Alzheimer's disease[20,21].

Ergosterol and cholesterol, the major sterols in fungi and mammalian cells, respectively, are the products of a multi-step biosynthesis pathway (Figure S1A)[22]. One sterol precursor, Farnesyl-PP, is a metabolite with multiple potential end-products such as heme, dolichol, and ubiquinone[22]. However, once Farnesyl-PP is processed to squalene, it is committed to be converted, by the post-squalene enzymes, into ergosterol or cholesterol (Figure S1A). Following sterol production, which occurs mostly in the ER and on lipid droplets (LD), the majority is immediately transferred to other organelles with the strongest accumulation being at the plasma membrane (PM)[23]. In the PM, sterols serve essential components, necessary for membrane integrity, fluidity, and proper function of multiple membrane proteins[24]. Alternatively, sterols can be stored as Sterol Esters (SEs) in LDs [25], which bud from the ER and are crucial for cellular metabolic homeostasis[26]. Hence, sterols are actively removed from the ER through diverse pathways to ensure an overall low level of this molecule in the ER membrane[27]. Despite that, they are still required for ER contact formation and function[12–15]. Thus, a central, unresolved, question in contact site biology is how the sterol-rich lipid subdomains are formed and retained in the sterol-poor environment of the ER.

In this study, we set out to find the ER protein that organizes the sterol-rich subdomains in the ER membrane of the yeast *Saccharomyces cerevisiae.* We found that Yet3 is a pan-ER contact site membrane protein that interacts with the post-squalene ergosterol biosynthesis enzymes, and recruits this synthome, dubbed the ERGosome[28], to contacts. This leads to a membrane environment enriched in sterols. We demonstrate that there is an inherent balance of sterols between contacts and the PM and thus, Yet3 is also a master regulator of PM lipid subdomains. Consequently, alterations in expression of Yet3 leads to global cellular metabolic changes, which are conserved upon alterations in the levels of its human homologue, BAP31. Our work sheds molecular light on how membrane domains, required for ER contact function, are formed and maintained, and provides clues to the diverse and central roles of BAP31 in human development and health.

Results

Yet3 is a pan-ER contact site protein

To identify lipid-organizing proteins, we searched for proteins enriched in more than one contact site using previous datasets for contact site proteomes[8–10]. As expected, we found proteins such as Vps13-family members, VAPs, and LAMs whose function in tethering or lipid transfer was already well defined [29–33, 47]. Surprisingly, we found one additional protein, of less characterized function, that had a similar distribution, Yet3 (Yeast Endoplasmic reticulum Transmembrane 3). Yet3 is a protein of the ER with three predicted transmembrane domains (TMD), which has two paralogs Yet1 and Yet2[34]. In addition, it is highly conserved to mammals with its human homolog being BAP31 (B-cell receptor Associated Protein of 31kDa) [34]. BAP31 is also an ER membrane protein, first discovered due to its role in B-cell receptor maturation[35]. It was previously found as an ER-Mitochondria contact (MAM) resident, and it was shown to affect both apoptosis[36–38] and autophagy[39]; processes known to require specific lipid subdomains containing both sterols and sphingolipids[16–18]. It was also described as a resident of ER-PM contacts[40] suggesting that also in mammalian cells it is a pan-contact site protein. While BAP31 was suggested to affect many ER pathways such as secretion, quality control, and contact site formation[38,41–44], its molecular function is still debated and unclear. Hence, we decided to follow up on Yet3 and BAP31 activity and understand their conserved role in ER contacts.

We first set off to verify the results from previous high-throughput work that suggested Yet3 as a resident of several ER contact sites[8,9]. We verified that tagging of Yet3 on its C terminus (C') preserves its activity (Figure S1B). With this functional fusion protein, we saw that while endogenous expression of Yet3 demonstrates a homogenous distribution in the ER, it becomes concentrated in specific ER subdomains (reminiscent of contacts) when overexpressed. This was distinct from its paralog, and heterodimer partner, Yet1 (Figure S1C and Figure S1D).

To map the extent of contact sites to which Yet3 resides, we assayed its co-localization with split-Venus reporters for ER contacts with various organelles[45,46]. To create the reporters, we tagged an abundant ER membrane protein, Snd3, with the N' portion of a split-Venus (Snd3-VN) and attached the other half of the Venus protein (VC) to abundant membrane proteins on opposing organelles: Pex25-VC for peroxisomes; Faa4-VC for LDs; Ina1-VC for PM; Tom20-VC for mitochondrion and Zrc1-VC for the vacuole. We have previously demonstrated that only in areas where contacts are formed (30-80nm), the two parts of the split-Venus protein are close enough to interact in trans, thus emitting a signal that allows visualization of contacts by fluorescence microscopy [46]. We found that Yet3-mScarlet foci partially co-localized with every contact site reporter that we assayed, suggesting that Yet3 is found in multiple ER contacts (Figure 1A).

While the synthetic reporters do not cause formation of aberrant contact sites[46], they do affect contact dynamics. Hence, to verify that Yet3 is localized to endogenous contacts without relying on reporters, we assayed contact site co-localization using known tethers for most organelles, or organelle markers for peroxisomes and LDs (Pex7-mCherry and Tgl3-mCherry, respectively) (Figure 1B). We used these organelle markers since imaging contacts in the absence of a reporter is more challenging for peroxisomes and LDs, the size of which (~100nm in diameter) is below the resolution of conventional light microscopes (~250nm). At this resolution it is not possible to say if the protein indeed resides in the contact or merely co-localizes with the entire organelle. For all other ER contacts, we visualized known tethers such as Tcb2 and Lam2[47,48] for ER-PM; Lam6 and Mmm1[30,33,49] for ER-Mitochondria, Nvj1 and Nvj2[50,51] for ER-Vacuole, and Num1 and Mdm36 for the three-way contact site between the Mitochondria-ER-Cortex (PM), also known as the MECA[52]. We found that they all indeed partially co-localized with Yet3 puncta (Figure 1B).

To further verify and visualize the presence of Yet3 in contacts at a higher resolution, we performed correlative light and electron microscopy (CLEM). CLEM enables easy detection of ER-mitochondria and ER-PM contacts, and indeed we found overexpressed Yet3-GFP concentrates abundantly at these two contacts (Figure 1C).

Put together, our results demonstrate that Yet3 is a pan-ER contact membrane protein.

Yet3 levels affect organelles in an Opi1-independent manner

Contact residents can often influence the opposing organelles[9,49]. Therefore, we set out to find how Yet3 overexpression affects the organelles with whom the ER makes contact. To visualize the various organelles, we C' tagged with mCherry either Pex3 (peroxisomes), Tgl3 (LDs) or Tom20 (mitochondria). For vacuole membrane visualization, we used the $FM_{4\text{-}64}$ dye. We found that all organelles tested were affected by the high levels of Yet3: peroxisome numbers increased significantly, LD numbers were significantly reduced, vacuoles were enlarged, and mitochondrial shape was altered (Figure 2A and Figure S2A).

To test if this effect is conserved to BAP31, we overexpressed BAP31-GFP in HeLa S3 cells. While BAP31 was shown to be homogenously distributed in the ER[53,54], its overexpression led to its concentration at specific subdomains in the ER, similar to the Yet3 foci observed in yeast (Figure 2B). Additionally, the number of LDs as visualized with BODIPY red, was dramatically reduced (Figure 2B), suggesting that BAP31's cellular effect is conserved from yeast to humans.

How can Yet3 expression levels cause such global cellular effects? Previous work showed that Yet3 and its paralog Yet1, create a heterodimeric complex that regulates the inositol biosynthesis pathway by binding the master regulator of inositol biosynthesis, Opi1[55]. In summary, when inositol is present, Opi1 hinders inositol synthesis by entering the nucleus and inhibiting Ino2/Ino4 transcriptional activation, causing reduced expression of both inositol and phospholipid biosynthesis enzymes such as Ino1 and Cho2 (Figure S2B). In contrast, inositol depletion causes Opi1 to bind the Yet1-Yet3 heterodimer together with the yeast VAP, Scs2, on the nuclear membrane. This inhibits Opi1 entrance into the nucleus and enables the activation of all Ino2/Ino4 transcriptional targets (Figure S2B). *Yet3* or *yet1* deletion, therefore, disturbs the tethering of Opi1 to the nuclear-ER in case of inositol depletion from the media, and could cause dramatic cellular rewiring. Yet3 overexpression, conversely, could cause Opi1 to be consistently sequestered to the nuclear envelope, even when inositol is present, thereby altering its capacity to downregulate inositol production. Indeed, all our experiments thus far were performed in inositol-rich media, a condition under which it could be deleterious to prevent Opi1 from entering the nucleus.

To test if excessive or dysregulated inositol biosynthesis is the direct reason for the organelle number and morphology changes observed, we imaged Opi1-GFP while manipulating the expression levels of Yet3. In media depleted of inositol, Opi1 was found on the nuclear membrane in either control or overexpression of Yet3, as expected. Moreover, Opi1 remained inside the nucleus in a Δ*yet3* background, as was previously reported (Figure 2C)[55]. However, increased levels of Yet3 did not affect nuclear Opi1 localization in media containing inositol (Figure 2C). This may be because Yet1 levels remain unchanged and hence the heterodimeric complex levels do not increase. Regardless of the mechanistic explanation, this suggested that mis-localization of Opi1 is not the underlying reason for the phenotypes that we observed. This also prompted us to rely more on Yet3 overexpression from here on forward.

To verify that the phenotypes are not an indirect effect of Opi1 sequestration, we examined whether overexpression of Opi1 (which should lead to free Opi1 capable of entering the nucleus[56]) can rescue Yet3 overexpression phenotypes. Using LD number and mitochondrial shape as our phenotypic readout, we found that increased expression of Opi1 could not rescue these phenotypes (Figure 2D). Furthermore, when we imaged an *opi1* mutant, which would mimic a state of

increased Opi1 tethering to the nuclear membrane –leading to elevated concentration of inositol in the cell[56] (Figure S2B), we found that it did not imitate the effect of overexpressing Yet3 (Figure 2E).

Put together, our results all demonstrate that Yet3 has an Opi1-independent role whose expression levels dramatically alter organelles architecture.

Yet3 interacts with the post-squalene ergosterol biosynthesis machinery affecting sterol distribution in the cell

If Yet3 is not working through its heterodimeric role with Yet1 to sequester Opi1, what is it doing at contact sites and how does it cause such a broad cellular effect when overexpressed? To investigate the additional role of Yet3, we identified its interactors using immunoprecipitation followed by Mass Spectrometry (IP-MS). Interestingly, we found that overexpressed Yet3-GFP showed an enrichment of all the post-squalene ergosterol biosynthesis proteins (Figure 3A, Figure S1A) (Table S1)[22]. This suggested that Yet3 somehow affects the committed step in sterol biosynthesis at contact sites.

To further explore the connection between Yet3 overexpression and ergosterol, we followed free ergosterol distribution using the free-sterol biosensor, D4H[57], tagged with mCherry. In the control strain, we found the D4H signal mainly on the PM as previously reported[57]. Interestingly, both Yet3 overexpression and deletion led to reduced PM staining and re-localization of D4H to internal foci (see discussion) (Figure 3B).

Since there was an effect on sterol distribution at the PM, we assayed how Yet3 levels affect cell growth in the presence of the antifungal drug fluconazole. Fluconazole inhibits Erg11, an essential enzyme in the post-squalene ergosterol biosynthesis pathway, which leads to reduction of ergosterol levels in the cell (Figure S1A). Since the majority of ergosterols are transferred to the PM[23], it would also be the membrane most affected by fluconazole addition[58]. Indeed, the strain overexpressing Yet3 was susceptible to fluconazole (Figure 3C). It was also shown that reduced sterols increase the levels of long-chain sphingolipids as a compensatory mechanism[59]. Indeed, lipidomic analysis demonstrated reduced sterol levels in strains overexpressing Yet3 (Figure S3A), and elevated levels of long-chain sphingolipids (Figure S3B) (Table S2).

Reduced sterols on the PM should cause mis-localization of PM proteins that depend on sterol-rich subdomains for their localization. Examples of such proteins are Gap1 and Agp1, two broad-range amino acid permeases[60–62]. Indeed, Gap1-GFP and Agp1-GFP are both mis-localized on the background of *yet3* deletion and Yet3 overexpression (Figure S3C). Polar metabolite profiling analysis further supports this change in PM permeases since the levels of several amino acids are reduced in the overexpressed Yet3 strain compared to the control (Figure S3D) (Table S3). In addition, the amino acid responsive transcription factor, Gcn4, translocate to the nucleus, indicative of reduced overall amino acid levels (Figure S3E)[63].

Another known outcome of sterol reduction on the PM, is the activation of the ergosterol sensor and transcription factor Upc2[64]. Loss of PM sterols causes Upc2 to reveal a nuclear localization sequence, resulting in its nuclear accumulation and upregulation of transcripts encoding for ergosterol biosynthesis enzymes[64]. Indeed, Upc2-GFP shifted its localization from cytosolic to nuclear when Yet3 was overexpressed (Figure 3D). In addition, transcriptomic analysis by RNA-Seq verified that cells overexpressing Yet3 have increased levels of Upc2 and its targets, the post-squalene enzyme transcripts, compared to control cells (Figure 3E) (Table S4).

If the increased mRNAs for all the post-squalene biosynthetic enzymes indeed cause elevated ERG protein production and function, then also oxygen consumption rates should increase since some enzymes in the pathway require oxygen, such as Erg11, Erg3 and Erg5 (Figure S1A). To see if

oxygen consumption levels are affected by Yet3, we measured oxygen consumption rate (OCR) via Seahorse for different Yet3 expression levels (Table S5). Strains were grown in glucose, and then transferred to galactose containing medium for the analysis. Interestingly, both the Yet3 overexpressed strain and the deletion strain of *yet3* showed an increase in OCR compared to the control (Figure 3F). OCRs were most likely not elevated due to increased cellular respiration since translation of mitochondrial transcripts encoding the electron transport chain subunits were decreased in overexpression of Yet3 (Figure S3F); and mitochondrial respiration during growth in the non-fermentable carbon source, ethanol, was unchanged in overexpressed Yet3, and only slightly elevated in Δ*yet3* (Figure S3G). Altogether our data suggest that mitochondrial respiration is not upregulated, and that instead the increased OCR may result from oxygen shunted for sterol production.

Sterol production also requires large amounts of the carbon precursor, acetyl-CoA. In support for central carbon metabolism being shunted to provide this precursor in strains overexpressing Yet3, RNAseq results show that central carbon metabolism is downregulated at the transcriptional level (Table S4). Moreover, polar metabolite profiling analysis uncovered a reduction in the intermediate metabolites of glycolysis (Figure S3H) and tricarboxylic acid (TCA) cycle (Figure S3I) (Table S3), with a concomitant increase in pyruvic acid, the exit metabolite of glycolysis, and citrate, the entry metabolite of the TCA cycle (Figure S3H and Figure S3I). Indeed, pyruvic acid is important for acetyl Co-A production[22]. Moreover, two of the four amino acids whose amount increased upon overexpression of Yet3, alanine and arginine (Figure S3D), are important for CoA synthesis, which is the precursor for acetyl CoA[65,66].

We next tested heme levels, since this is an essential co-factor of several enzymes of the post-squalene pathway. Our RNA-Seq data showed increased transcript levels of *HEM13*, which encodes the heme biosynthetic enzyme coproporphyrinogen oxidase, in the Yet3 overexpression strain (Figure 3E). To measure total heme concentrations more directly, we used a porphyrin fluorescence assay. This assay revealed elevated overall heme levels in cells overexpressing Yet3 as would be expected from the higher levels of Hem13 (Figure 3G). Further, we used the genetically encoded ratiometric fluorescent heme sensor HS1-M7A to assess free heme levels[67]. The fractional heme occupancy of HS1-M7A is proportional to the heme available to the sensor. Free heme in the cytosol was diminished, despite the nuclear and mitochondrial fractions being elevated (Figure 3H). These results are consistent with an increased utilization of heme by the ergosterol biosynthesis enzymes that face the cytosol.

Altogether, our data demonstrate that Yet3 interacts with the post-squalene enzymes and affects sterol distribution in the cell. Despite the increase in heme levels, oxygen consumption, and *ERG* gene transcription – PM sterols remain low. This raises the question of whether the produced ergosterol is somehow sequestered by Yet3 in ER contacts.

Yet3 recruits the ERGosome to provide on-demand sterol biosynthesis at ER contact sites

Since Yet3 interacts with all the post-squalene pathway enzymes and affects sterol distribution, we hypothesized that it plays a role in sequestering the ergosterol enzymes at contact sites. To this end, we tagged 13 out of the 15 post-squalene ergosterol biosynthesis enzymes with mCherry on their N' (tagging that allowed their clear visualization at their native locations[68]) and imaged the effect of Yet3 expression on their localization. Strikingly, we found that upon overexpression of Yet3, the localization of all 13 tagged enzymes was shifted from their homogenous distribution on either the ER or in LDs, to co-localize with Yet3-GFP puncta (Figure 4A and Figure S4A). This was in sharp contrast to the pre-squalene enzymes Hmg1/2 whose localization was not altered upon overexpression of Yet3 (Figure 4A and Figure S4A). Our data suggest that Yet3 sequesters, directly or indirectly, all the post-squalene biosynthesis enzymes to create a "synthome",

previously dubbed the ERGosome[28], for on-demand ergosterol biosynthesis at contact sites. The ERGosome was also observed as a potential high molecular weight complex harboring Yet3 by blue native gel electrophoresis (Figure S4B). This is further supported by previous complexome analysis of mitochondrial proteins where Yet3 associated with a complex of approximately 750kDa also shared by Erg4 and Erg26[69].

If indeed Yet3 recruits the ERGosome to contact sites, we would also expect to see ergosterol accumulating at Yet3 foci. In support of this, using the mCherry-D4H reporter, we observed that free ergosterols were mainly co-localized with Yet3 containing foci when Yet3 was overexpressed (Figure 4B).

Previous reports showed that Yet3 heterodimerizes with its paralog Yet1, for inositol biosynthesis regulation[55,70]. Although we already eliminated inositol biosynthesis regulation as the pathway by which Yet3 affects contact sites (Figure 2), it could still be that its heterodimerization with Yet1 is important for its role in ERGosome scaffolding. However, our data supports a Yet1-independent role for Yet3 for three reasons. First, we observed Yet3 is much more abundant than its paralogs (Yet1 or Yet2), suggesting heterodimer-independent activity (Figure S1D and S4C). Second, blue native gel analysis indicated that deleting *yet1* does not dramatically affect the high molecular weight complex assembly (Figure S4B). Third, deletion of *yet1* increased the number and size of overexpressed Yet3 subdomain puncta and caused elevated ergosterol levels in the contacts, as shown by D4H, while overexpressing *YET1* reduced Yet3 puncta and decreased the amount of ergosterols in the contacts (Figure S4D). Hence, Yet1 does not support the role of Yet3 in ERGosome scaffolding, but rather it may sequester Yet3 for its role in Opi1 localization, thus regulating its capacity to translocate to contact sites and induce local sterol production.

So far, our data demonstrate that overexpression of Yet3 causes it to accumulate at contacts, initiating scaffolding of the ERGosome and increasing ergosterol levels at contacts at the expense of their trafficking to the PM. While this suggests that Yet3 is sufficient to induce local sterol production, it does not clearly demonstrate that it is necessary for this process when expressed under its own endogenous promoter. We therefore examined whether endogenous Yet3-GFP is also recruited to contacts. We hypothesized that Yet3 will be recruited to contacts during ergosterol deficiency, in other words, when ergosterol is in demand. Indeed, when grown in the presence of fluconazole, resulting in an ergosterol-depleted environment (shown by accumulation of Upc2 in the nucleus), we observed Yet3 (Figure 4C) and the ergosterol biosynthesis proteins (Figure S4E) concentrated at subdomains. This was also seen in iron-depleted medium that should cause reduction in free ergosterol due to reduced heme production (Figure S4F).

To support our assumption that native Yet3 is necessary for “on demand” sterol biosynthesis at the contacts, we relied on the fact that addition of fluconazole pheno-mimicked the organellar changes observed when Yet3 was overexpressed: fewer LDs and bulkier mitochondria (supported by a report that showed mitochondrial morphology changes when the ergosterol pathway is blocked[71]) (Figure 4D). The fact that the combination of growth in fluconazole alongside overexpression of Yet3 exacerbated the phenotypes supports the idea that each of these changes cause an independent reduction in total ergosterol. Importantly, deletion of *yet3* rescued the phenotypes of fluconazole treatment (Figure 4D). This evidence strongly supports that under endogenous conditions, the presence of Yet3 causes a certain fraction of ergosterol to be sequestered at contacts. Freeing this fraction by deletion of *yet3* releases the ergosterols from contact sites to other metabolic uses in the cell, thus rescuing the overall phenotypic consequences of reduced sterol levels.

If on-demand sterol biosynthesis at contact sites is a central function of Yet3, then we would expect it to be conserved to its human homolog BAP31. Indeed, cholesterol was concentrated more in the ER than on the PM in BAP31 overexpression compared to the control (Figure 4E).

Taken together, our results uncover a novel mechanism that orchestrates the formation and maintenance of lipid subdomains at contact sites. Furthermore, the role of Yet3/BAP31 may

elucidate the extensive involvement of BAP31 in numerous pathways, many of which are dependent on sterol enriched subdomains. This, in turn, provides a new perspective on its potential impact on a multitude of developmental processes and in disease states.

Discussion

In recent years it has become apparent that the ER membrane has subdomains with unique lipid compositions. One type of such subdomain consists of sterol-rich areas that are required for the formation of contact sites. Additional functions of ER subdomains have been demonstrated such as during fusion of tubules required for ER shaping, translocation of unique substrates, and trafficking of special cargo at ER exit sites[72–75]. While the proteome of ER contact sites was extensively studied over the last decade, how the distinctive lipid composition of these subdomains is formed and maintained, had remained elusive.

In this study, we uncovered the molecular mechanism that enables the formation of unique lipid domains enriched with sterols at ER contact sites. Ergosterol is the final product of a multi-step enzymatic biosynthesis pathway (Figure S1A). Once the dedicated intermediate, squalene, is formed – the pathway is made efficient by organization of the post-squalene enzymes as a synthome, dubbed the ERGosome[28]. Here, we show that the ERGosome is recruited to ER contact sites by Yet3, an ER membrane spanning protein. Moreover, this recruitment underlies the formation of the sterol-rich environment of contacts (Figure 5). We observed that while Yet3 can be found at all ER contact sites, it is more frequently found at the ER-mitochondria, ER-PM, and ER-LD contacts and less with ER-peroxisome contacts (Figure 1A). This is in line with findings that document a higher requirement for sterols in the former contacts[76].

Building ergosterols by the ERGosome requires heme, oxygen, iron, and 18 molecules of acetyl-CoA for each molecule of ergosterol (Figure S1A) [22]. This costly sterol is therefore tightly regulated, and its formation is highly controlled. It is not surprising, therefore, that we see a “tug of war” between contact sites and the PM (the cell’s most sterol-rich membrane) for the limited amount of sterols in the cell. Indeed, we demonstrated that overexpression of Yet3 or BAP31 leads to reduced content of ergosterol/cholesterol in the PM (Figure 3B, Figure 4E). Moreover, when we compared the transcriptome profile of cells overexpressing Yet3 (Figure 3E) to the transcriptome of strains from the deletion collection[77], we found that the closest resemblance is to Δ*erg2*— a strain deleted for an enzyme responsible for converting fecosterol to episterol in the ergosterol biosynthesis pathway (Figure S1A). This indicates that losing ergosterol biosynthesis has similar cellular consequences to depleting it from the PM by enriching sterols in contacts. This behavior can also explain the growth defect upon overexpression of Yet3 (Figure S1B). We hypothesize that elevated levels of Yet3 force the cell to direct its building blocks and energy for ergosterol synthesis, while other metabolites such as amino acids and lipids, that are required for cell duplication, are reduced (Figure S3D, Table S2, S3).

It was previously suggested that ERGosome assembly occurs at ER exit sites for vesicular trafficking[78]. This suggests that on-demand, efficient and local, sterol biosynthesis may be a widely used mechanism for creation of subdomains. Moreover, it could very well be that Yet3 may have a function in more ER subdomains, in addition to its role in ER contacts, to assemble the ERGosome, where local sterol synthesis is required. In support of this, it has been shown that Yet3 binds the SEC translocon complex which may enable translocation of specific substrates, such as GPI anchor proteins, that require high sterol and sphingolipid concentrations[70]. Another process requiring a sterol-rich subdomain is the fusion of ER tubules[79]. We found Yet3 foci co-localized with both Sey1 and Rtn1. Sey1 is the dynamin like GTPase required for fusion of tubules and Rtn1is the reticulon that maintains tubular morphology (Figure S5A). Moreover, our pull-down experiments with Yet3 also show a physical interaction with Sey1 as well as with Yop1 that works with it[80,81] (Table S1). Indeed, looking at the ER shape, we found that overexpression of Yet3 elevates the

extent of peripheral ER tubules (Figure S5B and Figure S5C). These suggest that during ER membrane shaping events, Yet3 may recruit the ERGosome to specific sites for modulating the physical properties of the lipid bilayer.

Other uses for ergosterols in the ER can be during ER stress. One of the main outcomes of ER stress is clustering of the ER stress sensor, Ire1. Ire1 clustering leads to sustained activation of the unfolded protein response (UPR) and requires upregulated sterol biosynthesis in the ER membrane[82]. It was already demonstrated that *YET3* mRNA levels[83,84] and Yet3 protein expression[70] are upregulated following addition of the UPR inducer dithriothreitol (DTT). Moreover, we noticed that upon UPR induction, Yet3-GFP accumulates in specific areas on the ER (Figure S5D), which support increased Ire1 clustering overtime (Figure S5E and Figure S5F). Conversely, a dysfunctional Yet3 form (tagged on its N') (Figure S1B) cannot support Ire1 assembly (Figure S5E). This suggests that the accumulation of Yet3 in specific areas of the ER may sequester the ERGosome to create local ergosterol enrichments required for proper Ire1 clustering.

The hypothesis that Yet3 may function in additional areas of the ER for making ergosterol-rich subdomains, can also explain our surprising observation that in many cases the depletion of *YET3* and its overexpression lead to similar phenotypes (Figure 3B, Figure S3C and Figure 3F). Indeed, depletion of *YET3* disrupts the normal accumulation of ergosterol in designated membrane areas, while overexpression of Yet3 enables the formation of the ERGosome, but recruits substantial amount of ergosterols into contacts, depleting them from other locations. In essence, the two manipulations will have similar effects on non-contact subdomains.

More mechanistically, it is not clear how Yet3 recruits the large ERGosome complex to specific domains. All ERGosome proteins harbor TMDs, and Yet3 itself possesses three predicted TMDs, which constitute approximately 50% of its protein sequence. While Yet3 and BAP31 are conserved throughout their sequence (Figure S6A), it is their TMDs that exhibit the most remarkable conservation (Figure S6B). Moreover, previous report suggests that BAP31 interacts with client membrane proteins via its TMD and may also engage with cholesterol, as demonstrated using a sterol-probe assay[85]. Interestingly, AlphaFold2 predictions[86] suggest that as a homotrimer, Yet3 could form a hydrophobic pocket that could potentially bind ergosterol (Figure S6C). This hydrophobic channel may be important for slowing the fast sterol diffusion in the ER membrane, thus maintaining the high concentration of this molecule in the ER subdomains where Yet3 is enriched. Taken together, we hypothesize that both Yet3 and BAP31 function as scaffold proteins, facilitating the recruitment of ergosterol/cholesterol biosynthesis proteins through their TMDs. However, to fully elucidate the molecular mechanisms underlying Yet3 and BAP31 function, further structural experiments are needed.

Another intriguing question is how Yet3 itself is recruited to sites of contact to initiate local sterol accumulation. One option is that it is pulled in by interactions with VAP proteins, Scs2 and Scs22 in yeast, that also localize to all ER contacts and have been shown to interact with Yet3 (and also come up in our pull-down assays) (Table S1)[55,87]. However, in our hands, the double deletion of Scs2 and Scs22 did not abolish Yet3 accumulation at ER subdomains (Data not shown). To address this question in an unbiased approach, we imaged overexpressed Yet3-GFP on the background of the yeast knockout library (Figure S6D). This library comprises yeast strains, each carrying a targeted mutation in one specific gene[88,89]. Our preliminary results reveal that genes related to ER membrane lipid composition and LD formation, affect the localization of Yet3. Specifically, deletion of genes such as *ice2*, *loa1* and *nem1*, that under normal conditions affect the formation of di- and tri-acyl glycerol (DAG and TAG, respectively), led to a reduction in the recruitment of Yet3 to subdomains (Figure S6E). These observations suggest that the lipid milieu of the ER membrane influences the recruitment of Yet3. This may also explain why overexpressed Yet3, in contrast to other overexpressed tethers that disperse along the ER, in fact accumulates in ER subdomains. This nonstandard behavior may be the result of a feedback loop: Yet3 may accumulate itself in unique membrane micro-domains. As Yet3 accumulates, it recruits the ERGosome and

increases the ergosterol concentration. Elevation of ergosterol in the contacts may encourage the assembly of more Yet3 molecules that are influenced by the ER membrane lipid composition, thus resulting in even more sterol accumulation in these subdomains and stronger Yet3 recruitment. However, to fully understand Yet3 recruitment, further comprehensive studies are needed.

Our studies focused on Yet3. However, Yet3 has two close paralogs, Yet1 and Yet2. Do they also have a role in ERGosome recruitment? A previous report[70] and our data (Figure S4C) showed that compared to Yet1 and Yet3, Yet2 does not express constitutively, which may suggest it fulfills a different function. However, heterodimerization of Yet3 and Yet1 plays a crucial role in modulating the inositol biosynthesis pathway (Figure S2B)[55]. Moreover, deletion of *yet3* results in a reduction of Yet1 levels[70]. Surprisingly, deletion of *yet1* does not affect Yet3 expression levels but alters its distribution on the ER membrane[70]. Rather than being homogenously distributed, *yet1* deletion promotes accumulation of Yet3 in subdomains, reminiscent of the phenotype observed upon overexpression of Yet3[70]. We moreover show that deletion of *yet1,* which leads to increased recruitment of Yet3 to subdomains, also influences the distribution of ergosterol (Figure S4D). We propose therefore that the presence of Yet1 modulates Yet3 function – in its presence, heterodimerization occurs recruiting Yet3 to its role as an Opi1 regulator, while in the absence or reduced expression of Yet1, or during conditions of increased Yet3 levels – Yet3 functions independently as a scaffold for ERGosome formation. This regulatory interplay between inositol biosynthesis and ergosterol concentration underscores the multifunctional nature of Yet3. Opi1, the inhibiting factor for inositol production, also disturbs the creation of Phosphatidylethanolamine (PE) and Phosphatidylcholine (PC) by reducing the expression levels of the enzymes required to synthesize these phospholipids, Psd1, Cho2 and Opi3. This may be an efficient way to control and balance the amount of ergosterols and phospholipids in the cell. Inositol is also an essential building block for phosphatidylinositol (PI), another common phospholipid. Intriguingly, strains lacking LDs as observed in Yet3 overexpression (Figure 2A), exhibit significantly reduced PI levels even under continuous growth in the presence of inositol[90]. The reduction in overall PI content within cells overexpressing Yet3 supports our hypothesis that it serves to promote the crosstalk between both lipid metabolism pathways.

Other than the two paralogs in yeast, Yet3 also has a highly conserved human homolog, BAP31. BAP31 was reported to have roles in diverse cellular functions such as: ER stress through the UPR; lipid and glucose metabolism[41,42]; mitochondrial homeostasis; autophagy[39]; and regulation of proliferation and migration of cells[43,44]. Moreover, it is known to be involved in the activation of caspase-8 and apoptosis[36,37]. Similar to Yet3, BAP31 was shown to be a resident protein in the ER-PM contact[40] and in MAMs, where it may regulate autophagy and apoptosis [38,39,91]. Both pathways are known to necessitate sterol-rich domains. Although BAP31 was suggested to function as a tether protein that binds either TOM40 or FIS1[54,92] in MAMs, this was never fully demonstrated, and a clear demonstration of a tether activity was not shown [45]. Our results suggest that while BAP31 is indeed a resident protein in these contacts, its role may be in concentrating cholesterol at specific ER subdomains. In support of this, BAP31 interacts with SREBP1C and INSIG1, both key players in the regulation of cholesterol metabolism[93] , and with OSBP[91], which is a lipid transfer protein that controls cholesterol transfer. BAP31 deletion induced lipogenesis and cholesterol accumulation in hepatocytes[41] and LD accumulation in white adipose tissue[94]. Interestingly, the overexpression of both BAP31 and Yet3 resulted in reduction of LD number (Figure 2A and Figure 2B). Like Yet3, BAP31 binds proteins that are required for ER tubule shaping such as the reticulon RTN3, and the dynamin like GTPase ATL3[91], which are also enriched in sterol rich domains. This could hint that BAP31 might also accumulate in multiple subdomains to create the optimal membrane environment for cholesterol dependent pathways.

BAP31 was first discovered due to its role in B-cell receptor maturation[35]. Since the sterol regulatory binding protein (SREBP) signaling pathway is crucial for effective antibody responses[95], BAP31 involvement in secretion of antibodies may be through its function in cholesterol subdomain regulation. Interestingly, BAP31 selectively binds Immunoglobulin D (IgD) (and not

Immunoglobulin M (IgM))[96] and is required for optimal targeting of the Major Histocompatibility Complex (MHC) class I molecules to ER exit sites[97]. BAP31 is also involved in T cell activation and proliferation by regulating the expression of key members in the T cell receptor (TCR) signaling pathways[98]. IgD, MHC and the TCR, are all known to be enriched in sterol-rich subdomains[99]. Therefore, it could be that the reason that BAP31 knockdown increases MHC class II expression in macrophage cell surface[100] is the opposite result of BAP31 overexpression, where we observe high concentration of cholesterol on the ER and less on the PM (Figure 4E). The connection of BAP31 to so many pathways that regulate cellular homeostasis may explain why it is associated with a variety of diseases such as different types of cancer[101–104], neurological disorders[105,106], metabolic syndromes[41,42], and viral infectivity[107,108]. We suggest that BAP31 is involved in many of these diseases due to its role in regulating the cholesterol distribution in the cell.

More globally, to our knowledge, our study is the first to reveal a lipid organizing protein in contact sites. It also suggests a conserved function for BAP31 in creation of sterol-rich domains, which may explain its involvement in many cellular pathways, and surely will shed more light about its actions during development and in the course of disease.

Acknowledgements

We thank Emma Fenech and Ofir Klein for critical reading of the manuscript. We are grateful for insightful and helpful conversations with Charles Barlowe, Robin Klemm, Tim Levine, Avner Fink, Ines Castro and Yury Bykov. We thank Michal Eisenberg-Bord for support during the initial stages of this project. We thank Emma Fenech, Mor Angel, Reut Ester Avraham, Yeynit Asraf, Hadar Meyer, Tat Cheng and Ariel Feler for helping with experimental work. We thank Yoav Peleg for cloning support and Charles Barlowe for sharing Yet3 antibody. We thank Sophie Martin from the University of Geneva and Eelco van Anken from Università Vita-Salute San Raffaele for generously sharing reagents. We thank Orly Laufman for sharing HeLa S3 cell line.

This work was supported by a collaborative grant from the Deutsche Forschungsgemeinschaft (DFG) to DR and MS (DFGRA 1028/11-1) and by a collaborative grant from the DFG to PR, RFB and MS SFB1190 (P11, P13 and P22 respectively). The robotic system of the Schuldiner lab was purchased through the kind support of the Blythe Brenden-Mann Foundation. MS is an Incumbent of the Dr. Gilbert Omenn and Martha Darling Professorial Chair in Molecular Genetics. PR is additionally supported by the DFG under Germany's Excellence Strategy EXC 2067/1-390729940; SFB1002 (A06, PR), and the Max Planck Society. ARR is supported by the US National Institutes of Health (NIH) grants GM145350 and ES025661, a US National Science Foundation (NSF) grant 1552791, and the Georgia Institute of Technology Blanchard and Vasser-Woolley professorships. RFB is supported by the European Research Council (CoG 101088355 - cryoNERVE), and the DFG through Germany's Excellence Strategy - EXC 2067/1- 390729940.

Materials and Methods

Yeast strains and plasmids

The laboratory strain BY4741[109] served as the basis for the *S. cerevisiae* strains used in this study. We performed genetic manipulations using the lithium acetate, polyethylene glycol, single-stranded DNA method[110]. The plasmids used for PCR-mediated homologous recombination have been previously documented[111,112]. We designed the primers using Primers4-Yeast[113]. Prof. Sophie Martin from the University of Geneva generously provided the pDA179-mCherry-D4H plasmid. The Ire1-mCherry plasmid was graciously given by Prof. Eelco van Anken from Università Vita-

Salute San Raffaele. The plasmids and strains utilized in this study are listed in Table S6 and Table S7, respectively.

Culturing of yeast

Yeast cells were incubated overnight at a temperature of 30°C in synthetic minimal medium, which consisted of 0.67% (wt/vol) yeast nitrogen base (YNB) with ammonium sulfate, supplemented with amino acids and 2% glucose (SD). The following antibiotics were used for selection: nourseothricin (NAT, Quimigen) at a concentration of 0.2g/l; G418 (Formedium) at a concentration of 0.5g/l; and hygromycin (HYG, Formedium) at a concentration of 0.5g/l.

Subsequently, cells were diluted and cultivated until they reached mid-logarithmic phase, characterized by an optical density (OD_{600}) ranging from 0.4 to 0.9. For the different growth conditions used in this study, strains were cultured as mentioned below: 2mM DTT (Sigma); 10µg/ml Fluconazole (Sigma), medium depleted of inositol using YNB without inositol (Formedium), or medium depleted of iron, using YNB without iron.

In experiments involving the mCherry-D4H reporter for free sterols, yeast strains were diluted and incubated for approximately 3 hours at 30°C. followed by transfer to a temperature of 37°C and incubation for an additional hour prior to imaging.

Manual fluorescence microscopy and organelle staining

Cell cultures were incubated overnight in a 96-well round-bottom plate (ThermoFisher) containing 100µl of SD media, supplemented with the necessary amino acids and/or antibiotics (as mentioned above). The cells were incubated at 30°C with slight agitation. The day after, 5µl of the overnight culture was diluted into 195µl of SD media and incubated for approximately 4 hours at 30°C with slight agitation. For the observation of the mCherry-D4H ergosterol reporter, the cultures were transferred to 37°C after approximately 3 hours. 50µl of the culture was then transferred to a 384-well glass-bottomed microscopy plate (Matrical Bioscience) coated with 0.25mg/ml Concanavalin A (ConA, Sigma). Cells in the mid-logarithmic phase were adhered to the plates by incubating at room temperature for 15 minutes. Following adherence, the cells were washed and imaged in synthetic minimal medium.

For mitochondrial staining, after adherence to the ConA, the media was replaced with synthetic minimal medium containing 50nM MitoTracker (MitoTracker Orange CMTMRos; Invitrogen) and incubated at room temperature (RT) for 10 minutes, washed once, and imaged in SD media.

For lipid droplet staining, after adherence to the ConA the media was replaced with phosphate buffered saline (PBS) containing 100µM MDH (AUTODOT™ Visualization Dye Monodansylpentane, Abgent), cells were incubated at RT for 15 minutes, washed, and imaged in PBS.

For vacuole staining, after adherence to the ConA the media was replaced with synthetic minimal medium containing 16µM $FM_{4\text{-}64}$ (FM™ 4-64 Dye (N-(3-Triethylammoniumpropyl)-4-(6-(4-(Diethylamino) Phenyl) Hexatrienyl) Pyridinium Dibromide, Invitrogen), incubated at 30°C for 1 hour, washed, and imaged in SD media.
For vacuole area per cell quantification, images of the vacuoles with CMAC (CellTracker™ Blue CMAC (Invitrogen C2110)) dye were imaged. after adherence to the ConA the media was replaced with synthetic minimal medium containing 10µM CMAC and incubated at RT for 30 minutes, washed twice and imaged in SD media.

Imaging was performed at RT using a VisiScope Confocal Cell Explorer system, which consists of a Zeiss Yokogawa spinning disk scanning unit (CSU-W1) coupled with an inverted IX83

microscope (Olympus). Single-focal-plane and Z-stack images were acquired with a 60× oil lens (NA 1.4) and were captured using a PCO-Edge sCMOS camera, controlled by VisiView software (GFP [488 nm], RFP [561 nm], or BFP [405 nm]).

High-resolution imaging was performed at room temperature using an automated inverted fluorescence microscope system (Olympus) equipped with a spinning disk high-resolution module (Yokogawa CSU-W1 SoRa confocal scanner with double micro lenses and 50-µm pinholes). Images of cells in the 384-well plates were captured using a 60× oil lens (NA 1.42) and a Hamamatsu ORCAFlash 4.0 camera. Fluorophores were excited by a laser and images were captured in the GFP channel (excitation wavelength 488 nm, emission filter 525/50nm). All images were taken in a Z-stack, and processed using cellSens software. Images were deconvoluted using cellSens software for noise reduction and the best focal plane for presentation was selected.

Images captured using a 100X oil lens were imaged using a Hamamatsu flash orca 4.0 camera, and a CSU-W1 Confocal Scanner Unit of Yokogawa with a 50µm pinhole disk at room temperature. For images with the ergosterol sensor, the strains were maintained at 37°C during imaging. Fluorophores were excited by a laser and images were captured in two channels: GFP (excitation wavelength 488nm, emission filter 525/50nm) and mCherry (excitation wavelength 561nm, emission filter 617/73nm).

All acquired images were manually inspected and brightness adjustments were performed using ImageJ[114]. All quantifications in Figure 2A were done by ScanR Olympus soft imaging solutions version 3.2.

Electron Tomography and Correlative Fluorescent Imaging

Pelleted yeast cells were placed in an aluminum disc with a depression of 100µm and outer diameter of 3mm (Engineering Office M. Wohlwend GmbH), then covered with a matching flat disc. The sandwiched sample was high-pressure frozen using an EM ICE high pressure-freezing device (Leica Microsystems, GmbH, Germany). Frozen samples were dehydrated in a temperature-controlled AFS2 Freeze substitution device, (Leica Microsystems) at − 90°C for 55 hours, in dry acetone containing 0.1% Uranyl Acetate (EMS, Hatfield, PA, USA). The temperature was then raised to −45°C (5°C/hour) for 9 hours followed by three acetone washes. Infiltration with Lowicryl HM20 (EMS) was carried out at increasing concentrations (10%, 25%, for 2 hours each). The temperature was then raised to −25°C (5°C/hour) and infiltration with higher concentrations of Lowicryl HM20 (50%, 75%, 2 hour each) was carried out. Finally, 100% Lowicryl HM20 was exchanged three times for every 10 hours followed by polymerization under UV light for 48 hours. The temperature was increased to 20°C (5°C/hour) and left under UV light for 48 hours. Sections of 200nm thickness were produced using an EMUC7 ultramicrotome (Leica microsystems) and were mounted on formvar coated 200 mesh copper grids.

Grids were labeled with vacuolar membrane $FM_{4\text{-}64}$ dye (1:100, T13320, Thermo Fisher Scientific) for 15 minutes. Multi-color wide-field fluorescence imaging of the sections was performed using a VUTARA SR352 system (Bruker) in the presence of an imaging buffer composed of 5mM cysteamine, oxygen scavengers (7µM glucose oxidase and 56nM catalase) in 50mM Tris with 10mM NaCl and 10% glucose at pH 8.0. Images were recorded using 1.3 NA 60x silicon oil immersion objective (Olympus) and excitation lasers of 488nm and 561nm. Z slices of 150nm were collected in order to compensate for the curvature of the grid. Chromatic correction and alignment of the 488nm and 561nm channels was performed prior to data collection using a glass slide with tetraspeck beads (T7279, Invitrogen). Images of the channels were aligned using Vutara SRX software (Bruker).

After fluorescence mapping, grids were stained with Reynolds lead citrate for 10 minutes and transmission electron microscopy (TEM) was performed with a Tecnai TF20 Field Emission microscope (Thermo Fisher Scientific) operating at 200kV. The sample was pre-exposed to an intense flux of electrons in order to induce shrinkage of the embedded material, to prevent sample changes during tomogram acquisition. Low-magnification montaged TEM maps of the sample grids were obtained using SerialEM software[115] The fluorescence maps were superimposed over the TEM montages using the vacuole fluorescent labeling as markers, and targets were chosen where bright puncta appeared in the cells. TEM tomograms were acquired with SerialEM, with 1nm/pixel resolution and images collected every one degree between -60 and 60 degrees. Electron tomographic datasets were reconstructed using IMOD software[116].

High precision overlays of the fluorescence and tomographic reconstructions for specific cells was done using the vacuole labeling as a fiducial marker. For each cell, the best fluorescence Z slice was selected and overlaid with the corresponding tomographic virtual section using Adobe Photoshop. Figure 1C shows superimposed fluorescence maps overlaying virtual sections from the cellular tomographic reconstructions.

Cryo-electron tomography

Sample vitrification: Yeast expressing either endogenous or overexpressing Yet3-GFP were cultured to OD_{600} 0.9. Glow-discharged Cryo-EM grids (R1.2/1.3, Cu 200 mesh grid, Quantifoil microtools) were mounted on a Vitrobot Mark IV (Thermo Fisher Scientific) and a drop of 3.5µL of culture was deposited on their carbon side. Excess liquid was removed by back-blotting with filter paper (Whattman 597) prior to vitrification by quick plunging into a liquid ethane/propane mixture at liquid nitrogen temperature. The grids were stored in grid boxes in liquid nitrogen until further use.

Sample thinning: Lamellae were prepared using an Aquilos 2 Cryo focused ion beam (FIB)/scanning electron microscope (SEM) (Thermo Fisher Scientific) at cryogenic temperature. A protective layer of organometallic platinum was deposited on the grid with the gas injection system (GIS) for 35 seconds. The sample was tilted to an angle of 20° and 200nm thick lamellae were prepared sequentially, starting with the Ga2+ ion beam at 30kV and 300 pA beam current for rough milling and followed by fine milling at 30kV and 50 pA. SEM imaging at 3kV and 13 pA was used to monitor the milling process.

Data acquisition: Tilt series from -46° to +64° at increments of 3° using the dose-symmetric acquisition scheme[117] of the lamellae were acquired using a Krios G4 Cryo- transmission electron microscope (Thermo Fisher Scientific) equipped with a 300kV field emission gun, Selectris energy filter, and a Falcon 4i direct electron detector camera, at a magnification of 33000x (3.653Å/pixel) at a defocus of -5 to -7µm. The target total dose per tomogram was around 120 e-/A^2. The camera was operated in dose-fractionation mode and between 700 to 900 EER frames were generated per tilt image. Frames were subsequently aligned using Motioncor2 and the new tilts series were reconstructed using patch tracking in IMOD 4.11[118] and weighted back-projected to reconstruct a tomogram. Tomograms were binned to 14.61 Å/pixel and isotopically reconstructed using IsoNe[119].
Tomogram segmentation: automatic membrane segmentation was performed using MemBrain-Seg[120]. Segmentations were then manually curated and colored using Amira (Thermo Fisher Scientific). Images were produced using UCSF Chimera[121].

Electron Microscopy

Processing of the samples was conducted using the Tokuyasu technique (Tokuyasu, 1973). Initially, the specimens were subjected to fixation using a solution of 0.1% glutaraldehyde (EMS)

and 4% paraformaldehyde (EMS) in a 0.1M cacodylate buffer (synthesized from dimethylarsinic acid sodium salt trihydrate; Sigma-Aldrich) with an addition of 5mM CaCl2 (pH 7.4; Sigma-Aldrich). This fixation process was carried out for a duration of 2 hours. Subsequently, the samples were rinsed and embedded in a 10% gelatin solution (EMS) and subjected to an additional fixation period of 24 hours at a temperature of 4°C.

Following this, the samples underwent a cryoprotection process, which involved infiltration with a 2.3M sucrose solution (J.T. Baker) for a period of 48 hours at RT, and were then frozen by immersion in liquid nitrogen. Ultrathin frozen sections, ranging from 70 to 90nm in thickness, were prepared using a Leica EM UC7 cryo-ultramicrotome. These sections were then transferred onto formvar-coated 200-mesh nickel transmission electron microscopy (EM) grids (EMS).

The grids were subsequently rinsed and embedded in a solution of 2% methyl cellulose (Sigma-Aldrich) and 0.4% uranyl acetate (EMS). The final imaging was performed using a Thermo Fisher Scientific Tecnai T12 transmission electron microscope, equipped with a bottom-mounted TVIPS TemCam-XF416 4k × 4k CMOS camera.

Library preparation and high-throughput screening

An automated methodology was employed for the integration of specific genomic manipulations into yeast libraries, as described in previous studies[68,122]. The query strains utilized for the procedure were constructed based on a strain YMS721[123]. The handling of libraries was facilitated using a RoToR bench-top colony array instrument (Singer Instruments). In brief, the query strains were mated with library strains on rich medium plates to yield diploid cells. These cells were subsequently transferred to nitrogen starvation media for a period of seven days to induce sporulation. Haploid cells were isolated using canavanine and thialysine (Sigma-Aldrich), with the absence of leucine serving as a selection marker for MATalpha. The final library was constructed by selecting for the desired combination of manipulations. Strains representative of the final library were validated using both microscopy and check-PCR.

For the purpose of screening, libraries were imaged using a Hamamatsu flash orca 4.0 camera and a CSU-W1 Confocal Scanner Unit of Yokogawa, equipped with a 50µm pinhole disk. The ScanR Olympus soft imaging solutions acquisition 3.2 software was used for image acquisition, with images captured using a 60× air lens (NA 0.9, GFP [488 nm]). For the secondary screen aimed at hit validation, strains were imaged using a 100× oil lens (NA 0.9, GFP [488 nm]). Libraries were imaged at RT during mid-logarithmic growth phase. Manual inspection of images was performed using ImageJ software[114].

Drop dilution assay

Serial dilutions of the cells were cultivated on synthetic minimal medium supplemented with glucose. The cells were initially incubated overnight with the appropriate selection markers. Following this, yeast strains were back-diluted to achieve an OD_{600} of 0.2 in synthetic media and incubated for approximately 4 hours at 30°C. After undergoing at least one cell division or upon reaching mid-logarithmic phase, the strains were back-diluted again to an OD_{600} of 0.1 and subsequently diluted in 10-fold increments. 2.5µL from each dilution was then plated onto either SD agar plates or SD agar plates supplemented with 10µg/ml Fluconazole (Sigma-Aldrich), both of which contained all necessary amino acids. The plating was performed in triplicate using a multichannel pipette (Gilson). Following 3 days of growth at 30°C, images of the plates were captured using a Canon PC1591 digital camera.

Growth assay

The growth assay was conducted in Transparent 96-well plates (Greiner) using a Spark plate reader (Tecan). The cells were incubated at a temperature of 30°C with shaking speed of 200 rpm in a Liconic incubator for 72 hours. Following a resuspension on a Bioshake 3000 plate shaker operating at 1,200 rpm, samples were measured at hourly intervals. The OD_{600} was recorded at a wavelength of 600nm.

Western blots

Yeast strains expressing C' GFP-tagged Yet1, Yet2, or Yet3 for figure S3C or C' GFP-tagged Yet1 and Yet3 either endogenously expressed or overexpressed for figure S1D, were cultured at 30°C in SD complete media until they reached mid-logarithmic phase. Cell density was adjusted to an OD_{600} of 5, corresponding to approximately 20µg of protein per sample (checked by BCA). The cells were harvested by centrifugation at 3,000 x g for 3 minutes and washed with 1ml of nuclease-free water. The cell pellet was resuspended in 200µL of lysis buffer (8M urea, 50mM Tris, pH 7.5, and protease inhibitors; Merck) and lysed by vortexing with glass beads (Scientific Industries) at 4°C for 10 minutes. Subsequently, 25µL of 20% SDS was added to each sample, followed by incubation at 45°C for 15 minutes. The lysate was separated from the glass beads by piercing the bottom of the microcentrifuge tubes, placing them in 5ml tubes, and centrifuging at 4,000 x g for 10 minutes. The flow-through was transferred to a new 1.5ml microcentrifuge tube and centrifuged at 20,000 x g for 5 minutes. The supernatant was collected and mixed with 4x SDS sample buffer (Laemmli buffer) and fresh 1M DTT, followed by incubation at 45°C for 15 minutes. The protein samples were separated by SDS-PAGE on a 4–20% gradient gel (Bio-Rad) and transferred to a 0.45-µm nitrocellulose membrane (Pall Corporation) using the Trans-Blot Turbo transfer system (Bio-Rad). The membrane was blocked with SEA BLOCK buffer (Thermo Scientific; diluted 1:5 in PBS) for 1 hour at RT and incubated overnight at 4°C with primary antibodies (rabbit anti-GFP, ab290, 1:2500; Abcam and mouse anti-Actin, ab170325, 1:5000, Abcam) diluted in a 2% wt/vol BSA/PBS solution containing 0.01% NaN_3. After washing, the membrane was probed with secondary antibodies (800CW Goat anti-Rabbit IgG, ab216773; Abcam and 680CW Goat anti-Mouse IgG, ab216776, Abcam) diluted 1:10,000 in 5% wt/vol nonfat milk/ Tris-buffered saline with 0.05% Tween 20 (TBST) for 1 hour at room temperature. The blots were washed and imaged using the LI-COR Odyssey Infrared Scanner.

Blue Native PAGE experiments

Isolation of crude organelles was performed on yeast cells (200ml) constitutively expressing the indicated GFP tagged proteins and cultured in rich media (YP) supplemented with 2% glucose till logarithmic phase. The cells were harvested (3000 x g, 5 minutes, RT), resuspended in DTT buffer (100mM Tris, 10mM DTT) and incubated at 30°C for 15 minutes. The cells were then washed once with spheroplasting buffer (1.2M Sorbitol, 20mM KPI, pH 7.2) and incubated with spheroplasting buffer supplemented with zymolyase (6mg/g of cells) for 1 hour at 30°C, to digest the cell wall. Further steps were carried out on ice. The spheroplasts were resuspended in homogenization buffer (0.6M Sorbitol, 10mm Tris, pH 7.4, 1mM EDTA, 0.2% fatty acid-free BSA with 2mM PMSF). To obtain cell lysate, the spheroplasts were dounce homogenized. The cell debris and nuclei were removed by centrifugation (2000 x g, 10 minutes, 4°C). The supernatant containing the crude organelles were isolated by centrifugation (18,000 x g, 15 minutes, 4°C). The pellets were resuspended in SEM buffer (250mM Sucrose, 1mM EDTA, 10mM MOPS) containing 2mM PMSF and stored at -80°C.

Blue Native gels were run with the crude organelle samples (150µg) solubilized in 100µL SEM buffer supplemented with Triton X-100 with a protein to detergent ratio of 1:2. The sample was

incubated for 30 minutes on ice. The supernatant containing the solubilized fraction was isolated by centrifugation (30,000 x g, 30 minutes, 4°C), and was mixed with the 10X loading dye (5% (w/v) Coomassie blue G, 500mM 6-amino-N-caproic acid, 100mM Bis-Tris, pH 7.0). The sample was loaded on a gel containing 6%-16% acrylamide gradient. The gels were run (150V, 15mA, 2 hours, 4°C) with Cathode buffer A (500mM Tricine, 150mM Bis-Tris, 0.2% Coomassie blue G, pH 7.0). The buffer was replaced with Cathode buffer B (500mM Tricine, 150mM Bis-Tris, pH 7.0) and the gels run was continued (50V, 15mA, 16 hours, 4°C). The proteins were blotted onto a polyvinylidene fluoride (PVDF) membrane and immunodecorated with a GFP antibody (Torrey Pines Biolabs Inc) in a 1:1000 dilution. Secondary antibody, Goat anti-rabbit IgG (H+L)-HRP conjugate (Bio-Rad) was applied in 1:10,000 dilution.

Mitochondrial translation rate analysis

Wild type and overexpressed Yet3 strains were cultured overnight in YPGal. The next morning, the $OD6_{00}$ was measured and adjusted to approximately 0.5 in YPGal. The cultures were then incubated for an additional 5 hours to ensure similar growth cycles and OD across all strains. For each reaction, 0.5 OD of culture was centrifuged at 4000 rpm for 5 minutes, washed with 500µl KPi buffer + 2% galactose, and resuspended in 500µl KPi + galactose. The cultures were then incubated for 10 minutes at 30°C in Methionine starvation medium. To block cytosolic protein synthesis, 10µl of Cycloheximide was added for 5 minutes. Subsequently, 2µl of [35S] Methionine was added for a 10-minute pulse. Then,10µl of cold Methionine was added and the samples were immediately placed on ice. The samples were then centrifuged at maximum speed for 1 minute at 4°C and frozen for further processing. The pellet was resuspended in 500µl water, mixed with 74µl of 2M NaOH and 6µl of 2-Mercaptoethanol (2-ME), and incubated on ice for 10 minutes. 80µl of 50% TCA (2M NaOH, 2-ME, TCA, acetone) was added and the mixture was incubated on ice for 10 minutes. The samples were then centrifuged at maximum speed for 20 minutes at 4°C. The pellet was finally dissolved in 50µl of 1xLoading buffer. 25µl of each sample was loaded onto a 10-18% Tris-Tricine gel. The gel was run at 25V and 250mA for 2.5 hours, stained, destained, dried, and exposed to a screen for 2 days for autoradiography.

Immunoprecipitation and LC–MS/MS sample preparation

Approximately 5 OD_{600} of cell pellets were resuspended in 400µl of lysis buffer, which contained 150mM NaCl, 50mM Tris-HCl (pH 8.0), 5% Glycerol, 1% digitonin (Sigma), 1mM MgCl2, protease inhibitors (Merck), and benzonase (Sigma). The cell suspension was then transferred to a 2ml FastPrep™ tube (lysing matrix C, MP Biomedicals). Lysis was performed by six cycles of one minute at maximum speed on a FastPrep-24™ cell homogenizer (MP Biomedicals), with a 5 minutes cooling period on ice between each cycle. The lysates were then centrifuged at 16,000 g for 10 minutes at 4°C, and the supernatant was transferred to a new microcentrifuge tube. For the purification of Protein-GFP, the samples were incubated with 40µl of pre-washed GFP-Trap Agarose beads (Chromotek) for 1 hour at 4°C. The beads were then washed twice with 200µl of digitonin wash buffer (150mM NaCl, 50mM Tris-HCl pH 8.0, 1% digitonin) and four times with basic wash buffer (150mM NaCl, 50mM Tris-HCl pH 8.0). The beads were then incubated with 50µl of elution buffer (2M urea, 20mM Tris-HCl pH 8.0, 2mM DTT and 0.5µl trypsin (0.5µg/µl, Promega, #V5111)) per sample for 90 minutes. The eluate was then separated from the beads and collected in a new microcentrifuge tube. 50µl of alkylation buffer (2M urea, 20mM Tris-HCl pH 8.0, 50mM iodoacetamide (IAA)) was added to the beads and incubated for 10 minutes. This buffer was also separated from the beads and combined with the first eluate. Finally, the beads were washed with 50µl of urea buffer (2M urea, 20mM Tris-HCl pH 8.0) for an additional 10 minutes, and this buffer was also separated and combined with the previous mixture. All elution steps were performed at RT in the dark with shaking at 1,400 rpm. The combined eluate (150µl total volume) was incubated overnight at RT in the dark at 800 rpm. The following morning, 1µl of 0.25µg/µl

trypsin was added to each sample and incubated for an additional 4 hours at RT in the dark at 800 rpm. Following digestion, peptides were desalted using Oasis HLB, µElution format (Waters, Milford, MA, USA). The samples were vacuum dried and stored in -80˚C until further analysis.

LC–MS/MS Proteomics

The mass spectrometry proteomics data have been deposited to the ProteomeXchange Consortium via the PRIDE [124] partner repository with the dataset identifier PXD052060 and 10.6019/PXD052060.

Liquid chromatography was used with ULC/MS grade solvents. Each sample was loaded using split-less nano-Ultra Performance Liquid Chromatography (10 kpsi nanoAcquity; Waters, Milford, MA, USA). The mobile phase was: A) H_2O + 0.1% formic acid and B) acetonitrile + 0.1% formic acid. The peptides were then separated using a T3 HSS nano-column (75µm internal diameter, 250mm length, 1.8µm particle size; Waters) at 0.35µL/minute except for the first 13 minutes. Peptides were eluted from the column into the mass spectrometer using the following gradient: 3%B for 13 minutes at flow of 0.4µL/minute, 3% to 30%B in 42 minutes, 30% to 90%B in 5 minutes, maintained at 90% for 5 minutes and then back to initial conditions[125].

Mass Spectrometry was performed with the nanoUPLC coupled online through a nanoESI emitter (10µm tip; New Objective; Woburn, MA, USA) to a quadrupole orbitrap mass spectrometer (Q Exactive HF, Thermo Scientific) using a FlexIon nanospray apparatus (Proxeon). Data was acquired in data dependent acquisition (DDA) mode, using a Top10 method. MS1 resolution was set to 120,000 (at 200m/z), mass range of 375-1650m/z, AGC of 3e6 and maximum injection time was set to 60 milli-seconds. MS2 resolution was set to 15,000, quadrupole isolation 1.7m/z, AGC of 1e5, dynamic exclusion of 20 seconds and maximum injection time of 60 milli-seconds[125.]

Raw data was processed with MaxQuant v2.0.1.0[126]. The data was searched with the Andromeda search engine against the SwissProt *S. cerevisiae* ATCC204508/S288c proteome database (January 2023 version, 6060 entries) in addition to the MaxQuant contaminants database. All parameters were kept as default except: Minimum peptide ratio was set to 1 and match between runs was enabled. Carbamidomethylation of C was set as a fixed modification. Oxidation of M and protein N-term acetylation were set as variable modifications. The LFQ intensities were used for further calculations using Perseus v1.6.2.3[127]. Decoy hits were filtered out, as well as proteins that were identified on the basis of a modified peptide only. The LFQ intensities were log2-transformed and only proteins that had at least 2 valid values in at least one experimental group were kept. The remaining missing values were imputed by a random low range distribution. Student's t-tests were performed between the relevant groups to identify significant changes in protein levels.

Data analysis was done using GraphPad Prism 10.2.2.

Metabolomics and lipidomics sample preparation

Endogenously expressed Yet3, Yet3 overexpression, and Yet3 knockout yeast strains were cultured overnight at 30°C in a synthetic minimal medium supplemented with 2% glucose and the appropriate selection marker. On the following day, 50µl of each sample was transferred to a the same medium without any selection markers, and incubated overnight at 30°C. Subsequently, the cells were diluted and grew until they reached mid-log phase, as indicated by an OD_{600} measurement. For the collection of cells, 25 OD_{600}, or 10 OD_{600} specifically for free and total ergosterol level measurements, were harvested and washed twice with DDW. The cells were then flash-frozen in liquid nitrogen and stored at -80°C for future analysis.

Metabolite extraction for polar and lipid metabolite analysis

Extraction and analysis of lipids and polar metabolites were performed as previously described [128,129] with some modifications: Cell pellets were extracted with 1ml of a pre-cooled (−20˚C) homogenous methanol: methyl-tert-butyl-ether (MTBE) 1:3 (v/v) mixture, containing following internal standards: 0.1µg/ml of Phosphatidylcholine (17:0/17:0) (Avanti), 0.4µg/ml of Phosphatidylethanolamine (17:0/17:0, 0.15nmol/ml of Ceramide/Sphingoid Internal Standard Mixture II (Avanti, LM6005), 0.0267µg/ml d5-TG Internal Standard Mixture I (Avanti, LM6000) and 0.1µg/ml Palmitic acid-13C (Sigma, 605573). The tubes were vortexed and then sonicated for 30 minutes in an ice-cold sonication bath (taken for a brief vortex every 10 minutes). Then, UPLC-grade water (DDW): methanol (3:1, v/v) solution (0.5ml), containing internal following standards: C13 and N15 labeled amino acids standard mix (Sigma, 767964) (1:1500), was added to the tubes followed by vortex and centrifugation. The upper organic phase was transferred into a 2mL Eppendorf tube. The polar phase was re-extracted as described above, with 0.5mL of MTBE. Both organic phases were combined and dried in a Speedvac and then stored at −80˚C until analysis. The lower polar phase, used for polar metabolite analysis, was treated in a similar way. For analysis, the dried lipid extracts were re-suspended in 150µl mobile phase B (see below) and centrifuged at 20800rcf (4˚C for 10 minutes). Then 120µL were transferred to the HPLC vials for injection. Polar dry samples were re-suspended in 120µL methanol: DDW (50:50) and centrifuged twice to remove the debris. 70µL were transferred to the HPLC vials for injection.

Lipid extracts were analyzed by LC-MS lipidomics using a Waters ACQUITY I class UPLC system coupled to a mass spectrometer (Thermo Exactive Plus Orbitrap) which was operated in switching positive and negative ionization mode. The analysis was performed using Acquity UPLC System combined with chromatographic conditions as described[128] with small alterations. Briefly, the chromatographic separation was performed on an ACQUITY UPLC BEH C8 column (2.1×100mm, i.d., 1.7µm) (Waters Corp., MA, USA). The mobile phase A consisted of DDW: Acetonitrile: Isopropanol 46:38:16 (v/v/v) with 1% 1M NH4Ac, 0.1% acetic acid. Mobile phase B composition is DDW: Acetonitrile: Isopropanol 1:69:30 (v/v/v) with 1% 1M NH4Ac, 0.1% acetic acid. The column was maintained at 40˚C, and the flow rate of the mobile phase was 0.4ml/min. Mobile phase A was run for 1 minute at 100%, then it was gradually reduced to 25% at 12 minutes, following a decrease to 0% at 16 minutes. Then, mobile phase B was run at 100% till 21 minutes, and mobile phase A was set to 100% at 21.5 minutes. Finally, the column was equilibrated at 100% A till 25 minutes. Lipid identification and quantification was performed using LipidSearch™ software (Thermo Fisher Scientific). The validation of the putative identification of lipids was performed by comparing it to the homemade library, which contains lipids produced by various organisms, and the correlation between retention time and carbon chain length and degree of unsaturation. Relative levels of lipids were normalized to the internal standards and the protein amount in the examined samples.

LC-MS polar metabolite analysis (Metabolic profiling) was performed as described[129] with minor modifications: Briefly, analysis was performed using Acquity I class UPLC System combined with mass spectrometer Q Exactive Plus Orbitrap™ (Thermo Fisher Scientific) which was operated in a negative ionization mode. The LC separation was done using the SeQuant Zic-pHilic (150mm × 2.1mm) with the SeQuant guard column (20mm × 2.1mm) (Merck). The Mobile phase B: acetonitrile and Mobile phase A: 20mM ammonium carbonate with 0.1% ammonia hydroxide in DDW: acetonitrile (80:20, v/v). The flow rate was kept at 200µl/minute and gradient as follow: 0-2minutes 75% of B, 14 minutes 25% of B, 18 minutes 25% of B, 19 minutes 75% of B, for 4 minutes, 23 minutes 75% of B. Data processing was done using Compound discoverer v3.3 (Thermo Fisher Scientific) software when detected compounds were identified by retention time, and fragments were verified using an in-house-generated mass spectra library.

Data analysis was done using GraphPad Prism 10.2.2.

Targeted analysis of free ergosterol

Extraction and analysis of ergosterol were performed as previously described[130] with some modifications: For analysis of free ergosterol the cell pellet was extracted with 400ul of a pre-cooled (−20˚C) homogenous methanol: methyl-tert-butyl-ether (MTBE) 1:3 (v/v) mixture, containing epicholesterol (10uL, 1mg/mL) as internal standard. The mixture was incubated, shaking, with added zirconium beads at 30Hz, for 1.5 minutes (Retsch MM400) and then mixed at at 1,200rpm for 1 hour (Thermomixer C Eppendorf) at RT. Then, water (100uL) was added for phase separation, and the upper organic phase was collected and dried. The obtained residue was derivatized with N-trimethylsilylimidazole/ trimethylchlorosilane reagent (TMSI:TMCS, 99:1, v/v; 50uL; both from Merck) and pyridine (50uL) in a shaker at 800rpm for 1 hour at 60˚C; Thermomixer C Eppendorf). The obtained solution was transferred to the GC-MS vials for injection.

Data analysis was done using GraphPad Prism 10.2.2.

Respiration test

Yeast strains were grown on YPD plates containing NAT for a day at 30°C. The yeast colonies were transferred to liquid YPD (containing 2% glucose) and incubated overnight at 30°C with slight agitation. On the day of the experiment, cell density (OD_{600}) was measured after 12 hours of growth. The cultures were diluted to an OD_{600} of 0.5 and incubated for another 2.5 hours at 30°C with slight agitation. One day before the measurement the Seahorse, XFe96/XF Pro Cell Culture microplate (Agilent) was coated with 0.1mg/ml Poly-D-Lysine (Sigma Aldrich), and was incubated with the coating solution at 4°C overnight. The yeast cells were pelleted down at 500 x g after which they were resuspended in either YPGal (containing 1% galactose) for determining basal respiration or Assay Medium (0.67% yeast nitrogen base, 2% potassium acetate, and 2% ethanol) for measuring maximal respiration[131] to an OD_{600} of 0.1. 180µl of cell suspension was added per well to the Seahorse XFe96/XF Pro Cell Culture microplate. After seeding, the cells were incubated for 30 minutes at 30°C. The measurement was done under basal conditions and upon the addition of 40µM CCCP, and 2.5µM Antimycin A in a Seahorse XFe96 Analyzer (Agilent) at 30°C. Three cycles of mixing (for 3 minutes) and measuring (for 3 minutes) time were allotted to each condition. Data analysis was done using GraphPad Prism 10.2.2.

Heme level measurements

Total heme measurements were performed as previously described[132]. Briefly, for all total heme measurements, ~1x108 cells were harvested, washed in sterile ultrapure water, resuspended in 500µL of 20mM oxalic acid and stored in a closed box at 4°C overnight (16–18 hours). The next day, an equal volume (500µL) of 2M oxalic acid was added to the cell suspensions. The samples were split, with half the cell suspension transferred to a heat block set at 95°C and heated for 30 minutes and the other half of the cell suspension kept at RT for 30 minutes. All suspensions were centrifuged for 2 minutes on a table-top microfuge at 21,000g and the porphyrin fluorescence (excitation 400nm, emission 620nm) of 200µL of each sample was recorded on a Synergy Mx multi-modal plate reader using black Greiner Bio-one flat bottom fluorescence plates. Heme concentrations were calculated from a standard curve prepared by diluting 500–1500µM hemin chloride stock solutions in 0.1M NaOH into ultrapure water. In order to calculate heme concentrations, the fluorescence of the unboiled sample (taken to be the background level of protoporphyrin IX) was subtracted from the fluorescence of the boiled sample (taken to be the free base porphyrin generated upon the release of heme iron). The cellular concentration of heme was determined by dividing the moles of heme determined in this fluorescence assay by the number of cells analyzed, giving moles of heme per cell, and then converting to a cellular concentration by dividing by the volume of a yeast cell, taken to be 50fL.

Free heme measurements at steady-state was performed on cells expressing the HS1-M7A heme sensors cultured in 10mL SCE-LEU media, with or without 0.5mM succinylacetone, for ~14–16 hours to OD_{600} ~ 1–2. Cytosolic, nuclear and mitochondrial-targeted sensors were expressed on low copy centromeric plasmids and were driven by the *GPD* promoter (p415-GPD) [67,132] After culturing, cells were collected, washed in water, and resuspended in PBS solution to a density of 10 OD_{600} units per mL. 200µL of the cell suspension, corresponding to 2 OD_{600} units or 4 x 107 cells, was used to measure EGFP (excitation 488nm, emission 510nm) and mKATE2 (excitation 588nm, emission 620nm). Background autofluorescence of cells not expressing the sensors was recorded and subtracted from the EGFP and mKATE2 sensor fluorescence values. Fluorescence was recorded on a Synergy Mx multi-modal plate reader using black Greiner Bio-one flat bottom fluorescence plates.

To estimate fractional heme occupancy of the heme sensor, we used the following formula: [133]

$$\% \text{ Heme Occupancy} = (R - R_{min}) / (R_{max} - R_{min}) \times 100$$

where R_{min} was the sensor ratio obtained from heme depleted cells cultured with succinylacetone, R_{max} is the ratio obtained from cells expressing HS1, a high-affinity sensor that is quantitatively saturated with heme[65], and R is the steady-state ratio of the HS1-M7A heme sensor in a given strain.

Data analysis was performed using GraphPad Prism 10.2.2.

RNA sample collection, extraction, and sequencing

Endogenously expressed Yet3 and overexpressed Yet3 strains were cultured overnight at 30°C in synthetic minimal medium supplemented with 2% glucose and NAT. On the following day, cells were back-diluted and cells at 2.5 OD_{600} were pelleted, washed with DDW, frozen in liquid nitrogen and stored at −80°C until further analysis. RNA was extracted using a modified protocol of the Nucleospin 96 RNA kit (Macherey-Nagel, Duren, Germany). Cells were lysed in a 96 deep-well plate by adding 450µl of lysis buffer containing 1M sorbitol (Sigma-Aldrich), 100mM EDTA, and 0.45µl lyticase (10IU/µL) and incubating at 30°C for 30 minutes. Spheroplasts were centrifuged for 10 minutes at 1,300 x g and extraction was performed as per the kit protocol substituting β-mercaptoethanol with DTT.

RNA libraries were created as follows: poly(A) RNA was selected by reverse transcription with a barcoded poly(T) primer. The barcoded DNA–RNA hybrids were pooled and fragmented by a hyperactive variant of the Tn5 transposase. Tn5 was stripped off the DNA with 0.2% SDS followed by SPRI beads cleanup, and cDNA was amplified and sequenced with Illumina Novaseq 6000 using a primer complementary to the opposite adaptor to the poly(A).

Processing and analysis of RNA-seq data

50-bp reads of the RNA-seq of every sample were mapped to the *S. cerevisiae* genome (R64 in SGD) using bowtie2 (parameters: –very-sensitive –trim-to 40). After alignment to the genome, samples that had less than 150,000 reads were discarded from the analysis to prevent an artificial enrichment for highly expressed genes. For every sequence, we removed PCR-duplicates using UMIs and umitools. For each gene, we summed all the unique reads aligned to 400 bp upstream its 3′ end to 200-bp downstream in order to get the total expression of that gene. The number of reads for each sample was normalized to 10^6. Expression fold change was calculated between the log2-normalized means of the different samples and the p-value calculated based on expression values in individual repeats (n=3).

Data analysis was done using GraphPad Prism 10.2.2.

Mammalian cell culture

Human HeLa S3 cells (graciously shared by Orly Laufman, Weizmann Institute of Science) were maintained in DMEM/F-12 medium (Gibco, USA) supplemented with 10% fetal bovine serum (FBS, Gibco, USA) and 1% Penicillin-Streptomycin-Neomycin (Biological Industries, Israel).

Mammalian Plasmids and Transfections

HeLa S3 cells were transfected with plasmids expressing the pLenti-C-mGFP-P2A-Puro Lentiviral Gene Expression Vector (Origene) or BAP31 (BCAP3) Human Tagged Lenti ORF Clone plasmids (Origene) (1µg/ml) for 4 hours using Lipofectamine 2000 (Invitrogen, USA) and then were grown in DMEM/F-12 medium overnight.

Imaging and staining of Mammalian Cells

Cells were cultured on coverslips placed in a 12-well plate and subsequently fixed using 4% paraformaldehyde (PFA) for a duration of 20 minutes. The nuclei were stained with Hoechst H33342 (1:1000 dilution, Sigma, USA) for approximately 10 minutes, while LDs were stained with BODIPY 558/568 (1:2000 dilution, Invitrogen, D3835) for ~45 minutes at RT. The coverslips were then mounted using Immu-Mount mounting medium (Thermofisher scientific, USA).

For the purpose of cholesterol staining, cells were grown on a 12-well plate and fixed in 4% PFA for 15 minutes at RT. Following fixation, the cells were washed thrice with PBS. The fixed cells were then incubated with freshly prepared filipin III (F9765; Sigma-Aldrich) at a concentration of 50 µg/ml in PBS for ~1.5 hours at RT in the dark. After three additional washes with PBS, the cells were mounted using Immu-Mount mounting medium.

Image acquisition was performed using an Andor Dragonfly 505 confocal spinning disk system, operated via Fusion software. The system is integrated with a Leica Dmi8 inverted microscope, and images were captured using a Plan Apo 63x (1.40 N.A.) oil immersion lens. All images were subsequently edited using the Fiji image processing package[114].

Protein modelling and analysis

Yet3 and BAP31 sequences were retrieved from UniProt (PMC9825514) and monomeric or homotrimeric structures were obtain with ColabFold's (PMC9184281) implementation of AlphaFold2 (PMC8371605) (AlphaFold2_advanced_v2). Structures were visualized in ChimeraX (PMC10588335) software. Structural based alignments from ChimeraX were rendered in ESPript3 (PMC4086106). Hydrophobic cavities were calculated with MOLE (PMC6030847).

Figure Legends

Figure 1- Yet3 is a pan-ER contact site protein

A. Overexpressed (OE) Yet3-mScarlet concentrates at many ER contact sites. To visualize the localization of Yet3 at contacts using fluorescence microscopy, various split-Venus reporters were used: ER-Peroxisomes (Pex) reporter (Snd3-VN/Pex25-VC); ER-Lipid droplets (LD) reporter (Snd3-VN/Faa4-VC); ER-Plasma membrane (PM) reporter (Snd3-VN/Ina1-VC); ER-Mitochondria (Mito) reporter (Snd3-VN/Tom20-VC) and ER-Vacuole (Vac) reporter (Snd3-VN/Zrc1-VC). White arrows show areas of co-localization between Yet3 puncta and the indicated reporter signals. Strains were imaged with a 100x oil lens. Scale bar, 5µm.

B. Overexpressed (OE) Yet3-GFP localizes to contact sites in the absence of a synthetic reporter. Marker proteins (Pex7 and Tgl3 for Pex or LDs, respectively), and tether proteins (Tcb2 and Lam2 in the ER-PM contact, Lam6 and Mmm1 in the ER-Mito contact, Nvj1 and Nvj2 in the ER-Vac contact, Num1 and Mdm36 in the ER-mitochondria-plasma membrane (MECA) contact), were expressed under a constitutive promoter and tagged with mCherry on their N'. White arrows mark areas of co-localization between the Yet3 puncta and the mCherry tagged proteins. Strains were imaged with a 100x oil lens. Scale bar, 5µm.

C. Correlated Light and Electron Microscopy (CLEM) images showing that Yet3 localizes to both ER-mitochondria (Mito) and ER-plasma membrane (PM) contacts. The yellow arrows point to the contact site between the ER tubule and the indicated organelle, where the Yet3-GFP signal is bright. Scale bar, 500nm.

Figure 2-Yet3 levels affect organelles in an Opi1-independent manner

A. Microscopy images highlighting how multiple organelles are affected by overexpression (OE) of Yet3. In strains that overexpress Yet3, peroxisome number (marked using Pex3-mCherry) increased, while LD number (marked with Tgl3-mCherry) decreased. The vacuoles (dyed with $FM_{4\text{-}64}$) and mitochondria (shown by Tom20-mCherry) appear enlarged. The mean number of peroxisomes and LDs per cell was quantified and is presented in yellow at the bottom of each image, with standard error of mean. The mean of the vacuole area per cell was quantified and is presented in yellow at the bottom of the image, with standard error of mean. The differences were statistically significant using a two-tailed t-test, ****$p \leq 0.0001$. In the peroxisome analysis, N= 5188, 7090 for control and OE Yet3 respectively. In the LD analysis, N=5648, 6378 for control and OE Yet3 respectively. In the vacuole analysis, N= 6734, 6378 for control and OE Yet3 respectively. Cells were imaged with a 60x oil lens. Scale bar, 5µm

B. HeLa S3 cells display a decreased number of LDs following overexpression (OE) of the human homolog of Yet3, BAP31. HeLa S3 cells were transfected with either P2A-GFP plasmid as a control or BAP31-GFP plasmid for overexpressing BAP31. LDs were visualized using BODIPY red, and Hoechst dye was used for nuclear staining in blue. Shown are representative images from three replicates. Cells were imaged using a 63x glycerol lens. Scale bar, 10µm.

C. Increased expression of Yet3 does not cause mis-localization of Opi1. On the background of Yet3 overexpression (OE) or knockout (KO), Opi1-GFP consistently enters the nucleus when inositol is present. Depletion of inositol from the media showed an Opi1-GFP signal on the nuclear membrane in both control and Yet3 overexpression. However knockout of Yet3 led to Opi1 accumulating inside the nucleus as expected. All strains were imaged with a 60x oil lens. Scale bar, 5µm.

D. Increased levels of Opi1 in inositol-containing media did not rescue the phenotypes of overexpressed (OE) Yet3. Mitochondria were visualized by Tom20-GFP and LDs using Tgl3-GFP. Images were taken using a 60x oil lens. Scale bar, 5µm.

E. Knockout (KO) of *OPI1* does not mimic the Yet3 overexpression (OE) phenotypes. Mitochondria were imaged using Mitotracker Orange and LDs by using the blue MDH dye. Images were taken using a 60x oil lens. Scale bar, 5µm.

Figure 3- Yet3 interacts with the post-squalene ergosterol biosynthesis machinery, affecting sterol distribution in the cell

A. Ergosterol biosynthesis proteins are enriched as interactors of Yet3. A volcano plot showing -log(p-value) vs. log2(fold-change) of changes observed following Immunoprecipitation-Mass Spectrometry (IP-MS) to identify peptides of interacting proteins when compared to an overexpressed Tom20-GFP control. Highlighted are enriched interactors of overexpressed Yet3-GFP. Ergosterol biosynthesis proteins, shown in red, are both enriched and are statistically significant (*$p \leq 0.05$). Yet3 itself is represented by a purple dot, while Yet1 is represented in a blue dot. Shown are average enrichment values from biological triplicates.

B. Yet3 expression levels affect the distribution of plasma membrane sterols. mCherry-D4H, a reporter for free ergosterols, was expressed on the background of control, overexpressed (OE) Yet3 and Yet3 knockout (KO) strains, demonstrating altered sterol distribution in the cell. All samples were imaged with a 100x oil lens. Scale bar, 5µm.

C. Overexpression (OE) of Yet3 sensitized cells to the ergosterol-biosynthesis inhibiting drug, fluconazole. Drop dilution assay of control and overexpressed Yet3 strains grown on control (Untreated) or Fluconazole (20ug/ml) containing media. Images were acquired after three days at 30ºC. A representative image from three replicates is shown.

D. The transcriptional activator of ergosterol biosynthesis, Upc2, enters the nucleus upon overexpression (OE) of Yet3. Upc2, known to translocate from the cytosol to the nucleus upon sensing a reduction in PM ergosterols, was tagged with GFP on its C' to visualize its cellular localization by fluorescence microscopy using a 60x oil lens. Scale bar, 5µm.

E. mRNAs of ergosterol biosynthesis enzymes are upregulated in strains overexpressing Yet3 compared to control cells. The volcano plot shows -log(p-value) against log2(fold change) of changes recorded using RNA-Seq. Highlighted in red are the post-squalene pathway transcripts, *HEM13* is marked in blue and the *YET3* mRNA is in purple. Next Generation Sequencing (NGS) was performed in three replicas per strain.

F. Oxygen consumption rate (OCR) increases in overexpression (OE) of Yet3 and in the Yet3 knockout (KO). All samples were grown on glucose overnight and transferred to galactose for 24 hours before measuring their basal respiration. Significance of the changes for three independent replicates was tested using two-way ANOVA. ****$p \leq 0.0001$.

G. Total heme concentration in overexpressed (OE) Yet3 is higher than in control. A porphyrin fluorescence assay was used to measure heme concentration. Significance of the changes for three independent replicates was tested using an unpaired t-test. ***$p \leq 0.001$.

H. In contrast to mitochondria and the nucleus, cytosolic free heme was reduced in overexpression (OE) of Yet3. Unbound heme concentration was measured using the Heme Sensor1 (HS1). HS1 levels of heme were measured by heme dependent fluorescence emission compared to an independent fluorophore by percentage. The HS1 was targeted to the mitochondrial matrix by fusing it to the N' of Cox4, or to the nucleus by fusing it to the C' of SV40. Significance of the

changes from three independent replicates was tested using two-way ANOVA significance test. ***$p \leq 0.001$. ****$p \leq 0.0001$.

Figure 4- Yet3 recruits the ERGosome to provide on-demand sterols at ER contact sites

A. Yet3 overexpression (OE) alters the localization of post-squalene biosynthesis pathway proteins to specific subdomains on the ER membrane. Constitutively expressed post-squalene proteins tagged with mCherry on their N' were homogeneously distributed in strains expressing endogenous Yet3-GFP. Upon overexpression of Yet3, they concentrated in ER subdomains that co-localize with Yet3 puncta. The pre-squalene enzyme, mCherry-Hmg1, did not alter its distribution nor concentrate together with overexpressed Yet3 puncta, which demonstrates that this is not an unspecific restructuring of the ER as a whole. Images were taken with a 100x oil lens. Scale bar, 5µm.

B. Yet3-GFP containing foci co-localized with sterol-rich areas (measured using the free ergosterol reporter mCherry-D4H), showcasing that internal ergosterol accumulates at contact sites when Yet3 is overexpressed. Strains were imaged with a 100x oil lens. Scale bar, 5µm.

C. During conditions of decreased ergosterol abundance in the cell (created by treating the cells with the ergosterol biosynthesis inhibitor Fluconazole), Yet3, expressed under its own promoter, accumulates at ER subdomains. Endogenously expressed Yet3-GFP is homogenously distributed around the ER. Applying Fluconazole (20ug/ml), caused sterol depletion from cells as can be seen by the translocation into the nucleus of Upc2-GFP, a transcription factor that senses ergosterol reduction in the PM and enters the nucleus. Under these conditions, Yet3-GFP also accumulates in subdomains of the ER, while another ER protein, Sec63-GFP, does not change. Strains were imaged in 60x lens. Scale bar, 5µm.

D. Yet3 depletion rescues Fluconazole induced cellular alterations. Yeast strains with endogenous (Control), overexpressing (OE) or knocked out (KO) for Yet3 were imaged in regular media or treated with Fluconazole (20ug/ml) to inhibit ergosterol biosynthesis. Fluconazole addition reduced LD number and altered the shape of mitochondria (Mito) in a way that pheno-mimicked the Yet3 overexpression alone. Combined overexpression of Yet3 and growth in fluconazole led to enhanced phenotypes. Importantly, knockout of Yet3 rescued both LD abundance and mitochondrial morphology in cells treated with Fluconazole compared to untreated control cells. Mitochondria were stained with Mitotracker Orange, and LDs were stained using MDH. Strains were imaged in PBS. Scale bar, 5µm.

E. BAP31 overexpression alters cholesterol distribution. Confocal images of HeLa S3 cells transfected with an overexpression (OE) BAP31-GFP plasmid, demonstrate changes in cholesterol (visualized using Filipin III dye) distribution in the cell. P2A-GFP plasmid was transfected to HeLa S3 as control. White arrows in cells overexpressing BAP31 indicate co-localization between cholesterol concentrations and BAP31 puncta on the ER. Cells were imaged using a 63x glycerol lens. Scale bar, 10µm.

Figure 5- Schematic illustration of our model for Yet3 molecular function.

Yet3 accumulates at ER contact sites and recruits the post-squalene proteins in the ergosterol biosynthesis pathway to create the ERGosome. There, it increases the concentration of ergosterols, which create the sterol rich domains essential for contact formation and function.

Figure S1- Overexpression of Yet3 tagged on its C' has the same growth rate as untagged Yet3, and accumulates at ER subdomains.

A. Illustration of the ergosterol biosynthesis pathway. The scheme contains all the enzymes and metabolites required for ergosterol synthesis, divided to the pre-squalene and post-squalene steps. Fluconazole, an inhibitor of Erg11, reduces ergosterol amounts in the cell.

B. A growth assay of strains overexpressing (OE) Yet3 fused to GFP on either its C' or N'. While overexpressed, N' tagged Yet3 shows the same growth rate as control (BY4741 strain) and Yet3 knockout (KO), the C' tagged overexpressed Yet3 has a similar growth rate to an untagged overexpressed Yet3 strain, demonstrating that tagging on this terminus preserves the function of the protein. Strains were grown overnight in synthetic minimal medium, back diluted to an OD_{600} of ~0.01 and monitored for growth over 48 hours.

C. Yet3-GFP overexpression shows high protein concentration at specific subdomains of the ER. One of the Yet3 paralogs in yeast, Yet1-GFP, is homogenously distributed across the ER both when endogenously expressed and when overexpressed. GFP intensity between the control and overexpressed strains was adjusted for brightness. Images were taken with a 100x oil lens. Scale bar, 5µm.

D. A strong promoter for overexpressing (OE) Yet1 and Yet3 results in higher protein levels. Western blot analysis of strains with Yet1 and Yet3, either endogenously expressed or overexpressed from a *TEF* promoter, all C' tagged with GFP. Immunoblotting was performed with antibodies against GFP and Actin, as a loading control.

Figure S2- Yet3 overexpression affects mitochondrial morphology

A. Mitochondria are enlarged in overexpressed (OE) Yet3 compared to a control strain. EM images of yeast show the mitochondrial size in different Yet3 expression levels. M, mitochondrion. Scale bar, 200nm.

B. Schematic illustration of the inositol biosynthesis regulation in yeast. In an inositol-rich environment, Opi1 inhibits the transcription activators Ino2/Ino4 and prevents expression of Ino1 and other phospholipid synthesis related-proteins. Depletion of inositol from the media results in sequestering Opi1 to the nuclear-ER, where it binds the Yet1-Yet3 heterodimeric complex, together with Scs2.

Figure S3- Overexpression of Yet3 rewires cellular metabolism

A. Free ergosterol measurements show lower concentrations of ergosterols in overexpression (OE) of Yet3 compared to the control strain. GC-MS lipid profile of sterols extracted from control, overexpressed Yet3, and Yet3 knockout (KO) strains in mid-logarithmic growth phase were analyzed. P-values were calculated from the three replicates of each strain using a one-way ANOVA test. *$p \leq 0.05$, **$p<0.01$, NS=non-significant.

B. Long-chain sphingolipids (SPH d22:2) are more abundant in strains overexpressing (OE) Yet3, that also have lower ergosterol levels (Figure S3A). Extraction and analysis of lipids by lipidomic analysis was done on independent triplicates from each strain. One-way ANOVA was tested for significance. *$p \leq 0.05$, NS=non-significant.

C. Gap1 and Agp1, two amino acid permeases that require ergosterol rich regions for trafficking to the plasma membrane, are mis-localized due to altered expression of Yet3. Both proteins were tagged with GFP on their C'. Strains were imaged using a 60x oil lens. Scale bar, 5µm.

D. Levels of various amino acids in overexpression (OE) of Yet3 compared to control. Triplicates from each sample were analyzed using polar metabolite profiling. Presented are only amino acids with significant changes as tested using two-way ANOVA. *p<0.05, **p<0.01, ****p ≤ 0.0001.

E. The transcription factor Gcn4 enters the nucleus when Yet3 is overexpressed (OE). Gcn4 was tagged with GFP on its C'. Images were taken with a 60X oil lens during their logarithmic growth phase. Scale bar, 5µm.

F. Overexpression (OE) of Yet3 reduces the translation rate of mitochondrial-encoded proteins. Translation rate was tested using a mitochondrial translation assay. Three replicates were performed and significance was tested by a two-tailed unpaired t-test, **p<0.01.

G. Different expression levels of Yet3 do not affect basal Oxygen Consumption Rate (OCR) in non-fermentable carbon source. Yeast strains were grown on glucose and then transferred to ethanol-based buffer for Seahorse measurements. Overexpression (OE) of Yet3 did not show any significant differences compared to the control strain. Knockout (KO) of Yet3 OCR had a small difference compared to control OCR. Three biological repeats and two technical repeats were performed. *p<0.05, NS=non-significant.

H. All intermediate metabolites of glycolysis are reduced in overexpression (OE) of Yet3. The exit metabolite in glycolysis, Pyruvic acid, is increased in Yet3 overexpression. Presented are only metabolites with significant changes. Triplicates from control and overexpressed strains were analyzed using polar metabolite profiling. Significant changes were tested using two-way ANOVA. **p<0.01, ***p ≤ 0.001, ****p ≤ 0.0001.

I. TCA cycle intermediate metabolites are reduced in overexpression (OE) of Yet3. Citrate, the entry point for the TCA cycle, is increased in Yet3 overexpression. Presented are only metabolites with significant changes. Triplicates from control and overexpression strains were analyzed using polar metabolite profiling. Significant changes were tested using two-way ANOVA. ****p ≤ 0.0001.

Figure S4- Yet3 assembles the post-squalene biosynthesis enzymes at ER contact sites, independently from its paralog Yet1.

A. Overexpression (OE) of Yet3 changes the positioning of proteins involved in the post-squalene biosynthesis pathway, directing them to subdomains on the ER membrane. In strains of Yet3-GFP expressed at normal levels, post-squalene proteins, which were tagged with mCherry at their N' and under control of a constitutive promoter, were evenly distributed. Overexpressed Yet3 recruits these proteins into specific ER subdomains that aligned with Yet3 puncta. The fact that the pre-squalene protein, mCherry-Hmg2, did not change its localization shows that this is not due to a general reorganization of ER proteins. The images were captured using a 100x oil lens. Scale bar, 5µm.

B. Potential high molecular weight complexes observed by blue native gel analysis. Two potential complexes of the ERGosome together with Yet3 are shown migrating at ~720kDa and ~480kDa, emphasized by red triangles. Yet3 is overexpressed and tagged with GFP on its C' while the ergosterol proteins are constitutively expressed and tagged with GFP on their N'. Crude preparations enriched for mitochondria and the ER were analysed and probed with anti-GFP antibody.

C. Endogenous Yet3 is more abundant than its two paralogs Yet1 and Yet2. Western blot analysis of three different strains, Yet1, Yet2 and Yet3, all tagged with GFP on their C' and under regulation of their native promoter. Immunoblotting was performed with antibodies against GFP and Actin as a loading control.

D. Yet1 expression levels affect the presence of Yet3 puncta amount and size, and change the free ergosterol distribution in the cell. Yet1 knockout (KO) decreases the signal of overexpressed (OE) Yet3 in the ER and increases its punctate distribution. Under these conditions, the free ergosterol is more concentrated inside the cell. However, Yet1 overexpression causes Yet3 to redistribute homogeneously on the ER surface and restores ergosterol distribution on the PM. Yet3 was, in both strains, tagged with GFP on its C'. Free ergosterols were tracked by mCherry-D4H reporter. White arrows represent co-localization between the mCherry-D4H and Yet3 foci. All samples were imaged with a 100x oil lens. Scale bar, 5µm.

E. Reduced amount of cellular ergosterols lead to accumulation of Yet3 in ER subdomains together with the ergosterol biosynthesis pathway proteins. Addition of 10ug/ml Fluconazole, caused endogenous Yet3-GFP signal that is usually distributed homogeneously around the ER, to accumulate in ER subdomains. Different constitutively expressed ergosterol biosynthesis proteins tagged with mCherry on their N' moved from their even distribution on the ER membrane or the LD, to ER subdomains too when treated with Fluconazole. White arrows highlight cases of co-localization with Yet3. As a control, the localization of Hmg1, a pre-squalene pathway enzyme, was not affected by Fluconazole. Images of the strains were taken with a 100x oil lens. Scale bar, 5µm.

F. Iron depletion from the media enhance overexpressed (OE) Yet3 puncta shape and induced endogenous Yet3 accumulation in ER subdomains. Yet3-GFP strains, either endogenously expressed or overexpressed, were grown under iron-free conditions. In these conditions, Yet3 shows enhanced localization to subdomains unlike the control ER protein Sec63 tagged with GFP on its C' remained that remained distributed along the entire ER membrane. White arrows highlight Yet3 foci formation in lower concentration of iron. The images were captured using a 60x oil lens Scale bar, 5µm.

Figure S5- Yet3 may recruit the ERGosome to additional ER subdomains that require ergosterol rich areas to function.

A. Sey1 and Rtn1 accumulations co-localize with Yet3 at ER subdomains. Yet3 was overexpressed (OE) and C' tagged with GFP. Sey1 and Rtn1 were constitutively expressed and tagged with mCherry on their N'. White arrows indicate the co-localization of Yet3 puncta with Sey1 and Rtn1 accumulation. Images were taken in 100x magnification. Scale bar, 5µm.

B. Overexpression (OE) of Yet3 shows a higher extent of ER tubules at the cell periphery. The ER was marked by overexpression of Emc6 tagged on its N'. Both images were taken in the same Z-plane (that highlights peripheral ER tubules) using a 60x oil lens SORA. Scale bar, 5µm.

C. Increased number of ER tubules in overexpressed (OE) Yet3 as visualized using cryo-ET. Tomographic slices (left) and corresponding segmentations of cryo-FIB (right) milled strains expressing endogenous (top) or overexpressing (bottom) Yet3-GFP. Scale bars, 200nm.

D. Endogenous Yet3-GFP accumulates in specific ER subdomains upon DTT treatment. Yet3 tagged with GFP on its C' was grown overnight in synthetic minimal media and back diluted to 2mM DTT for 4 hours before imaging. White arrows show Yet3 concentration in the ER membrane. Images were taken with a 60x oil lens. Scale bar, 5µm.

E. The functional form of Yet3 is necessary for clustering Ire1 in response to ER stress induced by DTT (2mM, 4 hours). Overexpression (OE) of Yet3 tagged on its C' (the functional form, Figure S1B) enables Ire1 clustering, while tagging on its N' (non-functional form) does not. Ire1-mCherry was visualized using a plasmid. Scale bar, 5µm.

F. Quantification of Ire1 clustering upon UPR induction by DTT treatment. Overexpression (OE) of Yet3 increased the percentage of cells with visible Ire1 clusters compared to control cells after DTT induction (2mM for 2 hours). Cells were counted manually using Image J.

Figure S6- Yet3 concentration in subdomains are dependent on proteins that change the ER membrane lipid composition.

A. Comparison of the Yet3 and BAP31 amino acid sequence and secondary structure showing high conservation of the transmembrane domains (TMDs). Each α represents one alpha helix of the proteins, starting from the N' until the C'. Red triangles are identical amino acids situated in the same place for both Yet3 and BAP31. White triangles represent amino acids with the same charge.

B. Yet3 and BAP31 TMDs are highly conserved according to AlphaFold2 prediction. A structural based sequence alignment of Yet3 (yellow) and BAP31 (blue) monomers. The N' of both Yet3 and BAP31 contain the three TMDs and the C' faces the cytosol.

C. A model of a Yet3 homotrimer predicted using AlphaFold2. Three Yet3 molecules with three membrane spanning domains each, create a hydrophobic cavity (seen in purple).

D. Schematic of the high content screen for finding genes that affect Yet3's capacity to localize to subdomains. Overexpression (OE) of Yet3 tagged with GFP on its C' was integrated to a deletion/hypomorphic allele library. In this library, every colony harbors a loss-of-function mutant in each of the ~6,000 yeast genes. All strains were imaged by automated microscopy, followed by manual inspection to identify proteins that are either required for, or suppress, the subdomain localization.

E. Results of the screen to uncover which mutated genes affected Yet3 accumulation at a specific subdomain of the ER. Deletion of either *ice2*, *loa1* or *nem1*, all proteins related to the ER lipid composition and LD formation, reduces Yet3 subdomain association. For a full list of hits see Supplementary Table S8. Scale bar, 5µm.

References

1. Zung, N., & Schuldiner, M. (2020). New horizons in mitochondrial contact site research. In Biological Chemistry (Vol. 401, Issue 6). https://doi.org/10.1515/hsz-2020-0133.

2. Eisenberg-Bord, M., Shai, N., Schuldiner, M., & Bohnert, M. (2016). A Tether Is a Tether Is a Tether: Tethering at Membrane Contact Sites. In Developmental Cell (Vol. 39, Issue 4). https://doi.org/10.1016/j.devcel.2016.10.022.

3. Scorrano, L., De Matteis, M.A., Emr, S., Giordano, F., Hajnóczky, G., Kornmann, B., Lackner, L.L., Levine, T.P., Pellegrini, L., Reinisch, K., et al. (2019). Coming together to define membrane contact sites. Nat Commun *10*. 10.1038/s41467-019-09253-3.

4. Shai, N., Yifrach, E., Van Roermund, C.W.T., Cohen, N., Bibi, C., Ijlst, L., Cavellini, L., Meurisse, J., Schuster, R., Zada, L., et al. (2018). Systematic mapping of contact sites reveals tethers and a function for the peroxisome-mitochondria contact. Nat Commun *9*. 10.1038/s41467-018-03957-8.

5. Bernhard,W., and Rouiller, C. (1956). Close topographical relationship between mitochondria and ergastoplasm of liver cells in a definite phase of cellular activity. J Biophys Biochem Cytol *2*, 73–78. 10.1083/JCB.2.4.73.

6. Phillips, M.J., and Voeltz, G.K. (2015). Structure and function of ER membrane contact sites with other organelles. Nature Reviews Molecular Cell Biology 2015 17:2 *17*, 69–82. 10.1038/nrm.2015.8.

7. Prinz, W. A., Toulmay, A., & Balla, T. (2020). The functional universe of membrane contact sites. In Nature Reviews Molecular Cell Biology (Vol. 21, Issue 1). https://doi.org/10.1038/s41580-019-0180-9

8. Castro, I.G., Shortill, S.P., Dziurdzik, S.K., Cadou, A., Ganesan, S., Valenti, R., David, Y., Davey, M., Mattes, C., Thomas, F.B., et al. (2022). Systematic analysis of membrane contact sites in Saccharomyces cerevisiae uncovers modulators of cellular lipid distribution. Elife *11*. 10.7554/ELIFE.74602.

9. Eisenberg-Bord, M., Zung, N., Collado, J., Drwesh, L., Fenech, E.J., Fadel, A., Dezorella, N., Bykov, Y.S., Rapaport, D., Fernandez-Busnadiego, R., et al. (2021). Cnm1 mediates nucleus-mitochondria contact site formation in response to phospholipid levels. J Cell Biol *220*. 10.1083/JCB.202104100.

10. Elbaz-Alon, Y., Rosenfeld-Gur, E., Shinder, V., Futerman, A.H., Geiger, T., and Schuldiner, M. (2014). A dynamic interface between vacuoles and mitochondria in yeast. Dev Cell *30*, 95–102. 10.1016/j.devcel.2014.06.007.

11. Cohen, Y., Klug, Y.A., Dimitrov, L., Erez, Z., Chuartzman, S.G., Elinger, D., Yofe, I., Soliman, K., Gärtner, J., Thoms, S., et al. (2014). Peroxisomes are juxtaposed to strategic sites on mitochondria. Mol Biosyst *10*. 10.1039/c4mb00001c.

12. Ardail, D., Popa, I., Bodennec, J., Louisot, P., Schmitt, D., and Portoukalian, J. (2003). The mitochondria-associated endoplasmic-reticulum subcompartment (MAM fraction) of rat liver contains highly active sphingolipid-specific glycosyltransferases. Biochemical Journal *371*. 10.1042/BJ20021834.

13. Fujimoto, M., Hayashi, T., and Su, T.P. (2012). The role of cholesterol in the association of endoplasmic reticulum membranes with mitochondria. Biochem Biophys Res Commun *417*. 10.1016/j.bbrc.2011.12.022.

14. Hayashi, T., and Fujimoto, M. (2010). Detergent-resistant microdomains determine the localization of σ-1 receptors to the endoplasmic reticulum-mitochondria junction. Mol Pharmacol *77*. 10.1124/mol.109.062539.

15. Pani, B., Hwei, L.O., Liu, X., Rauser, K., Ambudkar, I.S., and Singh, B.B. (2008). Lipid rafts determine clustering of STIM1 in endoplasmic reticulum-plasma membrane junctions and regulation of store-operated Ca2+ entry (SOCE). Journal of Biological Chemistry *283*. 10.1074/jbc.M800107200.

16. Garofalo, T., Matarrese, P., Manganelli, V., Marconi, M., Tinari, A., Gambardella, L., Faggioni, A., Misasi, R., Sorice, M., and Malorni, W. (2016). Evidence for the involvement of lipid rafts localized at the ER-mitochondria associated membranes in autophagosome formation. Autophagy *12*. 10.1080/15548627.2016.1160971.

17. Sano, R., Annunziata, I., Patterson, A., Moshiach, S., Gomero, E., Opferman, J., Forte, M., and d'Azzo, A. (2009). GM1-Ganglioside Accumulation at the Mitochondria-Associated ER Membranes Links ER Stress to Ca2+-Dependent Mitochondrial Apoptosis. Mol Cell *36*. 10.1016/j.molcel.2009.10.021.

18. Manganelli, V., Matarrese, P., Antonioli, M., Gambardella, L., Vescovo, T., Gretzmeier, C., Longo, A., Capozzi, A., Recalchi, S., Riitano, G., et al. (2021). Raft-like lipid microdomains drive autophagy initiation via AMBRA1-ERLIN1 molecular association within MAMs. Autophagy *17*. 10.1080/15548627.2020.1834207.

19. Hayashi, T., and Su, T.P. (2010). Cholesterol at the endoplasmic reticulum: Roles of the sigma-1 receptor chaperone and implications thereof in human diseases. Subcell Biochem *51*. 10.1007/978-90-481-8622-8_13.

20. Montesinos, J., Pera, M., Larrea, D., Guardia-Laguarta, C., Agrawal, R.R., Velasco, K.R., Yun, T.D., Stavrovskaya, I.G., Xu, Y., Koo, S.Y., et al. (2020). The Alzheimer's disease-associated

C99 fragment of APP regulates cellular cholesterol trafficking. EMBO J *39*. 10.15252/embj.2019103791.

21. Area-Gomez, E., Del Carmen Lara Castillo, M., Tambini, M.D., Guardia-Laguarta, C., De Groof, A.J.C., Madra, M., Ikenouchi, J., Umeda, M., Bird, T.D., Sturley, S.L., et al. (2012). Upregulated function of mitochondria-associated ER membranes in Alzheimer disease. EMBO Journal *31*. 10.1038/emboj.2012.202.

22. Jordá, T., & Puig, S. (2020). Regulation of ergosterol biosynthesis in saccharomyces cerevisiae. In Genes (Vol. 11, Issue 7). https://doi.org/10.3390/genes11070795

23. Sokolov, S. S., Trushina, N. I., Severin, F. F., & Knorre, D. A. (2019). Ergosterol Turnover in Yeast: An Interplay between Biosynthesis and Transport. In Biochemistry (Moscow) (Vol. 84, Issue 4). https://doi.org/10.1134/S0006297919040023

24. Zheng Koh, D. H., & Saheki, Y. (2021). Regulation of Plasma Membrane Sterol Homeostasis by Nonvesicular Lipid Transport. In Contact (Vol. 4). https://doi.org/10.1177/25152564211042451

25. Gu, Y., Jiao, X., Ye, L., & Yu, H. (2021). Metabolic engineering strategies for de novo biosynthesis of sterols and steroids in yeast. In Bioresources and Bioprocessing (Vol. 8, Issue 1). https://doi.org/10.1186/s40643-021-00460-9

26. Olzmann, J. A., & Carvalho, P. (2019). Dynamics and functions of lipid droplets. In Nature Reviews Molecular Cell Biology (Vol. 20, Issue 3). https://doi.org/10.1038/s41580-018-0085-z.,

27. Mesmin, B., & Maxfield, F. R. (2009). Intracellular sterol dynamics. In Biochimica et Biophysica Acta - Molecular and Cell Biology of Lipids (Vol. 1791, Issue 7). https://doi.org/10.1016/j.bbalip.2009.03.002

28. Mo, C., and Bard, M. (2005). A systematic study of yeast sterol biosynthetic protein-protein interactions using the split-ubiquitin system. Biochim Biophys Acta Mol Cell Biol Lipids *1737*. 10.1016/j.bbalip.2005.11.002.

29. Kumar, N., Leonzino, M., Hancock-Cerutti, W., Horenkamp, F.A., Li, P.Q., Lees, J.A., Wheeler, H., Reinisch, K.M., and De Camilli, P. (2018). VPS13A and VPS13C are lipid transport proteins differentially localized at ER contact sites. Journal of Cell Biology *217*. 10.1083/JCB.201807019.

30. Elbaz-Alon, Y., Eisenberg-Bord, M., Shinder, V., Stiller, S.B., Shimoni, E., Wiedemann, N., Geiger, T., and Schuldiner, M. (2015). Lam6 Regulates the Extent of Contacts between Organelles. Cell Rep *12*. 10.1016/j.celrep.2015.06.022.

31. Costello, J.L., Castro, I.G., Hacker, C., Schrader, T.A., Metz, J., Zeuschner, D., Azadi, A.S., Godinho, L.F., Costina, V., Findeisen, P., et al. (2017). ACBD5 and VAPB mediate membrane associations between peroxisomes and the ER. Journal of Cell Biology *216*. 10.1083/jcb.201607055.

32. Loewen, C.J.R., and Levine, T.P. (2005). A highly conserved binding site in vesicle-associated membrane protein-associated protein (VAP) for the FFAT motif of lipid-binding proteins. Journal of Biological Chemistry *280*. 10.1074/jbc.M500147200.

33. Murley, A., Sarsam, R.D., Toulmay, A., Yamada, J., Prinz, W.A., and Nunnari, J. (2015). Ltc1 is an ER-localized sterol transporter and a component of ER-mitochondria and ER-vacuole contacts. Journal of Cell Biology *209*. 10.1083/jcb.201502033.

34. Toikkanen, J.H., Fatal, N., Hildén, P., Makarow, M., and Kuismanen, E. (2006). YET1, YET2 and YET3 of Saccharomyces cerevisiae encode BAP31 homologs with partially overlapping functions. Journal of Biological Sciences *6*, 446–456. 10.3923/JBS.2006.446.456.

35. Kim, K.M., Adachi, T., Peter, J.N., Terashima, M., Lamers, M.C., Köhler, G., and Reth, M. (1994). Two new proteins preferentially associated with membrane immunoglobulin D. EMBO J *13*, 3793. 10.1002/J.1460-2075.1994.TB06690.X.

36. Ng, F.W.H., Nguyen, M., Kwan, T., Branton, P.E., Nicholson, D.W., Cromlish, J.A., and Shore, G.C. (1997). p28 Bap31, a Bcl-2/Bcl-XL- and procaspase-8-associated protein in the endoplasmic reticulum. J Cell Biol *139*, 327–338. 10.1083/JCB.139.2.327.

37. Breckenridge, D. G., Nguyen, M., Kuppig, S., Reth, M., & Shore, G. C. (2002). The procaspase-8 isoform, procaspase-8L, recruited to the BAP31 complex at the endoplasmic reticulum. Proceedings of the National Academy of Sciences of the United States of America, 99(7), 4331–4336. https://doi.org/10.1073/PNAS.072088099

38. Iwasawa, R., Mahul-Mellier, A.L., Datler, C., Pazarentzos, E., and Grimm, S. (2011). Fis1 and Bap31 bridge the mitochondria-ER interface to establish a platform for apoptosis induction. EMBO Journal *30*. 10.1038/emboj.2010.346.

39. Namba, T. (2019). BAP31 regulates mitochondrial function via interaction with Tom40 within ER-mitochondria contact sites. Sci Adv *5*. 10.1126/SCIADV.AAW1386.

40. Jing, J., He, L., Sun, A., Quintana, A., Ding, Y., Ma, G., Tan, P., Liang, X., Zheng, X., Chen, L., et al. (2015). Proteomic mapping of ER-PM junctions identifies STIMATE as a regulator of Ca 2+ influx. Nat Cell Biol *17*. 10.1038/ncb3234.

41. Xu, J.L., Li, L.Y., Wang, Y.Q., Li, Y.Q., Shan, M., Sun, S.Z., Yu, Y., and Wang, B. (2018). Hepatocyte-specific deletion of BAP31 promotes SREBP1C activation, promotes hepatic lipid accumulation, and worsens IR in mice. J Lipid Res *59*, 35. 10.1194/JLR.M077016.

42. Wu, Z., Yang, F., Jiang, S., Sun, X., and Xu, J. (2018). Induction of Liver Steatosis in BAP31-Deficient Mice Burdened with Tunicamycin-Induced Endoplasmic Reticulum Stress. Int J Mol Sci *19*. 10.3390/IJMS19082291.

43. Dang, E., Yang, S., Song, C., Jiang, D., Li, Z., Fan, W., Sun, Y., Tao, L., Wang, J., Liu, T., et al. (2018). BAP31, a newly defined cancer/testis antigen, regulates proliferation, migration, and invasion to promote cervical cancer progression. Cell Death & Disease 2018 9:8 *9*, 1–15. 10.1038/s41419-018-0824-2.

44. Kim, W.T., Choi, H.S., Lee, H.M., Jang, Y.J., and Ryu, C.J. (2014). B-cell receptor-associated protein 31 regulates human embryonic stem cell adhesion, stemness, and survival via control of epithelial cell adhesion molecule. Stem Cells *32*, 2626–2641. 10.1002/STEM.1765.

45. Eisenberg-Bord, M., Shai, N., Schuldiner, M., & Bohnert, M. (2016). A Tether Is a Tether Is a Tether: Tethering at Membrane Contact Sites. In Developmental Cell (Vol. 39, Issue 4). https://doi.org/10.1016/j.devcel.2016.10.022

46. Shai, N., Yifrach, E., Van Roermund, C.W.T., Cohen, N., Bibi, C., Ijlst, L., Cavellini, L., Meurisse, J., Schuster, R., Zada, L., et al. (2018). Systematic mapping of contact sites reveals tethers and a function for the peroxisome-mitochondria contact. Nat Commun *9*. 10.1038/s41467-018-03957-8.

47. Gatta, A.T., Wong, L.H., Sere, Y.Y., Calderón-Noreña, D.M., Cockcroft, S., Menon, A.K., and Levine, T.P. (2015). A new family of StART domain proteins at membrane contact sites has a role in ER-PM sterol transport. Elife *4*. 10.7554/eLife.07253.

48. Manford, A.G., Stefan, C.J., Yuan, H.L., MacGurn, J.A., and Emr, S.D. (2012). ER-to-Plasma Membrane Tethering Proteins Regulate Cell Signaling and ER Morphology. Dev Cell *23*. 10.1016/j.devcel.2012.11.004.

49. Kornmann, B., Kornmann, B., Currie, E., Currie, E., Collins, S.R., Collins, S.R., Schuldiner, M., Schuldiner, M., Nunnari, J., Nunnari, J., et al. (2009). An ER-Mitochondria Tethering Complex Revealed by a Synthetic Biology Screen. Science (1979) *325*.

50. Pan, X., Roberts, P., Chen, Y., Kvam, E., Shulga, N., Huang, K., Lemmon, S., and Goldfarb, D.S. (2000). Nucleus-vacuole junctions in Saccharomyces cerevisiae are formed through the direct interaction of Vac8p with Nvj1p. Mol Biol Cell *11*. 10.1091/mbc.11.7.2445.

51. Toulmay, A., and Prinz, W.A. (2012). A conserved membrane-binding domain targets proteins to organelle contact sites. J Cell Sci *125*. 10.1242/jcs.085118.

52. Lackner, L.L., Ping, H., Graef, M., Murley, A., and Nunnari, J. (2013). Endoplasmic reticulum-associated mitochondria-cortex tether functions in the distribution and inheritance of mitochondria. Proc Natl Acad Sci U S A *110*. 10.1073/pnas.1215232110.

53. Geiger, R., Andritschke, D., Friebe, S., Herzog, F., Luisoni, S., Heger, T., and Helenius, A. (2011). BAP31 and BiP are essential for dislocation of SV40 from the endoplasmic reticulum to the cytosol. Nat Cell Biol *13*, 1305–1314. 10.1038/NCB2339.

54. Namba, T. (2019). BAP31 regulates mitochondrial function via interaction with Tom40 within ER-mitochondria contact sites. Sci Adv *5*. 10.1126/SCIADV.AAW1386.

55. Wilson, J.D., Thompson, S.L., and Barlowe, C. (2011). Yet1p-Yet3p interacts with Scs2p-Opi1p to regulate ER localization of the Opi1p repressor. 10.1091/mbc.E10-07-0559.

56. Wagner, C., Blank, M., Strohmann, B., & Schüller, H. J. (1999). Overproduction of the Opi1 repressor inhibits transcriptional activation of structural genes required for phospholipid biosynthesis in the yeast Saccharomyces cerevisiae. Yeast, 15(10 A). https://doi.org/10.1002/(SICI)1097-0061(199907)15:10A<843::AID-YEA424>3.0.CO;2-M

57. Marek, M., Vincenzetti, V., and Martin, S.G. (2020). Sterol biosensor reveals LAM-family ltc1-dependent sterol flow to endosomes upon arp2/3 inhibition. Journal of Cell Biology *219*. 10.1083/JCB.202001147.

58. Berkow, E. L., & Lockhart, S. R. (2017). Fluconazole resistance in Candida species: A current perspective. In Infection and Drug Resistance (Vol. 10). https://doi.org/10.2147/IDR.S118892

59. Kim, Y., Mavodza, G., Senkal, C.E., and Burd, C.G. (2023). Cholesterol-dependent homeostatic regulation of very long chain sphingolipid synthesis. Journal of Cell Biology *222*. 10.1083/jcb.202308055.

60. Jauniaux, J. - and Grenson, M. (1990). GAP1, the general amino acid permease gene of Saccharomyces cerevisiae Nucleotide sequence, protein similarity with the other bakers yeast amino acid permeases, and nitrogen catabolite repression. Eur J Biochem *190*. 10.1111/j.1432-1033.1990.tb15542.x.

61. Schreve, J.L., Sin, J.K., and Garrett, J.M. (1998). The Saccharomyces cerevisiae YCC5 (YCL025c) gene encodes an amino acid permease, Agp1, which transports asparagine and glutamine. J Bacteriol *180*. 10.1128/jb.180.9.2556-2559.1998.

62. Bianchi, F., van't Klooster, J.S., Ruiz, S.J., and Poolman, B. (2019). Regulation of Amino Acid Transport in Saccharomyces cerevisiae. Microbiology and Molecular Biology Reviews *83*. 10.1128/mmbr.00024-19.

63. Natarajan, K., Meyer, M.R., Jackson, B.M., Slade, D., Roberts, C., Hinnebusch, A.G., and Marton, M.J. (2001). Transcriptional Profiling Shows that Gcn4p Is a Master Regulator of Gene Expression during Amino Acid Starvation in Yeast. Mol Cell Biol *21*. 10.1128/mcb.21.13.4347-4368.2001.

64. Yang, H., Tong, J., Lee, C.W., Ha, S., Eom, S.H., and Im, Y.J. (2015). Structural mechanism of ergosterol regulation by fungal sterol transcription factor Upc2. Nature Communications 2015 6:1 *6*, 1–13. 10.1038/ncomms7129.

65. White, W.H., Gunyuzlu, P.L., and Toyn, J.H. (2001). Saccharomyces cerevisiae Is Capable of de Novo Pantothenic Acid Biosynthesis Involving a Novel Pathway of β-Alanine Production from Spermine. Journal of Biological Chemistry *276*. 10.1074/jbc.M009804200.

66. Boss, P.K., Pearce, A.D., Zhao, Y., Nicholson, E.L., Dennis, E.G., and Jeffery, D.W. (2015). Potential grape-derived contributions to volatile ester concentrations in wine. Molecules *20*. 10.3390/molecules20057845.

67. Hanna, D. A., Harvey, R. M., Martinez-Guzman, O., Yuan, X., Chandrasekharan, B., Raju, G., Outten, F. W., Hamz, I., & Reddi, A. R. (2016). Heme dynamics and trafficking factors revealed by genetically encoded fluorescent heme sensors. Proceedings of the National Academy of

Sciences of the United States of America, 113(27), 7539–7544. https://doi.org/10.1073/PNAS.1523802113

68. Breker, M., Gymrek, M., and Schuldiner, M. (2013). A novel single-cell screening platform reveals proteome plasticity during yeast stress responses. Journal of Cell Biology *200*. 10.1083/jcb.201301120.

69. Schulte, U., den Brave, F., Haupt, A., Gupta, A., Song, J., Müller, C.S., Engelke, J., Mishra, S., Mårtensson, C., Ellenrieder, L., et al. (2023). Mitochondrial complexome reveals quality-control pathways of protein import. Nature *614*. 10.1038/s41586-022-05641-w.

70. Wilson, J.D., and Barlowe, C. (2010). Yet1p and Yet3p, the yeast homologs of BAP29 and BAP31, interact with the endoplasmic reticulum translocation apparatus and are required for inositol prototrophy. Journal of Biological Chemistry *285*, 18252–18261. 10.1074/jbc.M109.080382.

71. Altmann, K., and Westermann, B. (2005). Role of essential genes in mitochondrial morphogenesis in Saccharomyces cerevisiae. Mol Biol Cell *16*. 10.1091/mbc.E05-07-0678.

72. Del Dedo, J.E., Fernández-Golbano, I., Pastor, L., Meler, P., Ferrer-Orta, C., Rebollo, E., and Geli, M.I. (2021). Coupled sterol synthesis and transport machineries at er–endocytic contact sites. Journal of Cell Biology *220*. 10.1083/jcb.202010016.

73. Runz, H., Miura, K., Weiss, M., and Pepperkok, R. (2006). Sterols regulate ER-export dynamics of secretory cargo protein ts-O45-G. EMBO Journal *25*. 10.1038/sj.emboj.7601205.

74. Lee, M., Moon, Y., Lee, S., Lee, C., and Jun, Y. (2019). Ergosterol interacts with Sey1p to promote atlastin-mediated endoplasmic reticulum membrane fusion in Saccharomyces cerevisiae. FASEB Journal *33*. 10.1096/fj.201800779RR.

75. Lewis, P.M., Dunn, M.P., McMahon, J.A., Logan, M., Martin, J.F., St-Jacques, B., and McMahon, A.P. (2001). Cholesterol modification of sonic hedgehog is required for long-range signaling activity and effective modulation of signaling by Ptc1. Cell *105*. 10.1016/S0092-8674(01)00369-5.

76. King, C., Sengupta, P., Seo, A.Y., and Lippincott-Schwartz, J. (2020). ER membranes exhibit phase behavior at sites of organelle contact. Proc Natl Acad Sci U S A *117*. 10.1073/pnas.1910854117.

77. Kemmeren, P., Sameith, K., Van De Pasch, L.A.L., Benschop, J.J., Lenstra, T.L., Margaritis, T., O'Duibhir, E., Apweiler, E., Van Wageningen, S., Ko, C.W., et al. (2014). Large-scale genetic perturbations reveal regulatory networks and an abundance of gene-specific repressors. Cell *157*. 10.1016/j.cell.2014.02.054.

78. Del Dedo, J.E., Fernández-Golbano, I., Pastor, L., Meler, P., Ferrer-Orta, C., Rebollo, E., and Geli, M.I. (2021). Coupled sterol synthesis and transport machineries at er–endocytic contact sites. Journal of Cell Biology *220*. 10.1083/jcb.202010016.

79. Lee, M., Moon, Y., Lee, S., Lee, C., and Jun, Y. (2019). Ergosterol interacts with Sey1p to promote atlastin-mediated endoplasmic reticulum membrane fusion in Saccharomyces cerevisiae. FASEB Journal *33*. 10.1096/fj.201800779RR.

80. Voeltz, G.K., Prinz, W.A., Shibata, Y., Rist, J.M., and Rapoport, T.A. (2006). A class of membrane proteins shaping the tubular endoplasmic reticulum. Cell *124*. 10.1016/j.cell.2005.11.047.

81. Hu, J., Shibata, Y., Zhu, P.P., Voss, C., Rismanchi, N., Prinz, W.A., Rapoport, T.A., and Blackstone, C. (2009). A Class of Dynamin-like GTPases Involved in the Generation of the Tubular ER Network. Cell *138*. 10.1016/j.cell.2009.05.025.

82. Cohen, N., Breker, M., Bakunts, A., Pesek, K., Chas, A., Argemí, J., Orsi, A., Gal, L., Chuartzman, S., Wigelman, Y., et al. (2017). Iron affects Ire1 clustering propensity and the amplitude of endoplasmic reticulum stress signaling. J Cell Sci *130*, 3222–3233. 10.1242/JCS.201715.

83. Travers, K.J., Patil, C.K., Wodicka, L., Lockhart, D.J., Weissman, J.S., and Walter, P. (2000). Functional and genomic analyses reveal an essential coordination between the unfolded protein response and ER-associated degradation. Cell *101*, 249–258. 10.1016/S0092-8674(00)80835-1.

84. Gasch, A.P., Spellman, P.T., Kao, C.M., Carmel-Harel, O., Eisen, M.B., Storz, G., Botstein, D., and Brown, P.O. (2000). Genomic expression programs in the response of yeast cells to environmental changes. Mol Biol Cell *11*. 10.1091/mbc.11.12.4241.

85. Hulce, J.J., Cognetta, A.B., Niphakis, M.J., Tully, S.E., and Cravatt, B.F. (2013). Proteome-wide mapping of cholesterol-interacting proteins in mammalian cells. Nat Methods *10*. 10.1038/nmeth.2368.

86. Jumper, J., Evans, R., Pritzel, A., Green, T., Figurnov, M., Ronneberger, O., Tunyasuvunakool, K., Bates, R., Žídek, A., Potapenko, A., et al. (2021). Highly accurate protein structure prediction with AlphaFold. Nature *596*. 10.1038/s41586-021-03819-2.

87. Loewen, C.J.R., and Levine, T.P. (2005). A highly conserved binding site in vesicle-associated membrane protein-associated protein (VAP) for the FFAT motif of lipid-binding proteins. Journal of Biological Chemistry *280*. 10.1074/jbc.M500147200.

88. Giaever, G., Chu, A.M., Ni, L., Connelly, C., Riles, L., Véronneau, S., Dow, S., Lucau-Danila, A., Anderson, K., André, B., et al. (2002). Functional profiling of the Saccharomyces cerevisiae genome. Nature *418*. 10.1038/nature00935.

89. Breslow, D.K., Cameron, D.M., Collins, S.R., Schuldiner, M., Stewart-Ornstein, J., Newman, H.W., Braun, S., Madhani, H.D., Krogan, N.J., and Weissman, J.S. (2008). A comprehensive strategy enabling high-resolution functional analysis of the yeast genome. Nat Methods *5*. 10.1038/nmeth.1234.

90. Gaspar, M.L., Hofbauer, H.F., Kohlwein, S.D., and Henry, S.A. (2011). Coordination of storage lipid synthesis and membrane biogenesis: Evidence for cross-talk between triacylglycerol metabolism and phosphatidylinositol synthesis. Journal of Biological Chemistry *286*. 10.1074/jbc.M110.172296.

91. Cho, N.H., Cheveralls, K.C., Brunner, A.D., Kim, K., Michaelis, A.C., Raghavan, P., Kobayashi, H., Savy, L., Li, J.Y., Canaj, H., et al. (2022). OpenCell: Endogenous tagging for the cartography of human cellular organization. Science (1979) *375*. 10.1126/science.abi6983.

92. Iwasawa, R., Mahul-Mellier, A.L., Datler, C., Pazarentzos, E., and Grimm, S. (2011). Fis1 and Bap31 bridge the mitochondria-ER interface to establish a platform for apoptosis induction. EMBO Journal *30*. 10.1038/emboj.2010.346.

93. Cho, N.H., Cheveralls, K.C., Brunner, A.D., Kim, K., Michaelis, A.C., Raghavan, P., Kobayashi, H., Savy, L., Li, J.Y., Canaj, H., et al. (2022). OpenCell: Endogenous tagging for the cartography of human cellular organization. Science (1979) *375*. 10.1126/science.abi6983.

94. Wei, X., Li, L., Zhao, J., Huo, Y., Hu, X., Lu, J., Pi, J., Zhang, W., Xu, L., Yao, Y., et al. (2023). BAP31 depletion inhibited adipogenesis, repressed lipolysis and promoted lipid droplets abnormal growth via attenuating Perilipin1 proteasomal degradation. Int J Biol Sci *19*. 10.7150/ijbs.82178.

95. Luo, W., Adamska, J.Z., Li, C., Verma, R., Liu, Q., Hagan, T., Wimmers, F., Gupta, S., Feng, Y., Jiang, W., et al. (2023). SREBP signaling is essential for effective B cell responses. Nat Immunol *24*. 10.1038/s41590-022-01376-y.

96. Geisberger, R., Lamers, M., & Achatz, G. (2006). The riddle of the dual expression of IgM and IgD. In Immunology (Vol. 118, Issue 4). https://doi.org/10.1111/j.1365-2567.2006.02386.x

97. Paquet, M.-E., Cohen-Doyle, M., Shore, G.C., and Williams, D.B. (2004). Bap29/31 Influences the Intracellular Traffic of MHC Class I Molecules. The Journal of Immunology *172*. 10.4049/jimmunol.172.12.7548.

98. Niu, K., Xu, J., Cao, Y., Hou, Y., Shan, M., Wang, Y., Xu, Y., Sun, M., and Wang, B. (2017). BAP31 is involved in T cell activation through TCR signal pathways. Sci Rep *7*. 10.1038/srep44809.

99. Drake, D.R., and Braciale, T.J. (2001). Cutting Edge: Lipid Raft Integrity Affects the Efficiency of MHC Class I Tetramer Binding and Cell Surface TCR Arrangement on CD8+ T Cells. The Journal of Immunology *166*. 10.4049/jimmunol.166.12.7009.

100. Zhao, B., Sun, L., Yuan, Q., Hao, Z., An, F., Zhang, W., Zhu, X., and Wang, B. (2023). BAP31 Knockout in Macrophages Affects CD4+T Cell Activation through Upregulation of MHC Class II Molecule. Int J Mol Sci *24*. 10.3390/ijms241713476.

101. Xu, K., Han, B., Bai, Y., Ma, X.Y., Ji, Z.N., Xiong, Y., Miao, S.K., Zhang, Y.Y., and Zhou, L.M. (2019). MiR-451a suppressing BAP31 can inhibit proliferation and increase apoptosis through inducing ER stress in colorectal cancer. Cell Death & Disease 2019 10:3 *10*, 1–16. 10.1038/s41419-019-1403-x.

102. Wang, A., Zhang, Y., and Cao, P. (2019). Inhibition of BAP31 expression inhibits cervical cancer progression by suppressing metastasis and inducing intrinsic and extrinsic apoptosis. Biochem Biophys Res Commun *508*, 499–506. 10.1016/J.BBRC.2018.11.017.

103. Chen, J., Guo, H., Jiang, H., Namusamba, M., Wang, C., Lan, T., Wang, T., and Wang, B. (2019). A BAP31 intrabody induces gastric cancer cell death by inhibiting p27kip1 proteasome degradation. Int J Cancer *144*, 2051–2062. 10.1002/IJC.31930.

104. Yu, S., Wang, F., Fan, L., Wei, Y., Li, H., Sun, Y., Yang, A., Jin, B., Song, C., and Yang, K. (2015). BAP31, a promising target for the immunotherapy of malignant melanomas. J Exp Clin Cancer Res *34*. 10.1186/S13046-015-0153-6.

105. Liu, X., Jiao, K., Jia, C. cong, Li, G. xun, Yuan, Q., Xu, J. kai, Hou, Y., and Wang, B. (2019). BAP31 regulates IRAK1-dependent neuroinflammation in microglia. J Neuroinflammation *16*. 10.1186/S12974-019-1661-7.

106. Wang, T., Chen, J., Hou, Y., Yu, Y., and Wang, B. (2019). BAP31 deficiency contributes to the formation of amyloid-β plaques in Alzheimer's disease by reducing the stability of RTN3. FASEB J *33*, 4936–4946. 10.1096/FJ.201801702R.

107. Regan, J.A., and Laimins, L.A. (2008). Bap31 is a novel target of the human papillomavirus E5 protein. J Virol *82*, 10042–10051. 10.1128/JVI.01240-08.

108. Geiger, R., Andritschke, D., Friebe, S., Herzog, F., Luisoni, S., Heger, T., and Helenius, A. (2011). BAP31 and BiP are essential for dislocation of SV40 from the endoplasmic reticulum to the cytosol. Nat Cell Biol *13*, 1305–1314. 10.1038/NCB2339.

109. Brachmann, C.B., Davies, A., Cost, G.J., Caputo, E., Li, J., Hieter, P., and Boeke, J.D. (1998). Designer deletion strains derived from Saccharomyces cerevisiae S288C: A useful set of strains and plasmids for PCR-mediated gene disruption and other applications. Yeast *14*. 10.1002/(SICI)1097-0061(19980130)14:2<115::AID-YEA204>3.0.CO;2-2.

110. Gietz, R.D., and Woods, R.A. (2006). Yeast transformation by the LiAc/SS Carrier DNA/PEG method. Methods Mol Biol *313*. 10.1385/1-59259-958-3:107.

111. Janke, C., Magiera, M.M., Rathfelder, N., Taxis, C., Reber, S., Maekawa, H., Moreno-Borchart, A., Doenges, G., Schwob, E., Schiebel, E., et al. (2004). A versatile toolbox for PCR-based tagging of yeast genes: New fluorescent proteins, more markers and promoter substitution cassettes. Yeast *21*. 10.1002/yea.1142.

112. Longtine, M.S., McKenzie, A., Demarini, D.J., Shah, N.G., Wach, A., Brachat, A., Philippsen, P., and Pringle, J.R. (1998). Additional modules for versatile and economical PCR-based gene deletion and modification in Saccharomyces cerevisiae. Yeast *14*. 10.1002/(SICI)1097-0061(199807)14:10<953::AID-YEA293>3.0.CO;2-U.

113. Yofe, I., and Schuldiner, M. (2014). Primers-4-Yeast: A comprehensive web tool for planning primers for Saccharomyces cerevisiae. Yeast *31*. 10.1002/yea.2998.

114. Schindelin, J., Arganda-Carreras, I., Frise, E., Kaynig, V., Longair, M., Pietzsch, T., Preibisch, S., Rueden, C., Saalfeld, S., Schmid, B., Tinevez, J. Y., White, D. J., Hartenstein, V., Eliceiri, K., Tomancak, P., & Cardona, A. (2012). Fiji: An open-source platform for biological-image analysis. In Nature Methods (Vol. 9, Issue 7). https://doi.org/10.1038/nmeth.2019

115. Mastronarde, D.N. (2005). Automated electron microscope tomography using robust prediction of specimen movements. J Struct Biol *152*. 10.1016/j.jsb.2005.07.007.

116. Kremer, J.R., Mastronarde, D.N., and McIntosh, J.R. (1996). Computer visualization of three-dimensional image data using IMOD. J Struct Biol *116*. 10.1006/jsbi.1996.0013.

117. Hagen, W.J.H., Wan, W., and Briggs, J.A.G. (2017). Implementation of a cryo-electron tomography tilt-scheme optimized for high resolution subtomogram averaging. J Struct Biol *197*. 10.1016/j.jsb.2016.06.007.

118. Mastronarde, D.N., and Held, S.R. (2017). Automated tilt series alignment and tomographic reconstruction in IMOD. J Struct Biol *197*. 10.1016/j.jsb.2016.07.011.

119. Liu, Y.T., Zhang, H., Wang, H., Tao, C.L., Bi, G.Q., and Zhou, Z.H. (2022). Isotropic reconstruction for electron tomography with deep learning. Nat Commun *13*. 10.1038/s41467-022-33957-8.

120. Lamm, L., Zufferey, S., Righetto, R.D., Wietrzynski, W., Yamauchi, K.A., Burt, A., Liu, Y., Zhang, H., Martinez-Sanchez, A., Ziegler, S., et al. (2024). MemBrain v2: an end-to-end tool for the analysis of membranes in cryo-electron tomography. bioRxiv.

121. Pettersen, E.F., Goddard, T.D., Huang, C.C., Couch, G.S., Greenblatt, D.M., Meng, E.C., and Ferrin, T.E. (2004). UCSF Chimera - A visualization system for exploratory research and analysis. J Comput Chem *25*. 10.1002/jcc.20084.

122. Tong, A.H.Y., and Boone, C. (2006). Synthetic genetic array analysis in Saccharomyces cerevisiae. Methods Mol Biol *313*. 10.1385/1-59259-958-3:171.

123. Breslow, D.K., Cameron, D.M., Collins, S.R., Schuldiner, M., Stewart-Ornstein, J., Newman, H.W., Braun, S., Madhani, H.D., Krogan, N.J., and Weissman, J.S. (2008). A comprehensive strategy enabling high-resolution functional analysis of the yeast genome. Nat Methods *5*. 10.1038/nmeth.1234.

124. Perez-Riverol, Y., Bai, J., Bandla, C., García-Seisdedos, D., Hewapathirana, S., Kamatchinathan, S., Kundu, D.J., Prakash, A., Frericks-Zipper, A., Eisenacher, M., et al. (2022). The PRIDE database resources in 2022: A hub for mass spectrometry-based proteomics evidences. Nucleic Acids Res *50*. 10.1093/nar/gkab1038.

125. Elinger, D., Gabashvili, A., and Levin, Y. (2019). Suspension Trapping (S-Trap) Is Compatible with Typical Protein Extraction Buffers and Detergents for Bottom-Up Proteomics. J Proteome Res *18*. 10.1021/acs.jproteome.8b00891.

126. Cox, J., Hein, M.Y., Luber, C.A., Paron, I., Nagaraj, N., and Mann, M. (2014). Accurate proteome-wide label-free quantification by delayed normalization and maximal peptide ratio extraction, termed MaxLFQ. Molecular and Cellular Proteomics *13*. 10.1074/mcp.M113.031591.

127. Tyanova, S., Temu, T., Sinitcyn, P., Carlson, A., Hein, M. Y., Geiger, T., Mann, M., & Cox, J. (2016). The Perseus computational platform for comprehensive analysis of (prote)omics data. In Nature Methods (Vol. 13, Issue 9). https://doi.org/10.1038/nmeth.3901

128. Malitsky, S., Ziv, C., Rosenwasser, S., Zheng, S., Schatz, D., Porat, Z., Ben-Dor, S., Aharoni, A., and Vardi, A. (2016). Viral infection of the marine alga Emiliania huxleyi triggers lipidome remodeling and induces the production of highly saturated triacylglycerol. New Phytologist *210*. 10.1111/nph.13852.

129. Zheng, L., Cardaci, S., Jerby, L., Mackenzie, E.D., Sciacovelli, M., Johnson, T.I., Gaude, E., King, A., Leach, J.D.G., Edrada-Ebel, R., et al. (2015). Fumarate induces redox-dependent senescence by modifying glutathione metabolism. Nat Commun *6*. 10.1038/ncomms7001.

130. Dong, Y., Steffenson, B.J., and Mirocha, C.J. (2006). Analysis of ergosterol in single kernel and ground grain by gas chromatography-mass spectrometry. J Agric Food Chem *54*. 10.1021/jf060149f.

131. Zhang, Y., Karmon, O., Das, K., Wiener, R., Lehming, N., and Pines, O. (2022). Ubiquitination Occurs in the Mitochondrial Matrix by Eclipsed Targeted Components of the Ubiquitination Machinery. Cells *11*. 10.3390/cells11244109.

132. Martinez-Guzman, O., Willoughby, M.M., Saini, A., Dietz, J. V., Bohovych, I., Medlock, A.E., Khalimonchuk, O., and Reddi, A.R. (2020). Mitochondrial-nuclear heme trafficking in budding yeast is regulated by GTPases that control mitochondrial dynamics and ER contact sites. J Cell Sci *133*. 10.1242/jcs.237917.

133. Hanna, D.A., Moore, C.M., Liu, L., Yuan, X., Dominic, I.M., Fleischhacker, A.S., Hamza, I., Ragsdale, S.W., and Reddi, A.R. (2022). Heme oxygenase-2 (HO-2) binds and buffers labile ferric heme in human embryonic kidney cells. Journal of Biological Chemistry *298*. 10.1016/j.jbc.2021.101549.

Zunger et al, Figure 1

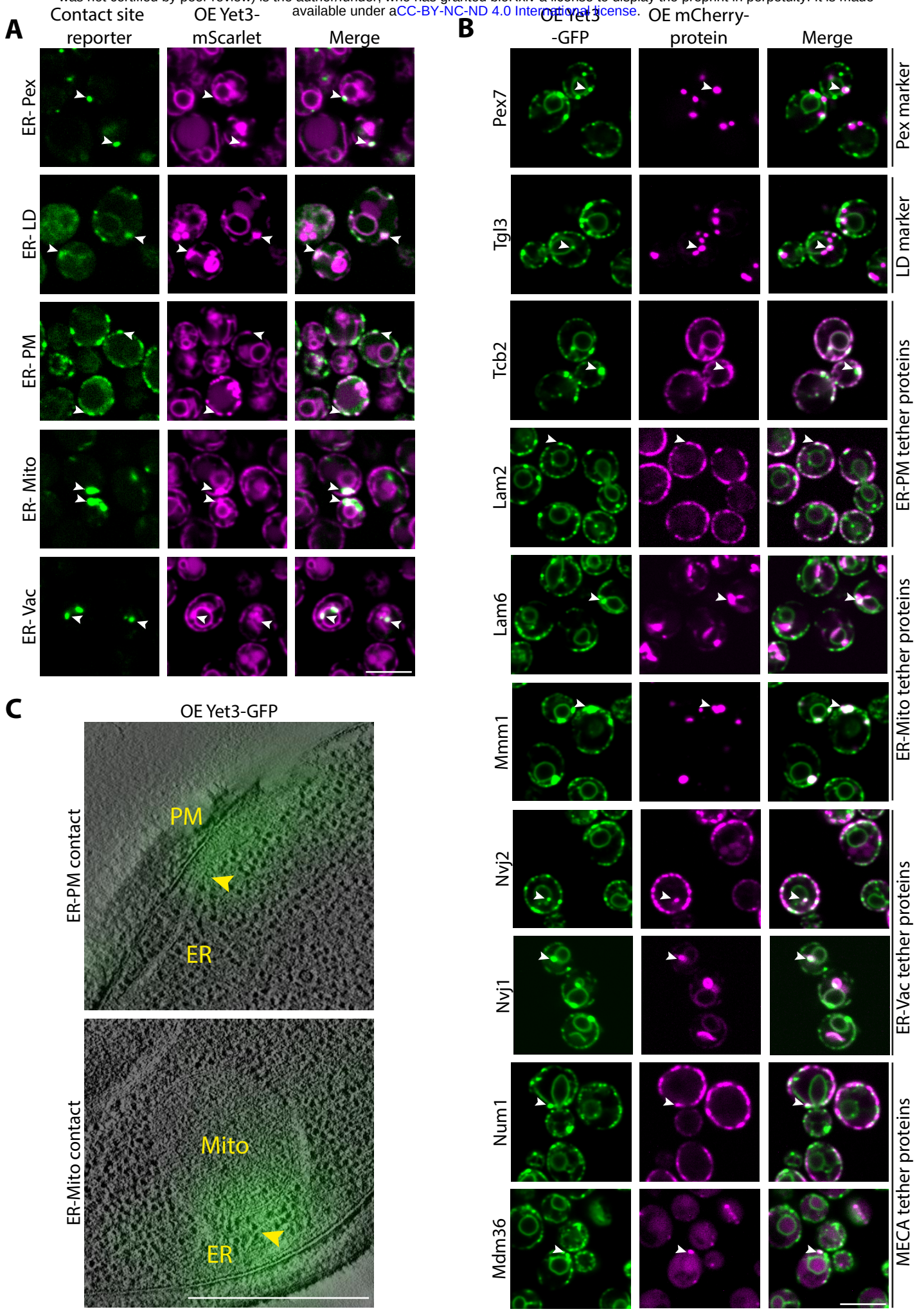

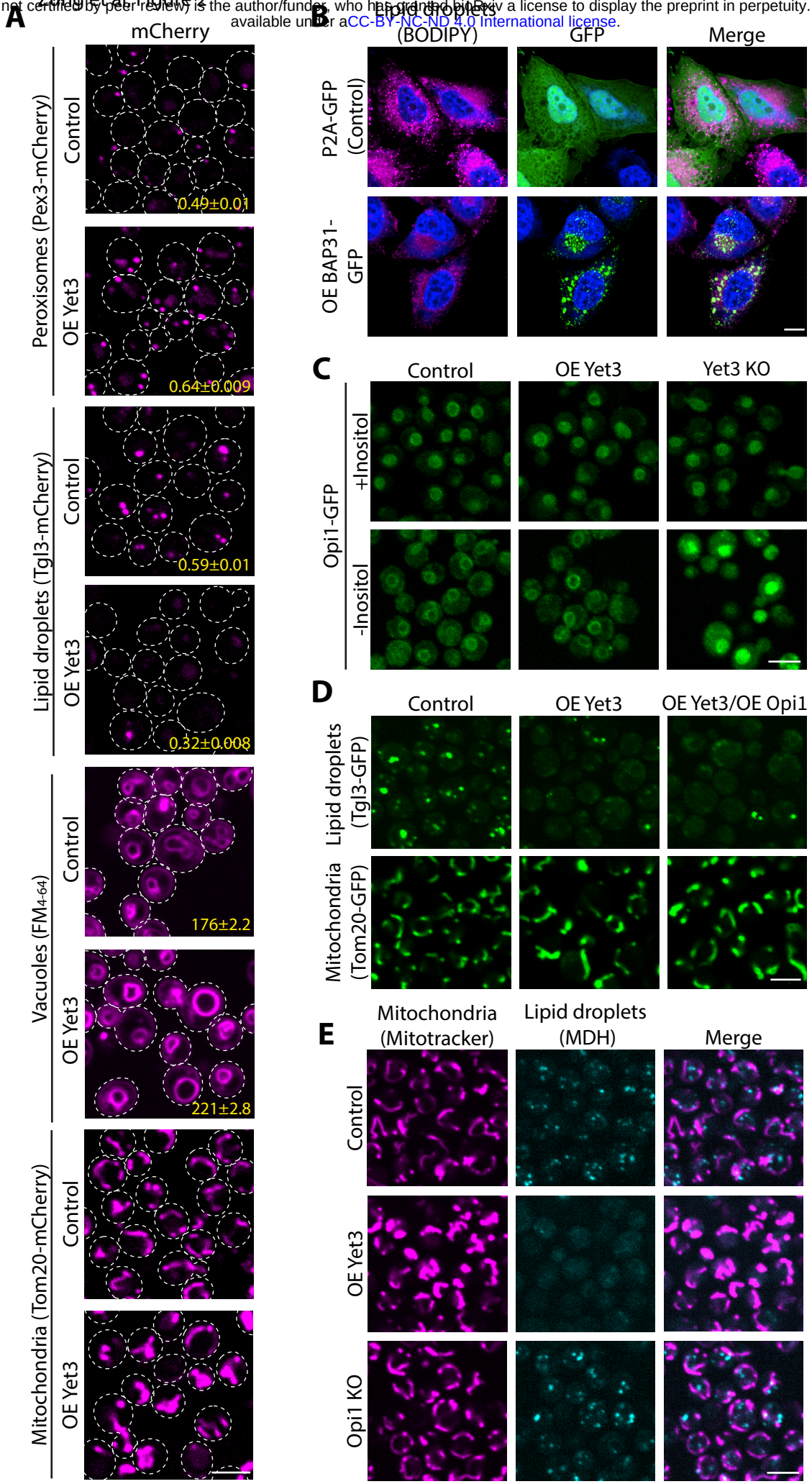

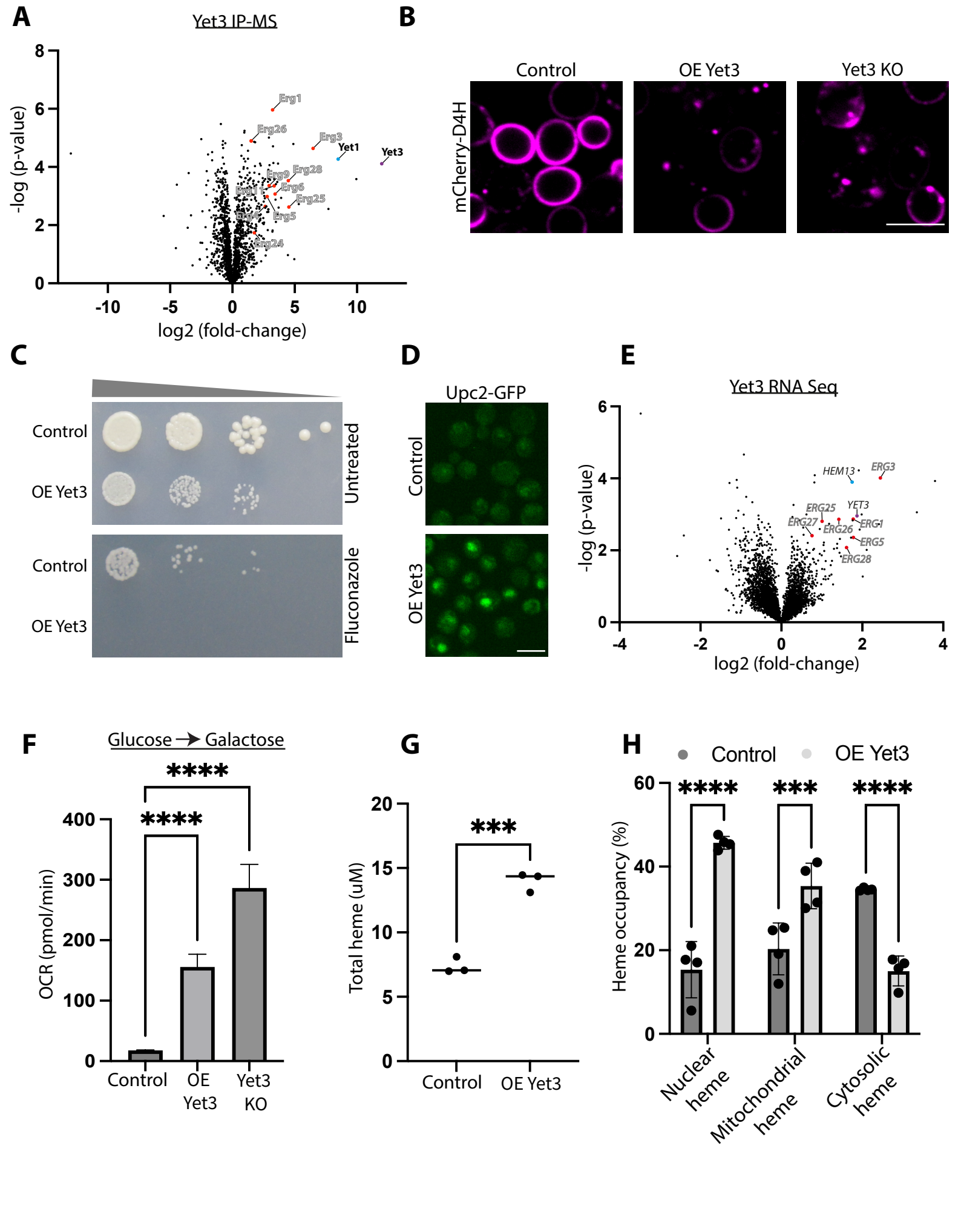

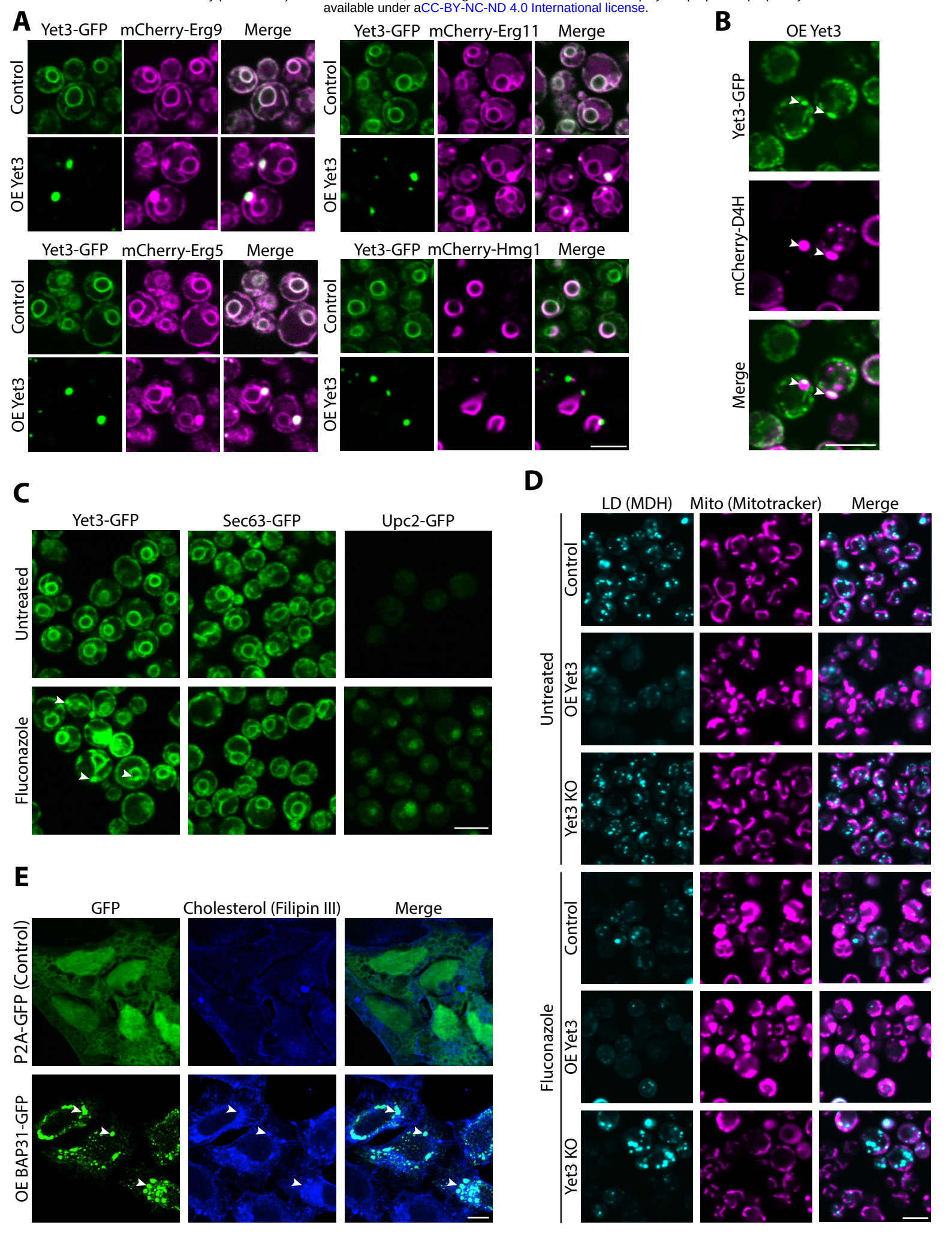

Zung et al, Figure 5